

**Synthesis and Characterization of New Binuclear Cu(I)
Diimine and Phosphine Mixed Ligand Complexes.
Catalytic Application in the Coupling of
Phenylacetylene with Halobenzene**

BY

Atif Fazal

A Dissertation Presented to the
DEANSHIP OF GRADUATE STUDIES

KING FAHD UNIVERSITY OF PETROLEUM & MINERALS

DHAHRAN, SAUDI ARABIA

In Partial Fulfillment of the
Requirements for the Degree of

DOCTOR OF PHILOSOPHY

In

Chemistry

January, 2010

KING FAHD UNIVERSITY OF PETROLEUM & MINERALS
DHAHRAN 31261, SAUDI ARABIA

DEANSHIP OF GRADUATE STUDIES

This dissertation, written by **Atif Fazal** under the direction of his thesis advisor and approved by his thesis committee, has been presented to and accepted by Dean of Graduate Studies, in partial fulfillment of the requirements for the degree of
DOCTOR OF PHILOSOPHY IN CHEMISTRY.

Dissertation Committee

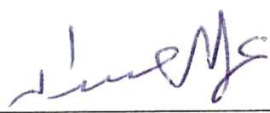

Dr. Mohammed Fettouhi (Advisor)



Dr. Abdulrahman Al-Arfaj (Co-Advisor)


Dr. Bassam El Ali (Member)


Dr. Mohammad A. Gondal (Member)


Dr. Anvarhusein Isab (Member)


Dr. Abdullah J. Hamdan
Department Chairman


Dr. Salam S. Zummo
Dean of Graduate Studies

23/2/19

[Date]



ACKNOWLEDGMENT

In the name of Allah (SWT) who alone is the most powerful and the most merciful. Peace and blessings be upon the last Prophet (SAW), his progeny and noble companions.

I wish to express my reverence and gratitude to my esteemed and lovable advisor, Dr. Mohammed Fettouhi without his expert guidance this dissertation would not have been possible. Not only was he readily available for me, as he so generously. But he always read and responded to the drafts of each chapter of my work more quickly than I could have hoped. His oral and written comments are always extremely perceptive, helpful, and appropriate. I am thankful to my dissertation co-advisor Dr. Abdulrahman Al-Arfaj and Dr. Bassam El Ali, our graduate advisor for their amiable personality and guidance during the course of my work. I wish to acknowledge the support offered by Dr. Muhammad Ashraf Gondal for utilizing his lab facilities. I am thankful to Dr. Lahcene Ouahab from Rennes 1 University, France for offering x-ray analysis support, which was pivotal for the present work. I also offer my thanks to Dr. Anvarhusein Isab my committee member. My teachers Dr. Abdallah Abulkibash, Dr. Muhammad Shahid Ansari (my M. Phil advisor) for their prayers and support. I would like to thank Dr. Zaki S. Seddigi and Dr. Abdallah Jaffar Al-Hamdan previous and present chairman of the department for their professional support.

Far too many people to mention individually have assisted in so many ways during my work at KFUPM. They all have my sincere gratitude. In particular, I would like to thank my wonderful friends Khizar hayat, Tawfik A. Saleh, Sabee and Tariq for their support during tough time. Ahmed Al-Harbi, Dr. Hafiz Muhammad Afzal, Dr. Altaf, Dr. Waqar, Dr. Shemsi, Shahid, Ishfaq, Nazeer-ud-din, Al-Maythality, Rami, Basim Moosa, Monim, Nidal, Moheeduin, Abdullah Manda, Hatim, Khalid, Aftab, Farhan, Osama, Salman, Tahir, Aijaz, Naveed, Nimr, Abdul Nasir. Mr. Arab, Farooqi, Bahauddin,

Dastageer, Mansoor Zaki, Aiman, Saleem, Ismail, Kashif, Haider, Shahid, Nasir, Inayat, Nooh, Mr.Baig and Saleem wangde.

A penultimate and most heartfelt thank-you goes to my wonderful parents, especially my mother. For always being there when I needed them most, and never once complaining. They have been a beacon of love and modesty. They deserve far more credit than I can ever give them. My brothers Waseem, Waqar, Javed, Aamir, Waqas, Asim, Asif; my sisters Naheed, Nosheen and Muniba. My sisters and brothers-in-law. My nieces and nephews for their support and prayers throughout my life. I also wish to acknowledge my parents-in-law for their love and supplications for my happiness and success.

My final, and heartfelt, acknowledgment must go to my wife Maria. She has worked industriously, and successfully, since our marriage to make life more tranquil. Her support, encouragement, and companionship has turned my journey successful. For all that, and for being everything I am not, she has my everlasting admiration. I cannot leave this page without mentioning Mahveen (my adorable daughter), her birth has truly been a blessing in disguise for me. Finally, I am extremely thankful to King Fahd University of Petroleum and Minerals, Dhahran, Saudi Arabia for sponsoring my Ph.D. studies.

DEDICATED TO MY PARENTS
MARIA, MAHVEEN and MARWA

TABLE OF CONTENTS

List of Abbreviations	xiv
List of Tables	xvi
List of Figures	xx
Abstract (English)	xxv
Abstract (Arabic)	xxvii
CHAPTER 1	1
1.1 Introduction	1
1.2 Role of Copper(I) complexes in the catalysis of carbon-carbon bond formation.....	2
1.3 Current status of the problem	6
1.4 Objectives of The Present Study.....	6
Chapter 2.....	9
Binuclear Copper(I) mixed ligand complexes with	9
bis(diphenylphosphino)acetylene (dppa)	9
2.1 Synthesis.....	9
2.1.1 $[\text{Cu}_2(\text{dppa})_2(\text{bipy})_2][\text{BF}_4]_2$ (1)	9

2.1.2	$[\text{Cu}_2(\text{dppa})_2(4,4'\text{-Me}_2\text{bipy})_2][\text{BF}_4]_2$ (2)	10
2.1.3	$[\text{Cu}_2(\text{dppa})_2(5,5'\text{-Me}_2\text{bipy})_2][\text{BF}_4]_2$ (3)	10
2.1.4	$[\text{Cu}_2(\text{dppa})_2(6,6'\text{-Me}_2\text{bipy})_2][\text{BF}_4]_2$ (4)	11
2.1.5	$[\text{Cu}_2(\text{dppa})_2(\text{phen})_2][\text{BF}_4]_2$ (5)	11
2.1.6	$[\text{Cu}_2(\text{dppa})_2(4\text{-Mephen})_2][\text{BF}_4]_2$ (6)	12
2.1.7	$[\text{Cu}_2(\text{dppa})_2(2,9\text{-Me}_2\text{phen})_2][\text{BF}_4]_2$ (7)	12
2.1.8	$[\text{Cu}_2(\text{dppa})_2(4,7\text{-Me}_2\text{phen})_2][\text{BF}_4]_2$ (8)	12
2.2	Characterization of the complexes 1-8	13
2.2.1	Elemental Analysis and Melting points	13
2.2.2	Ultraviolet and Visible Spectroscopy	14
2.2.3	Emission Spectroscopy	17
2.2.4	Fourier-Transformed Infrared Spectroscopy (FT-IR)	20
2.2.5	Raman Spectroscopy	22
2.2.6	Single Crystal X-ray Analysis	24
2.2.7	Nuclear Magnetic Resonance Spectroscopy	33
Chapter 3		37
	Binuclear Copper(I) mixed ligand complexes with	37

trans-1,2-bis(diphenylphosphino)ethylene (dppethy).....	37
3.1 Synthesis of $[\text{Cu}_2(\text{dppethy})_3(\text{CH}_3\text{CN})_2][\text{BF}_4]_2$ Precursor-B.....	37
3.1.1 Synthesis of binuclear complexes.....	38
3.1.2 $[\text{Cu}_2(\text{dppethy})_2(\text{bipy})_2][\text{BF}_4]_2$ (9)	38
3.1.3 $[\text{Cu}_2(\text{dppethy})_2(4,4'\text{-Me}_2\text{bipy})_2][\text{BF}_4]_2$ (10)	38
3.1.4 $[\text{Cu}_2(\text{dppethy})_2(5,5'\text{-Me}_2\text{bipy})_2][\text{BF}_4]_2$ (11)	39
3.1.5 $[\text{Cu}_2(\text{dppethy})_2(6,6'\text{-Me}_2\text{bipy})_2][\text{BF}_4]_2$ (12)	39
3.1.6 $[\text{Cu}_2(\text{dppethy})_2(\text{phen})_2][\text{BF}_4]_2$ (13)	40
3.1.7 $[\text{Cu}_2(\text{dppethy})_2(4\text{-Mephen})_2][\text{BF}_4]_2$ (14)	40
3.1.8 $[\text{Cu}_2(\text{dppethy})_2(2,9\text{-Me}_2\text{phen})_2][\text{BF}_4]_2$ (15)	41
3.1.9 $[\text{Cu}_2(\text{dppethy})_2(4,7\text{-Me}_2\text{phen})_2][\text{BF}_4]_2$ (16)	41
3.2 Characterization of Precursor-B and Complexes 9-16.....	42
3.2.1 Elemental Analysis	42
3.2.2 Ultraviolet and Visible Spectroscopy	43
3.2.3 Fourier-Transformed Infrared Spectroscopy (FT-IR)	44
3.2.4 Nuclear Magnetic Resonance Spectroscopy	46
Chapter 4.....	50

Binuclear Copper(I) mixed ligand complexes with	50
4,4'-bipyridine bridging ligand (4,4'-bipy)	50
4.1 Synthesis.....	50
4.1.1 $[\text{Cu}_2(4,4'\text{-bipy})(\text{PPh}_2(\text{i-Pr}))_2(\text{bipy})_2][\text{BF}_4]_2$ (17).....	50
4.1.2 $[\text{Cu}_2(4,4'\text{-bipy})(\text{m-Tol}_3\text{P})_2(\text{bipy})_2][\text{BF}_4]_2$ (18)	51
4.1.3 $[\text{Cu}_2(4,4'\text{-bipy})(\text{DAP-DP})_2(\text{bipy})_2][\text{BF}_4]_2$ (19).....	51
4.1.4 $[\text{Cu}_2(4,4'\text{-bipy})(\text{PPh}_2(\text{i-Pr}))_2(6,6'\text{-Me}_2\text{bipy})_2][\text{BF}_4]_2$ (20)	52
4.1.5 $[\text{Cu}_2(4,4'\text{-bipy})(\text{PPh}_2(\text{i-Pr}))_2(\text{phen})_2][\text{BF}_4]_2$ (21)	52
4.1.6 $[\text{Cu}_2(4,4'\text{-bipy})(\text{m-Tol}_3\text{P})_2(\text{phen})_2][\text{BF}_4]_2$ (22)	52
4.1.7 $[\text{Cu}_2(4,4'\text{-bipy})(\text{PCy}_3)_2(\text{phen})_2][\text{BF}_4]_2$ (23).....	53
4.1.8 $[\text{Cu}_2(4,4'\text{-bipy})(\text{PCy}_3)_2(4\text{-Me phen})_2][\text{BF}_4]_2$ (24).....	53
4.1.9 $[\text{Cu}_2(4,4'\text{-bipy})(\text{PPh}_2(\text{i-Pr}))_2(2,9\text{-Me}_2\text{phen})_2][\text{BF}_4]_2$ (25).....	54
4.2 Characterization of the complexes 17-25	54
4.2.1 Elemental Analysis and Melting points.....	54
4.2.2 Ultraviolet and Visible Spectroscopy	55
4.2.3 Emission spectroscopy	57
4.2.4 Fourier-Transformed Infrared Spectroscopy (FT-IR)	59

4.2.5	Single Crystal X-ray Analysis.....	61
4.2.6	Nuclear Magnetic Resonance Spectroscopy	67
Chapter 5.....		71
Binuclear Copper(I) mixed ligand complexes with		71
trans-1,2-bis(4-pyridyl)ethylene (bpe) bridging ligand		71
5.1	Synthesis.....	71
5.1.1	[Cu ₂ (bpe)(PPh ₂ (i-Pr)) ₂ (6,6'-Me ₂ bipy) ₂][BF ₄] ₂ (26)	72
5.1.2	[Cu ₂ (bpe)(PPh ₂ i-Pr) ₂ (phen) ₂][BF ₄] ₂ (27)	72
5.1.3	[Cu ₂ (bpe)(PCy ₃) ₂ (phen) ₂][BF ₄] ₂ (28)	72
5.1.4	[Cu ₂ (bpe)(Cy ₂ PhP) ₂ (phen) ₂][BF ₄] ₂ (29).....	73
5.1.5	[Cu ₂ (bpe)(m-Tol ₃ P) ₂ (phen) ₂][BF ₄] ₂ (30).....	73
5.1.6	[Cu ₂ (bpe)(PCy ₃) ₂ (4-Mephen) ₂][BF ₄] ₂ (31)	74
5.1.7	[Cu ₂ (bpe)(Ph ₃ P) ₂ (4,7-Me ₂ phen) ₂][BF ₄] ₂ (32)	74
5.2	Characterization of the Complexes 25-32	74
5.2.1	Elemental Analysis	74
5.2.2	Ultraviolet and Visible Spectroscopy	75
5.2.3	Emission spectroscopy	77

5.2.4 Single Crystal X-ray Analysis.....	78
5.2.5 Nuclear Magnetic Resonance Spectroscopy	81
Chapter 6.....	83
Binuclear Copper(I) mixed ligand complexes with	83
2,2'-bipyrimidine (bpm) bridging ligand.....	83
6.1 Synthesis	84
6.1.1 $[\text{Cu}_2(\text{bpm})(\text{PPh}_2(\text{i-Pr}))_2(\text{Br})_2]$ (33).....	84
6.1.2. $[\text{Cu}_2(\text{bpm})(\text{PPh}_2(\text{i-Pr}))_2(\text{I})_2]$ (34).....	84
6.1.3. $[\text{Cu}_2(\text{bpm})(\text{TCP})_2(\text{Br})_2]$ (35).....	85
6.1.4. $[\text{Cu}_2(\text{bpm})(\text{TCP})_2(\text{Br})_2]$ (36).....	85
6.2 Characterization of the complexes (33-36)	85
6.2.1 Elemental Analysis and Melting points	86
6.2.2 Ultraviolet and Visible Spectroscopy	86
6.2.3 Fourier-Transformed Infrared Spectroscopy (FT-IR).....	88
6.2.4 Far-Infrared analysis	89
6.2.5 Single crystal X-ray crystallography	90
6.2.6 Nuclear Magnetic Resonance Spectroscopy.....	95

Chapter 7.....	96
Copper(I) mixed ligand complexes with	96
2,3-bis(2-pyridyl)pyrazine (bpp) bridging ligand	96
7.1 Synthesis	97
7.1.1. $[\text{Cu}_2(\text{bpp})(\text{TCP})_2(\text{Br})_2]$ (37)	97
7.1.2. $[\text{Cu}(\text{bpp})(\text{PPh}_2(\text{i-Pr}))(\text{Br})]$ (38)	97
7.1.3. $[\text{Cu}(\text{bpp})(\text{Ph}_3\text{P})(\text{Br})]$ (39)	98
7.1.4. $[\text{Cu}(\text{bpp})(\text{PPh}_2(\text{i-Pr}))(\text{I})]$ (40)	98
7.2 Characterization of the complexes (37-40)	98
7.2.1 Elemental Analysis and Melting points	98
7.2.2 Ultraviolet and Visible Spectroscopy	100
7.2.3 Fourier-Transformed Mid Infrared Spectroscopy (MidFT-IR)	101
7.2.4 FAR-IR analysis	102
7.2.5 Single crystal X-ray crystallography	103
Chapter 8.....	108
Mononuclear Copper(I) mixed ligand complexes with different phosphines.....	108
8.1 Synthesis	108

8.1.1 [Cu(m-Tol ₃ P) ₂ (bipy)][BF ₄] (41)	108
8.1.2 [Cu(PPh ₂ (i-Pr)) ₂ (bipy)][BF ₄] (42)	109
8.1.3 [Cu(p-Tol ₃ P) ₂ (bipy)][BF ₄] (43)	109
8.1.4 [Cu(DAP-DP) ₂ (bipy)][BF ₄] (44)	110
8.1.5 [Cu(^t BuPh ₂ P) ₂ (bipy)][BF ₄] (45)	110
8.1.6 [Cu(PPh ₃) ₂ (4,4'-Me ₂ bipy)][BF ₄] (46)	110
8.1.7 [Cu(p-Tol ₃ P) ₂ (4,4'-Me ₂ bipy)][BF ₄] (47)	111
8.1.8 [Cu(PPh ₂ (i-Pr)) ₂ (4,4'-Me ₂ bipy)][BF ₄] (48)	111
8.1.9 [Cu(m-Tol ₃ P) ₂ (4,4'-Me ₂ bpy)][BF ₄] (49)	111
8.1.10 [Cu(TCP) ₂ (phen)][BF ₄] (50)	112
8.1.11 [Cu(p-Tol ₃ P) ₂ (phen)][BF ₄] (51)	112
8.1.12 [Cu(PPh ₂ (i-Pr)) ₂ (4-Mephen)][BF ₄] (52)	113
8.1.13 [Cu(PPh ₃) ₂ (4-Mephen)][BF ₄] (53)	113
8.1.14 [Cu(p-Tol ₃ P) ₂ (4-Mephen)][BF ₄] (54)	114
8.1.15 [Cu(PPh ₃) ₂ (2,9-Me ₂ phen)][BF ₄] (55)	114
8.2 Characterization of the complexes (41-55)	115
8.2.1 Elemental Analysis	115

8.2.2 Electronic Spectra of Complexes.....	117
8.2.3 Excitation and Emission spectroscopy.....	119
8.2.4 Fourier-Transformed Infrared Spectroscopy (FT-IR).....	121
8.2.5 Single Crystal X-ray Analysis	122
8.2.6 Nuclear Magnetic Resonance Spectroscopy	131
Chapter 9.....	135
Catalytic Application in the coupling of.....	135
phenylacetylene with halobenzene	135
9.1 Introduction.....	135
9.2 Catalytic properties of some mononuclear copper(I) mixed ligand complexes	136
9.2.1 Suggested Mechanism.....	137
9.3 Binuclear copper(I) catalysts for phenylacetylene and halobenzene coupling.	140
Chapter 10	142
Conclusion	142
References.....	145
Appendices	156

A-I.....	156
A-II.....	159
A-III.....	193
A-IV	206
A V.....	220
A- VII.....	248
A-VIII.....	269
Curriculum Vitae.....	273

LIST OF ABBREVIATIONS

Precursor-A	$[\text{Cu}_2(\text{dppa})_3(\text{CH}_3\text{CN})_2][\text{BF}_4]_2$
Precursor-B	$[\text{Cu}_2(\text{dppethy})_3(\text{CH}_3\text{CN})_2][\text{BF}_4]_2$
DPPA	bis(diphenylphosphino)acetylene
Dppethy	trans-1,bis(diphenylphosphino)ethylene
4,4'-bipy	4,4'-bipyridine
bpe	Trans-1,2-bis(4-pyridyl)ethylene
dpp	2,3-bis(2-pyridyl)pyrazine
bpm	2,2'-bipyrimidine
bipy	2,2'-bipyridyl
4,4'-Me ₂ bipy	4,4'-dimethyl-2,2'-bipyridyl
5,5'-Me ₂ bipy	5,5'-dimethyl-2,2'-bipyridyl
6,6'-Me ₂ bipy	6,6'-dimethyl-2,2'-bipyridyl
phen	1,10-phenanthroline
4-Mephen	4-methyl-1,10-phenanthroline
2,9-Me ₂ phen	2,9-dimethyl-1,10-phenanthroline

4,7-Me ₂ phen	4,7-dimethyl-1,10-phenanthroline
PPh ₂ (i-Pr)	iso-propyldiphenylphosphine
PCy ₃	tri-cyclohexylphosphine
PPh ₃	triphenyl phosphine
(m-Tol ₃)P	tri-meta-tolylphosphine
(p-Tol ₃)P	tri-para-tolylphosphine
^t BuPh ₂ P	tert-butyldiphenylphosphine
DAP-DP	4-(dimethylamino)phenyldiphenylphosphine
PhCy ₂ P	dicyclohexylphenylphosphine
TCP	tris(2-cyanoethyl)phosphine

LIST OF TABLES

Table 1. Results of Elemental Analysis and Melting Points of Complexes 1-8.....	13
Table 2. Results of Ultraviolet and Visible Spectroscopy for free Diimines	14
Table 3. Results of Ultraviolet and Visible Spectroscopy of Complexes 1-8.....	16
Table 4. Excitation and Emission Wavelengths of free Diimines.....	18
Table 5. Excitation and Emission Wavelengths of Complexes 1-6	19
Table 6. Infrared Frequencies (cm^{-1}) and assignment for Complexes 1-8	20
Table 7. Raman shifts for free Ligand and the Complexes	23
Table 8. Crystallographic Data Collection and Structure Refinement Parameters for Complexes 2, 3 and 4.....	24
Table 9. Selected Bond Lengths (\AA) and Bond Angles ($^{\circ}$) of Complexes 2-4.....	26
Table 10. Crystallographic Data Collection and Structure Refinement Parameters for Complexes 5, 7 and 8.....	29
Table 11. Selected Bond Lengths (\AA) and Bond Angles ($^{\circ}$) of the complexes 5, 7 and 8	30
Table 12. ^1H NMR shifts for free Diimines	34
Table 13. ^1H and ^{31}P NMR Shifts for Complexes 1- 8.....	35
Table 14. Results of Elemental Analysis and Melting Points of Precursor-B and complexes 9-16	42
Table 15. Results of Ultraviolet and Visible Spectroscopy for Precursor-B and Complexes 9-16	43

Table 16. Infrared Frequencies (cm^{-1}) and assignment for Ligand, Precursor-B and Complexes 9-12	45
Table 17. ^1H NMR and ^{31}P shifts for Ligand, Precursor-B and Complexes 9-13 and 15-16.....	48
Table 18. Results of Elemental Analysis and Melting Points of Complexes 17-25.....	54
Table 19. Results of Ultraviolet and Visible Spectroscopy for free Ligands and Complexes 17-25	56
Table 20. Excitation and Emission Wavelengths for Complexes 17 and 21.....	59
Table 21. Infrared Frequencies (cm^{-1}) and assignment for Complexes 17-22 and 24 ...	60
Table 22. Crystallographic Data Collection and Structure Refinement Parameters for Complexes 17 and 20	62
Table 23. Crystallographic Data Collection and Structure Refinement Parameters for Complexes 21 and 25.....	63
Table 24. Selected Bond Lengths (\AA) and Bond Angles ($^\circ$) of the complexes 17 and 20	63
Table 25. Selected Bond Lengths (\AA) and Bond Angles ($^\circ$) of the complexes	64
Table 26. ^1H NMR shifts for free ligands.....	69
Table 27. ^1H and ^{31}P NMR shifts for complexes 17-21 and 23-25	69
Table 28. Results of Elemental Analysis.....	75
Table 29. Results of Ultraviolet and Visible Spectroscopy for bpe and Complexes 26-32.....	76
Table 30. Excitation and Emission Wavelengths for Complexes 27, 28 and 31.....	77

Table 31. Crystallographic Data Collection and Structure Refinement Parameters for Complexes 26.....	78
Table 32. Selected Bond Lengths (Å) and Bond Angles (°) of the complexes	79
Table 33. ¹ H NMR shifts for free Ligand and Complexes	82
Table 34. Results of Elemental Analysis and Melting Points of the complexes 33-36..	86
Table 35. Results of Ultraviolet and Visible Spectroscopy free Ligands and Complexes 33-36	87
Table 36. Infrared frequencies (cm ⁻¹) and assignment for Complexes 33-36	88
Table 37. Far-IR absorption data for Cu-Br bond in Complex 33 and 35	90
Table 38. Crystallographic Data Collection and Structure Refinement Parameters for Complexes 33-35	90
Table 39. Selected Bond Lengths (Å) and Bond Angles (°) of the complexes 33-35....	92
Table 40. ¹ H and ³¹ P-NMR shifts for Complexes 34-36	95
Table 41. Results of Elemental Analysis and Melting Points of the Complexes 37- 40	99
Table 42. Results of Ultraviolet and Visible Spectroscopy for bpp and Complexes 38- 40.....	100
Table 43. Infrared frequencies (cm ⁻¹) and assignment for Complexes 37-39	101
Table 44. Far-IR absorption data for Cu-Br bond Strechthing in Complexes (37-38)....	102
Table 45. Crystallographic Data Collection and Structure Refinement Parameters for Complexes 37-38 and 40.....	103

Table 46. Selected Bond Lengths (Å) and Bond Angles (°) of the complexes 38 and 40	104
Table 47. Results of Elemental Analysis of the Complexes 41-55	115
Table 48. Results of Ultraviolet and Visible Spectroscopy for free Ligands and Complexes 42-51 and 54-55	117
Table 49. Excitation and Emission Wavelengths of Complexes 42-44, 47 and 52.....	119
Table 50. Infrared frequencies (cm ⁻¹) and assignment for Ligand and Complexes 42-46 & 48-49	121
Table 51. Crystallographic Data Collection and Structure Refinement Parameters for Complexes 41-44	122
Table 52. Crystallographic Data Collection and Structure Refinement Parameters for Complexes 45-48 and 53, 55.....	123
Table 53. Selected bond lengths (Å) and bond angles (°) of Complexes 41-44.....	125
Table 54. Selected Bond Lengths (Å) and Bond Angles (°) (of Complexes 45-49 and 53, 55)	126
Table 55. ¹ H and ³¹ P NMR shifts of Complexes 42-54.....	132
Table 56. Isolated yields of the Reaction of Aryl-halides with Phenylacetylene in the Presence 10 mol % of 56-59	137
Table 57. Isolated yields of the Reaction of Aryl-halides with Phenylacetylene in the Presence 5 mol % of 33-37	140

LIST OF FIGURES

Figure 1. UV-Visible Spectrum of Complex 2.....	15
Figure 2. Excitation and Emission Spectra of 2,2'-bipyridyl.....	18
Figure 3. FT-IR Spectrum of Precursor-A	20
Figure 4. Raman Spectrum of bis(diphenylphosphino)acetylene.....	22
Figure 5. X-ray structure of Complex 2 showing thermal ellipsoids drawn at the 30 % probability level. Hydrogen atoms and BF_4^- anions are omitted for clarity. Only ipso carbons of C_6H_5 group are shown for clarity	27
Figure 6. X-ray structure of Complex 3 showing thermal ellipsoids drawn at the 30 % probability level. Hydrogen atoms and BF_4^- anions are omitted for clarity. Only the ipso carbons of C_6H_5 groups are shown for clarity	27
Figure 7. X-ray structure of Complex 4 showing thermal ellipsoids drawn at the 30 % probability level. Hydrogen atoms and BF_4^- anions are omitted for clarity. Only the ipso carbons of C_6H_5 groups are shown for clarity	28
Figure 8. X-ray structure of Complex 5 showing thermal ellipsoids drawn at the 30 % probability level. Hydrogen atoms and BF_4^- anions are omitted for clarity. Only the ipso carbons of C_6H_5 groups are shown for clarity	31
Figure 9. X-ray structure of Complex 7 showing spheres drawn at the 30 % probability level. Hydrogen atoms, phenyl rings of dppa bridge and BF_4^- anions are omitted for clarity. Only the ipso carbons of C_6H_5 groups are shown for clarity.....	31

Figure 10. X-ray structure of Complex 8 showing thermal ellipsoid drawn at the 30 % probability level. Hydrogen atoms and BF_4^- anions are omitted for clarity. Only the ipso carbons of C_6H_5 groups are shown for clarity	32
Figure 11. ^1H -NMR Spectrum of Complex 5.....	33
Figure 12. ^{31}P -NMR Spectrum of Complex 5	34
Figure 13. FT-IR Spectrum of Complex 11	44
Figure 14. ^1H -NMR Spectrum of Complex 12.....	47
Figure 15. ^{31}P -NMR Spectrum of Complex 11	47
Figure 16. UV-Visible Spectrum of Complex 20.....	56
Figure 17. Excitation Spectrum of Complex 21	58
Figure 18. Emission Spectrum of Complex 21.	58
Figure 19. FT-IR Spectrum of Complex 20	60
Figure 20. X-ray structure of Complex 17 showing thermal ellipsoid drawn at the 30 % probability level. Hydrogen atoms and BF_4^- anions are omitted for clarity.....	65
Figure 21. X-ray structure of Complex 20 showing thermal ellipsoid drawn at the 30 % probability level. Hydrogen atoms and BF_4^- anions are omitted for clarity.....	65
Figure 22. X-ray structure of Complex 20 showing thermal ellipsoid drawn at the 30 % probability level. Hydrogen atoms and BF_4^- anions are omitted for clarity.....	66
Figure 23. X-ray structure of Complex 20 showing thermal ellipsoid drawn at the 30 % probability level. Hydrogen atoms and BF_4^- anions are omitted for clarity.....	66
Figure 24. X-ray structure of Complex 25 showing thermal ellipsoid drawn at the 30 % probability level. Hydrogen atoms and BF_4^- anions are omitted for clarity.....	67

Figure 25. ^1H NMR Spectrum (only the aromatic region) of Complex 20	68
Figure 26. ^{31}P NMR Spectrum of Complex 20	68
Figure 27. Excitation and Emission Spectrum of Complex 28	77
Figure 28. X-ray structure of Complex 26 showing thermal ellipsoid drawn at the 30 % probability level. Hydrogen atoms and BF_4^- anions are omitted for clarity.....	80
Figure 29. X-ray structure of Complex 28 showing thermal ellipsoid drawn at the 30 % probability level. Hydrogen atoms and BF_4^- anions are omitted for clarity.....	81
Figure 30. ^1H -NMR Spectrum of Complex 26.....	81
Figure 31. ^{31}P -NMR Spectrum of Complex 26	82
Figure 32. Electronic Spectrum of Complex 33	87
Figure 33. X-ray structure of Complex 33. Thermal ellipsoids are drawn at 30 % probability. Hydrogen atoms and DMF molecule are omitted for clarity.....	94
Figure 34. X-ray structure of Complex 34. Thermal ellipsoids are drawn at 30 % probability. Hydrogen atoms are omitted for clarity.....	94
Figure 35. X-ray structure of Complex 35. Thermal ellipsoids are drawn at 30 % probability. Hydrogen atoms are omitted for clarity.....	95
Figure 36. UV-Visible Spectrum of Complex 37.....	100
Figure 37. X-ray structure of Complex 37. Thermal ellipsoids are drawn at 30% probability. Hydrogen atoms are omitted for clarity.....	105
Figure 38. X-ray structure of Complex 38. Thermal ellipsoids are drawn at 30% probability. Hydrogen atoms are omitted for clarity.....	105

Figure 39. X-ray structure of Complex 39. Spheres are drawn at 30% probability.	
Hydrogen atoms are omitted for clarity	106
Figure 40. X-ray structure of Complex 40. Thermal ellipsoids are drawn at 30% probability. Hydrogen atoms are omitted for clarity.....	106
Figure 41. UV-Visible Spectrum of Complex 46.....	117
Figure 42. Excitation Spectrum of Complex 42.....	120
Figure 43. Emission Spectrum of Complex 42	120
Figure 44. X-ray structure of Complex 42 showing thermal ellipsoid drawn at 15 %.	
Hydrogen atoms, BF_4^- anion and one meta-tolyl ring is omitted for clarity	127
Figure 45. X-ray structure of Complex 43 showing thermal ellipsoid drawn at 15 %.	
Hydrogen atoms, 4,4'-bipy molecule and BF_4^- anion are omitted for clarity	127
Figure 46. X-ray structure of Complex 44 showing thermal ellipsoid drawn at 15 %.	
Hydrogen atoms, BF_4^- anion are omitted for clarity	128
Figure 47. X-ray structure of Complex 45 showing thermal ellipsoid drawn at 15 %.	
Hydrogen atoms, BF_4^- anion are omitted for clarity	128
Figure 48. X-ray Structure of Complex 47 showing thermal ellipsoid drawn at 15 %.	
Hydrogen atoms, BF_4^- anion are omitted for clarity	129
Figure 49. X-ray structure of Complex 49 showing thermal ellipsoid drawn at 15 %.	
Hydrogen atoms, BF_4^- anion are omitted for clarity	129
Figure 50. X-ray structure of Complex 50 showing thermal ellipsoid drawn at 15 %.	
Hydrogen atoms, BF_4^- anion are omitted for clarity	130

Figure 51. X-ray structure of Complex 52 showing thermal ellipsoid drawn at 15 %.

Hydrogen atoms, BF_4^- anions, two para-tolyl rings are omitted for clarity130

Figure 52. X-ray structure Complex 55 showing thermal ellipsoid drawn at 15 %.

Hydrogen atoms, BF_4^- anion are omitted for clarity131

Figure 53. ^1H -NMR (only the aromatic region) of Complex 45132

Dissertation Abstract

Name of Student: Atif Fazal

Title of Study: Synthesis and Characterization of new binuclear Cu(I) diimine and phosphine mixed ligand complexes. Catalytic application in the coupling of phenylacetylene with halobenzene.

Major Field: Inorganic Chemistry

Date of Degree: January 2010

In the present study binuclear mixed ligand complexes of copper(I) with phosphine and diimine derivatives with diphosphine and dinitrogen bridges have been successfully synthesized. Characterization of the mixed ligand complexes was carried out using elemental analysis, UV-Visible, FT-IR, NMR spectroscopy and solution luminescence. Single crystal X-ray diffraction analyses were conducted on series of complexes to determine their molecular structure. Catalytic properties towards the coupling of phenylacetylene with halobenzene have been studied.

DOCTOR OF PHILOSOPHY DEGREE

KING FAHD UNIVERSITY OF PETROLEUM & MINERALS

DHAHRAN SAUDI ARABIA

ملخص الرسالة

عاطف فضل	الاسم:
تصنيع و توصيف معقدات جديدة للنحاس الأحادي ثنائية النواة ذات متصلات مختلطة من الفوسفينات و الأيمينات الثنائية. التطبيقات التحفيزية على تفاعلات ازدواج الفينيلاستلين مع هاليدات البنزين.	عنوان الرسالة:
كيمياء غير عضوية	التخصص:
١٤٣١/٢	تاريخ التخرج:

تم في هذا البحث تصنيع معقدات جديدة للنحاس الأحادي ثنائية النواة ذات متصلات مختلطة من الفوسفينات الثلاثية و الأيمينات الثنائية من مشتقات 2, 2'-بابردين و 10,1-فناثرولين. وتم توصيف هذه المركبات بواسطة تقنية تحليل العناصر ومطيافية الأشعة المرئية و فوق البنفسجية و الأشعة تحت الحمراء و الرنين النووي المغناطيسي و كذلك وميض الانبعاث للمحاليل. وتم التوصيف أيضا بتقنية حيود الأشعة السينية على البلورات للإيجاد التركيبية البلورية. وتم دراسة الخصائص التحفيزية على تفاعلات ازدواج الفينيلاستلين مع هاليدات البنزين.

درجة الدكتوراه في الكيمياء

جامعة الملك فهد للبترول و المعادن

الظهران- المملكة العربية السعودية

CHAPTER 1

1.1 Introduction

Multinuclear coordination complexes are currently widely investigated for their physical and chemical properties with potential applications in catalysis, molecular recognition, solar energy conversion, luminescence based sensing, display devices, probes of biological systems and phototherapy [1-15]. Applications of copper complexes are of interest because of the lower cost of copper compared to the other metals offering similar properties. In this context, copper(I) halides are known to react with tertiary phosphines to yield the mono, di and polynuclear complexes with a variety of structures. This is a result of geometric flexibility of copper(I) and its ability to adopt two, three or four coordination numbers [16-21]. Interest in these copper(I) complexes arises from their catalytic [22-28], photophysical [29-34] and biological applications [35-37].

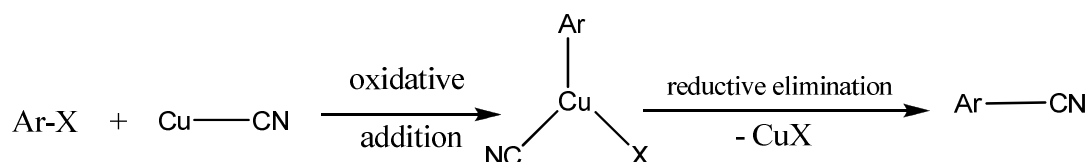
Recently, mixed ligand mononuclear copper(I) complexes containing phosphines and chelating diimines have been found to be versatile species. They exhibit interesting photophysical properties [38-42]; because of their ready availability and the prevalence of low lying charge transfer (CT) excited states. Blaskie and McMillin [43] have reported tetragonally flattened geometry for these excited states and tetrahedral-like coordination geometry for ground state appropriate for a closed shell ion [44-45]. They were also found to catalyze different chemical reactions such as carbon-carbon and carbon heteroatom bond formation reactions [46-47]. On the ground of the above mentioned properties of the mononuclear copper(I) complexes

containing phosphines and chelating diimines, binuclear species with the same coordination sphere appear very attractive, as they can provide intriguing mixed – valence species that are regarded as prototypes for molecular switches and wires. Copper functionalized dye sensitized solar cells, employing diimine-copper(I) complexes as dyes, are remarkably efficient. Maximum radiative emission is achieved by preventing the non-emissive geometric reorganization path, typically by increasing the steric bulk of the substituents or by electronic control [48-52]. Cu(I) complexes are challenging to synthesize due to the intrinsic instability of the cuprous oxidation state; under many conditions disproportionation of Cu(I) to Cu(0) to Cu(II) is thermodynamically favored. As a matter of fact literature reports of such binuclear species are rare. Those having a diphosphine bridge are based for instance on methylenediphenylphosphine [53-59], 1,2-bis(diphenylphosphino)ethane [60-62] or 1,2-bis(diphenylphosphino)acetylene a trifunctional ligand [63-71] capable of forming dinuclear and polynuclear or even polymeric complexes. The dominant coordination modes, which leave the ligand intact, are end-on terminal and end-on bridging through the phosphorous functions [64, 67]. Those having a dipyridyl bridge are based for instance on 4,4'-bipyridine [72-74], trans-1,2-bis(4-pyridyl)ethene [75-76], 2,2'-bipyrimidine and 2,3-bis(2-pyridyl)pyrazine [77].

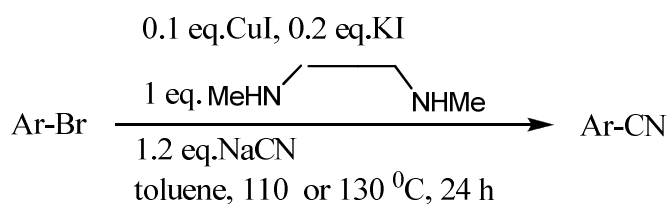
1.2 Role of Copper(I) complexes in the catalysis of carbon-carbon bond formation

Aryl-acetylene and aryl-heteroatom bonds are prevalent in many compounds that are of biological, pharmaceutical and materials interest. The coupling of phenylacetylene with halobenzene is an important transformation both from organic synthesis viewpoint and industrial manufacturing. In recognition of the widespread importance, over the years, many synthetic methods have emerged for the coupling of phenylacetylene with halobenzenes like Hartwig-Büchwald [78, 79], Sonogashira coupling [80] Castro and Stephens [81]. These reaction; have similarities with the much older Rosenmund-von Braun synthesis (1916) [82] between aryl halides and

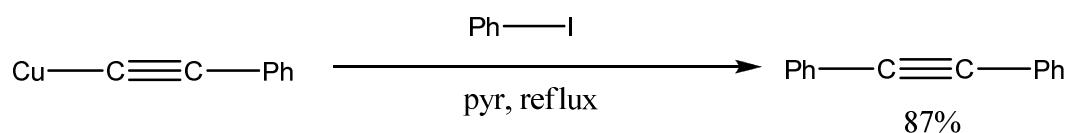
copper(I) cyanide and the mechanism probably involves the formation of a Cu(III) species through oxidative addition of the aryl halide. Subsequent reductive elimination then leads to the product:



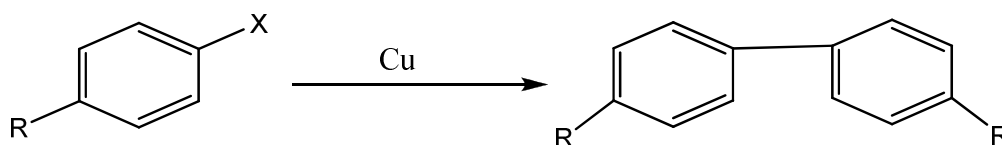
The excess of copper cyanide and the use of a polar, high-boiling point solvent makes the purification of the products difficult. In addition, elevated temperatures (up to 200 °C) lower the functional group tolerance. The use of alkali metal cyanides or cyanation reagents such as cyanohydrins, a catalytic amount of copper(I) iodide and kalium iodide, allows a mild, catalytic cyanation of various aryl bromides.



Rosenmund-von Braun synthesis was itself modified in 1973 by the Sonogashira coupling by adding a palladium catalyst and preparing the organocopper compound in situ. A typical reaction is the coupling of iodobenzene with the copper acetylide of phenylacetylene in refluxing pyridine to diphenylacetylene:

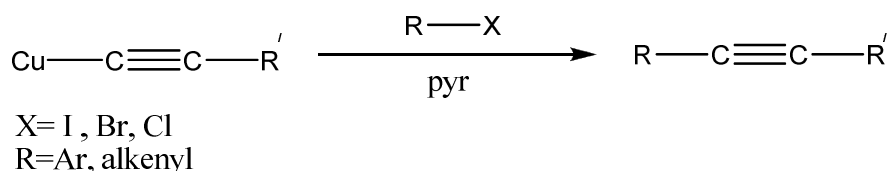


The Ullmann coupling is a coupling reaction between aryl halides with copper. The reaction is named after Fritz Ullmann [83].

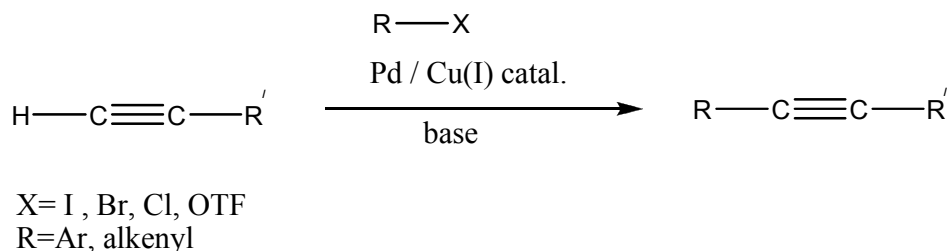


The traditional version of the Ullmann reaction requires harsh reaction conditions, and the reaction has a reputation for erratic yields. Since its discovery some improvements and alternative procedures have been introduced [84]. The reaction mechanism of the Ullmann reaction is extensively studied. Electron spin resonance rules out a radical intermediate. The oxidative addition / reductive elimination sequence observed with palladium catalysts is unlikely for copper because copper(III) is rarely observed. The reaction probably involves the formation of an organocopper compound (RCuX) which reacts with the other aryl reactant in a nucleophilic aromatic substitution. Alternative mechanisms do exist such as σ -bond metathesis [85].

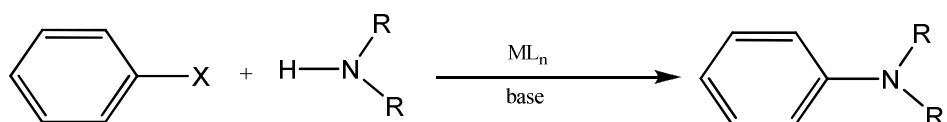
The Castro-Stephens Coupling is a cross coupling reaction between a Copper(I) acetylide and an aryl halide forming a disubstituted alkyne and a copper(I) halide.



The reaction was discovered in 1963 by chemists Castro and Stephens and is used as a tool in the organic synthesis of organic compounds [80]. The Stephens-Castros coupling also have some drawbacks; like most copper(I) salts are insoluble in organic solvents, and hence, the reactions are often heterogeneous and require high reaction temperatures. Sonogashira reaction was first reported by Kenkichi Sonogashira and Nobue Hagihara in 1975 [81]. It is a coupling reaction of terminal alkynes with aryl or vinyl halides.



Typically, two catalysts are needed for this reaction: a zerovalent palladium complex and a halide salt of copper(I). The palladium complex activates the organic halides by oxidative addition into the carbon-halogen bond. Phosphine-palladium complexes such as tetrakis(triphenylphosphine)palladium(0) are used for this reaction, but palladium(II) complexes are also available because they are reduced to the palladium(0) species by the consumption of terminal alkynes in the reaction medium. The oxidation of triphenylphosphine to triphenylphosphine oxide can also lead to the formation of Pd(0) *in situ* when catalysts such as bis(triphenylphosphine)palladium(II) chloride are used. In contrast, copper(I) halides react with the terminal alkyne and produce copper(I) acetylide, which acts as an activated species for the coupling reactions. The Büchwald-Hartwig reaction in its original scope is an organic reaction describing a coupling between an aryl halide and an amine in presence of base and a palladium catalyst forming a new carbon-nitrogen bond.



The primary or secondary amine substituents can be any organic residue and the metal M in the reactions original scope is Palladium and the ligand L can be a wide range of phosphines such as triphenylphosphine. Another regular catalyst ligand combination is tris(dibenzylideneacetone)dipalladium(0). The base can be sodium bis(trimethylsilyl)amide or a tert-butoxide. Moreover, the reactions are sensitive to functional groups on aryl halides and the yields are often irreproducible. It replaced, to an extent, the Copper catalyzed Golderberg reaction [86]. It was shown by Weingarten in 1964 [87], Cohen in 1976 [88], and more recently, by others that if the solubility of

copper salts is increased then the aryl coupling reactions tend to occur at milder temperatures. D. Venkataraman et al; [46-47] have shown that $\text{Cu}(\text{phen})(\text{PPh}_3)\text{Br}$ can be used as catalyst for coupling of aryl iodides with aryl acetylenes using K_2CO_3 as the base, in toluene at 110-120 °C. This mononuclear copper(I)-based catalytic system shows catalytic conversions under mild conditions and is tolerant to functional groups and does not require the use of expensive metal like Palladium.

1.3 Current status of the problem

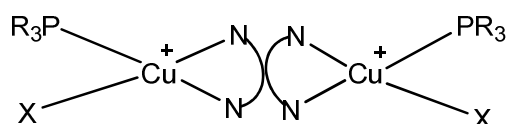
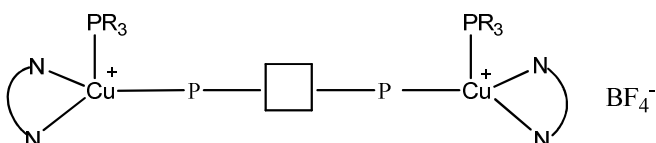
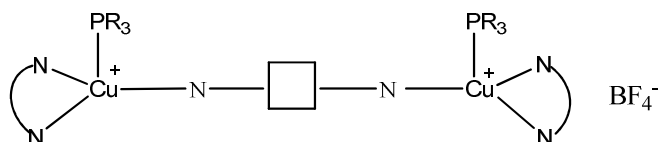
Copper(I) bimetallic mixed ligand complexes based on phosphines and chelating diimines and having bridging bis(diphenylphosphino)acetylene [53-59] or trans-1,2-bis(diphenylphosphinoethene) [60-62] are rare in literature. Copper(I) bimetallic mixed ligand complexes based on phosphines and chelating diimines having bridging 4,4'-bipyridine [56-58], trans-1,2-bis(4-pyridyl)ethylene [75-76], 2,2'-bipyrimidine or 2,3-bis(2-pyridyl)pyrazine [77] are also rare in literature. To date systematic modification of the chelating diimine and the phosphine in such complexes is absent in literature. The result of this study will first enhance the understanding of the coordination chemistry of copper(I) towards chelating diimine and bridging ligands. Moreover, this study will result in new materials with potential applications in photoactive devices. In addition to this, the crystallographic data will allow to rationalize the effect of the nature of the coordination sphere and its correlation with the photophysical properties and the catalytic activity of the complexes.

The screening of copper(I) mixed ligand complexes as effective catalysts for the formation of carbon-carbon bonds instead of the costly palladium counterparts will give preliminary results about the catalytic performance of these complexes. This may open wide perspectives to the design and application of efficient catalytic systems for the formation of carbon-carbon bonds.

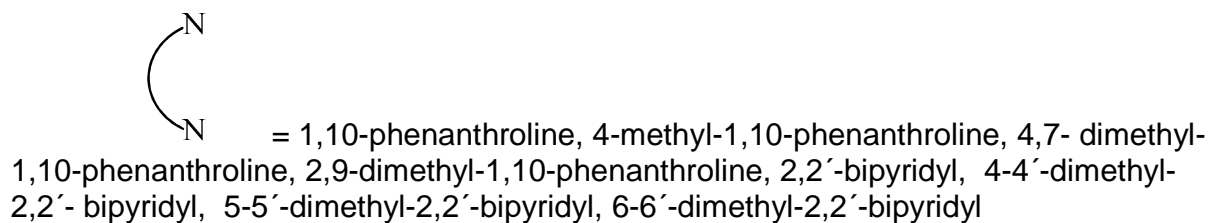
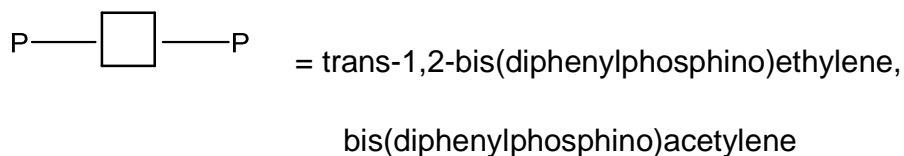
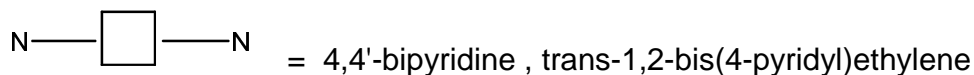
1.4 Objectives of The Present Study

The objectives of the present study are listed below.

1. Synthesis of the following binuclear mixed ligand coordination cationic complexes using diphosphine and dinitrogen bridging ligands, and various diimine ligands with the following general formula:



Where



2. Characterization of these complexes using, Nuclear Magnetic Resonance (^1H , ^{13}C , ^{31}P), Elemental Analysis (EA), Mass Spectrometry (MS), Fourier Transformed Infra Red Spectroscopy (FT-IR), Raman and Ultraviolet-Visible (UV-Vis) Spectroscopy.
3. Study of the luminescence of these complexes.
4. Crystal growth of crystals suitable for single crystal X-ray diffraction analysis.
5. Determination of the single crystal X-ray structures.
6. Study of the efficacy of these complexes as catalysts in the coupling of phenylacetylene with halobenzene.

Chapter 2

Binuclear Copper(I) mixed ligand complexes with bis(diphenylphosphino)acetylene (dppa)

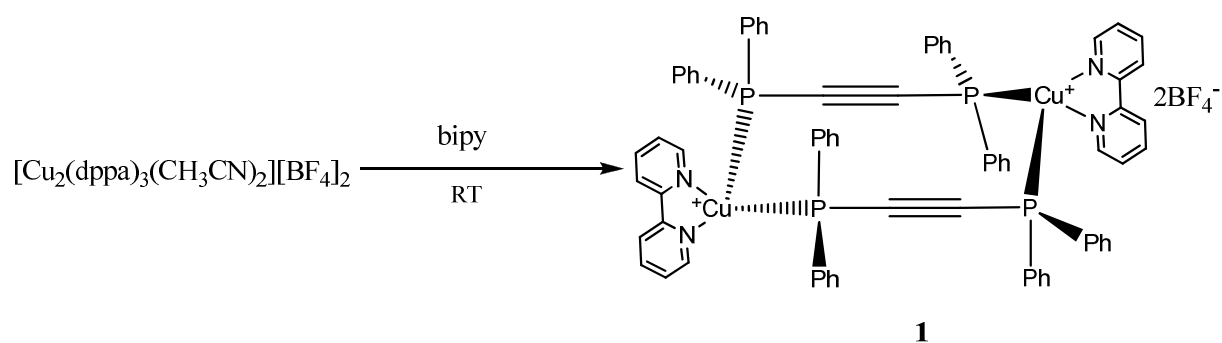
Bis(diphenylphosphino)acetylene is a potentially trifunctional ligand, where the two phosphorus centers are normally coordinated to metals in advance of the acetylene group due to stronger net donor capability of the phosphine ligand compared with alkyne [89]. However, the rigidity of the linear C≡C backbone constrains the dppa ligand to bridge between metal centers, forming either dimeric or polymeric coordination compounds [90–94]. We present the syntheses and characterization of binuclear Cu(I) diimine complexes bridged by two dppa ligands.

2.1 Synthesis

A following general procedure was followed for the synthesis of compounds (1-8). $[\text{Cu}_2(\text{dppa})_3(\text{CH}_3\text{CN})_2][\text{BF}_4]_2$ (0.015 mmol) (Precursor-A), prepared by the method of Y.-C.Liu et al [72] and diimine (0.038 mmol) were placed in an oven dried 100 ml Schlenk flask in glove box, sealed with rubber septum and taken out. Freshly distilled, dried dichloromethane (10.0 ml) was injected through the septum using a long needle. The mixture was stirred at room temperature for 8h to result in a clear yellow solution. The resultant solution was filtered and the filtrate carefully layered with 20 ml of diethyl ether to afford yellow color binuclear product.

2.1.1 $[\text{Cu}_2(\text{dppa})_2(\text{bipy})_2][\text{BF}_4]_2$ (1)

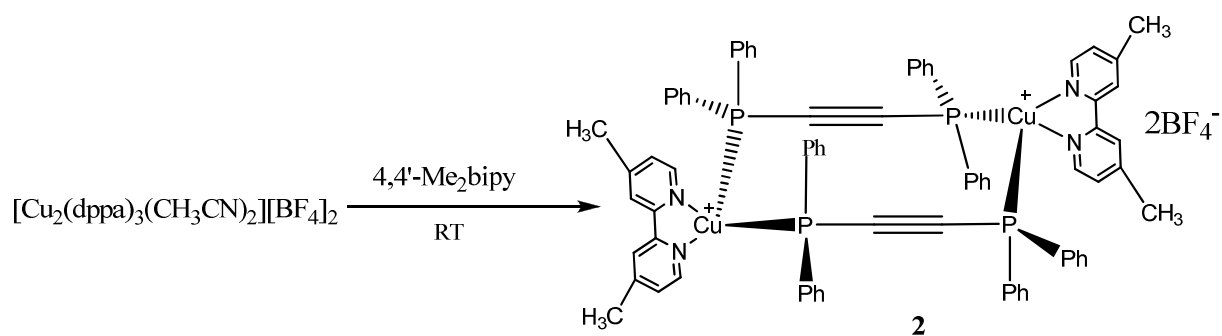
The compound was obtained as yellow crystalline material. Yield, 90%



Scheme 2.1

2.1.2 $[\text{Cu}_2(\text{dppa})_2(4,4'\text{-Me}_2\text{bipy})_2][\text{BF}_4]_2$ (**2**)

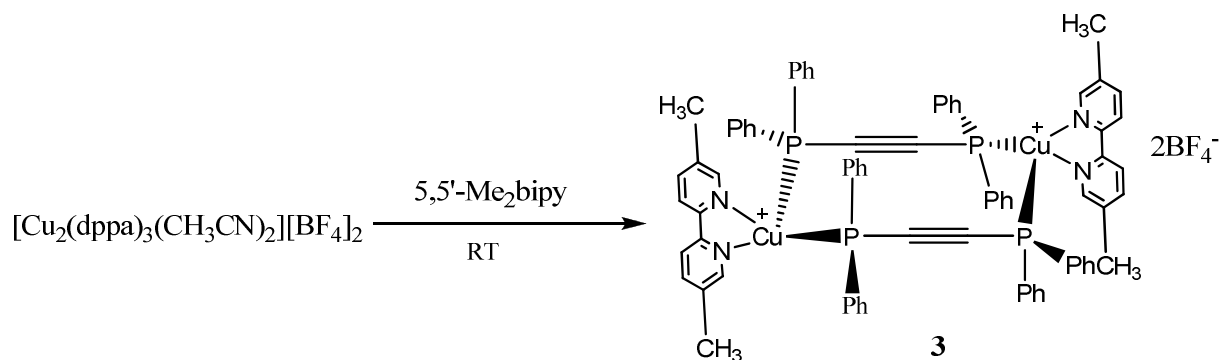
The compound was obtained as yellow crystalline material. Yield, 96%.



Scheme 2.2

2.1.3 $[\text{Cu}_2(\text{dppa})_2(5,5'\text{-Me}_2\text{bipy})_2][\text{BF}_4]_2$ (**3**)

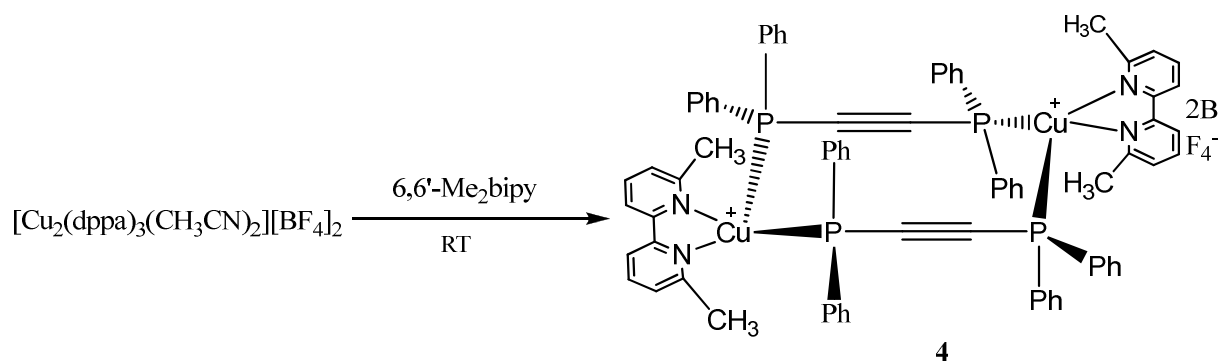
The compound was obtained as yellow crystalline material. Yield, 93%.



Scheme 2.3

2.1.4 $[\text{Cu}_2(\text{dppa})_2(6,6'\text{-Me}_2\text{bipy})_2][\text{BF}_4]_2$ (4)

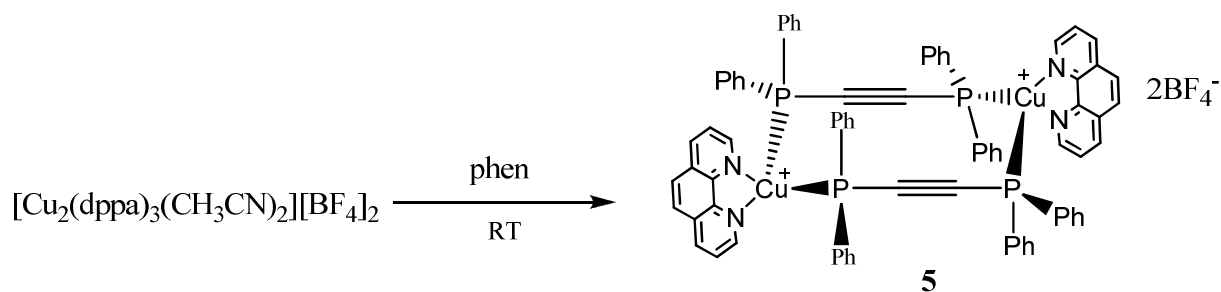
The compound was obtained as yellow crystalline material. Yield, 98%.



Scheme 2.4

2.1.5 $[\text{Cu}_2(\text{dppa})_2(\text{phen})_2][\text{BF}_4]_2$ (5)

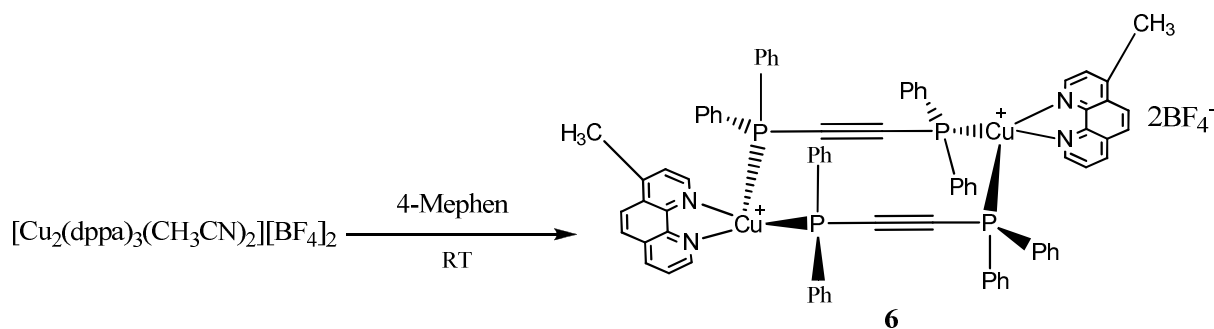
The compound was obtained as yellow crystalline material. Yield, 90 %



Scheme 2.5

2.1.6 $[\text{Cu}_2(\text{dppa})_2(4\text{-Mephen})_2][\text{BF}_4]_2$ (6)

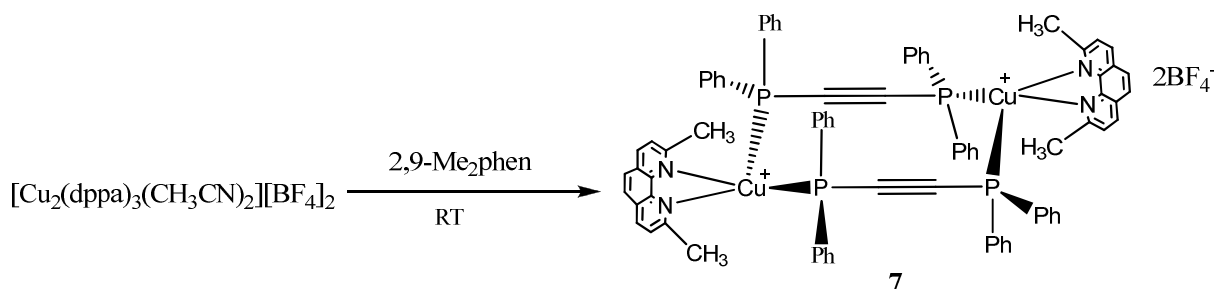
The compound was obtained as yellow crystalline material Yield, 89%.



Scheme 2.6

2.1.7 $[\text{Cu}_2(\text{dppa})_2(2,9\text{-Me}_2\text{phen})_2][\text{BF}_4]_2$ (7)

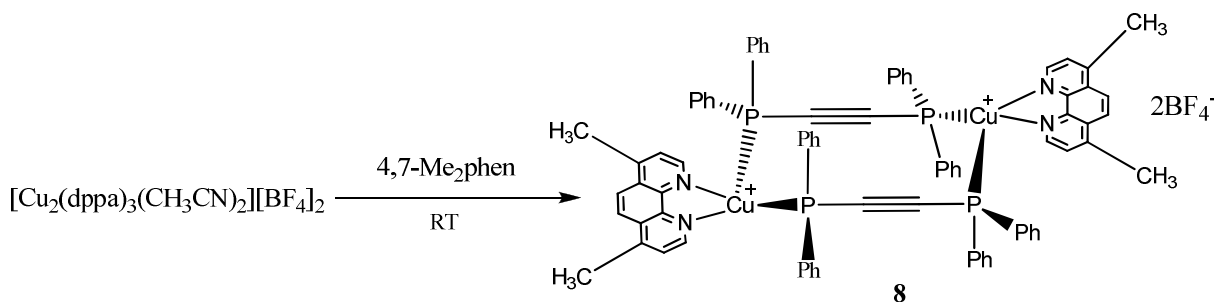
The compound was obtained as yellow crystalline material Yield, 85 %.



Scheme 2.7

2.1.8 $[\text{Cu}_2(\text{dppa})_2(4,7\text{-Me}_2\text{phen})_2][\text{BF}_4]_2$ (8)

The compound was obtained as yellow crystalline material Yield, 80%.



Scheme 2.8

2.2 Characterization of the complexes 1-8

2.2.1 Elemental Analysis and Melting points

Elemental analysis was performed on Perkin Elmer EA 3000 CHNS/O Elemental Analyzer. Melting Points were measured using Buchi 510 Melting Point apparatus. The samples were dried prior to analysis. The results of the complexes are given in table 1.

Table 1. Results of Elemental Analysis and Melting Points of Complexes 1-8

Complex	C %	H %	N %	MP ($^{\circ}$ C)
1	Calc: 61.32	4.16	4.13	215-218
	Found: 61.40	4.17	3.80	
2	61.35	4.54	3.97	237-238
	61.59	4.82	3.85	
3	61.35	4.54	3.97	242-243
	61.61	4.38	3.91	
4	61.35	4.54	3.97	234-235
	61.55	4.30	3.89	
5	61.70	3.99	3.99	232-233
	61.75	3.69	3.97	
6	62.22	4.06	3.92	212-214
	62.51	4.30	3.65	

7	63.30	4.35	4.00	235-237
	63.10	4.17	3.71	
8	62.60	4.39	3.84	218-220
	62.65	3.69	3.75	

2.2.2 Ultraviolet and Visible Spectroscopy

The UV-Vis spectra of the complexes were recorded in dichloromethane.

2.2.2.1 Electronic Spectra of Ligands

Electronic spectra of bipyridyls and phenanthrolines ligands used were recorded in dichloromethane.

Table 2. Results of Ultraviolet and Visible Spectroscopy for free Diimines

Compound	Conc. M	$\lambda_{nm}(\epsilon_{molar} \times 10^{-3})$
bipy	5.32×10^{-5}	283.0s (14.1×10^3)
4,4'-Me ₂ bipy	4.06×10^{-5}	281.5s(16.57×10^3), 295.0sh(9.8×10^3)
5,5'-Me ₂ bipy	4.52×10^{-5}	289.5s(19.58×10^3), 310.0sh(6.85×10^3), 320.0 (0.77×10^3)
6,6'-Me ₂ bipy	1.26×10^{-4}	291.5s(15.96×10^3), 303.5sh(9.47×10^3)
phen	1.01×10^{-4}	264.5s(17.89×10^3) , 278.5sh(8.67×10^3) , 322.0 (0.297×10^3)
4-Mephen	3.86×10^{-5}	265.0s(16.11×10^3), 278.5sh(8.67×10^3), 299.0sh(3.50×10^3)

2,9-Me ₂ phen	4.60×10^{-5}	270.0s(43.47×10^3), 312.5sh(2.47×10^3), 329.5sh(1.60×10^3)
4,7-Me ₂ phen	5.0×10^{-5}	265.0s(25.52×10^3), 303.0sh(4.84×10^3), 323.0br(1.0×10^3)

Wavelength (λ_{\max}) is in nanometer (nm) and molar extinction coefficient

ϵ_{molar} ($\text{M}^{-1} \text{cm}^{-1}$) is given in parenthesis. (s = sharp, sh = shoulder, br = broad)

The UV portion of the spectra is characterized by the intense bands typical of the π - π^* transitions of the diimine ligands. The molar absorption coefficients (ϵ_{molar}) are of the order of 0.297×10^3 to $43.47 \times 10^3 \text{ M}^{-1} \text{cm}^{-1}$.

2.2.2.2 Electronic Spectra of Complexes

The absorption data of complexes (1-8) are given in table 2. The absorption maxima are listed for all energy bands. The representative spectrum of complex 2 is given in figure 1 below. UV-Vis spectra are given in Appendix A-II.

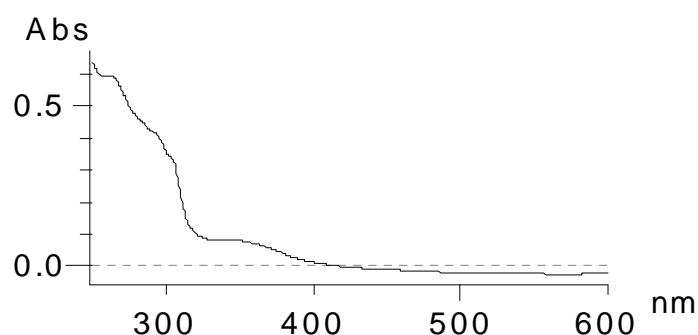


Figure 1. UV-Visible Spectrum of Complex 2

Table 3. Results of Ultraviolet and Visible Spectroscopy of Complexes 1-8

Compound	Conc. M	$\lambda_{nm}(\epsilon_{molar} \times 10^{-3})$
1	1.27×10^{-4}	277.5sh(8.2), 266.5sh(6.92), 293.5sh(8.6), 286.5sh(7.8) 360.0br
2	3.03×10^{-5}	265.0s(30.99), 284.0s(23.99), 293.5s(21.75)
3	1.507×10^{-4}	278.5s(2.74), 287.0s(2.80), 545.5br(0.06)
4	1.64×10^{-4}	277.5s (6.34), 286.5 (6.09), 432.5br (0.18), 450.5br (0.30), 517.0br (0.04)
5	1.347×10^{-4}	277.5s (4.51), 286.5s, 294.5s(3.34), 360.0(0.90), 550.0br (0.05)
6	3.86×10^{-5}	272.0(36.0), 298.0(10.5)
7	4.60×10^{-5}	272.0s(72.552), 292.0s(25.93), 295.5s(23.48), 364.0(1.61), 383.5(1.04)
8	5.0×10^{-5}	361.5br(10.3)

Wavelength (λ_{max}) is in nanometer (nm) and molar extinction coefficient ϵ_{molar} ($\text{M}^{-1} \text{cm}^{-1} \times 10^3$) is given in parenthesis. (s = sharp, sh = shoulder, br = broad)

In UV region intense ligand-centred (LC) bands typical of the π - π^* transitions of the phenanthroline and bipyridyl ligands are observed for all complexes. The Visible part of the spectrum consists of weak absorption bands which arise from metal-to-ligand charge-transfer (MLCT) electronic transitions. These occur at low energy because the Cu^+ ion can be easily oxidized and the phen-type ligands possess low energy empty π^* orbitals. Direct evidence of the localized nature of the lowest-lying MLCT state of Cu(I)–diimine was achieved by Gordon and McGarvey *via* resonance raman experiment [95–96]. Substituted bipyridyls and phenanthrolines exhibit more intense absorption maxima than those of unsubstituted ones. In addition the methyl substitution at 6,6' and 2,9 positions strongly enhances the absorption [48].

2.2.3 Emission Spectroscopy

2.2.3.1 Emission study of diimines

Excitation and emission spectra of free diimines and coordination complexes were recorded in dichloromethane. A representative spectrum of 2,2'-bipyridyl is given below in figure 2. Excitation and emission spectra of all other compounds are given in Appendix-III

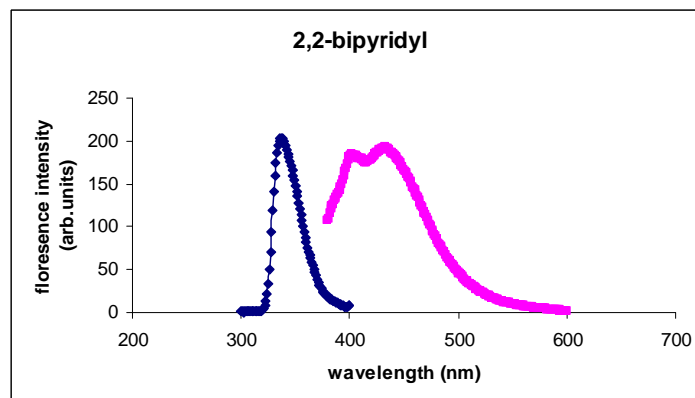


Figure 2. Excitation and Emission Spectra of 2,2'-bipyridyl

Table 4. Excitation and Emission Wavelengths of free Diimines

Diimines	λ_{ex}	λ_{em}
bipy	381	412
4,4'-Me ₂ bipy	340	381
5,5'-Me ₂ bipy	340	365
6,6'-Me ₂ bipy	340	362
phen	340	413
4-Mephen	340	410

2.2.3.2 Excitation and emission study of complexes

These studies were carried out in dichloromethane. The results are given in table 5.

Free diimines display emission maxima are in the range of 380 to 470 nm. In the complexes (1-6) it is observed that upon excitation in the UV region emission is

observed in the Visible region. The visible luminescence from Cu(I)–diimine arises in most of the cases from two MLCT excited states in thermal equilibrium, *i.e.* a singlet ($^1\text{MLCT}$) and a triplet ($^3\text{MLCT}$) [5]. The energy gap between these states is about 1500–2000 cm^{-1} and, at room temperature, the population of the lower lying $^3\text{MLCT}$ level largely exceeds that of $^1\text{MLCT}$, though the minority $^1\text{MLCT}$ excited molecules are responsible for most of the observed room temperature luminescence. Upon light excitation the lowest $^3\text{MLCT}$ excited state is populated, thus the metal centre changes its formal oxidation state from Cu(I) to Cu(II); the latter tends to assume a more flattened coordination geometry. In this ‘open’ structure a fifth coordination site is made available for the newly formed d^9 ion, that can be attacked by nucleophilic species such as solvent molecules and counterions, leading to pentacoordinated excited complexes (exciplexes), that deactivate *via* non-emissive deactivation paths. Direct spectroscopic evidence for these exciplexes is still lacking, however convincing clues for their formation have been given by McMillin *et al* [43].

Table 5. Excitation and Emission Wavelengths of Complexes 1-6

Complex	λ_{ex}	λ_{em}
1	290	340
2	290	340
3	290	340
4	290	340
5	290	340
6	340	417

2.2.4 Fourier-Transformed Infrared Spectroscopy (FT-IR)

The FT-IR spectra were recorded using KBr pellets in the range of 4000-400 cm^{-1} . The assignment of the different vibrations was carried out by comparison with literature data [97-99]. The absorption wavenumbers are presented in table 6 and a representative spectrum of the precursor-A is given in figure 3. FT-IR spectra are listed in Appendix-IV

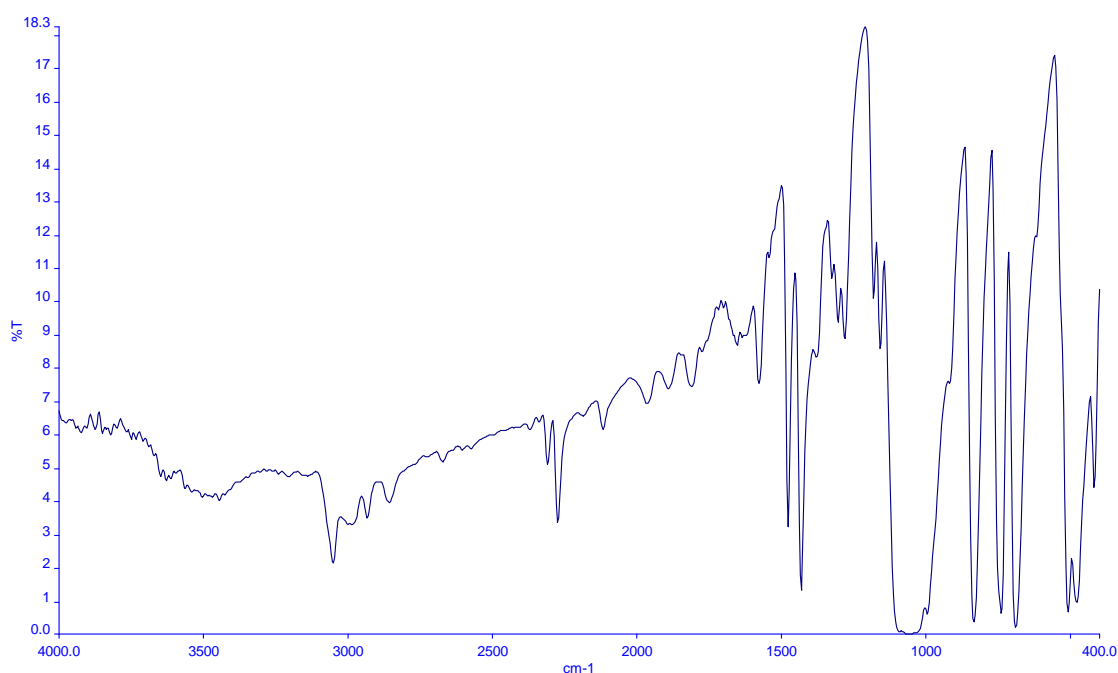


Figure 3. FT-IR Spectrum of Precursor-A

Table 6. Infrared Frequencies (cm^{-1}) and assignment for Complexes 1-8

Assignment	1	2	3	4	5	6	7	8
C-H stretch aromatics	3053s	3054s	3048s	3051s	3418br	3612 w	3423br	3042m
C-H stretch alkanes	2922	2922s	2922	2922	2926 w	2923 w	2918w	2922s

C-H bend		1610m	1664s				1620	
CH ₃ deformation		1593m	1576m	1596m		1512	1502 s	1574w,
CH in plane bend aromatic ring	1435.3 s,	1434	1435m	1435m		1043vs	1434s	1432s
CH ring stretch + bend	1055.6 w	1054m	1055m	1057m	1099s	1043vs	1059 vs	1055vs
C-H OOP bend aromatic ring	831.8s	828s	830s	825s	839s	826vs	862w	833s
CH OOP bend	751m	749m	748m	782m	742s	682s	742w	745s
Ring bend	694s	694s	694s	694s	692s	682s	694s	693s
Ring bend	512s	513s	513m	515m	511m	512w	512m	511s
Inter ring bend	476m	476m	480w	477w	489w	480w	485m	478m

All complexes show a strong absorption from 1043-1059 cm⁻¹ and 826-839 cm⁻¹ attributed to C-H in plane bending of the aromatic ring and C-H out of plane bending of the aromatic ring. Shift of 20 cm⁻¹ from 1039-1059 cm⁻¹ and 18 cm⁻¹ from 821-839 cm⁻¹ is attributed to complexation of diimines. These shifts are attributed to the change in

electron density in the pyridines and phenanthroline ring when the non bonding pair of electrons on the nitrogen atom is donated to the metal ion [9] The aromatic C=C stretching are found in the range of $1410\text{-}1640\text{ cm}^{-1}$. Raman study was carried out for symmetrically substituted C \equiv C bonds

2.2.5 Raman Spectroscopy

Raman spectra were recorded for the solid samples. The spectra are given in Appendix A-V. Typically 128 scans were used for spectra collection. They are presented in table 7 and a representative spectrum of bis(diphenylphosphino)acetylene is given in figure 4.

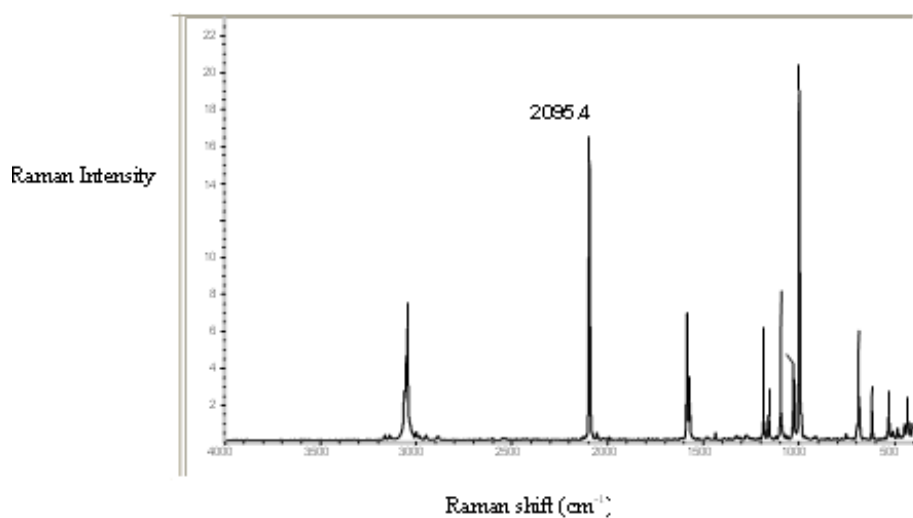
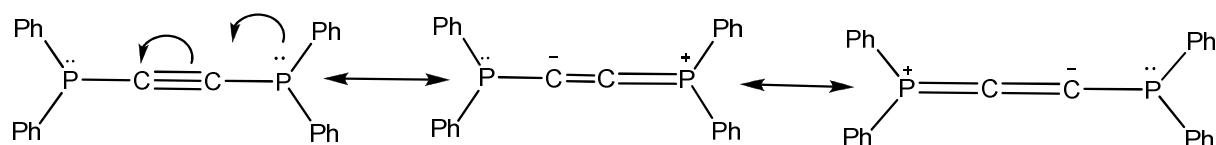


Figure 4. Raman Spectrum of bis(diphenylphosphino)acetylene

Table 7. Raman shifts for free Ligand and the Complexes

Complex	Raman Shift for —C≡C— (cm ⁻¹)	$\Delta v(\text{cm}^{-1}) = v_{\text{complex}} - v_{\text{dppa}}$
DPPA	2095.4	
Precursor-A	2116.0	20.6
1	2108.3	12.9
2	2107.1	11.7
3	2111.4	16
4	2111.4	16
5	2104.0	8.6
6	2109.0	13.5
7	2110.1	14.7
8	2115.1	19.7

$\nu(\text{C}\equiv\text{C})$ in dppa appears at 2095 cm^{-1} in Raman spectrum of free ligand(dppa) but is i.r. inactive both in free ligand and in complexes where the diphosphine is symmetrically bonded to 2 metal atoms via the phosphorus atoms only [63]. Raman spectra of complexes 1-8. Showed a $\nu(\text{C}\equiv\text{C})$ as an intense absorption from 2107 to 2115 cm^{-1} while in DPPA strong absorption was observed at 2095 cm^{-1} .



Considering the above resonance forms, the Shift upon coordination results from the bonding of phosphorous to the metal. Shift to higher wavenumber with in the series is due to strong pi-back donation from metal d-orbital to π^* of C-P bond of bis(diphenylphosphino)acetylene. The Raman shifts observed for $\text{C}\equiv\text{C}$ are in close agreement with the reported values [69] for complexes with the same coordination sphere.

2.2.6 Single Crystal X-ray Analysis

X-ray intensity data were recorded on a Bruker-Axs Smart Apex system equipped with a graphite monochromatized Mo $\text{K}\alpha$ radiation ($\lambda = 0.71073$). The data were corrected for Lorentz-polarization and absorption effects. Hydrogen atoms were included at calculated positions using a riding model [100]. The structures were solved with direct methods and refined by full matrix least square methods based on F^2 , using a structure determination and graphic package SHELXTL (version 5.10) [101]. The crystallographic data of complexes for which single crystals were successfully grown are given in tables-8 & 9 and selected bond lengths and bond angles are given in table 10 & 11 respectively.

Table 8. Crystallographic Data Collection and Structure Refinement Parameters for Complexes 2, 3 and 4

Complexes	2	3	4
Chemical Formula	$\text{C}_{72} \text{H}_{64} \text{B}_2 \text{Cu}_2 \text{F}_8 \text{N}_4 \text{P}_4$	$\text{C}_{72} \text{H}_{64} \text{B}_2 \text{Cu}_2 \text{F}_8 \text{N}_4 \text{P}_4$	$\text{C}_{72} \text{H}_{64} \text{B}_2 \text{Cu}_2 \text{F}_8 \text{N}_4 \text{P}_4$
Formula Mass , Da	1457.89	1457.89	1457.89

Space Group	$P2_1/c$	$P2_1/c$	$Pca2_1$
a, Å	12.0733(12)	12.2375(12)	16.870(2)
b, Å	12.9668(12)	12.4548(12)	17.3655(16)
c, Å	22.4245(12)	23.2815(12)	23.968(3)
α , deg	90	90	90
β , deg	91.8830(10)	93.6101(10)	90
γ , deg	90	90	90
V, Å ³	3508.7(5)	3541.4(5)	7021.6(15)
ρ_{calcd} , gcm ⁻³	1.380	1.367	1.457
Z	2	2	4
μ , mm ⁻¹	0.765	0.758	0.764
T, K	296(2)	296(2)	296(2)
λ , Å	0.71073	0.71073	0.71073
$R_1(Fo^2)^a$	0.0605	0.0497	0.0442
$WR_2(Fo^2)^b$	0.1368	0.1345	0.0907
GOF	1.145	1.021	1.052

$$^a R_1 = \Sigma(| | Fo| - | Fc| |) / \Sigma | Fo| \quad ^b WR_2 = [\Sigma(w | Fo|^2 - | Fc|^2) / \Sigma | Fo|^2]^{1/2}$$

Table 9. Selected Bond Lengths (Å) and Bond Angles (°) of Complexes 2-4

2	3	4
Cu1-N4 2.076(8)	Cu1-N2 2.043(2)	Cu1-N1 2.058(3)
Cu1-N3 2.126(8)	Cu1-N1 2.085(3)	Cu1-N2 2.086(3)
Cu1-P2 2.244(3)	Cu1-P2 2.2165(9)	Cu1-P1 2.2186(10)
Cu1-P3 2.274(4)	Cu1-P1 2.3035(9)	Cu1-P2 2.2900(10)
Cu2-N2 2.038(9)	N1-C1 1.336(4)	N1-C1 1.343(5)
Cu2-N1 2.051(9)	N1-C6 1.347(4)	N1-C6 1.356(5)
N1-Cu1-N2 79.67(12)	N2-Cu1-N1 80.60(10)	N4-Cu1-N3 78.4(4)
N1-Cu1-P1 129.49(9)	N2-Cu1-P2 134.39(7)	N4-Cu1-P2 115.0(3)
N2-Cu1-P1 113.52(9)	N1-Cu1-P2 117.02(7)	N3-Cu1-P2 117.9(3)
N1-Cu1-P2 98.98(9)	N2-Cu1-P1 98.67(7)	N4-Cu1-P3 112.2(3)
N2-Cu1-P2 98.55(9)	N1-Cu1-P1 99.60(7)	N3-Cu1-P3 112.8(3)
P1-Cu1-P2 124.49(4)	P2-Cu1-P1 117.20(3)	P2-Cu1-P3 115.31(12)

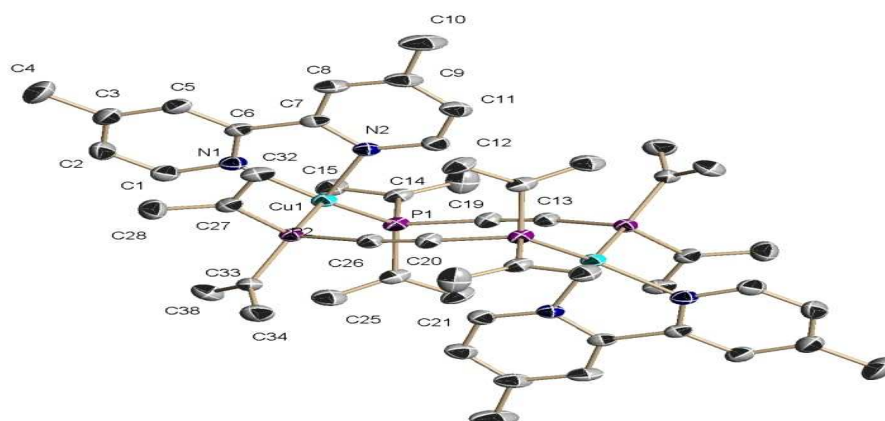


Figure 5. X-ray structure of Complex 2 showing thermal ellipsoids drawn at the 30 % probability level. Hydrogen atoms and BF_4^- anions are omitted for clarity. Only ipso carbons of C_6H_5 group are shown for clarity

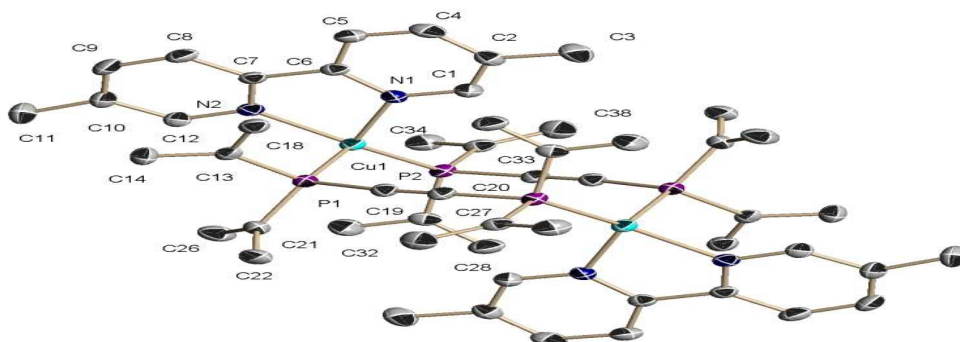


Figure 6. X-ray structure of Complex 3 showing thermal ellipsoids drawn at the 30 % probability level. Hydrogen atoms and BF_4^- anions are omitted for clarity. Only the ipso carbons of C_6H_5 groups are shown for clarity

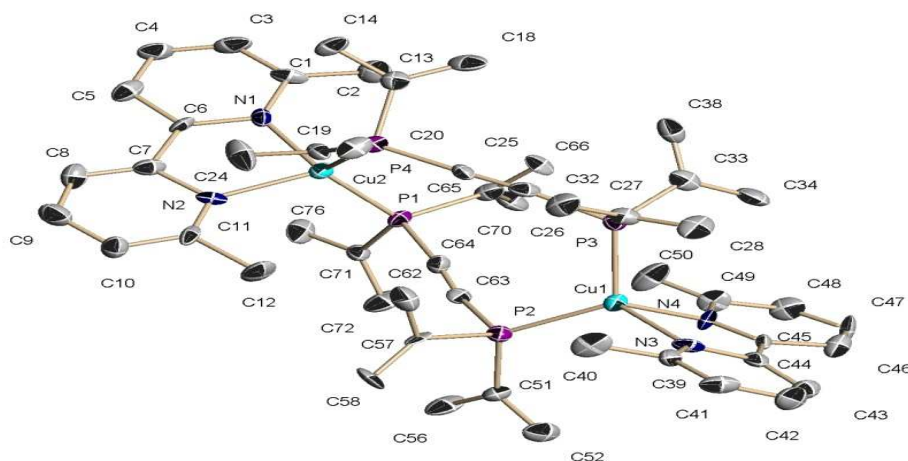


Figure 7. X-ray structure of Complex 4 showing thermal ellipsoids drawn at the 30 % probability level. Hydrogen atoms and BF_4^- anions are omitted for clarity. Only the ipso carbons of C_6H_5 groups are shown for clarity

The molecular structure of complexes 2, 3 and 4 are shown in figures 5-7. In complex 1 and 2 there is a crystallographic center of symmetry imposed on the molecule. In these three complexes $\text{Cu}_2(\text{dppa})_2$ moiety can be considered as a 10-membered chair like dimetallacycle. The chair conformation is twisted in complex 3 possibly due to steric hindrance of bipyridyl rings substituted at 6 position. Each Cu(I) atom is chelated by a bipy ligand, and the two Cu(bipy) groups are bridged by two dppa ligands. The Cu^+ ion adopts a distorted tetrahedral coordination, with the bond angles ranging from $79.67(12)^\circ$ to $82.2(3)^\circ$ for N-Cu-N bite and for P-Cu-N link the angles are between $98.67(7)^\circ$ to $117.9(3)^\circ$.

The P-Cu-P angles range from $115.31(12)^\circ$ to $124.49(4)^\circ$ significantly greater than the idealized bond angle of 109.5° . Likely due to repulsion between the phenyl and methyl groups in the complexes 2, 3 and 4 which adopt distorted tetrahedral geometry

P1,P2,C19,C20 in complex 2 , P1,P2,C19 and P4,P1 C25 ,C64 atoms are coplanar to within .01 Å⁰ P-Cu-P 124.49(4) ,117.20(3) and 115.31(12) makes a dihedral angle with P1-P2-C12-C25 plane and the N-Cu-N plane respectively. And the P-C=C are bowed from idealized 180⁰.

Table 10. Crystallographic Data Collection and Structure Refinement Parameters for Complexes 5, 7 and 8.

Complexes	5	7	8
Chemical Formula	C ₇₂ H ₅₆ B ₂ Cu ₂ F ₈ N ₄ P ₄	C ₇₇ H ₆₆ B ₂ Cu ₂ F ₄ N ₄ P ₄ F ₈ Cl ₂	C ₇₆ H ₆₄ B ₂ Cu ₂ F ₈ N ₄ P ₄
Formula Mass , Da	1457.89	717.03	1457.89
Space Group	P2 ₁ /c	P-1	P2 ₁ /c
a, Å	13.0674(12)	11.4859(18)	12.8260(12)
b, Å	12.3143(12)	12.8142(19)	13.1353(12)
c, Å	21.4167(12)	15.406(2)	20.9568(12)
α, deg	90.00	105.223(3)	90.00
β, deg	91.3213(10)	101.469(4)	90.5883(10)
γ, deg	90.00	108.022(3)	90.00
V, Å ³	3445.4(5)	1981.3(5)	3530.5(5)
ρ _{calcd} , gcm ⁻³	1.405	1.501	1.371

Z	2	2	2
μ , mm ⁻¹	0.779	0.638	0.760
T, K	296(2)	298(2)	296(2)
λ , Å	0.71073	0.71073	0.71073
$R_1(F\sigma^2)^a$	0.0506	0.0608	0.0518
$WR_2(F\sigma^2)^b$	0.1467	0.1365	0.1432
GOF	1.019	1.164	1.058

$$^aR_1 = \Sigma(| | Fo| - | Fc| | / \Sigma | Fo| . ^bWR_2 = [\Sigma(w | Fo|^2 - | Fc|^2) / \Sigma | Fo|^2]^{1/2}$$

Table 11. Selected Bond Lengths (Å) and Bond Angles (°) of the complexes 5, 7 and 8

5	7	8
Cu1-N1 2.043 (5)	Cu1-N3 2.102(16)	Cu1-N2 2.053(3)
Cu1-P2 2.2100 (16)	Cu1-N4 2.105(13)	Cu1-N1 2.073(3)
Cu1-P3 2.2867 (19)	Cu1-P5 2.211(5)	Cu1-P2 2.2091(9)
N3- Cu1-N4 80.6(5)	N2- Cu1-N1 81.88(11)	N1-Cu1-N2 80.8(2)
N3-Cu1-P5 122.3(4)	N2-Cu1-P2 134.37(8)	N1-Cu1-P2 129.60(16)
N4-Cu1-P5 120.2(4)	N1- Cu1-P2 117.28(8)	N2-Cu1-P2 112.58(17)
N3-Cu1-P3 107.8(4)	N2- Cu1- P1 98.99(8)	N1-Cu1-P3 100.16(16)
N4-Cu1-P3 99.5(4)	N1-Cu1-P1 100.44(8)	N2-Cu1-P3 97.46(17)
P5-Cu1-P3 118.71(18)	P2-Cu1-P1 115.62(3)	P2-Cu1-P3 123.94(7)

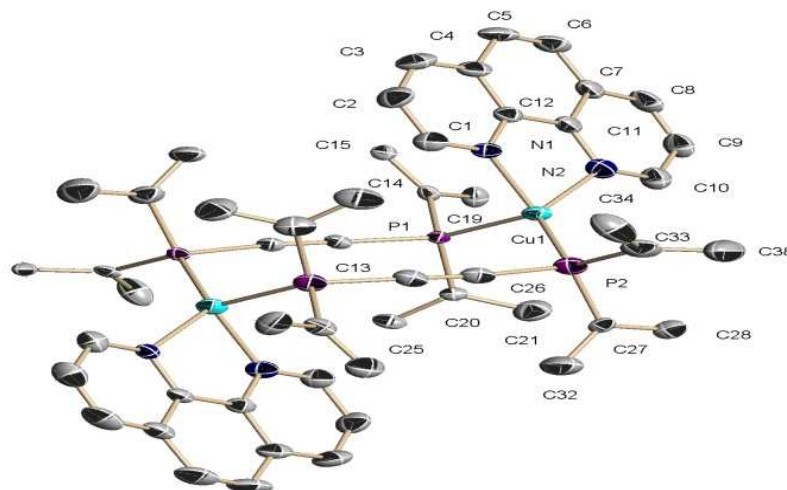


Figure 8. X-ray structure of Complex 5 showing thermal ellipsoids drawn at the 30 % probability level. Hydrogen atoms and BF_4^- anions are omitted for clarity. Only the ipso carbons of C_6H_5 groups are shown for clarity

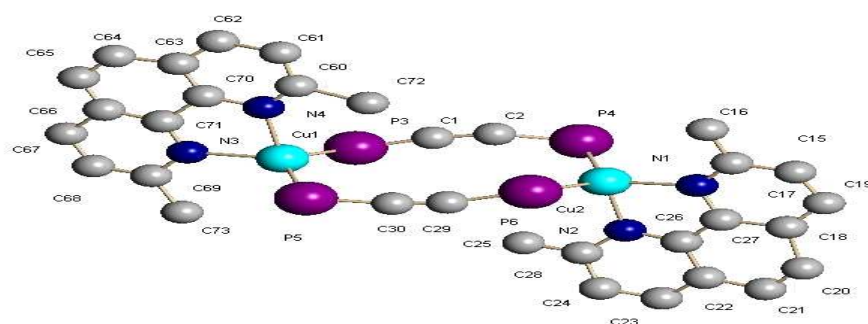


Figure 9. X-ray structure of Complex 7 showing spheres drawn at the 30 % probability level. Hydrogen atoms, phenyl rings of dppe bridge and BF_4^- anions are omitted for clarity. Only the ipso carbons of C_6H_5 groups are shown for clarity.

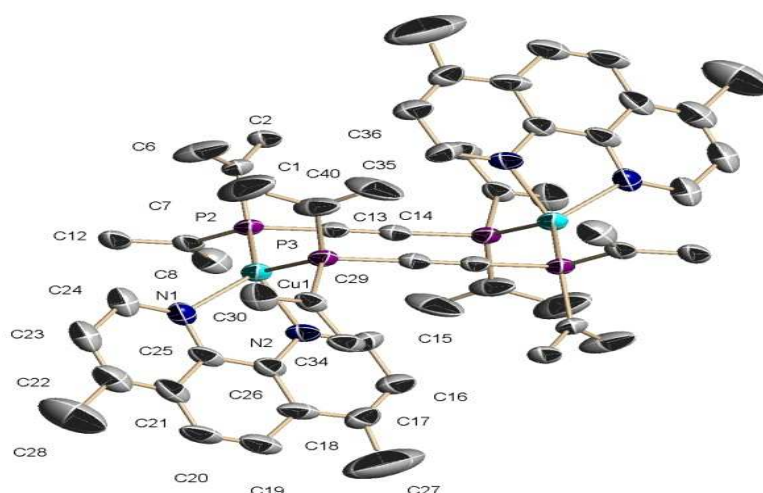


Figure 10. X-ray structure of Complex 8 showing thermal ellipsoid drawn at the 30 % probability level. Hydrogen atoms and BF_4^- anions are omitted for clarity. Only the ipso carbons of C_6H_5 groups are shown for clarity

The molecular structure of complexes 5, 7 and 8 are shown in figures 8-10. Similarly to their bipy analogs the three complexes are centrosymmetric. $\text{Cu}_2(\text{dppa})_2$ moiety can be considered as a 10-membered chair like dimetallacycle. The chair conformation is twisted in complex 7; possibly due to steric hindrance of phenanthroline rings substituted at 2,9 positions. Each Cu(I) atom is chelated by a phen ligand, and the two Cu(phen) groups are bridged by two dppa ligands. The Cu^+ ion adopts a distorted tetrahedral coordination, with the bond angles ranging from $80.6(5)^\circ$ to $81.88(11)^\circ$ for N-Cu-N bite and for P-Cu-N link the angles are between $98.99(7)^\circ$ to $112.58(17)^\circ$.

The bond distances between copper and phenanthroline nitrogen are in the range $2.043(5)$ to $2.073(3)^\circ\text{\AA}$. In complex 7 which has two methyl groups at 2,9 positions on the phenanthroline ring, has relatively large Cu-N distances, in the range $2.102(1)$ to

2.105(13) $^{\circ}$ A. The P-Cu-P angles range from 115.62(3) $^{\circ}$ to 123.94(4) $^{\circ}$ significantly greater than the idealized bond angle of 109.5 $^{\circ}$.

2.2.7 Nuclear Magnetic Resonance Spectroscopy

^1H NMR and ^{31}P spectra were recorded for free ligands and binuclear Cu(I) complexes in (CD_2Cl_2 or DMSO-d_6). Representative ^1H -NMR and ^{31}P -NMR spectra of complex 5 are given in figures 11 & 12. NMR spectra are given in appendix-VI & VII. NMR data is summarized in table 12.

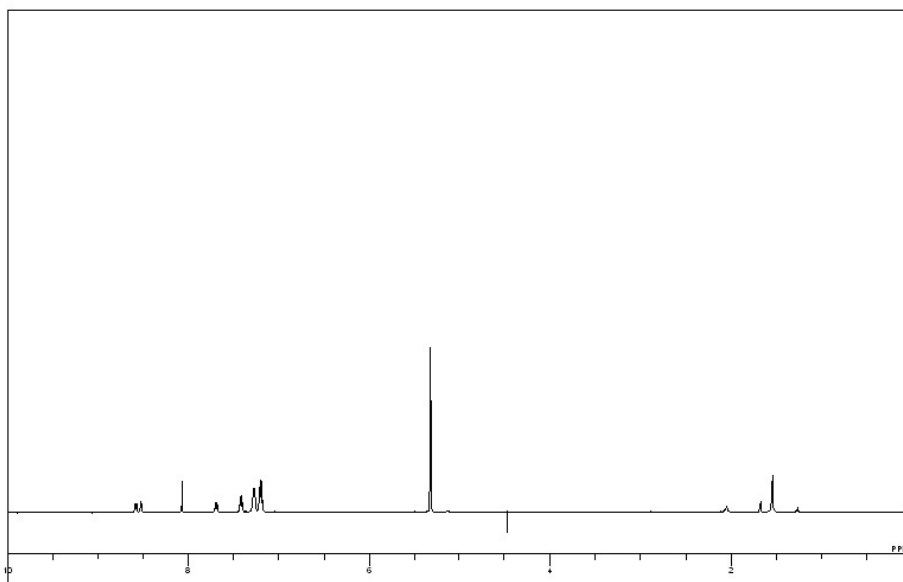


Figure 11. ^1H -NMR Spectrum of Complex 5

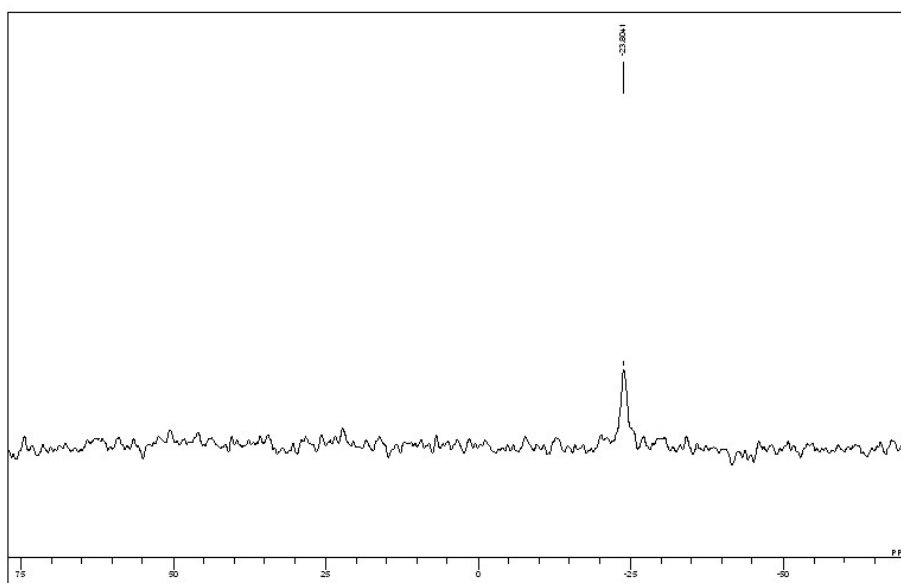


Figure 12. ^{31}P -NMR Spectrum of Complex 5

Table 12. ^1H NMR shifts for free Diimines

Free Ligand	H^1 -NMR shifts $\delta(\text{PPM})$
dppa	7.41 (d), 7.57-7.58 (m)
bipy	7.42(s), 7.92(s), 8.29(s), 8.62(s)
4,4'-Me ₂ bipy	2.07(s), 2.37(t), 2.48(s), 2.51(s), 7.26 (d) , 8.21 (t) , 8.51 (d),
5,5'-Me ₂ bipy	2.07(s), 2.20(s), 2.27(s), 2.33(s), 2.48(s), 2.49(s), 7.72(d) , 8.23 (d) , 8.47 (s),
6,6'-Me ₂ bipy	1.10(s), 2.44(s), 3.01(s), 7.22(s) , 7.74(s) , 8.11(s)

phen	7.23(d), 7.29 (s), 7.40(d), 7.75(s), 8.18(s) , 8.75(s)
4-Mephen	2.67(s), 2.80(s), 2.93(s), 7.65(d), 7.80(q), 8.15(dd), 8.52(d), 8.98(d), 9.14(d)
2,9-Me ₂ phen	2.48(s),2.76(s), 3.47(s), 7.59(d), 7.83(s), 8.31(d)
4,7-Me ₂ phen	2.72(s), 7.56(s), 8.06(s), 8.98(s)

Table 13. ¹H and ³¹P NMR Shifts for Complexes 1- 8

Compound	¹ H-NMR shifts δ(PPM)	³¹ P-NMR δ(PPM)	³¹ P δ(PPM)
DPPA	2.61(s,CH ₃ CN), 7.43-7.11(m, ph)	-33.52	
1	1.18(s), 1.47(s), 6.96 (t), 7.42- 7.23 (m) , 7.47-7.61 (m) , 8.01 (t) , 8.05(d) 8.29 (d)	-24.75(DMSO- <i>d</i> 6)	1.95
2	0.79(s), 1.18(s), 1.46(s), 1.59(s), 2.45(s), 7.02 , 7.19-7.30 , 7.44, 7.71, 7.86 , 8.24	-24.98(DMSO- <i>d</i> 6)	1.72
3	7.02, 7.19-7.30, 7.44, 7.71, 7.86, 8.24	-24.90(Cd ₂ Cl ₂)	1.8
4	1.54(d), 1.89(d), 2.23(s), 7.20- 7.31(m) , 7.44 (t) , 7.99 (t) , 8.06 (t) , 8.17 (d) , 8.32 (d)	-31.21(Cd ₂ Cl ₂)	-4.51

5	2.48(s), 7.23 (t), 7.29 (d) , 7.40 (t) , 7.75 (s) , , 8.17 (s) , 8.77(t)	-23.80(DMSO- <i>d</i> 6)	2.18
7	7.22(s,br),7.42(t),7.73(s), 7.75(d), 7.94(d), 8.73(d),8.21(d)	-33.51(DMSO- <i>d</i> 6)	-6.81
8	2.83(s),7.29(d),7.40(s),7.56(s), 8.26(s), 8.65(s)	-24.12(DMSO- <i>d</i> 6)	2.58

** Relative to 85% H₃PO₄ as an external standard.

*** $\Delta\delta(\text{PPM}) = \delta_{\text{complex}} - \delta_{\text{precursor}}$

³¹P NMR gave one broad signal for all complexes (1-8). Chemical shifts are in the range of -24.12 to -33.51 ppm. $\Delta\delta^{31}\text{P}$ of + 2.23 to -6.81 ppm is observed for complexes 1-8 with reference to the precursor. Complexes 4 and 7 show highly shielded phosphorous (-33.21, -33.51) consistent with high sigma donation power of 6,6'-Me₂bipy and 2,9-Mephen ligands.

Chapter 3

Binuclear Copper(I) mixed ligand complexes with trans-1,2-bis(diphenylphosphino)ethylene (dppethy)

Trans-1,2-bis(diphenylphosphino)ethylene is a conjugated diphosphine bridging ligand with sp^2 carbon chains between the two phosphorus donors [102-104]. Like the conjugated C- or N-donor ligands, the rodlike P-donor spacers also exhibit characteristics such as rigidity, conjugation, and photostability, as well as having molecular orbitals with suitable energies to overlap with those of the attached metal centers. In the present chapter detailed synthesis and characterization of binuclear copper(I) mixed ligand complexes using dppethy is presented.

3.1 Synthesis of $[\text{Cu}_2(\text{dppethy})_3(\text{CH}_3\text{CN})_2][\text{BF}_4]_2$ Precursor-B

$[\text{Cu}(\text{CH}_3\text{CN})_4][\text{BF}_4]$ (85 mg, 0.027 mmol) and dppethy ligand (170 mg, 0.43 mmol) were placed in an oven dried oven dried 100 ml Schlenk flask in glove box, sealed with rubber septum and taken out. Freshly distilled, dried acetonitrile (20 ml) was injected through the septum using a long needle. The mixture was stirred at room temperature for 18h to result in a clear yellow solution. The solution was filtered and concentrated to 5.0 ml under vacuum. The filtrate was carefully layered with 20 ml of diethyl ether to afford white powder of $[\text{Cu}_2(\text{dppethy})_3(\text{CH}_3\text{CN})_2][\text{BF}_4]_2$ (90 %)



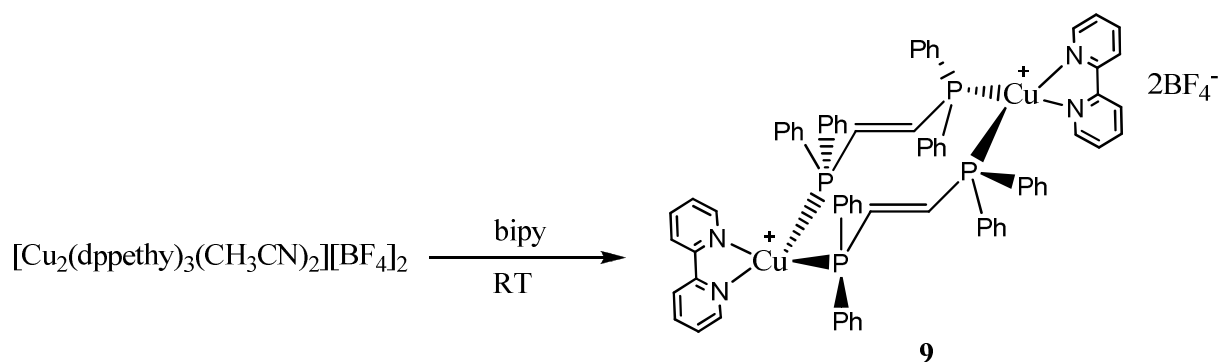
Scheme 3.1

3.1.1 Synthesis of binuclear complexes

A following general procedure was followed for the synthesis of compounds (9-16). $[\text{Cu}_2(\text{dppethy})_3(\text{CH}_3\text{CN})_2][\text{BF}_4]_2$ (0.015 mmol) (Precursor-B), and diimine (0.038 mmol) were placed in an oven dried 100 ml Schlenk flask in glove box, sealed with rubber septum and taken out. Freshly distilled, dried dichloromethane (10.0 ml) was injected through the septum using a long needle. The mixture was stirred at room temperature for 8h to result in a clear yellow solution. The resultant solution was filtered and the filtrate carefully layered with 20 ml of diethyl ether to afford yellow color binuclear product.

3.1.2 $[\text{Cu}_2(\text{dppethy})_2(\text{bipy})_2][\text{BF}_4]_2$ (9)

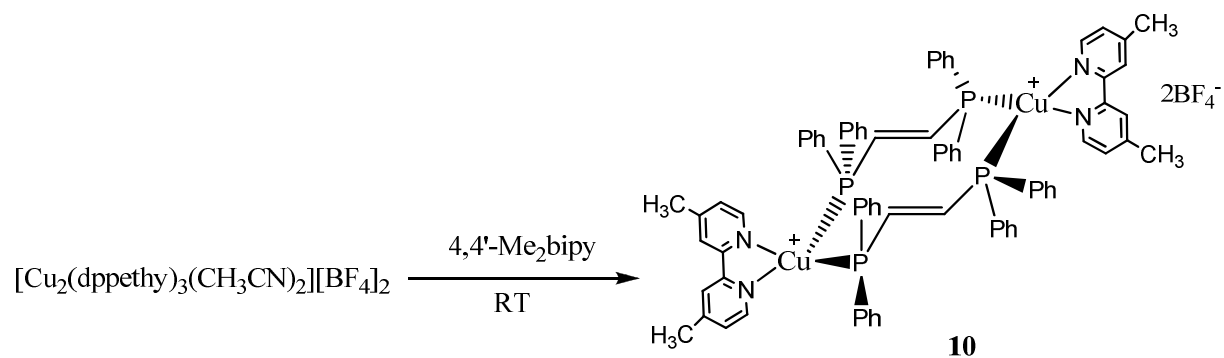
The compound was obtained as yellow crystalline material. Yield, 90%.



Scheme 3.2

3.1.3 $[\text{Cu}_2(\text{dppethy})_2(4,4'\text{-Me}_2\text{bipy})_2][\text{BF}_4]_2$ (10)

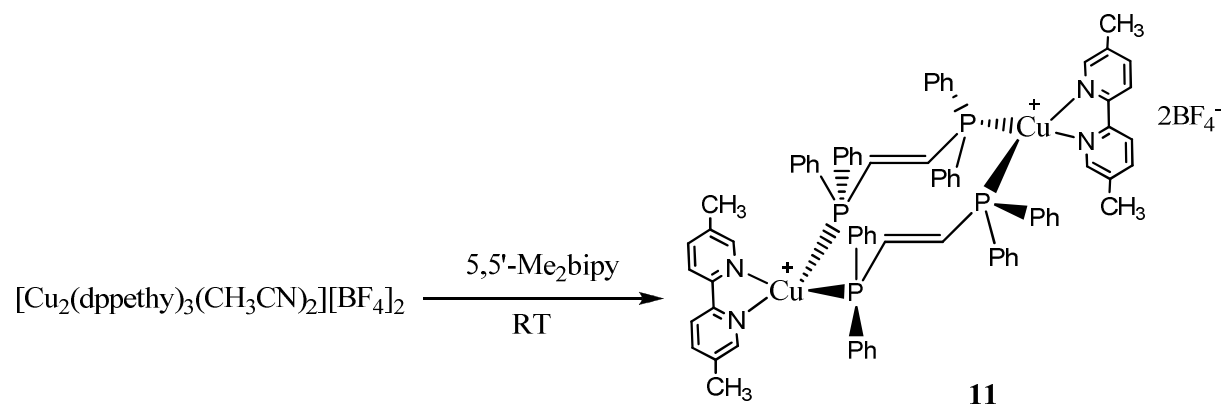
The compound was obtained as yellow crystalline material. Yield, 96%.



Scheme 3.3

3.1.4 $[\text{Cu}_2(\text{dppethy})_2(5,5'\text{-Me}_2\text{bipy})_2][\text{BF}_4]_2$ (11)

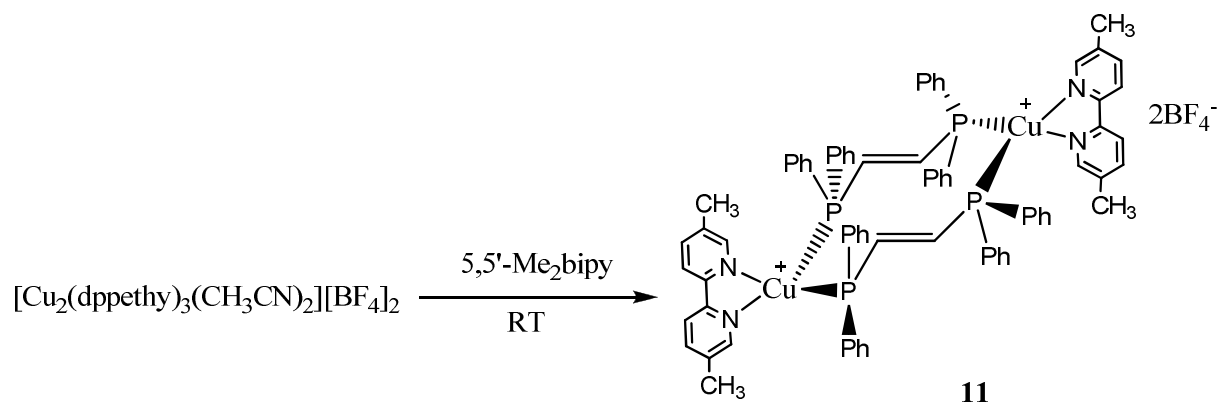
The compound was obtained as yellow crystalline material. Yield, 92%.



Scheme 3.4

3.1.5 $[\text{Cu}_2(\text{dppethy})_2(6,6'\text{-Me}_2\text{bipy})_2][\text{BF}_4]_2$ (12)

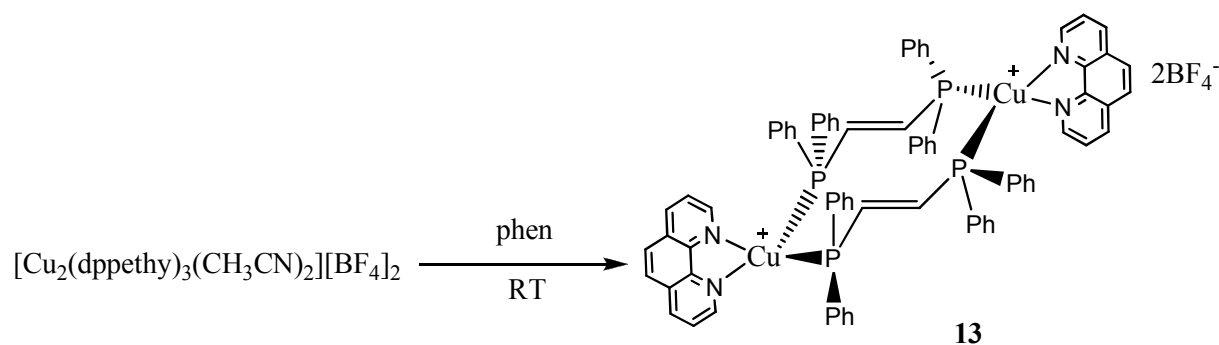
The compound was obtained as yellow crystalline material. Yield, 98%.



Scheme 3.5

3.1.6 $[\text{Cu}_2(\text{dppethy})_2(\text{phen})_2][\text{BF}_4]_2$ (**13**)

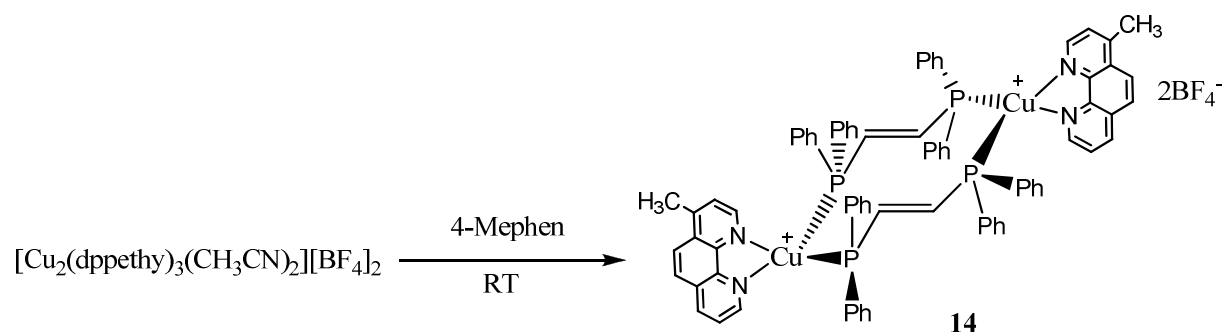
The compound was obtained as yellow crystalline material. Yield, 90 %.



Scheme 3.6

3.1.7 $[\text{Cu}_2(\text{dppethy})_2(4\text{-Mephen})_2][\text{BF}_4]_2$ (**14**)

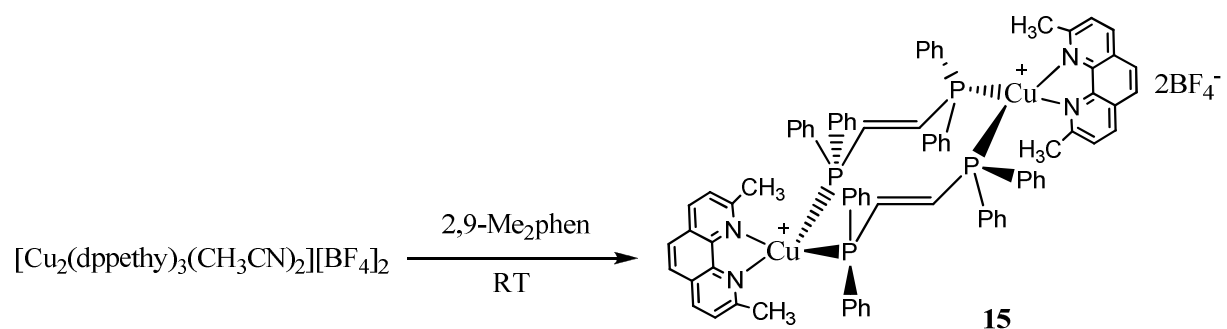
The compound was obtained as yellow crystalline material. Yield, 89 %.



Scheme 3.7

3.1.8 $[\text{Cu}_2(\text{dppethy})_2(2,9\text{-Me}_2\text{phen})_2][\text{BF}_4]_2$ (15)

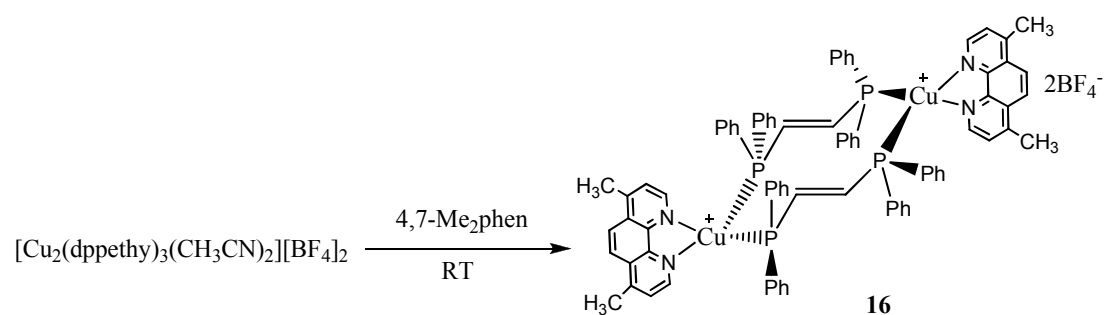
The compound was obtained as yellow crystalline material. Yield, 85%.



Scheme 3.8

3.1.9 $[\text{Cu}_2(\text{dppethy})_2(4,7\text{-Me}_2\text{phen})_2][\text{BF}_4]_2$ (16)

The compound was obtained as yellow crystalline material. Yield, 80 %.



Scheme 3.9

3.2 Characterization of Precursor-B and Complexes 9-16

3.2.1 Elemental Analysis

Elemental analysis was performed on Perkin Elmer EA 3000 CHNS/O Elemental Analyzer. Samples were dried prior to use.

Table 14. Results of Elemental Analysis and Melting Points of Precursor-B and complexes 9-16

Complex	C %	H %	N %
Precursor-B	Calc: 62.66	4.58	1.78
	Found: 62.82	4.79	2.09
9	61.53	4.26	3.98
	61.90	4.52	4.2
10	62.45	4.65	3.83
	62.72	4.87	4.1
11	62.45	4.65	3.83
	62.22	4.86	4
12	62.45	4.65	3.83
	62.25	4.52	3.61
13	62.17	4.19	3.92
	61.92	4.4	3.64
14	62.62	4.39	3.84
	62.35	4.17	3.82
15	63.05	4.57	3.77
	62.84	4.84	3.49
16	63.05	4.57	3.77
	63.3	4.29	3.82

3.2.2 Ultraviolet and Visible Spectroscopy

The UV-Vis spectra of the complexes were recorded in dichloromethane. The absorption data of precursor-B and complexes (9-16) is given in table 15. UV-Vis spectra are given in Appendix A-II.

Table 15. Results of Ultraviolet and Visible Spectroscopy for Precursor-B and Complexes 9-16

Compound	Conc. M	λ_{\max} ($\epsilon_{\text{molar}} \times 10^{-3}$)
Precursor-B	8.48×10^{-6}	277.5sh(30.88)
9	6.25×10^{-5}	276.5br(10.94), 284.5s(11.02), 308.0sh(7.02)
10	6.73×10^{-5}	265.5br(4.75), 273.5br(4.90), 287.0sh(4.80), 290.0br(4.72), 308.0sh(2.82)
11	8.21×10^{-5}	295.0br(2.47), 319.0sh(1.55)
12	1.52×10^{-5}	258.0br(8.42), 264.0br(8.48), 299.5br(6.05), 317.0sh(3.28)
13	2.09×10^{-5}	269.5s(15.88), 294.5sh(6.98), 341sh(0.28), 370.0br(.095), 383.5br(0.143)
15	3.36×10^{-5}	273.0s(3.77), 296.5sh(1.45), 458.5br
16	8.22×10^{-5}	271.0s(1.94), 282.5sh(1.05)

Wavelength (λ_{\max}) is in nanometer (nm) and molar extinction coefficient

ϵ_{molar} ($\text{M}^{-1} \text{cm}^{-1} \times 10^3$) is given in parenthesis. (s = sharp, sh = shoulder, br = broad)

In UV region a strong absorption band at 277.5 (30880) nm is observed for the precursor-B which is typical ligand-centred (LC) bands involving $\pi\text{-}\pi^*$ transitions. are observed for all Copper(I) diimine, phosphine coordination complexes. This LC band

shifts by 1.0-6.5 nm upon complexation with diimines. UV region of the complexes (9-16) beside this band shows weak to strong band from 264.0 (8480) to 341.0 (280) nm all of these bands involve LC π - π^* transitions. Visible part of the spectrum consists of weak absorption bands of diimine ligands, which arise from metal-to-ligand charge-transfer (MLCT) electronic transitions. These occur at low energy because the Cu^+ ion can be easily oxidized as the diimine ligands possess low energy empty π^* orbitals.

3.2.3 Fourier-Transformed Infrared Spectroscopy (FT-IR)

The FT-IR spectra were recorded using KBr pellets in the range of $4000\text{--}400\text{ cm}^{-1}$. The absorption wavenumbers are presented in table 16 and the representative spectrum of complex 11 is given in figure 13. FT-IR spectrum are listed in Appendix-IV.

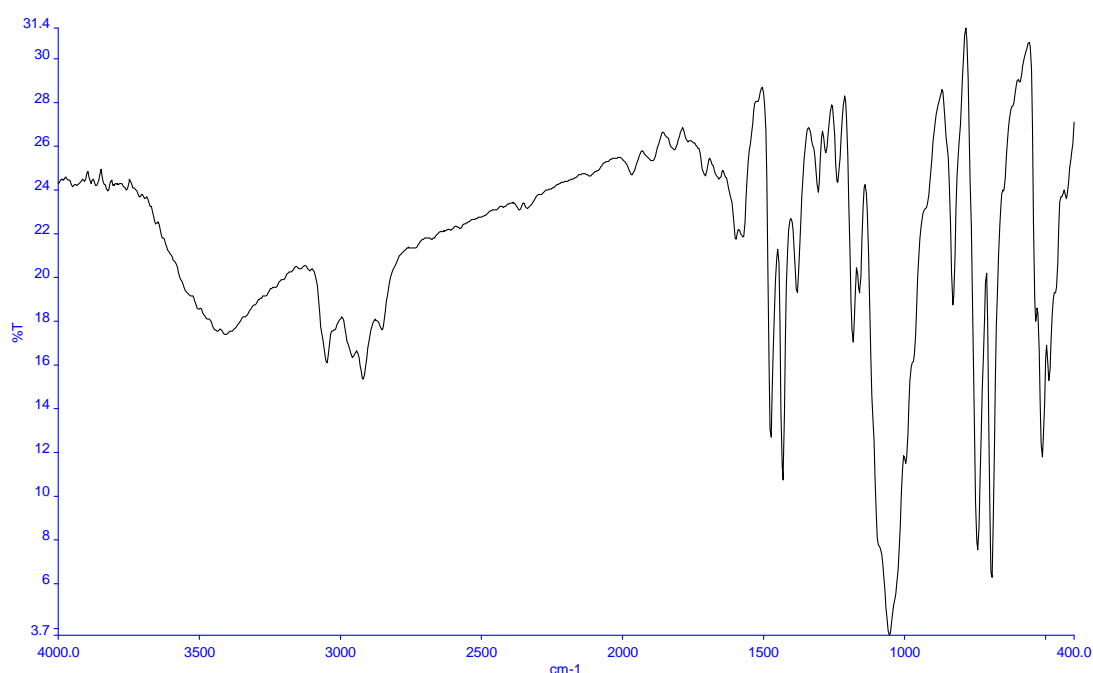


Figure 13. FT-IR Spectrum of Complex 11

In *trans*-1,2-bis(diphenylphosphino)ethylene and precursor-B C-H in plane bending of the aromatic ring is observed at 1093 and 1074 cm^{-1} and CH OOP bend . The aromatic C=C stretching are found in the range of 1427-1473 cm^{-1} In Copper(I) diimine complexes (9-16) show strong absorptions in the range of 1056-1060 cm^{-1} and 831-856 cm^{-1} attributed to C-H in plane bending of the aromatic ring and C-H out of plane bending of the aromatic ring respectively. Shift of 18.6 cm^{-1} from 1056-1075 cm^{-1} and 25.1 cm^{-1} from 831-856 cm^{-1} is attributed to complexation of diimines with the bridging ligand. These shifts are the consequence of the change in electron density in the pyridines and phenanthroline ring when the non bonding pair of electrons on the nitrogen atom is donated to the metal ion [92]. The aromatic C=C stretching are found in the range of 1430-1663 cm^{-1} .

Table 16. Infrared Frequencies (cm^{-1}) and assignment for Ligand, Precursor-B and Complexes 9-12

Assignment	Complexes					
	dppethy	P-B	9	10	11	12
C-H stretch aromatics	3050w	3054w	3050w		3051w	3047w
C-H stretch alkanes		2927w	2942w	2924m	2922w	2921m
C-H bend	1659w	1664s		1612s	1600w	1663w
C-H ring stretch	1472m	1473s	1476s	1480m	1477s	
C-H in plane bend aromatic ring	1427m	1303w	1434s	1435s	1434s	1436s

ring stretch + H bend	1303w	12780m	1310w	1308w	1309w	1303w
H in plane bend	1173m	1183w	1183 w	1184w	1186w	1184m
Ring stretch + Bend	1091m	1075br	1058br	1057br	1056br	1056br
C-H OOP bend aromatic ring		1074.8br				
H OOP bend				830m	830m	841w
Ring bend	739s	742s	741s	744s	744s	744s
Ring bend	692s	679s	693s	695s	694s	694s
Inter ring bend	491m	509w	510s	515s	514m	514m

3.2.4 Nuclear Magnetic Resonance Spectroscopy

^1H NMR and ^{31}P spectra were recorded for free ligands and binuclear Cu(I) complexes in DMSO- d_6 . Representative ^1H -NMR and ^{31}P -NMR spectrum of complex 12 are given in figure. NMR spectra are given in appendix-VI and VII. NMR results are tabulated in table17.

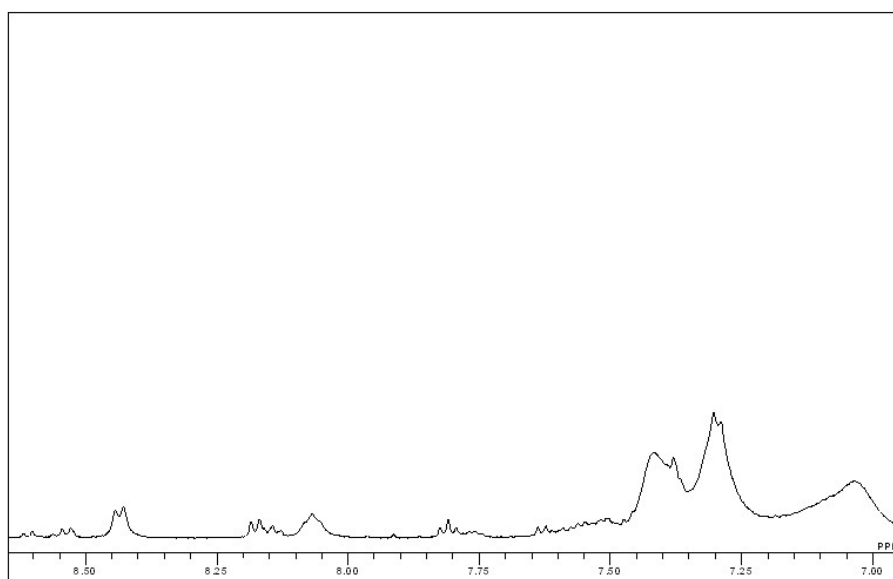


Figure 14. ^1H -NMR Spectrum of Complex 12

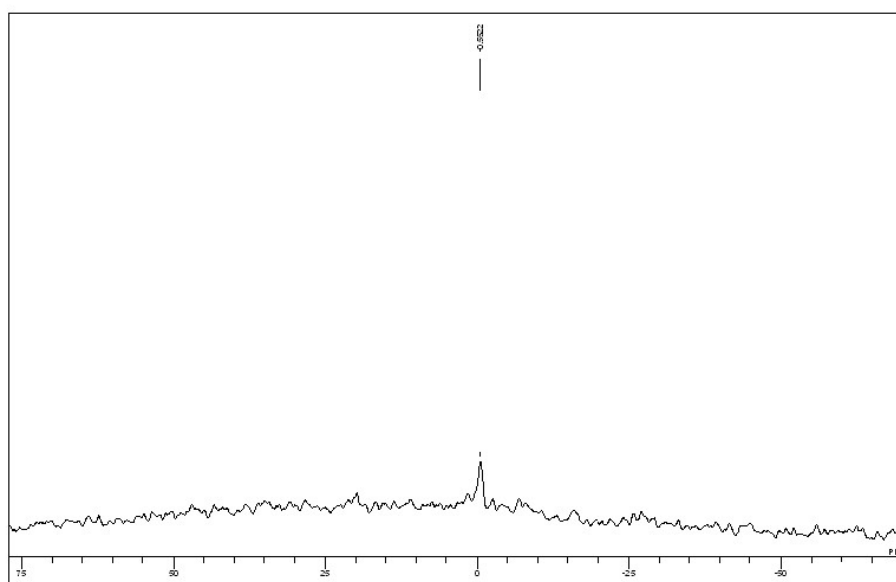


Figure 15. ^{31}P -NMR Spectrum of Complex 11

Table 17. ^1H NMR and ^{31}P shifts for Ligand, Precursor-B and Complexes 9-13 and 15-16

	^1H -NMR shifts $\delta(\text{PPM})$	^{31}P -NMR $\delta(\text{PPM})$	^{31}P -NMR $\Delta\delta(\text{PPM}) = \delta_{\text{complex}} - \delta_{\text{DPPETHY}}$
DPPETHY	6.71(t), 7.32(s), 7.37(s)	-9.031	
Precursor-B	6.71(s), 6.88(s), 6.95(s), 7.04(s), 7.13(t), 7.24(d), 7.28(s), 7.36(t)	-4.051	4.98
9	6.95(s), 7.09(s), 7.31(s), 7.47(s), 7.98(s), 8.13(s), 8.41(s), 8.59(s)	-1.003	8.02
10	1.40(m), 2.48(s), 2.50(s), 7.13(m), 7.40(m), 7.98(m), 8.20(s), 8.50(s)	-1.339	7.69
11	2.50(m), 6.90(s), 7.09(s), 7.31(s), 7.46(t), 8.12(s), 8.43(s), 8.57(s)	-0.552	8.47
12	1.66(s), 1.94(s), 2.18(s), 2.50(d), 2.55(s), 7.03(s), 7.30(d), 7.41(d), 7.50(m), 7.63(d), 7.80(t), 8.06(s), 8.16(t), 8.44(d), 8.52(s), 8.60(d)	-3.195	5.83
13	7.00(s), 7.02(s), 7.06(s), 7.24(t), 7.41(t), 7.86(q), 8.19(s), 8.75(d), 8.81(d)	-0.348	8.68
15	2.50(s), 7.40(m), 7.60(m), 7.74(t), 7.83(s), 7.87(s), 7.92(s), 7.95(d), 8.12(s), 8.22(s), 8.61(d), 8.74(d)	-0.506	8.52
16	1.20(s), 2.37(d), 3.32(m), 7.07(s), 7.23(s), 7.38(s), 7.51(s), 7.60(s), 8.23	-0.253	8.77

^{31}P NMR gave one broad signal for all complexes (9-16). The chemical shifts are in the range of -0.253 to -3.195 ppm. $\Delta\delta^{31}\text{P}$ of 5.83 to 8.77 ppm is observed for complexes 9-16 with reference to the precursor. The Upfield shift observed for complexes 12 & 15, which have 6,6'-dimethyl-2,2'-bipyridyl and 2,9-dimethyl-1,10-phenanthroline bonded to two Cu(dppethy) moieties, is a result of strong pi-back donation from metal to the phosphorous. This is enhanced by the stronger π donation of the diimine owing to the inductive effect of the methyl substituents. ^1H -NMR showed phenyl protons shifts in the range of 6.71-7.36 ppm; Bipyridyl and phenanthroline protons were also found in the of the coordination complexes in the range of 7.98-8.84 ppm. The shifts in the signals relatively to the free ligands are consistent with the complexation of diimine ligands with Cu(dppa) moiety. Signals found in the range of 1.20-3.32 ppm are attributed to the methyl protons of complexes 9-16 by comparing with the ^1H -NMR of free diimines.

Chapter 4

Binuclear Copper(I) mixed ligand complexes with 4,4'-bipyridine bridging ligand (4,4'-bipy)

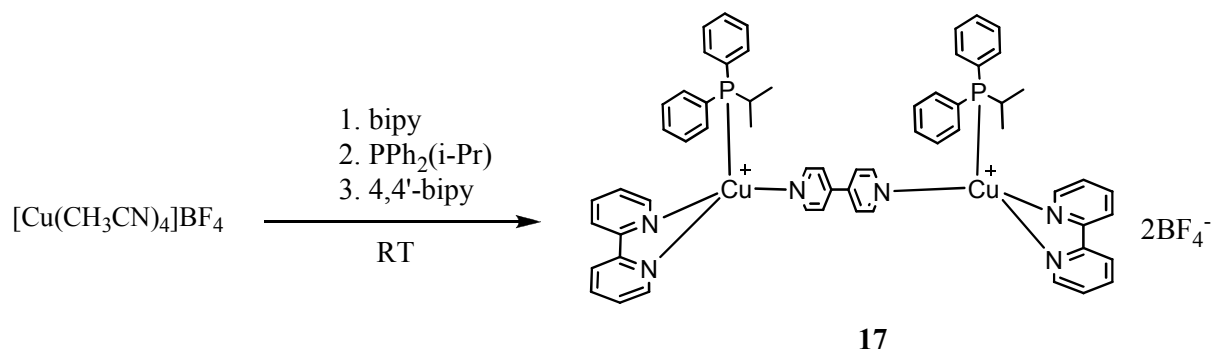
4,4'-Bipyridine (4,4'-bipy) is a bidentate ligand capable of bridging between metal centres to give coordination polymers. 4,4'-bipy has been successfully employed in the syntheses of homo- and heterometallic coordination polymers giving fascinating structures, robust microporosity, and highly luminescent properties [105].

4.1 Synthesis

A general procedure was followed for the synthesis of compounds (17-25). Diimine (1.00 mmol) and $[\text{Cu}(\text{CH}_3\text{CN})_4[\text{BF}_4]]$ (1.0 mmol) were placed in an oven dried 100 ml Schlenk flask in glove box, sealed with rubber septum and taken out. Freshly distilled, dried dichloromethane (30.0 ml) was injected through the septum using a long needle. The mixture was stirred at room temperature for 2h to result in a brown solution. Then a solution of phosphine (1.00 mmol) in dichloromethane (5.0 ml) was added drop wise with stirring, followed by the addition of 4,4'-bipy (0.5 mmol). The resulting blue solution was stirred for another 12h and filtered. The filtrate was carefully layered with 30.0 ml diethylether to get yellow color binuclear product. Recrystallization was carried out in dry dimethylformamide (DMF).

4.1.1 $[\text{Cu}_2(4,4'\text{-bipy})(\text{PPh}_2(\text{i-Pr}))_2(\text{bipy})_2][\text{BF}_4]_2$ (17)

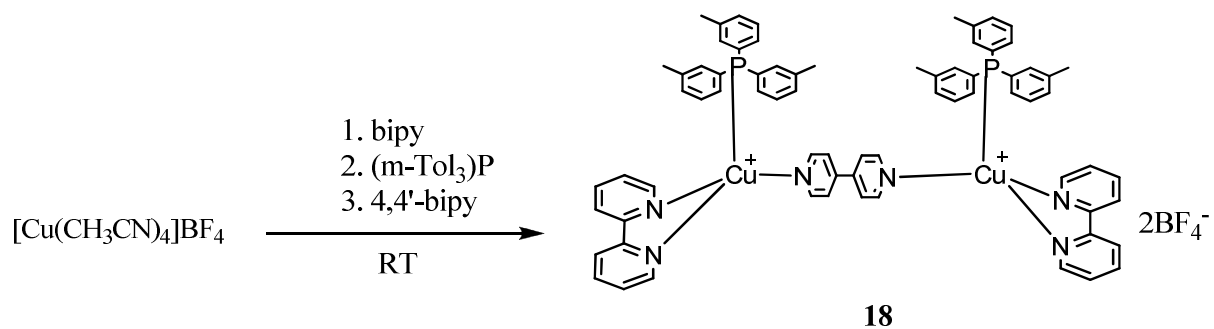
The compound was obtained as yellow crystalline material. Yield, 68%.



Scheme 4.1

4.1.2 $[\text{Cu}_2(4,4'\text{-bipy})(\text{m-Tol}_3\text{P})_2(\text{bipy})_2][\text{BF}_4]_2$ (**18**)

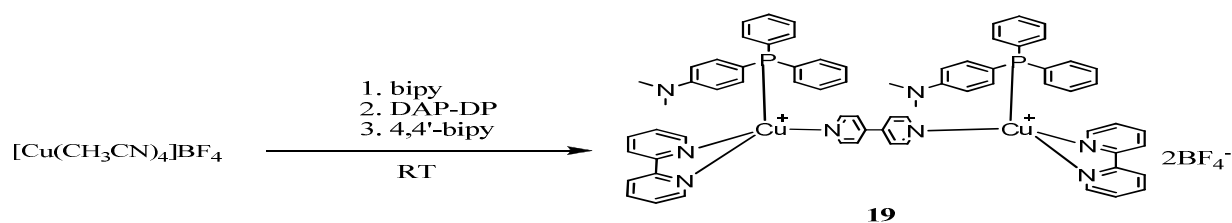
The compound was obtained as yellow crystalline material. Yield, 71%.



Scheme 4.2

4.1.3 $[\text{Cu}_2(4,4'\text{-bipy})(\text{DAP-DP})_2(\text{bipy})_2][\text{BF}_4]_2$ (**19**)

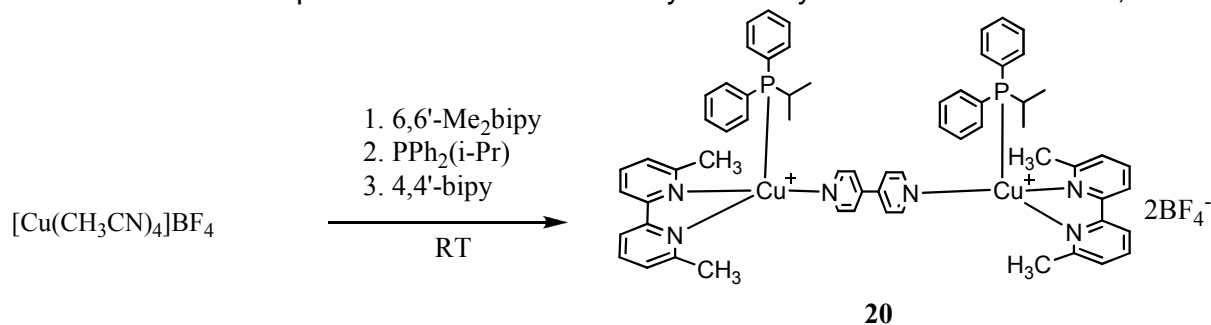
The compound was obtained as yellow crystalline material. Yield, 64%.



Scheme 4.3

4.1.4 $[\text{Cu}_2(4,4'\text{-bipy})(\text{PPh}_2(\text{i-Pr}))_2(6,6'\text{-Me}_2\text{bipy})_2][\text{BF}_4]_2$ (20)

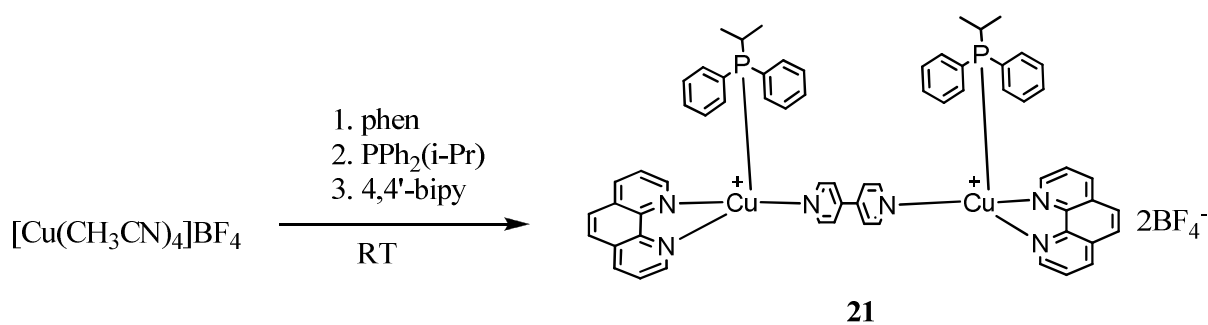
The compound was obtained as yellow crystalline material. Yield, 56%.



Scheme 4.4

4.1.5 $[\text{Cu}_2(4,4'\text{-bipy})(\text{PPh}_2(\text{i-Pr}))_2(\text{phen})_2][\text{BF}_4]_2$ (21)

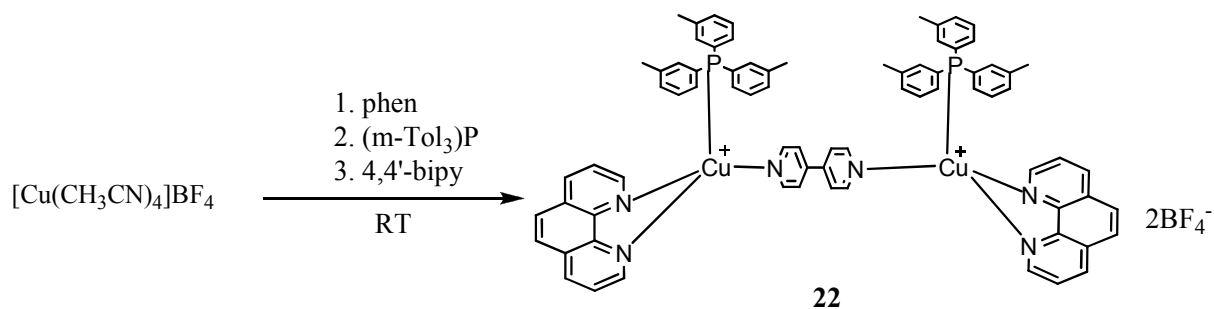
The compound was obtained as yellow crystalline material. Yield, 70%.



Scheme 4.5

4.1.6 $[\text{Cu}_2(4,4'\text{-bipy})(\text{m-Tol}_3\text{P})_2(\text{phen})_2][\text{BF}_4]_2$ (22)

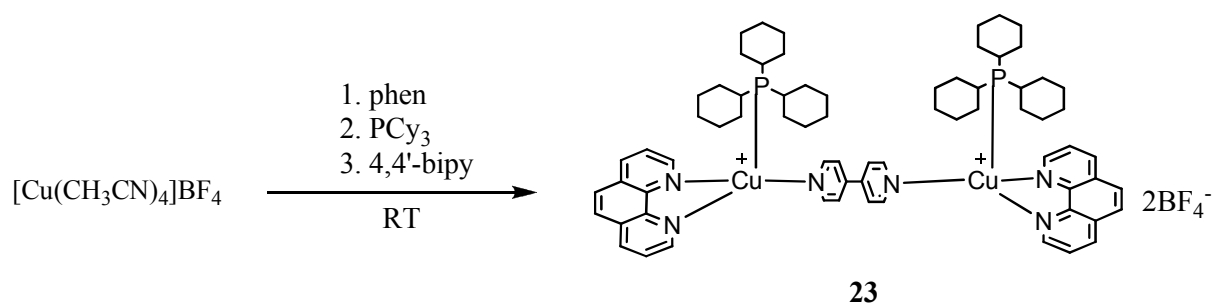
The compound was obtained as yellow crystalline material. Yield, 68%.



Scheme 4.6

4.1.7 $[\text{Cu}_2(4,4'\text{-bipy})(\text{PCy}_3)_2(\text{phen})_2][\text{BF}_4]_2$ (**23**)

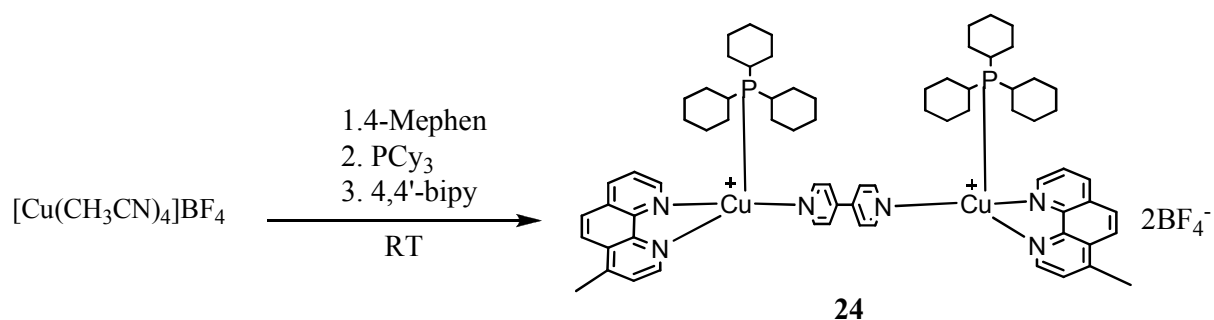
The compound was obtained as yellow crystalline material. Yield, 71%.



Scheme 4.7

4.1.8 $[\text{Cu}_2(4,4'\text{-bipy})(\text{PCy}_3)_2(4\text{-Me phen})_2][\text{BF}_4]_2$ (**24**)

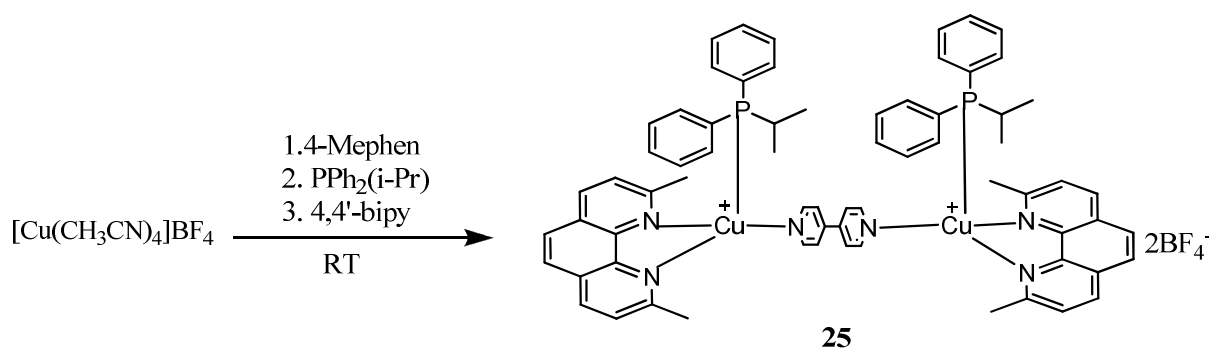
The compound was obtained as yellow crystalline material. Yield, 63%.



Scheme 4.8

4.1.9 $[\text{Cu}_2(4,4'\text{-bipy})(\text{PPh}_2(\text{i-Pr}))_2(2,9\text{-Me}_2\text{phen})_2][\text{BF}_4]_2$ (25)

The compound was obtained as yellow crystalline material. Yield, 67%.



4.2 Characterization of the complexes 17-25

4.2.1 Elemental Analysis and Melting points

Elemental analysis was performed on dried samples. UV-Vis spectra were recorded in dichloromethane for (17-25). UV-Vis spectra are given in Appendix A-II.

Table 18. Results of Elemental Analysis and Melting Points of Complexes 17-25

Complex	C %	H %	N %	MP ($^{\circ}$ C)
17	Calc: 58.8	4.73	6.85	180-183
	Found: 58.50	5.05	7.02	
18	62.11	4.87	6.20	152-155
	62.30	5.15	6.42	
	59.90	4.90	6.55	

19	60.22	5.20	6.28	215-219
20	61.43	4.96	6.31	221-224
	61.72	5.12	5.99	
21	61.43	4.96	6.31	234-237
	61.72	5.12	5.99	
22	64.00	4.48	5.89	212-215
	63.72	4.79	5.65	
23	58.88	6.89	6.43	210-213
	59.58	6.70	6.15	
24	59.46	7.05	6.30	203-206
	59.75	6.83	6.58	
25	61.43	4.95	6.31	230-233
	61.70	4.65	5.99	

4.2.2 Ultraviolet and Visible Spectroscopy

The UV-Vis spectra of the complexes were recorded in dichloromethane.

4.2.2.1 Electronic Spectra of Ligands and complexes

The absorption data of complexes (17-25) are given in table 19. The representative spectrum of complex 20 is given in figure 16 below. UV-Vis spectra are given in Appendix A-II

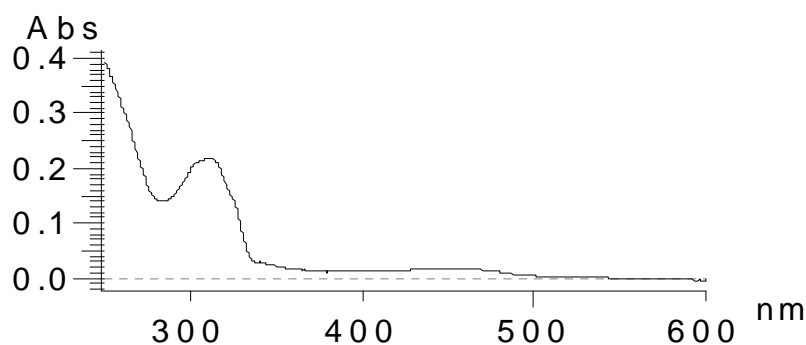


Figure 16. UV-Visible Spectrum of Complex 20

Table 19. Results of Ultraviolet and Visible Spectroscopy for free Ligands and Complexes 17-25

Compound	Conc. M	$\lambda_{\text{max}}(\epsilon_{\text{molar}} \times 10^{-3})$
$\text{PPh}_2(\text{i-Pr})$	1.31×10^{-4}	254.5s(9.16)
$(\text{m-Tol}_3)\text{P}$	1.69×10^{-4}	265.5(11.58), 266.5(11.59), 279.5sh(9.59), 376.5br(0.047), 447.0br(0.04)
DAP-DP	3.57×10^{-5}	287.0s(21.16)
17	8.35×10^{-5}	285.0s(23.36), 365.5br(2.51)
18	1.46×10^{-5}	274.0s(32.87), 378.0br(0.37), 372.0br(0.41)
19	2.19×10^{-5}	287.0s(68.49), 365.0br(1.82)
20	3.76×10^{-4}	283.0s(0.58), 312.5br(0.57), 327.0sh(0.35), 340.5br(0.079), 380.0br(0.031), 443.0br(0.026)

21	1.28×10^{-5}	270.0s(22.96), 299.0sh(5.54), 338.0br(0.46), 368.0br(0.39), 377.5br(0.31)
22	1.40×10^{-5}	271.0s(28.97), 318.0br(0.93), 331.0br(0.56), 345.5br(0.280)
23	2.14×10^{-5}	271.0s(28.97), 318.0br(0.93), 331.0br(0.56), 345.5br(0.280)
24	1.72×10^{-5}	272.5s(121.62), 300.5sh(22.67), 330.5br(2.32), 346.0br(1.51)
25	1.72×10^{-5}	272.5s(121.62), 300.5sh(22.67), 330.5br(2.32), 346.0br(1.51)

Wavelength (λ_{\max}) is in nanometer (nm) and molar extinction coefficient ϵ_{molar} ($\text{M}^{-1} \text{cm}^{-1} \times 10^3$) is given in parenthesis. (s = sharp, sh = shoulder, br = broad)

Free phosphines show strong absorptions in the UV region from 254.5(9.16×10^3) to 279.5(9.59×10^3) nm which are typical bands involving $\pi\text{-}\pi^*$ electronic transitions. This LC band shifts by 5.0-15.0 nm in complexes (17-25). The Visible part of the spectrum consists of weak band at 447.0(470.0) nm, which arises from metal-to-ligand charge transfer (MLCT) absorptions. In complex 20 MLCT absorption band appears at 443.0(260.0) nm.

4.2.3 Emission spectroscopy

4.2.3.1 Emission study of diimines

Excitation and Emission spectra of coordination complexes were recorded in dichloromethane. Representative excitation and emission spectrum of complex 21 is given below in figures 17 and 18.

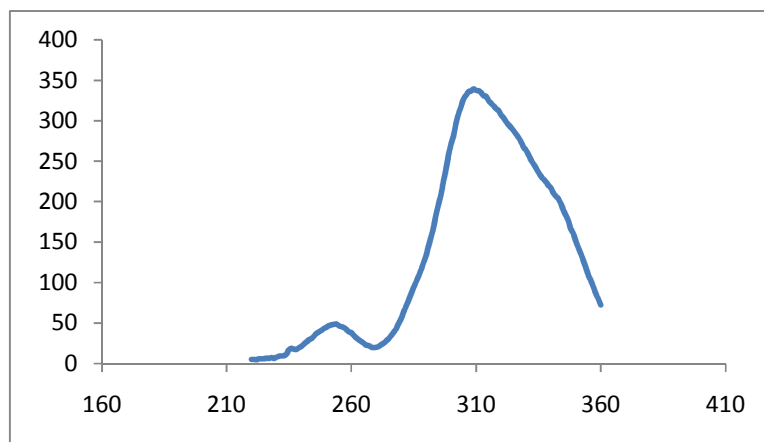


Figure 17. Excitation Spectrum of Complex 21

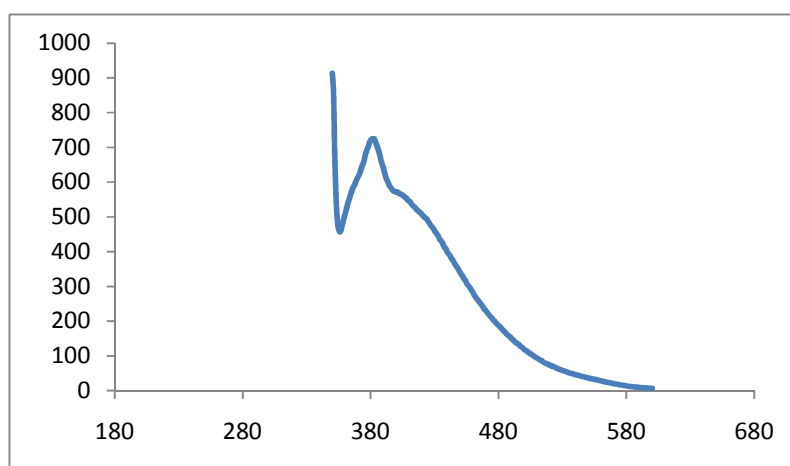


Figure 18. Emission Spectrum of Complex 21.

Excitation and emission spectrum are given in Appendix-IV

Table 20. Excitation and Emission Wavelengths for Complexes 17 and 21

Complex	λ_{ex}	λ_{em}
17	340	380
21	340	382

4.2.4 Fourier-Transformed Infrared Spectroscopy (FT-IR)

The FT-IR spectra were recorded using KBr pellets in the range of 4000-400 cm^{-1} . The absorption wavenumbers are presented in table 21 and the representative spectrum of complex 20 is given in figure 19. FT-IR spectra are listed in Appendix-IV



Figure 19. FT-IR Spectrum of Complex 20

Table 21. Infrared Frequencies (cm^{-1}) and assignment for Complexes 17-22 and 24

Assignment	17	18	19	20	21	22	24
C-H stretch aromatics	3054w	3027w	3047w	3047w	3039w	3051w	3054w
C-H stretch alkanes	2958w	2915w	2923w	2957m	2924s	2961w	2961w
C-H bend					1672s		
CH ₃ deformation	1594s	1590s	1598m	1594s	1588m	1600s	1600s
C-H in plane bend aromatic ring	1433s	1438m	1430w	1426s	1412m	1432m	1432m

H in plane bend	1159m			1175m	1213w		1220m
Ring +CH stretch Bend	1033br	1049s,br	1061s	1060s,br	1056s,br	1049s,br	1049br
C-H OOP bend aromatic ring	814m		839m	841m	852s	857s	
H OOP bend	757s	780s	786m	744m	731m	736s	736s
Ring bend	670s	692s	698m	644w	694w	698s	698m
Ring bend	516m	546m	523m	512m	520w	517m	517m
Inter ring bend		452s			470w		

In complexes (17-24) C-H in plane bending for the aromatic rings of diimines and the bridge is observed in the range of 1033 to 1060 cm^{-1} . The aromatic C=C stretching occurs from 1412 to 1440 cm^{-1} . Shift of 25.6 cm^{-1} from 1033 to 1060 cm^{-1} and 29.4 cm^{-1} from 810 to 39.3 cm^{-1} is attributed to the complexation of diimine and 4,4'-bipyridine with the copper ion.

4.2.5 Single Crystal X-ray Analysis

The crystallographic data of complexes for which single crystals were successfully grown are given in tables 22 & 23. Selected bond lengths and bond angles are given in tables 24 & 25 respectively.

Table 22. Crystallographic Data Collection and Structure Refinement Parameters for Complexes 17 and 20

Complexes	17	20
Chemical Formula	C ₆₀ H ₅₈ B ₂ Cu ₂ F ₈ N ₆ P ₂	C ₃₈ H ₃₇ B ₂ Cu ₂ F ₄ N ₄ P ₂
Formula Mass , Da	1225.76	752.48
Space Group	P21/c	P-1
a, Å	10.0289(12)	10.7897(6)
b, Å	13.5247(12)	11.4621(6)
c, Å	21.4524(12)	14.5588(8)
α, deg	90.00	81.0700(10)
β, deg	99.5905(10)	75.7920(10)
γ, deg	90.00	82.5760(10)
V, Å ³	2869.1(5)	1716.47(16)
ρ _{calcd} , gcm ⁻³	1.419	1.456
Z	2	2
μ, mm ⁻¹	0.868	0.816
T, K	293(2)	298(2)
λ, Å	0.71073	0.71073
R ₁ (F _o ²) ^a	0.1008	0.1010
WR ₂ (F _o ²) ^b	0.0413	0.3190
GOF	1.056	0.953

$$^a R_1 = \Sigma(| | F_o | - | F_c | |) / \Sigma | F_o | \quad ^b WR_2 = [\Sigma(w | F_o |^2 - | F_c |^2) / \Sigma | F_o |^2]^{1/2}$$

Table 23. Crystallographic Data Collection and Structure Refinement Parameters for Complexes 21 and 25.

Complexes	21	25
Chemical Formula	C ₃₈ H ₃₇ B Cu F N ₃ P	C ₃₈ H ₃₇ B Cu F ₄ N ₃ P
Formula Mass , Da	660.03	717.03
Space Group	P2(1)/n	P-1
a, Å	14.4309(6)	10.150(2)
b, Å	15.8009(6)	11.640(3)
c, Å	15.1812(6)	15.198(3)
α, deg	90.00	84.377(4)
β, deg	91.7750(10)	75.065(4)
γ, deg	90.00	85.885(4)
V, Å ³	3460.0(2)	1724.6(7)
ρ _{calcd} , gcm ⁻³	1.267	1.381
Z	4	2
μ, mm ⁻¹	0.713	0.733
T, K	298(2)	298(2)
λ, Å	0.71073	0.71073
R ₁ (F _o ²) ^a	0.0617	0.0862
WR ₂ (F _o ²) ^b	0.1835	0.2596
GOF	1.017	0.865

Table 24. Selected Bond Lengths (Å) and Bond Angles (°) of the complexes 17 and 20

17	20
----	----

Cu1-N1	2.060(2)	Cu1-N1	2.061(4)
Cu1-N2	2.081(2)	Cu1-N2	2.099(5)
Cu1-N3	2.092(2)	Cu1-N3	2.107(5)
Cu1-P1	2.2062(7)	Cu1-P1	2.212(15)
N1-Cu1-N2	110.07(8)	N1-Cu1-N3	108.28(19)
N1- Cu1-N3	104.75(8)	N2-Cu1-N3	78.2(2)
N2-Cu1-N3	79.02(9)	N1-Cu1-P1	120.02(14)
N1-Cu1-P1	116.37(6)	N2-Cu1- P1	121.00(14)
N2-Cu1-P1	115.18(6)	N3-Cu1-P11	14.62(15)
N3- Cu1-P1	125.47(6)		

Table 25. Selected Bond Lengths (Å) and Bond Angles (°) of the complexes

21		25	
Cu1-N2	2.061(3)	Cu2-N3	2.066(4)
Cu1-N3	2.074(3)	Cu2-N1	2.115(5)
Cu1-N1	2.074(3)	Cu2-N2	2.138(5)
Cu1-P1	2.210(10)	Cu2-P1	2.196(17)
N2-Cu1-N3	114.79(12)	N3-Cu2-N1	102.19(19)
N2-Cu1-N1	81.02(12)	N3-Cu2-N2	105.7(2)
N3-Cu1-N1	110.18(12)	N1-Cu2-N2	78.7(2)
N2-Cu1-P1	116.81(9)	N3-Cu2-P1	123.05(15)
N3-Cu1-P1	109.08(9)	N1-Cu2-P1	123.24(14)
N1-Cu1-P1	122.78(8)	N2-Cu2-P1	114.62(14)

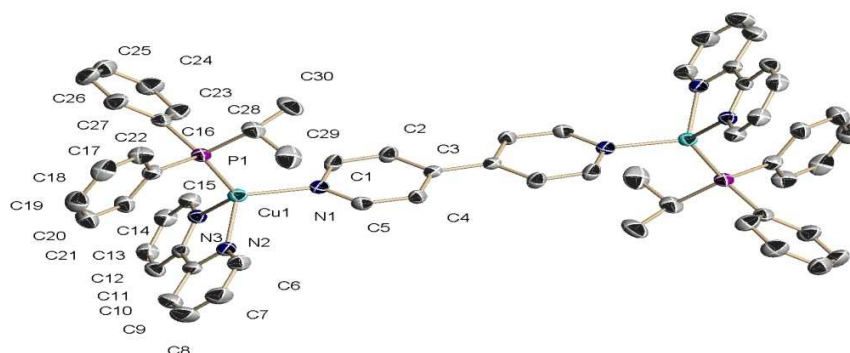


Figure 20. X-ray structure of Complex 17 showing thermal ellipsoid drawn at the 30 % probability level. Hydrogen atoms and BF_4^- anions are omitted for clarity

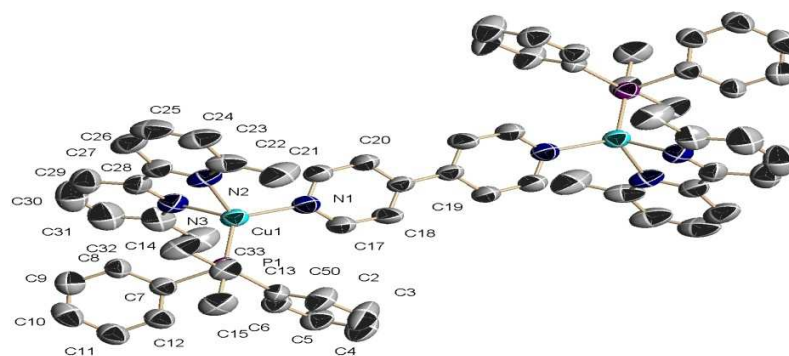


Figure 21. X-ray structure of Complex 17 showing thermal ellipsoid drawn at the 30 % probability level. Hydrogen atoms and BF_4^- anions are omitted for clarity

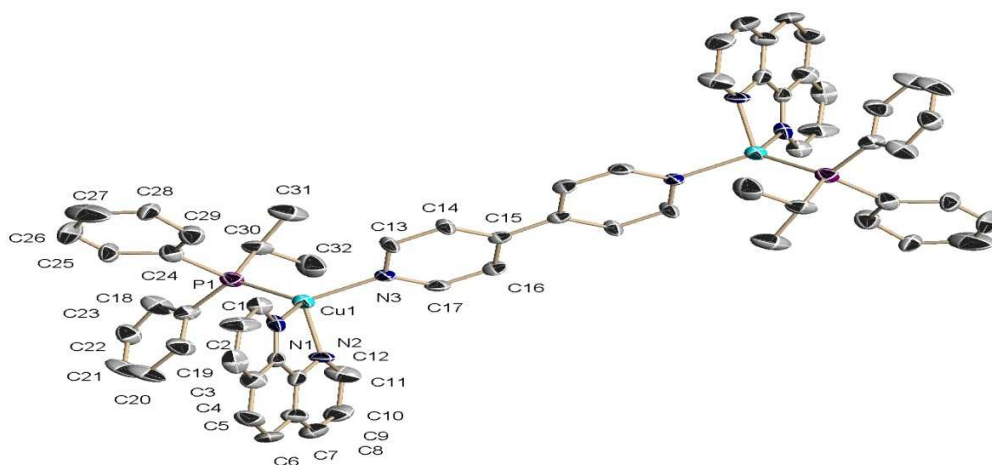


Figure 22. X-ray structure of Complex 20 showing thermal ellipsoid drawn at the 30 % probability level. Hydrogen atoms and BF_4^- anions are omitted for clarity

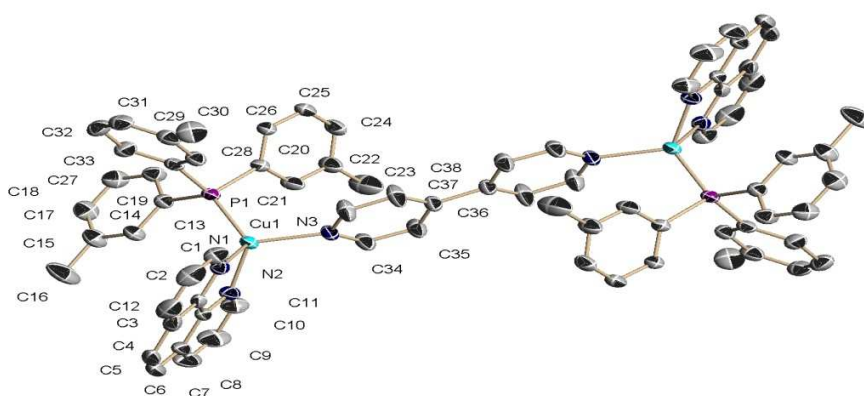


Figure 23. X-ray structure of Complex 21 showing thermal ellipsoid drawn at the 30 % probability level. Hydrogen atoms and BF_4^- anions are omitted for clarity

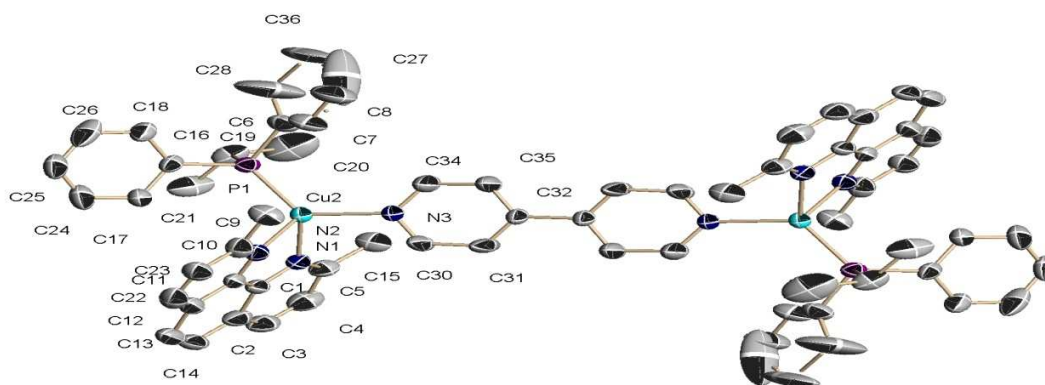


Figure 24. X-ray structure of Complex 22 showing thermal ellipsoid drawn at the 30 % probability level. Hydrogen atoms and BF_4^- anions are omitted for clarity

The X-ray structure of 17, 20, 21, 22 and 25 confirm the binuclear nature of the complexes with 4,4'-bipy bridging. Each copper(I) ion is bonded to two nitrogen atoms of chelating diimine, one nitrogen of the bridging ligand and phosphorous atom of phosphine. The geometry is distorted tetrahedral. The two pyridyl rings of the bridging ligand are almost coplanar. Except in complex 20 the binuclear molecule has crystallographic center of symmetry in the other four complexes.

4.2.6 Nuclear Magnetic Resonance Spectroscopy

^1H and ^{31}P NMR spectra were recorded for free ligands and binuclear Cu(I) complexes in DMSO-d_6 . Representative ^1H -NMR and ^{31}P -NMR spectrum of complex 20 are given in figures 25 & 26. NMR spectra are given in appendix-VI and VII. The data are summarized in tables 26 & 27.

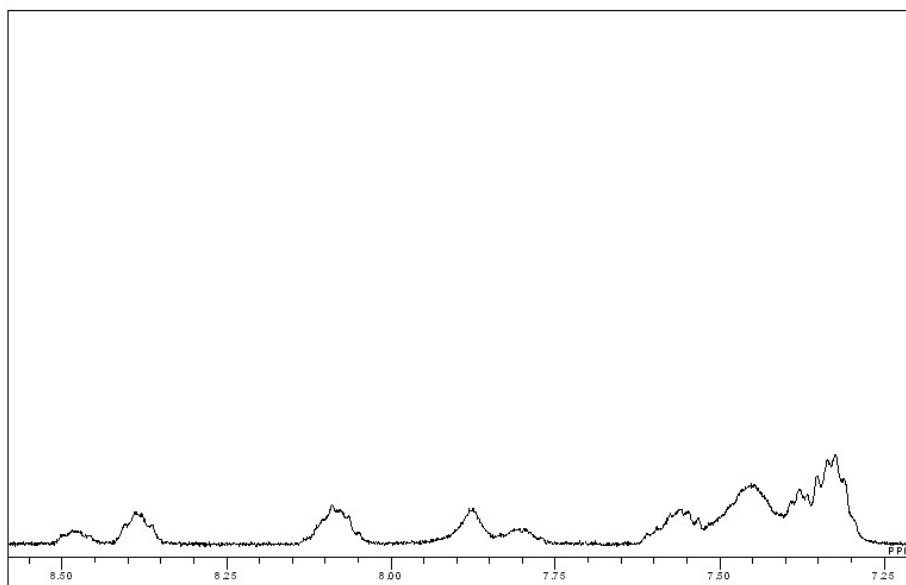


Figure 25. ^1H NMR Spectrum (only the aromatic region) of Complex 20

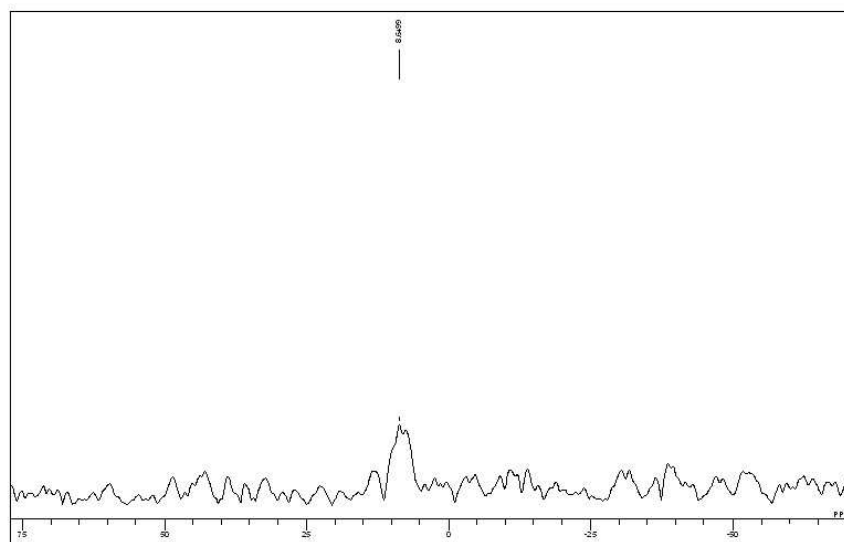


Figure 26. ^{31}P NMR Spectrum of Complex 20

Table 26. ^1H NMR shifts for free ligands.

Free Ligand	H^1 -NMR shifts $\delta(\text{PPM})$	^{31}P -NMR $\delta(\text{PPM})$
4,4'-dipyridyl hydrate	7.76(s), 8.66(s)	
$\text{PPh}_2(\text{i-Pr})$	0.94(q), 2.50(m), 7.32(q), 7.44(q)	-0.25, 35.34
$(\text{m-Tol}_3)\text{P}$	2.06(s), 2.23(s), 2.49(d), 6.95(t), 7.07(d), 7.18(d), 7.26(t)	-6.52
DAP-DP	2.06(s), 2.94(d), 6.70(d), 7.09(t), 7.17(t), 7.33(d), 7.50(s), 7.54(s), 7.56(s)	-8.64

Table 27. ^1H and ^{31}P NMR shifts for complexes 17-21 and 23-25

Complexes	H^1 -NMR shifts $\delta(\text{PPM})$	^{31}P -NMR $\delta(\text{PPM})$	^{31}P -NMR $\Delta\delta(\text{PPM}) = \delta_{\text{complex}} - \delta_{\text{PR3}}$
17	0.33(s), 0.43(m), 1.98(t), 2.33(m), 6.03(t), 6.29(d), 6.49(d), 6.92(m), 6.99(m), 7.34(q), 7.50(q), 7.75(s), 7.85(s), 7.93(s), 8.28(s, br)	11.96	12.21,
18	1.97(s), 2.00(s), 2.03(s), 2.06(d), 2.31(s), 2.48(d), 6.81(t), 7.19(q), 7.41(s), 7.57(s), 7.82(s), 8.15(s), 8.47(s), 8.61(s)	1.24	7.76

19	2.06(s),2.70(s),2.87(s),2.93(s),6.60(s),6.75(d),7.07(s,br),7.29(d),7.37(s),7.49(d),7.55(t),7.83(s),8.15(s),8.58(s)	0.42	9.02
20	0.88(s),0.98(m),1.05(q),2.04(d),2.13(d),2.50(s),2.87(s),7.33(q),7.36(t),7.45(s),7.53(d),7.80(s),7.87(s),8.08(s),8.38(q),8.48(q)	8.26	8.51
21	0.73(s),0.97(q),1.04(t),1.21(s),2.48(s),2.62(s),2.82(m),7.29(s),7.37(d),7.50(dd),7.82(m),8.00(d),8.22(s),8.70(d),8.79(d),9.06(s)	35.71	35.96
23	1.03(s),1.19(d),1.64(s),1.73(s),2.06(s),2.48(d),2.71(s),2.87(s),7.81(d),7.92(s),8.10(s),8.22(s),8.72(s),8.81(s),9.16(s)	50.39	1.55
24	1.00(s),1.25(m),1.63(s),1.71(s),1.78(s),2.06(s),2.48(d),2.71(s),2.87(s),6.77(s),7.28(s),7.81(d),7.93(s),8.24(d),8.32(d),8.71(s,br),8.80(d),8.96(s),9.12(s)	50.48,14.74	1.65
25	0.79(s),1.24(t),1.83(s),2.08(s),2.39(s),2.51(d),2.72(s),2.86(s),3.09(s),7.30(t),7.35(d),7.64(s,br),7.76(d),7.94(d),8.04(s),8.21(s),8.56(d),8.74(d)	9.98	9.76

** Relative to 85% H₃PO₄ as an external standard.

δ_{PR3} = PPh₂(i-Pr), PCy₃, (m-Tol)₃P and DAP-DP

³¹P-NMR gave one broad signal for all complexes (17-25). Chemical shifts observed are in the range -0.42 to 50.48 ppm. A shift $\Delta\delta^{31}\text{P}$ of 1.65 to 35.96 ppm with reference to free phosphines is observed. $\Delta\delta^{31}\text{P}$ -NMR of 8.26 and 9.76 for complex 20 and 25 are consistent with the observation that the π -back bonding from metal to phosphine is more in 6,6'-Me₂bipy and 2,9-Me₂phen; suggesting phosphorus atom is more shielded than the unsubstituted bpy & phen complexes (17 & 21) with the same phosphine and bridge.

Chapter 5

Binuclear Copper(I) mixed ligand complexes with trans-1,2-bis(4-pyridyl)ethylene (bpe) bridging ligand

Trans-1,2-bis(4-pyridyl)ethylene is a bidentate bridging ligand of considerable interest. Mixed ligand complexes with bpe result in diverse architectures with potential applications in catalysis and advanced materials such as magnetic, optic and electronic materials [106-110]. Recently Quadrangular metallocycles with elongated sides based on a trans-1,2-bis(4-pyridyl)ethylene motif have been reported [111]. These longer sides provided metallocycles with larger cavities and ideal distance between opposite sides with enhanced selectivity toward larger guests. In the present work, diimine and phosphine mixed ligand complexes with bpe bridge have been successfully synthesized and characterized and are presented below.

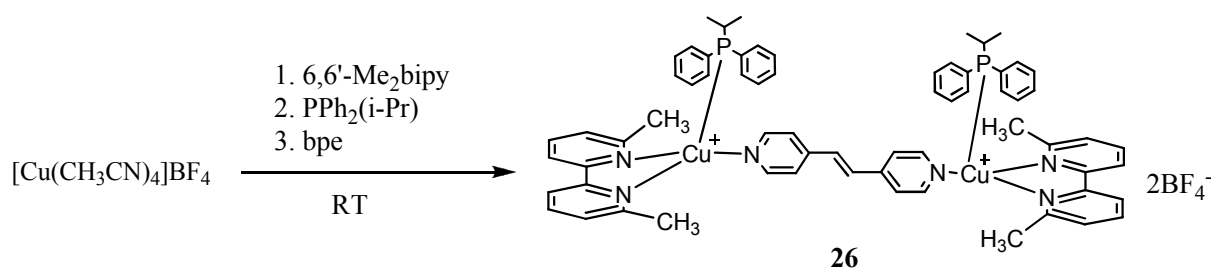
5.1 Synthesis

A general procedure was followed for the synthesis of compounds (26-33). Diimine (1.00 mmol) and $[\text{Cu}(\text{CH}_3\text{CN})_4[\text{BF}_4]]$ (1.0 mmol) were placed in an oven dried 100 ml Schlenk flask in glove box, sealed with rubber septum and taken out. Freshly distilled, dried dichloromethane (30.0 ml) was injected through the septum using a long needle. The mixture was stirred at room temperature for 2h to result in a brown solution.

Then a solution of phosphine (1.00 mmol) in dichloromethane (5.0 ml) was added drop wise with stirring, followed by the addition of trans-1,2-bis(4-pyridyl)ethylene (bpe) (0.500 mmol). The resulting blue solution was stirred for another 12h and filtered. The filtrate was carefully layered with 30.0 ml diethylether to get yellow color binuclear product. Recrystallization was carried out in dry dimethylformamide (DMF).

5.1.1 $[\text{Cu}_2(\text{bpe})(\text{PPh}_2(\text{i-Pr}))_2(6,6'\text{-Me}_2\text{bipy})_2][\text{BF}_4]_2$ (26)

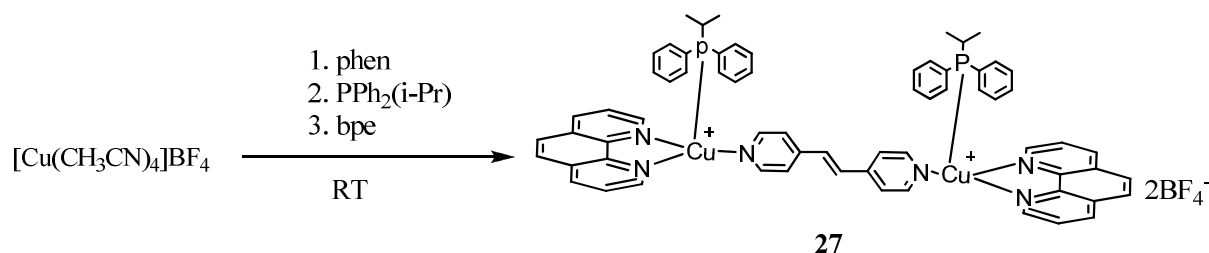
The compound was obtained as yellow crystalline material. Yield, 65%.



Scheme 5.1

5.1.2 $[\text{Cu}_2(\text{bpe})(\text{PPh}_2\text{i-Pr})_2(\text{phen})_2][\text{BF}_4]_2$ (27)

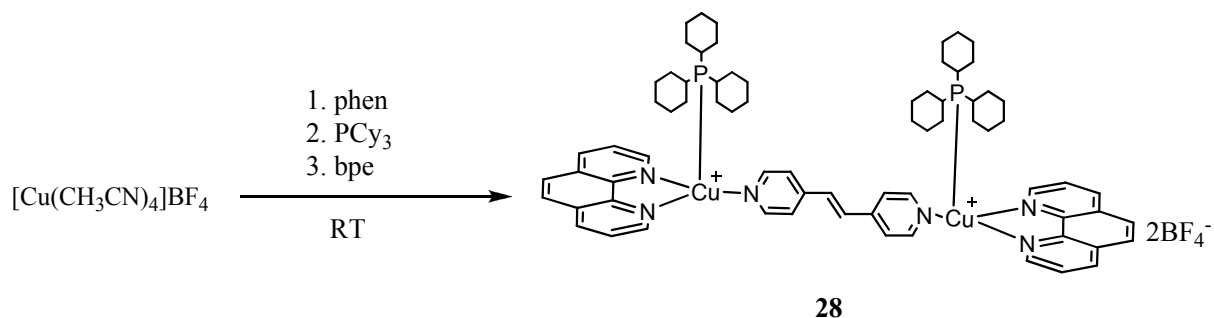
The compound was obtained as yellow crystalline material. Yield, 71%.



Scheme 5.2

5.1.3 $[\text{Cu}_2(\text{bpe})(\text{PCy}_3)_2(\text{phen})_2][\text{BF}_4]_2$ (28)

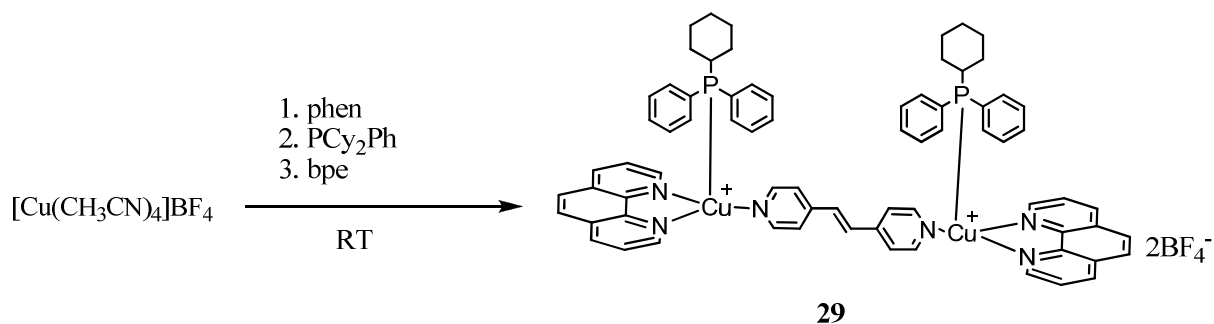
The compound was obtained as yellow crystalline material. Yield, 74%.



Scheme 5.3

5.1.4 $[\text{Cu}_2(\text{bpe})(\text{Cy}_2\text{PhP})_2(\text{phen})_2][\text{BF}_4]_2$ (29)

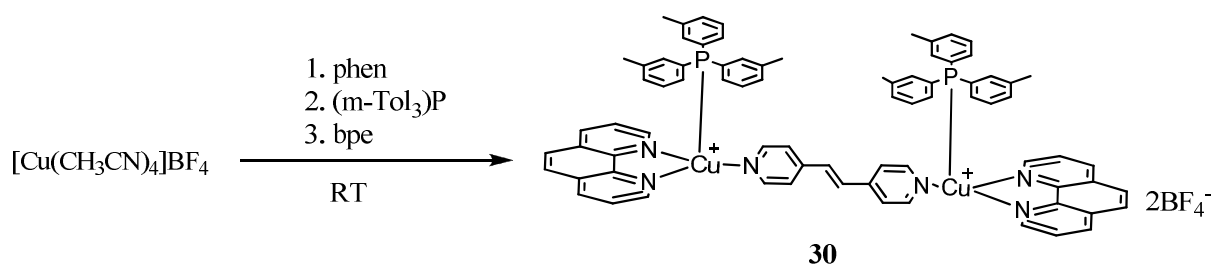
The compound was obtained as yellow crystalline material. Yield, 69%.



Scheme 5.4

5.1.5 $[\text{Cu}_2(\text{bpe})(\text{m-Tol}_3\text{P})_2(\text{phen})_2][\text{BF}_4]_2$ (30)

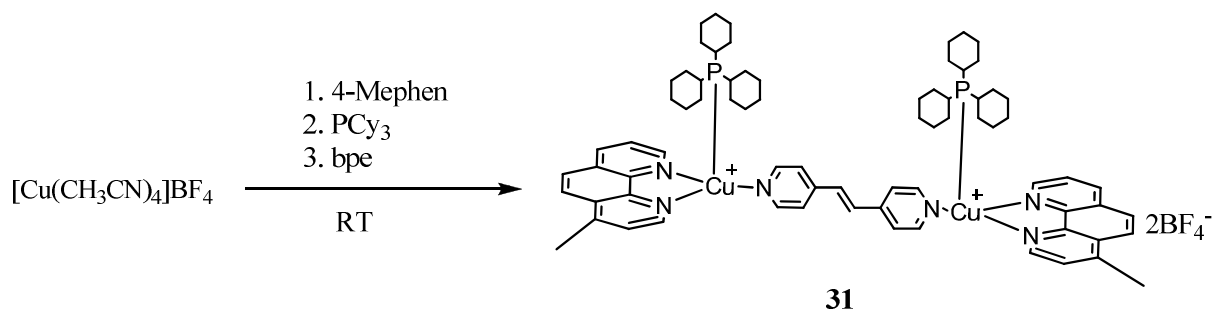
The compound was obtained as yellow crystalline material. Yield, 64%.



Scheme 5.5

5.1.6 $[\text{Cu}_2(\text{bpe})(\text{PCy}_3)_2(4\text{-Mephen})_2][\text{BF}_4]_2$ (31)

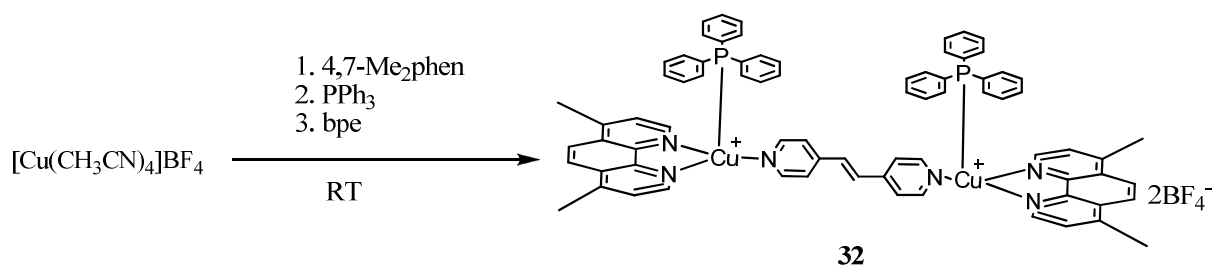
The compound was obtained as yellow crystalline material. Yield, 70%.



Scheme 5.6

5.1.7 $[\text{Cu}_2(\text{bpe})(\text{Ph}_3\text{P})_2(4,7\text{-Me}_2\text{phen})_2][\text{BF}_4]_2$ (32)

The compound was obtained as yellow crystalline material. Yield, 63%.



Scheme 5.7

5.2 Characterization of the Complexes 25-32

5.2.1 Elemental Analysis

Elemental analysis was performed on Perkin Elmer EA 3000 CHNS/ O Elemental Analyzer. The samples were dried prior to analysis. The results of the complexes are given in table 28

Table 28. Results of Elemental Analysis

Complex	C %	H %	N %
26	59.16	5.11	6.22
	59.32	4.83	6.26
27	61.00	4.61	6.46
	61.24	4.35	6.17
28	61.50	4.75	5.20
	61.56	4.90	4.83
29	62.80	4.79	6.10
	62.57	4.56	6.35
30	62.68	4.92	6.09
	62.69	4.83	6.30
31	62.25	6.14	5.88
	62.54	6.26	6.04
32	62.53	4.86	6.01
	62.59	4.93	6.30

5.2.2 Ultraviolet and Visible Spectroscopy

The UV-Vis spectra of the complexes were recorded in dichloromethane.

5.2.2.1 Electronic Spectra of Ligands and Complexes

Electronic spectra of trans-1, 2-bis(4-pyridyl)ethylene and complexes synthesized were recorded. The absorption data of complexes (26-32) is given in table 29. UV-Vis spectra are given in Appendix A-II.

Table 29. Results of Ultraviolet and Visible Spectroscopy for bpe and Complexes 26-32

Compound	Conc. M	λ_{\max} ($\epsilon_{\text{molar}} \times 10^{-3}$)
bpe	5.74×10^{-5}	289.0s(27.73), 298.0sh(26.96), 313.5sh(14.98)
26	1.62×10^{-5}	251.5s(2.77), 300.5s(37.96), 315.5sh(37.83), 328.0sh(12.83), 454.5br(2.77)
27	9.00×10^{-6}	271.0s(10.77), 295.5s(10.55), 315.5sh(4.66), 600.0br
28	1.28×10^{-5}	273.5s(27.18), 299.0sh(12.81), 315.0sh(6.17)
29	2.46×10^{-4}	270.5s(37.19), 298.5sh(13.08), 316.0sh(6.66), 379.5br(1.66)
30	1.51×10^{-5}	272.0s(40.12), 293.0sh(19.00), 315.0sh(6.35), 381.5br(0.73)
31	7.67×10^{-5}	273.5s(13.89), 299.0sh(7.49), 314.5sh(3.27), 345.5br(0.10)
32	2.38×10^{-5}	269.5s(54.62), 290.5sh(21.00), 370.5br(3.06), 372.0sh(2.94)

Wavelength (λ_{\max}) is in nanometer (nm) and molar extinction coefficient ($\epsilon_{\text{molar}} \text{ M}^{-1} \text{ cm}^{-1} \times 10^3$) is given in parenthesis. (s = sharp, sh = shoulder, br = broad)

Trans-1,2-bis(4-pyridyl)ethylene shows two strong ligand centered $\pi\text{-}\pi^*$ absorption bands in the UV region at 289.0(27730), 298.0(26960) nm and a shoulder at 313.5(14380) nm. These bands shift by 1.0 to 12.0 nm upon coordination with copper(I)

diimine-phosphine moiety. Visible part of the spectrum consists of weak absorption bands which are MLCT in nature. MLCT bands observed for complex 26 & 27 are the consequence of Cu(I) to Cu(II) oxidation.

5.2.3 Emission spectroscopy

5.2.3.1 Emission study of complexes

Excitation and Emission spectra of coordination complexes were recorded in dichloromethane. Emission spectra for complex 28 is given in figure 27. Excitation and emission spectrum are given in Appendix-IV

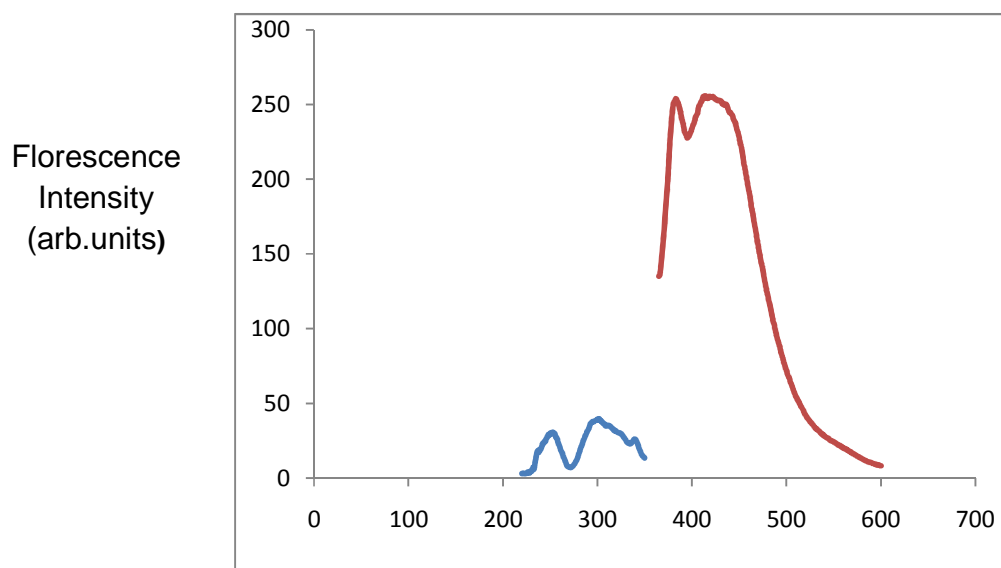


Figure 27. Excitation and Emission Spectrum of Complex 28

Table 30. Excitation and Emission Wavelengths for Complexes 27, 28 and 31

Complexes	$\lambda_{\text{ex,max}}(\text{nm})$	$\lambda_{\text{ex}}(\text{nm})$	$\lambda_{\text{em,max}}(\text{nm})$	$\lambda_{\text{em}}(\text{nm})$
27	255 297	340	363 382	382

	307		399	
28	239 246 248 316	340	382 406 409 417 421	380
31	236 249 329	340	395 383 420	380

In complexes (27, 28 & 31) upon excitation in the UV region emission is observed in the visible region. Each of these complexes show low energy bands in the range $\lambda_{em,max}$ 363-421nm which is likely due to MLCT or IL excited states.

5.2.4 Single Crystal X-ray Analysis

The crystallographic data of complexe 26 is given in table 31 and selected bond lengths and bond angles are given in table 32 respectively.

Table 31. Crystallographic Data Collection and Structure Refinement Parameters for Complexes 26

Complexes	27
Chemical Formula	C ₇₆ H ₆₄ B ₂ Cu ₂ F ₈ N ₄ P ₂
Formula Mass , Da	1528.79
Space Group	P-1
a, Å	11.3431(12)
b, Å	11.8001(12)
c, Å	14.8248(12)

α , deg	72.95
β , deg	71.2911(10)
γ , deg	77.16
V , Å ³	1778.8(3)
T , K	296(2)
λ , Å	0.71073
$R_1(FO^2)^a$	0.0960
$WR_2(FO^2)^b$	0.3310
GOF	1.132

$$aR_1 = \Sigma(| | Fo| - | Fc| | / \Sigma | Fo| . b WR_2 = [\Sigma(w | Fo|^2 - | Fc|^2) / \Sigma | Fo|^2]^{1/2}$$

Table 32. Selected Bond Lengths (Å) and Bond Angles (°) of the complexes

26	
Cu1-N3	2.058(5)
Cu1-N1	2.080(5)
Cu1-N2	2.092(6)
C21-P1	1.822(6)
C28-P1	1.860(7)
C16-P1	1.831(5)
N3-Cu1-N1	105.06(19)
N3-Cu1-N2	106.8(2)
N1-Cu1-N2	79.4(2)
N3-Cu1-P1	116.60(14)
N1-Cu1-P1	124.16(15)

N2-Cu1-P1	118.45(15)
-----------	------------

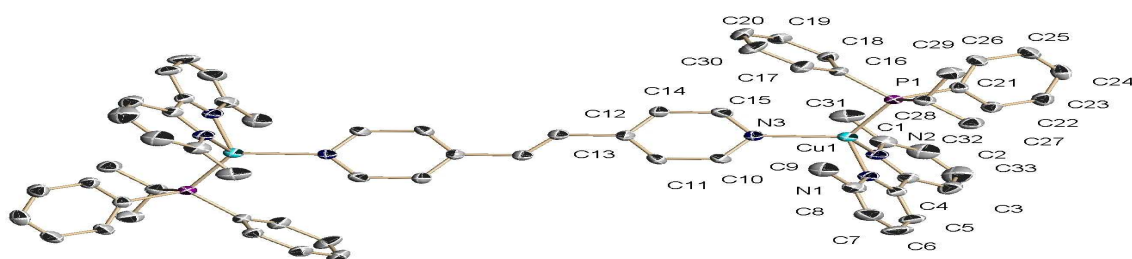


Figure 28. X-ray structure of Complex 26 showing thermal ellipsoid drawn at the 30 % probability level. Hydrogen atoms and BF_4^- anions are omitted for clarity.

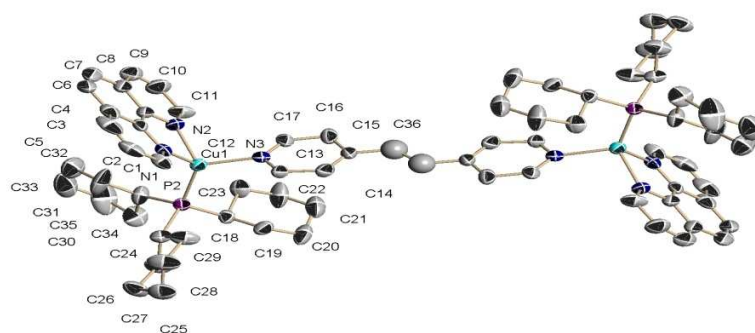


Figure 29. X-ray structure of Complex 28 showing thermal ellipsoid drawn at the 30 % probability level. Hydrogen atoms and BF_4^- anions are omitted for clarity

The single crystal X-ray structure of complexes 26 & 28 confirm the bimetallic nature of the complexes. Cu(I) ion is bonded to the diimine and phosphine forming a CuPN_2^+ . These are bridged by bpe ligand via the nitrogen atom on each side. Both complexes are centrosymmetric. The Cu(I) ion adopts a distorted tetrahedral geometry with N-Cu-N bond angles range in the range of $79.4(2)$ - $105.06(19)^\circ$. The P-Cu-N angles range from $113.9(5)$ to $124.16(15)^\circ$ which are significantly greater than the idealized bond angle of 109.5° .

5.2.5 Nuclear Magnetic Resonance Spectroscopy

^1H and ^{31}P NMR spectra were recorded for free ligands and binuclear Cu(I) complexes in DMSO-d_6 . Representative ^1H and ^{31}P -NMR spectra of complex 26 are given in figure 30 & 31. NMR spectra are given in appendix-vi & vii

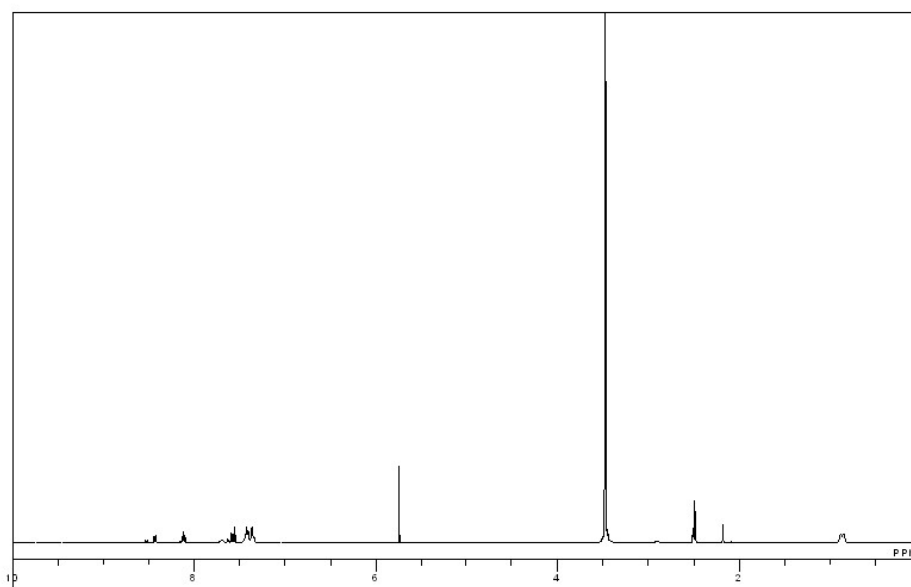


Figure 30. ^1H -NMR Spectrum of Complex 26

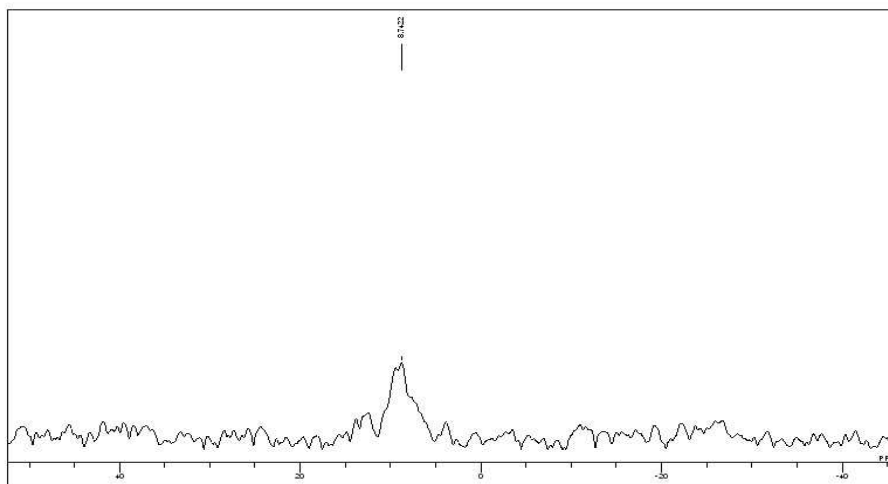


Figure 31. ^{31}P -NMR Spectrum of Complex 26

Table 33. ^1H NMR shifts for free Ligand and Complexes

Compound	H^1 -NMR shifts $\delta(\text{PPM})$	^{31}P - NMR $\delta(\text{PPM})$
bpe	2.14(s), 2.34(s), 2.57(s), 7.23(s), 7.58(d), 7.68(s), 7.79(s), 7.99(s), 8.65(s)	
27	0.86(t), 1.07(t), 2.07(s), 2.16(s), 2.25(s), 2.49(s), 2.71(s), 2.87(s), 2.90(s), 7.34(d), 7.40(t), 7.58(m), 8.11(m), 8.50(m)	9.1
28	0.82(s), 0.97(dd), 1.21(s), 2.06(s), 2.48(s), 2.71(s), 2.87(s), 3.25(s), 7.36(d), 7.50(d), 7.82(s), 7.93(s), 8.06(s), 8.24(s), 8.73(s), 8.81(d), 9.12(s)	15.18

29	0.91(s), 1.11(m), 1.27(d), 1.30(s), 1.32(m), 1.79(m), 2.42(s), 2.50(s), 7.11(d), 7.28(t), 7.60(s), 7.67(d), 8.15(s), 8.29(s), 8.66(s), 8.80(s), 9.24(s)	30.83
30	0.78(s), 1.17(s), 1.34(s), 1.53(s), 1.74(s), 1.97(s), 2.10(m), 2.31(s), 2.42(s), 2.74(s), 2.89(s), 7.34(s), 7.43(s), 7.58(s), 7.73(s), 7.87(s), 8.09(s), 8.28(s), 8.85(s), 9.15(s)	50.66
31	1.06(s), 1.18(s), 1.22(s), 1.24(s), 1.58(s), 1.60(s), 1.65(s), 1.67(s), 1.70(s), 1.75(s), 1.77(s), 1.82(s), 1.84(s), 1.93(s), 2.03(s), 2.09(s), 2.18(s), 2.86(s), 7.49(s), 7.69(s), 7.94(s), 8.09(s), 8.23(s), 8.32(s), 8.32(s), 8.80(s), 9.03(s), 9.17(s)	21.63, 50.63
32	2.06(s), 2.69(m), 2.84(m), 7.08(s), 7.24(t), 7.37(t), 7.54(t), 7.61(s), 8.12(s), 8.29(s), 8.59(s), 8.74(s)	7.81

Chapter 6

Binuclear Copper(I) mixed ligand complexes with 2,2'-bipyrimidine (bpm) bridging ligand

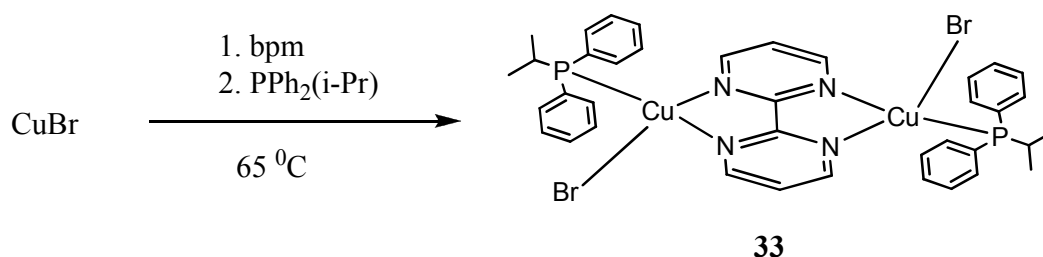
2,2'-bipyrimidine is a tetradentate aromatic nitrogen heterocycle employed as bridging ligand. It has played a major role because of its good coordinating properties and the ability to transmit electronic effects. 2,2'-bipyrimidine can adopt chelating and bis(chelating) coordination modes in its metal complexes yielding a plethora of extended systems [112-130].

6.1 Synthesis

A following general procedure was followed for the synthesis of compounds (33-36). PR_3 (1.0 mmol), CuX (1.0 mmol) and 2,2'-bipyrimidine (0.500 mmol) were placed in an oven dried 100 ml Schlenk flask in glove box, sealed with rubber septum and taken out. Freshly distilled, dried dimethylformamide (35.0 ml) was injected through the septum using a long needle. The mixture was stirred at room temperature for 2h to result in a red solution. The resulting solution was filtered and left over few days to get red crystals of binuclear product.

6.1.1 $[\text{Cu}_2(\text{bpm})(\text{PPh}_2(\text{i-Pr}))_2(\text{Br})_2]$ (33)

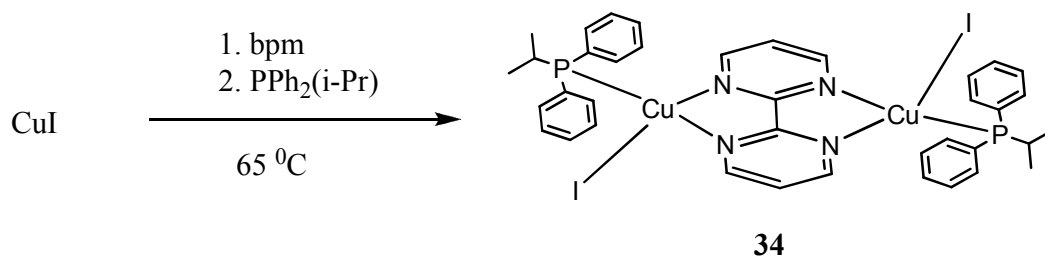
The compound was obtained as red crystalline material. Yield, 78 % .



Scheme 6.1

6.1.2. $[\text{Cu}_2(\text{bpm})(\text{PPh}_2(\text{i-Pr}))_2(\text{I})_2]$ (34)

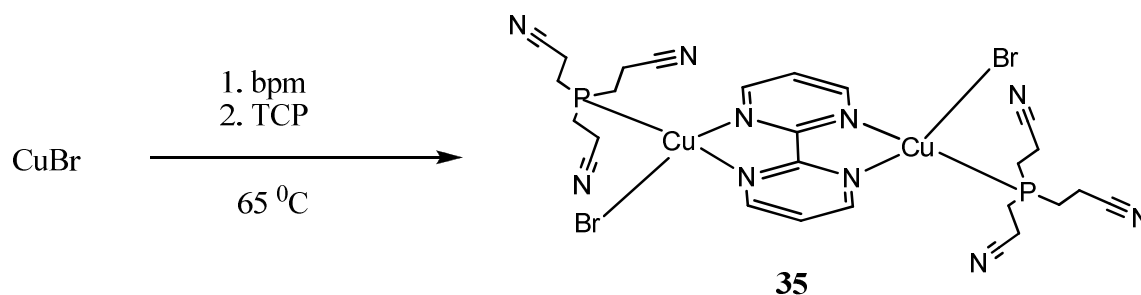
The compound was obtained as red crystalline material. Yield, 73 %.



Scheme 6.2

6.1.3. $[\text{Cu}_2(\text{bpm})(\text{TCP})_2(\text{Br})_2]$ (35)

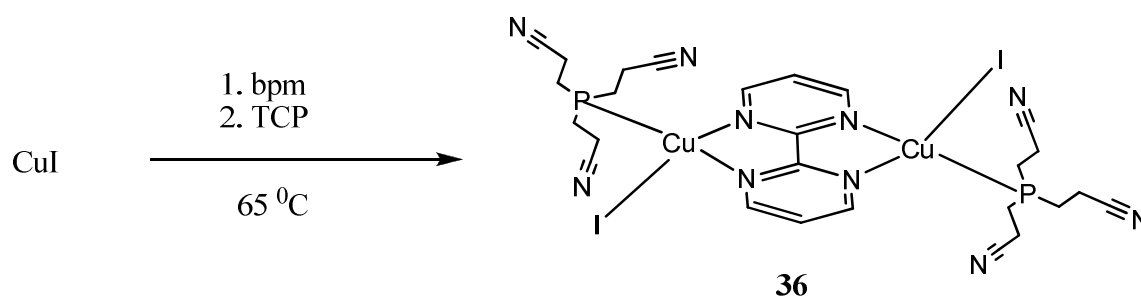
The compound was obtained as red crystalline material. Yield, 81%.



Scheme 6.3

6.1.4. $[\text{Cu}_2(\text{bpm})(\text{TCP})_2(\text{Br})_2]$ (36)

The compound was obtained as red crystalline material. Yield, 80 %



Scheme 6.4

6.2 Characterization of the complexes (33-36)

6.2.1 Elemental Analysis and Melting points

Elemental analysis was performed on Perkin Elmer EA 3000 CHNS/O Elemental Analyzer. Melting Points were measured using Buchi 510 Melting Point apparatus.

The samples were dried prior to analysis. The results are given in table 34.

Table 34. Results of Elemental Analysis and Melting Points of the complexes 33-36

Complex	C %	H %	N %	MP ($^{\circ}$ C)
33	50.79	4.51	8.07	200-203
	51.05	4.76	8.25	
34	41.89	3.72	6.66	205-208
	41.63	4.03	6.53	
35	38.98	3.24	17.05	194-197
	38.75	3.50	16.86	
36	32.39	2.69	14.16	190-193
	32.65	2.90	14.30	

6.2.2 Ultraviolet and Visible Spectroscopy

The UV-Vis spectra of the complexes were recorded in dichloromethane. Representative spectrum of complex 33 is given below in figure 32

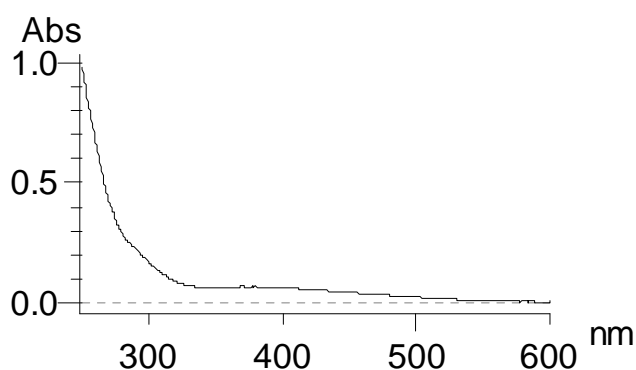


Figure 32. Electronic Spectrum of Complex 33

6.3.2.1 Electronic Spectra of Ligand and complexes

The absorption data of complexes (33-36) is given in table 35. UV-Vis spectra are given in Appendix A-II.

Table 35. Results of Ultraviolet and Visible Spectroscopy free Ligands and Complexes 33-36

Compound	Conc. M	$\lambda_{\text{max}} (\epsilon_{\text{molar}} \times 10^{-3})$
bmp	3.16×10^{-4}	280.0br(0.797), 291.0br(0.601)
TCP	2.02×10^{-4}	275.5s(0.495), 280.5s(0.445), 309.0br(0.346), 387.5br(0.024), 471.0br(0.012)
33	1.92×10^{-4}	266.5s(2.37), 294.0sh(1.01), 383.0br(0.338)
34	7.92×10^{-5}	270.5s(8.43), 291.0br(4.81), 379.5br(1.26)
35	1.01×10^{-4}	270.0s(1.55), 371.5br(0.613), 490.0br(0.316)

36	7.66×10^{-6}	270.0s(35.2), 283.0sh(30.28), 323.5br(11.71) 379.5br(11.09), 384.0br(11.61)
----	-----------------------	--

Wavelength (λ_{\max}) is in nanometer (nm) and molar extinction coefficient (ϵ_{molar} ($\text{M}^{-1} \text{cm}^{-1} \times 10^3$) is given in parenthesis. (s = sharp, sh = shoulder, br = broad) .

UV-Vis spectrum of 2,2'-bipyrimidine (bpm) shows broad absorption band at 280.0(797) and at 291.0(601) nm. These bands are ligand centered LC transitions. In bpm-phosphine complexes with bpm as a bridging ligand absorption band at 280.0(797) in free ligand shows a shift of 3.0-13.50 nm. Second broad absorption band in bpm ligand at 290.0 nm shows a shift of 4.0 nm. Broad bands at 383.0 (338), 490.0 (316), 379.5 (1260), 384.0 (11610), nm in Visible region of the spectrum are attributed to MLCT transitions as elaborated in previous chapters.

6.2.3 Fourier-Transformed Infrared Spectroscopy (FT-IR)

The FT-IR spectra were recorded using KBr pellets in the range of 4000-400 cm^{-1} . The assignment of the different vibrations was carried out by comparison with literature data [8].

The absorption wavenumbers are presented in table 36. FT-IR spectrum are listed in Appendix-V

Table 36. Infrared frequencies (cm^{-1}) and assignment for Complexes 33-36

Assignment	33	34	35	36
C-H stretch aromatics	3047w	3047w	3070w	3027w
C-H stretch alkanes	2914w	2915w	2903w	2919w
C-H bend	1648w	1671.0s	1648w	1648w

CH ₃ deformation	1550m	1550m	1559m	1554s
CH ring stretch	1427w	1427w	1403s	1403s
C-H in plane bend aromatic ring	1388s	1392s	1330w	
C-H OOP bend aromatic ring	822m	826m	826m	814w
Ring bend	690m	698m	667m	667m
Ring bend	512m	509m	504m	504m
Inter ring bend	478w	481w		

6.2.4 Far-Infrared analysis

Far-ir analysis were performed using high density polyethylene pellets (HDPE) .For Cu-X peak assignment we have used following empirical relationship proposed by Bowmaker et al [131]. Far-i.r. peak identification frequency is empirically correlated with the Cu-X bond length r . For CuCl and CuBr complexes, this relationship may be represented by

$$\nu/\text{cm}^{-1} = b(r/\text{\AA})^{-m} \quad (1)$$

where $b = 13800$ and 18000 and $m = 4.9$, 5.2 and 5.6 for $X = \text{Cl}$, Br and I respectively. The relationship was applied for bromocompounds 33 and 35 for which the x-ray analysis data are available.

Table 37. Far-Ir absorption data for Cu-Br bond in Complex 33 and 35

complex	$\overline{\nu}_{\text{Cu-Br}}^{\text{str}}$	
	$\overline{\nu}_{\text{Calc}}$	$\overline{\nu}_{\text{Obs}}$
33	182	180
35	179	181

A good agreement is obtained between the calculated and observed data. For compounds 33 and 35. Therefore, the Far-Ir absorptions at 180 and 181 cm^{-1} are assigned to $\overline{\nu}_{\text{Cu-Br}}^{\text{str}}$ in 33 and 35 respectively.

6.2.5 Single crystal X-ray crystallography

The crystallographic data of complexes whose single crystal were successful grown are given in table 38 and selected bond lengths and bond angles are given in table 39.

Table 38. Crystallographic Data Collection and Structure Refinement Parameters for Complexes 33-35

Complexes	33	34	35
Chemical Formula	$\text{C}_{44} \text{H}_{54} \text{Br}_2$ $\text{Cu}_2 \text{N}_6 \text{O}_2 \text{P}_2$	$\text{C}_{38} \text{H}_{37} \text{Cu I}_4$ $\text{N}_3 \text{O P}$	$\text{C}_{38} \text{H}_{37} \text{B Br}$ $\text{Cu N}_3 \text{P}$

Formula Mass , Da	1047.77	1153.82	720.94
Space Group	P-1	P-1	P-1
a, Å	9.5245(3)	9.6276(3)	10.9689(5)
b, Å	10.1619(3)	10.2665(3)	12.5742(6)
c, Å	14.2847(5)	14.2053(5)	12.9010(6)
α , deg	77.6700(10)	78.2520(10)	97.0690(10)
β , deg	73.8030(10)	74.5940(10)	104.1120(10)
γ , deg	62.3360(10)	63.1400(10)	93.5870(10)
V, Å ³	1170.17(7)	1201.87(7)	1704.61(14)
ρ_{calcd} , gcm ⁻³	1.487	1.594	1.405
Z	1	1	2
μ , mm ⁻¹	2.726	3.084	1.891
T, K	273(2)	298(2)	298(2)
λ , Å	0.71073	0.71073	0.71073
$R_1(F\sigma^2)^a$	0.0314	0.0337	0.0342
$WR_2(F\sigma^2)^b$	0.0859	0.0640	0.0627
GOF	1.038	0.746	0.606

$$^a R_1 = \sum (| | F_o | - | F_c | | / \sum | F_o | \quad ^b WR_2 = [\sum (w | F_o |^2 - | F_c |^2) / \sum | F_o |^2]^{1/2}$$

Table 39. Selected Bond Lengths (Å) and Bond Angles (°) of the complexes 33-35

33		34		35	
Cu1-N1	2.1134(15)	Cu1-N1	2.105(2)	Cu1-N2	2.091(2)
Cu1-N2	2.1500(15)	Cu1-N2	2.135(2)	Cu1- N1	2.096(2)
Cu1-P1	2.2079(5)	Cu1-P1	2.2089(9)	Cu1-P1	2.1774(9)
Cu1-Br1	2.4252(4)	Cu1-I1	2.5959(5)	Cu1-Br1	2.4237(5)
N1-Cu1	2.1134(15)	N2-Cu1	2.135(2)	Cu2-N3	2.089(2)
				Cu2-N4	2.123(3)
				Cu2-P2	2.1773(9)
				Cu2-Br2	2.4168(5)
N1-Cu1-N2	78.09(5)	N1-Cu1-N2	78.43(9)	N1-Cu1-N2	78.43(9)
N1-Cu1-P1	124.16(5)	N1-Cu1-P1	124.56(7)	N2-Cu1-P1	126.26(7)
N2-Cu1-P1	115.05(4)	N2-Cu1-P1	115.45(8)	N1-Cu1-P1	123.59(7)
N1-Cu1-Br1	108.98(5)	N1-Cu1-I1	107.78(7)	N2-Cu1-Br1	107.54(7)
N2-Cu1-Br1	107.87(5)	N2-Cu1-I1	108.63(7)	N1-Cu1-Br1	110.58(6)
N2-Cu1-I1	108.63(7)	P1-Cu1-I1	115.79(2)	P1-Cu1-Br1	106.62(3)

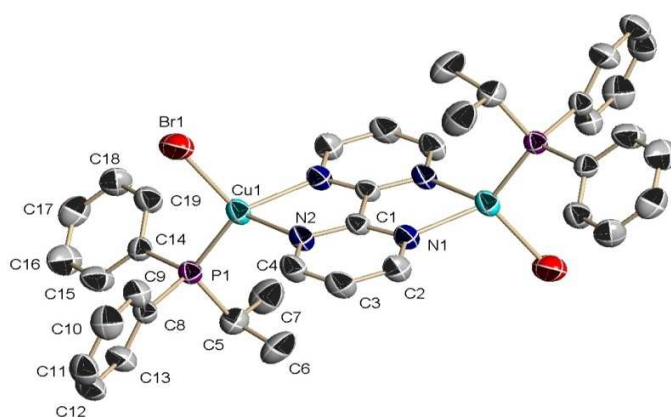


Figure 33. X-ray structure of Complex 33. Thermal ellipsoids are drawn at 30 % probability. Hydrogen atoms and DMF molecule are omitted for clarity

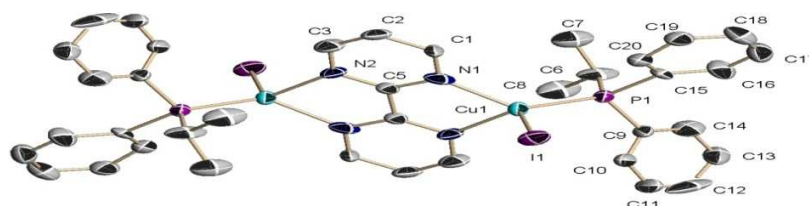


Figure 34. X-ray structure of Complex 34. Thermal ellipsoids are drawn at 30 % probability. Hydrogen atoms are omitted for clarity

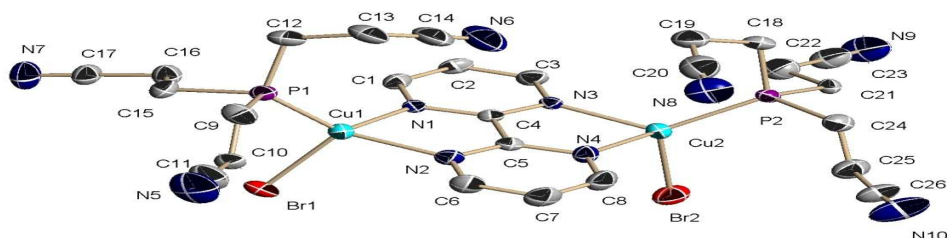


Figure 35. X-ray structure of Complex 35. Thermal ellipsoids are drawn at 30 % probability. Hydrogen atoms are omitted for clarity

The X-ray structure shows that complexes 33-35 are mixed ligand binuclear complexes. Two $\text{Cu}(\text{PR}_3)(\text{X})$ moieties are linked through nitrogen atoms of 2,2'-bipyrimidine bridge (bpm). In all complexes N-Cu-N bite show a range of $78.09(5)$ to $78.43(9)^\circ$ which is a deviation from a regular angle of 90° . The N-Cu-Br angle range observed is $106.90(7)$ to $108.98(5)^\circ$. Similarly for N-Cu-I $108.63(7)$ the deviation is observed on both type of bonds from normal tetrahedral geometry. For N-Cu-P link the deviation observed is greater (i.e. 16°) from tetrahedral bond angle in complexes 35 and 36. Which have bulky tris-(2-cyanoethyl)phosphine with the metal ion P-Cu-Br $114.73(3)$ and P-Cu-I $115.79(2)^\circ$ angles are also show large deviation from 109.5° . The deviation is likely the result of steric effects imposed by the bulky phosphine and halide ions.

6.2.6 Nuclear Magnetic Resonance Spectroscopy

^1H and ^{31}P -NMR analysis were performed by dissolving the samples in deuterated solvent $\text{DMSO}-d_6$

Table 40. ^1H and ^{31}P -NMR shifts for Complexes 34-36

Complexes	^1H -NMR shifts $\delta(\text{PPM})$	^{31}P -NMR $\delta(\text{PPM})$	^{31}P -NMR
34	0.830(s), 1.00(m), 2.06(s), 2.48(d), 2.70(s), 2.88(s), 7.38(m), 7.51(m), 7.80(m), 7.90(s), 8.58(s), 9.03(s)	37.32	37.17
35	1.02(m), 2.06(m), 7.95(m), 9.23(m)	-12.52	12.04
36	1.03(t), 2.06(t), 2.18(s), 2.30(s), 2.72(d), 3.58(m), 7.23(m), 7.41(s), 7.51(s), 7.95(m), 8.18(d), 8.74(d), 9.24(m)	-12.21	12.35

$$^{***} \Delta(\delta^{31}\text{P}) = \delta^{31}\text{P}_{\text{complex}} - \delta^{31}\text{P}_{(\text{PR}_3)}$$

Shifts from 0.83-3.54 ppm in ^1H -NMR are attributed to the methyl protons of phosphines. Shifts of 7.23-9.24 are the aromatic ring shifts of phosphines and bpm bridge. A $\Delta(\delta^{31}\text{P})$ resonance shift is observed after complexation. This is consistent with the coordination to the metal ion. Higher ^{31}P resonance shift of $\text{Ph}_2(\text{i-Pr})\text{P}$ ligand in compound 34 as compared with $[\text{NC}(\text{CH}_2)_2]_3\text{P}$ in compounds 35 and 36, is consistent with the relative basic character of the two phosphines.

Chapter 7

Copper(I) mixed ligand complexes with 2,3-bis(2-pyridyl)pyrazine (bpp) bridging ligand

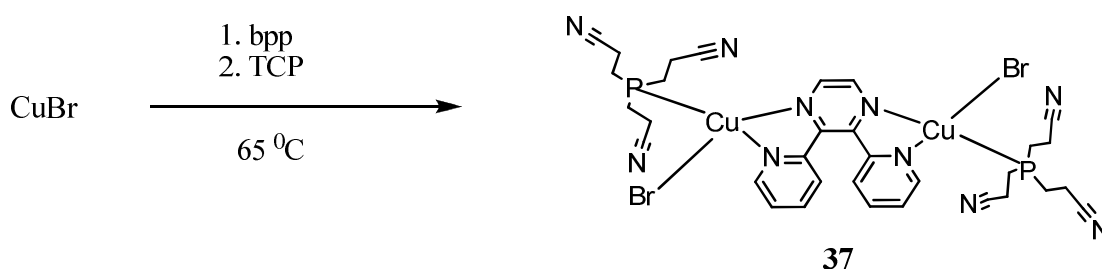
2,3-Bis(2-pyridyl)pyrazine (bpp) is a versatile polypyridyl type ligand with four nitrogen donor atoms like 2,2'-bipyrimidine but with a greater flexibility. The crystal structure of bpp was determined 18 years ago [133] and its complex formation with various metals has been the subject of several recent reports because of the spectroscopic, photochemical and photophysical properties of these bpp-containing compounds[134-135] concerning the complexes of bpp with first row transition metal ions, X-ray structures of complexes of bpp with Cu(I) [136] and Cu(II) [137-141] metal ion have shown that dpp can adopt not only the anticipated terminal bidentate and bridging bis-bidentate coordination modes but also the unexpected bidentate/monodentate [140] and bidentate / bis-monodentate [142] bridging modes. In this chapter synthesis and characterization of binuclear and mononuclear Cu(I)(PR₃)(X) bpp bridged mixed ligand complexes is described.

7.1 Synthesis

A following general procedure was followed for the synthesis of compounds (37-40). PR_3 (1.0 mmol), CuX (1.0 mmol) and 2,3-bis(2-pyridyl)pyrazine (0.5 mmol) were placed in an oven dried 100 ml Schlenk flask in glove box, sealed with rubber septum and taken out. Freshly distilled, dried dimethylformamide (35.0 ml) was injected through the septum using a long needle. The mixture was stirred at room temperature for 2h to result in a red solution. The resultant solution was filtered and left over few days to get red crystals of the product.

7.1.1. $[\text{Cu}_2(\text{bpp})(\text{TCP})_2(\text{Br})_2]$ (37)

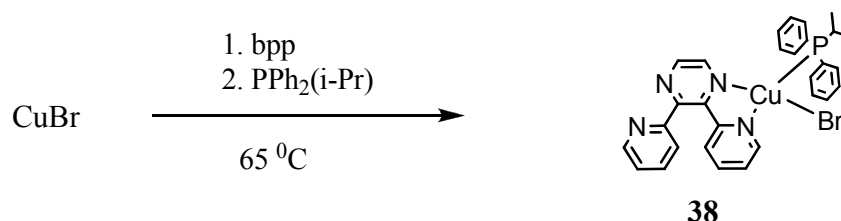
The compound was obtained as red crystalline material. Yield, 70 %.



Scheme 7.1

7.1.2. $[\text{Cu}(\text{bpp})(\text{PPh}_2(\text{i-Pr}))(\text{Br})]$ (38)

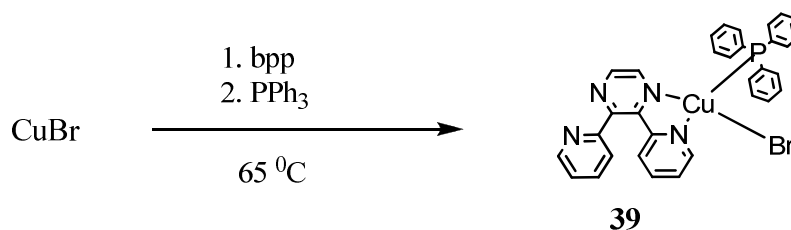
The compound was obtained as yellow crystalline material. Yield, 67 %.



Scheme 7.2

7.1.3. [Cu(bpp)(Ph₃P)(Br)] (39)

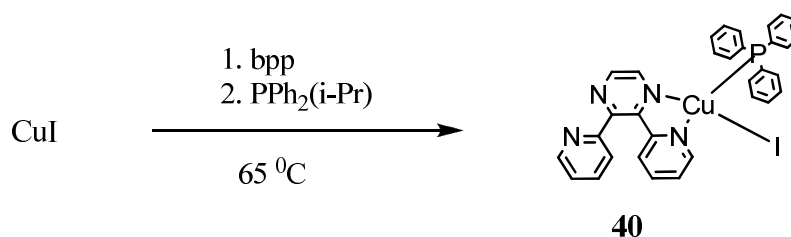
The compound was obtained as yellow crystalline material. Yield, 65 %.



Scheme 7.3

7.1.4. [Cu(bpp)(PPh₂(i-Pr))(I)] (40)

The compound was obtained as yellow crystalline material. Yield, 71% .



Scheme 7.4

7.2 Characterization of the complexes (37-40)

7.2.1 Elemental Analysis and Melting points

Elemental analysis was performed on Perkin Elmer EA 3000 CHNS /O Elemental Analyzer. The samples were dried prior to analysis. The results of the complexes are given in table 41

Table 41. Results of Elemental Analysis and Melting Points of the Complexes 37- 40

Complex	C %	H %	N %
37	42.37	3.74	15.43
	42.55	4.03	15.23
38	57.68	4.14	9.27
	57.35	4.24	9.38
39	60.07	3.90	8.75
	60.27	3.60	8.84
40	48.77	3.50	7.84
	48.90	3.70	7.93

7.2.2 Ultraviolet and Visible Spectroscopy

The UV-Vis spectra of the complexes were recorded in dichloromethane.

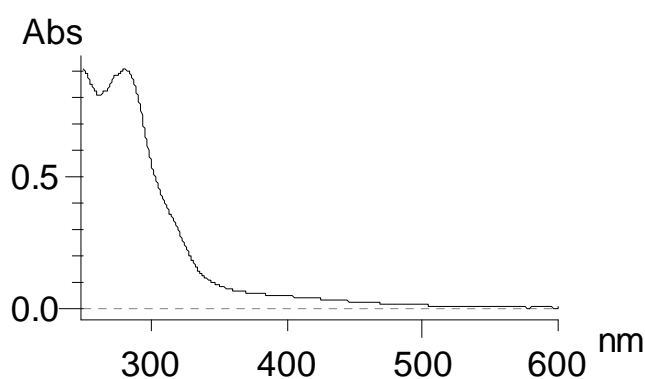


Figure 36. UV-Visible Spectrum of Complex 37

7.2.2.1 Electronic Spectra of Ligand and complexes

Electronic spectra of 2,3-bis(2-pyridyl)pyrazine and complexes synthesized were recorded. The absorption data of complexes is given in table 42. The representative spectrum is given in figure.33 above. UV-Vis spectra are given in Appendix A-III.

Table 42. Results of Ultraviolet and Visible Spectroscopy for bpp and Complexes 38-40

Compound	Conc. M	λ_{\max} ($\epsilon_{\text{molar}} \times 10^{-3}$)
bpp	2.15×10^{-4}	285.0s(2.41), 341.0br(0.232)
38	1.00×10^{-5}	282.5s(38.01), 303.0br(18.7), 383.5br(1.1), 452.5br(0.7)

39	3.31×10^{-5}	281.0s(27.50), 409.5br(1.38)
40	5.58×10^{-6}	282.5s(126.14), 315.0br(50.0), 385.0br(5.01)

Wavelength (λ_{\max}) is in nanometer (nm) and molar extinction coefficient ($\epsilon_{\text{molar}} \text{ M}^{-1} \text{ cm}^{-1} \times 10^3$) is given in parenthesis. (s = sharp, sh = shoulder, br = broad)

UV-Vis spectrum of 2,3-bis(2-pyridyl)pyrazine (bpp) showed strong absorption band at 285.0() nm and a weak shoulder at 341.5 () nm. Peak at 285.0() showed a shift of 4.0 nm upon coordination of bpe bridge with $\text{Cu}(\text{PR}_3)(\text{X})$ units. All absorptions are result of intra-ligand (IL π - π^*) transitions [13]. Broad bands seen in complexes from 383.5(1100) to 452.5(700) in Visible region of the spectrum are attributed to MLCT transitions.

7.2.3 Fourier-Transformed Mid Infrared Spectroscopy (MidFT-IR)

The FT-IR spectra were recorded using KBr pellets in the range of 4000-400 cm^{-1} . The absorption wavenumbers are presented in table 43 and the representative spectrum of the precursor-A is given in figure 7.3. FT-IR spectrum are listed in Appendix-V

Table 43. Infrared frequencies (cm^{-1}) and assignment for Complexes 37-39

Assignment	37	38	39
C-H stretch aromatics	3031w	3042w	3023w
C-H stretch alkanes	2914w	2922w	2907w
C-H in plane bend aromatic ring	1497m	1559m	1554w

C-H OOP bend aromatic ring	1156w	1151w	1163m
Ring bend	783m	791m	780m
Ring bend	663w	698m	663w
Inter ring bend	504w	512m	512m

7.2.4 FAR-IR analysis

In order to assign Cu-Br stretching frequencies for compounds 37-38, Bowmakers empirical formula was used [143]

Table 44. Far-IR absorption data for Cu-Br bond Strechthng in Complexes (37-38)

complex	$\bar{\nu}_{\text{Cu-Br}}^{\text{str}}$	
	$\bar{\nu}_{\text{Calc}}$	$\bar{\nu}_{\text{Obs}}$
37	Cu-Br	180
38	Cu-Br	186

On this ground the far-IR absorptions at 180 and 186 cm^{-1} were assigned to $\bar{\nu}_{\text{Cu-Br}}^{\text{str}}$ in complexes 37-38 respectively.

7.2.5 Single crystal X-ray crystallography

The crystallographic data of complexes for which single crystals were successfully grown are given in table 7.4 and selected bond lengths and bond angles are given in table 7.5.

Table 45. Crystallographic Data Collection and Structure Refinement Parameters for Complexes 37-38 and 40

Complexes	37	38	40
Chemical Formula	C ₃₈ H ₃₇ B Br Cu N ₃ P	C ₂₅ H ₃₀ Br ₂ Cu ₂ N ₄ P ₂	C ₃₅ H ₃₇ Cu I ₂ N ₄ P ₂
Formula Mass , Da	720.94	735.37	892.97
Space Group	P-1	P-1	P-1
a, Å	9.2725(7)	9.1204(3)	9.6850(5)
b, Å	9.6154(7)	9.9851(4)	12.0261(6)
c, Å	15.1185(12)	16.3342(6)	13.0218(7)
α, deg	85.238(2)	75.1260(10)	95.5660(10)
β, deg	89.636(2)	86.4920(10)	98.9920(10)
γ, deg	86.527(2)	86.3450(10)	102.9020(10)
V, Å ³	1340.83(18)	1433.21(9)	1446.46(13)

$\rho_{\text{calcd}}, \text{gcm}^{-3}$	2.404	1.704	2.050
Z	2	2	2
μ, mm^{-1}	1.786	4.405	3.037
T, K	298(2)	297(2)	296(2)
$\lambda, \text{\AA}$	0.71073	0.71073	0.71073
$R_1(F\sigma^2)^a$	0.0444	0.1340	0.0413
$WR_2(F\sigma^2)^b$	0.1371	0.3701	0.0772
GOF	0.0917	0.951	0.718

$$^a R_1 = \Sigma(| | F_o | - | F_c | | / \Sigma | F_o | . \quad ^b WR_2 = [\Sigma(w | F_o |^2 - | F_c |^2) / \Sigma | F_o |^2]^{1/2}$$

Table 46. Selected Bond Lengths (Å) and Bond Angles (°) of the complexes 38 and 40

38		40	
Cu1-N1	2.089(4)	Cu1-N1	2.085(9)
Cu1-N2	2.124(5)	Cu1-N2	2.098(8)
Cu1-P1	2.2076(15)	Cu1-P1	2.201(3)
Cu1-Br1	2.4153(9)	Cu1-Br2	2.4100(19)
N1-Cu1-N2	78.65(17)	N1-Cu1-N2	78.5(3)
N1-Cu1-P1	118.41(12)	N1-Cu1-P1	117.9(2)
N2-Cu1-P1	117.69(13)	N2-Cu1-P1	116.4(3)
N1-Cu1-Br1	105.25(12)		

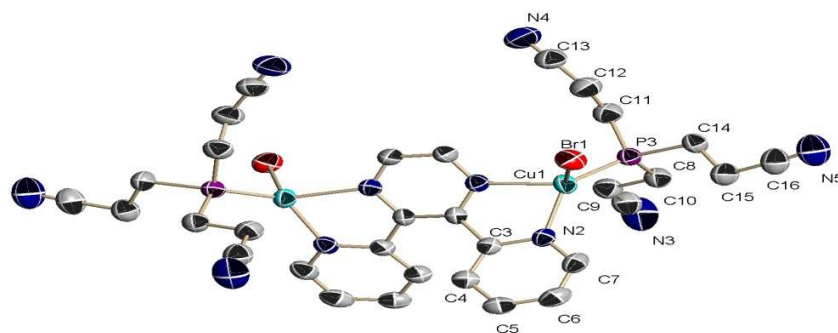


Figure 37. X-ray structure of Complex 37. Thermal ellipsoids are drawn at 30% probability. Hydrogen atoms are omitted for clarity

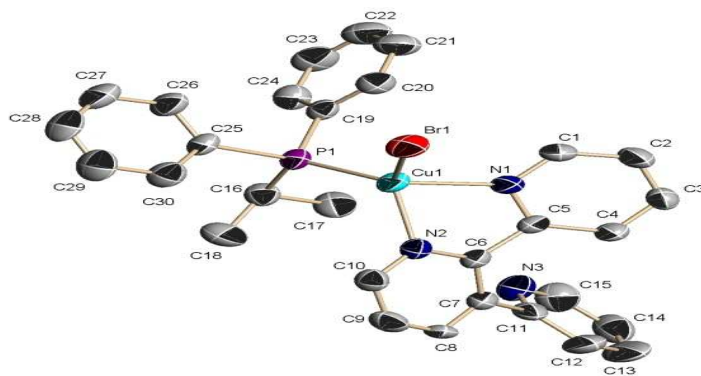


Figure 38. X-ray structure of Complex 38. Thermal ellipsoids are drawn at 30% probability. Hydrogen atoms are omitted for clarity

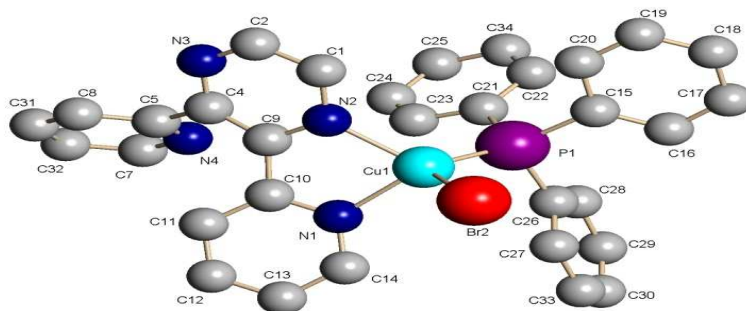


Figure 39. X-ray structure of Complex 39. Spheres are drawn at 30% probability. Hydrogen atoms are omitted for clarity

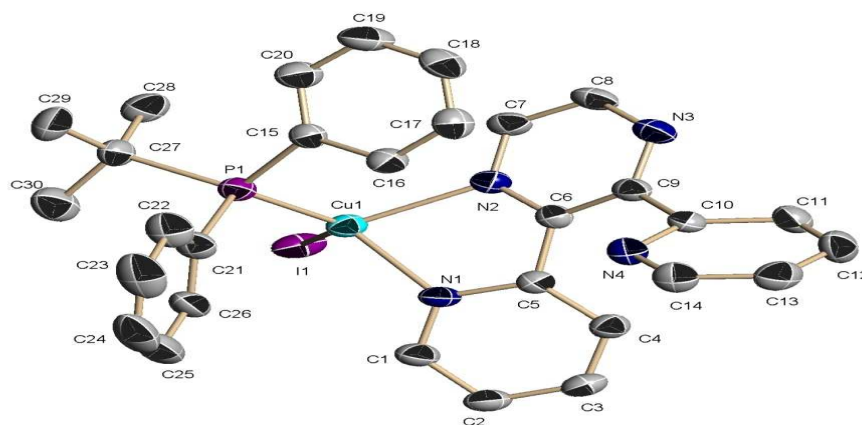


Figure 40. X-ray structure of Complex 40. Thermal ellipsoids are drawn at 30% probability. Hydrogen atoms are omitted for clarity

Among the complexes, only 37 was a binuclear complex; where two Cu(TCP)Br moieties are bridged by bpp ligand with a bis-bidentate coordination mode. Complex 38-40 were found to be mononuclear with a terminal bidentate coordination mode for bpp. In all complexes a distorted tetrahedral geometry is observed. The N-Cu-N and P-Cu-N bond angles are 77.78(11) to 117.90(2). The Cu-P and Cu-Br distances are in the ranges 2.201(3) to 2.2076(15) and 2.4100(19) to 2.4153(9) respectively.

Chapter 8

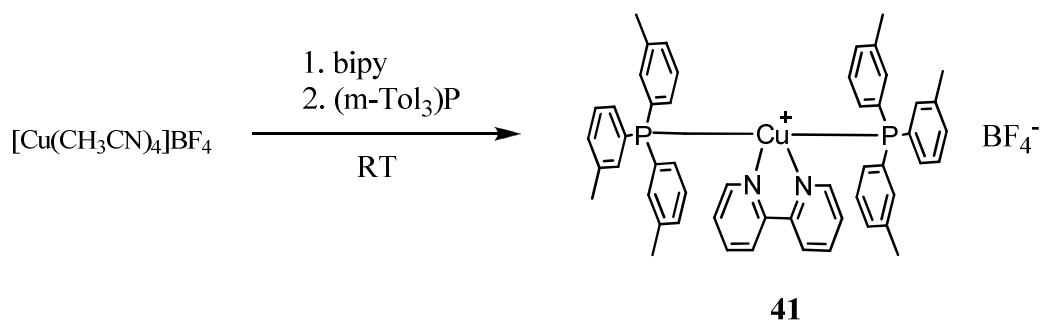
Mononuclear Copper(I) mixed ligand complexes with different phosphines

8.1 Synthesis

A general procedure was followed for the synthesis of compounds (41-55). Diimine (1.00 mmol) and $[\text{Cu}(\text{CH}_3\text{CN})_4[\text{BF}_4]]$ (1.0 mmol) were placed in an oven dried 100 ml Schlenk flask in glove box, sealed with rubber septum and taken out. Freshly distilled, dried dichloromethane (30.0 ml) was injected through the septum using a long needle. The mixture was stirred at room temperature for 2h to result in a brown solution. Then a solution of phosphine (1.00 mmol) in dichloromethane (5.0 ml) was added drop wise with stirring. Resultant blue green solution was stirred for another 12h and filtered; the filtrate was carefully layered with 30.0 ml diethylether to get yellow color binuclear product. Recrystallization was carried out in dry dimethylformamide (DMF).

8.1.1 $[\text{Cu}(\text{m-Tol}_3\text{P})_2(\text{bipy})][\text{BF}_4]$ (41)

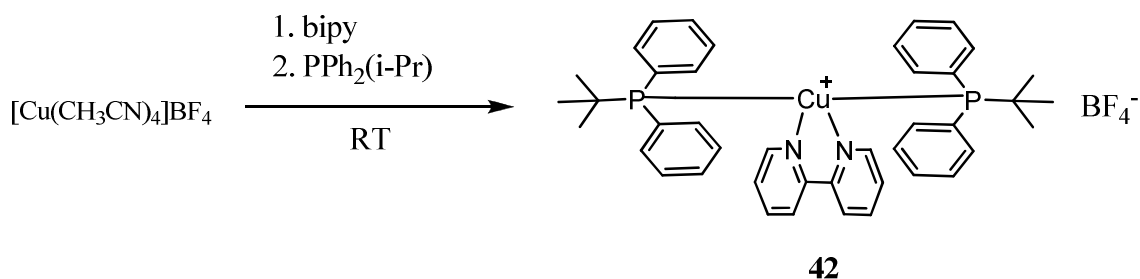
The compound was obtained as yellow crystalline material. Yield, 75 %



Scheme 8.1

8.1.2 $[\text{Cu}(\text{PPh}_2(\text{i-Pr}))_2(\text{bipy})][\text{BF}_4]$ (42)

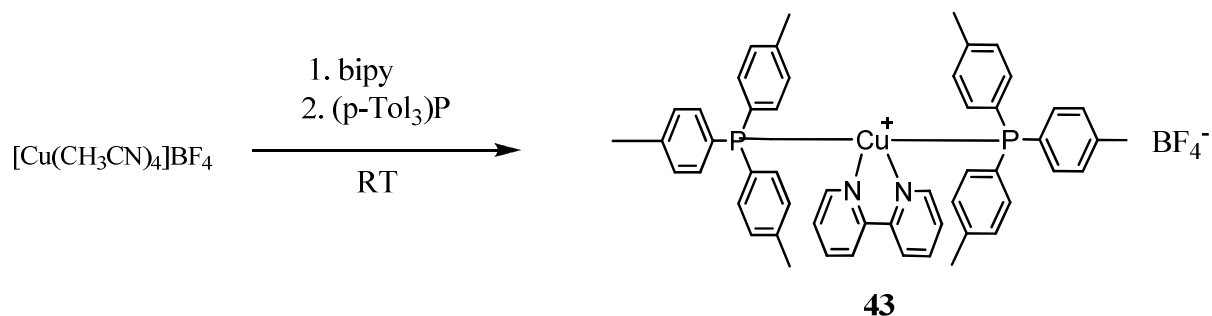
The compound was obtained as yellow crystalline material. Yield, 68 %



Scheme 8.2

8.1.3 $[\text{Cu}(\text{p-Tol}_3\text{P})_2(\text{bipy})][\text{BF}_4]$ (43)

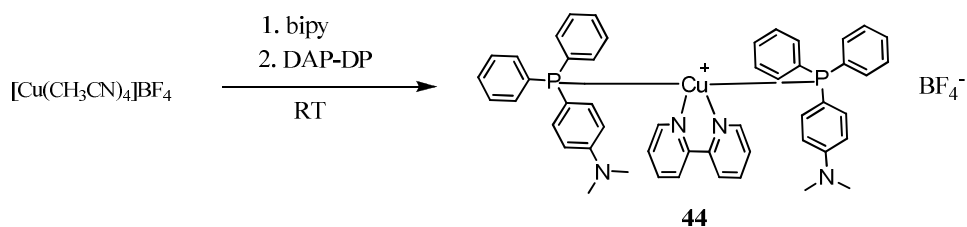
The compound was obtained as yellow crystalline material. Yield, 73 %



Scheme 8.3

8.1.4 [Cu(DAP-DP)₂(bipy)][BF₄] (44)

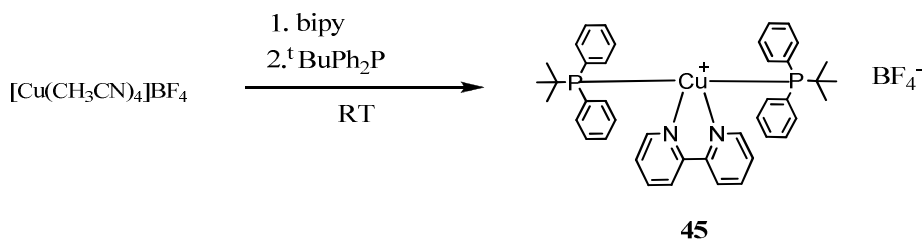
The compound was obtained as yellow crystalline material. Yield, 60 %



Scheme 8.4

8.1.5 [Cu(^tBuPh₂P)₂(bipy)][BF₄] (45)

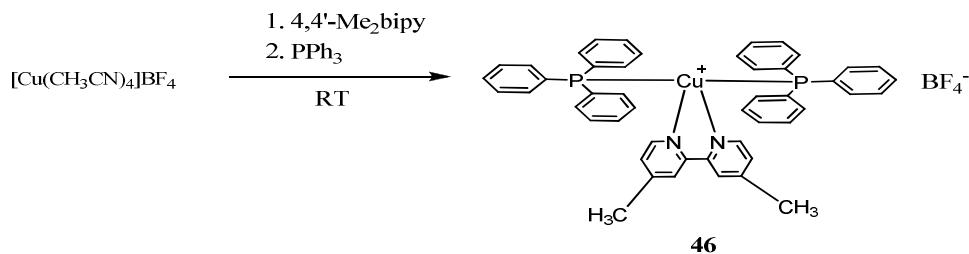
The compound was obtained as yellow crystalline material. Yield, 63 %



Scheme 8.5

8.1.6 [Cu(PPh₃)₂(4,4'-Me₂bipy)][BF₄] (46)

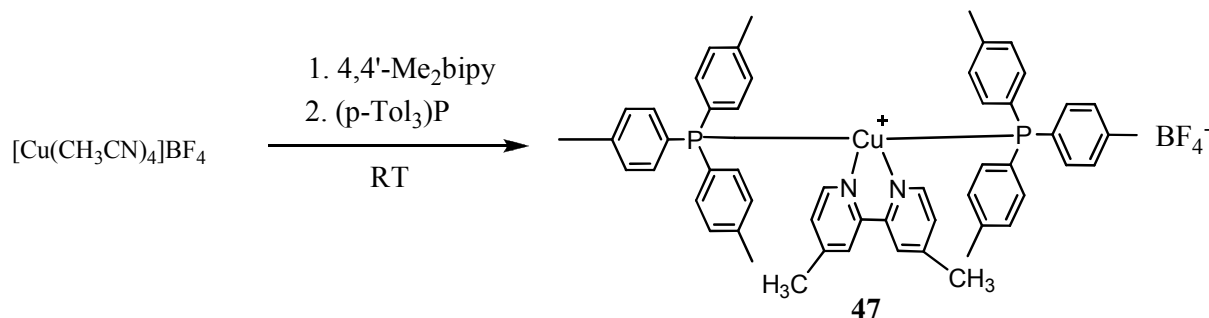
The compound was obtained as yellow crystalline material. Yield, 77 %



Scheme 8.6

8.1.7 [Cu(p-Tol₃P)₂(4,4'-Me₂bipy)][BF₄] (47)

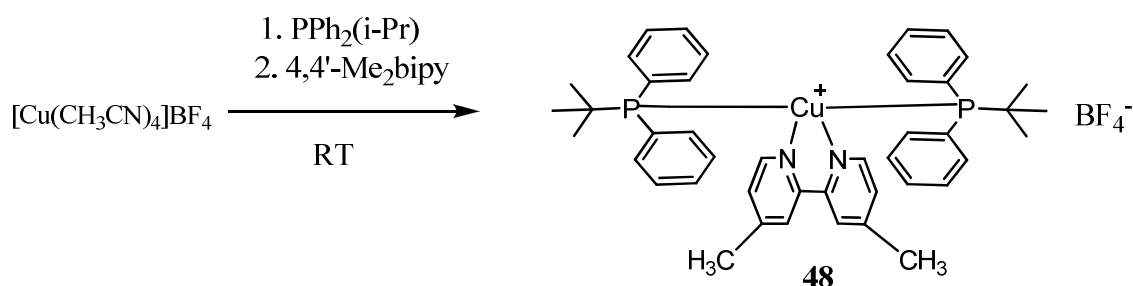
The compound was obtained as yellow crystalline material. Yield, 69%



Scheme 8.7

8.1.8 [Cu(PPh₂(i-Pr))₂(4,4'-Me₂bipy)][BF₄] (48)

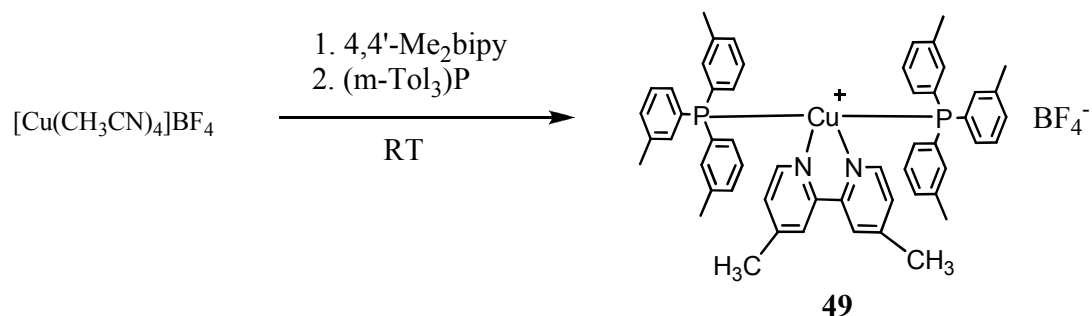
The compound was obtained as yellow crystalline material. Yield, 65 %



Scheme 8.8

8.1.9 [Cu(m-Tol₃P)₂(4,4'-Me₂bpy)][BF₄] (49)

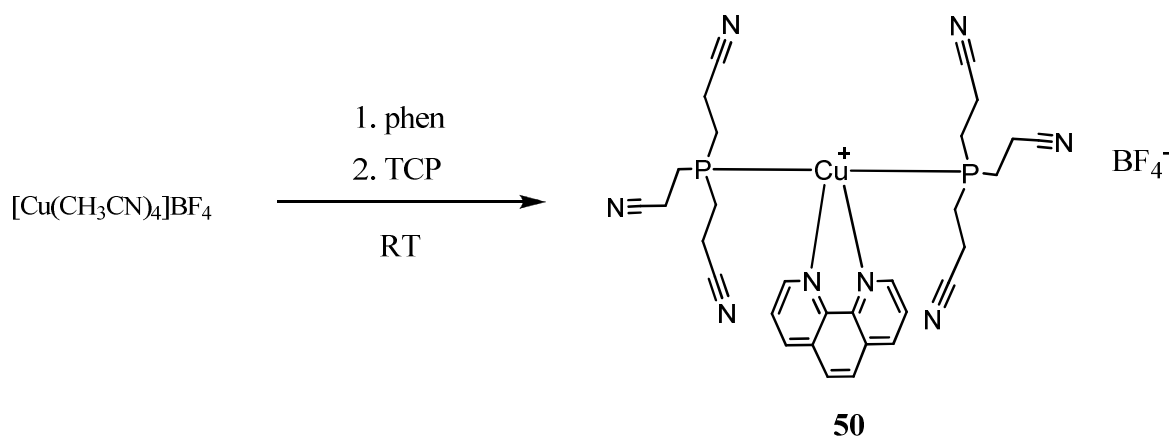
The compound was obtained as yellow crystalline material. Yield, 71%



Scheme 8.9

8.1.10 $[\text{Cu}(\text{TCP})_2(\text{phen})][\text{BF}_4]$ (50)

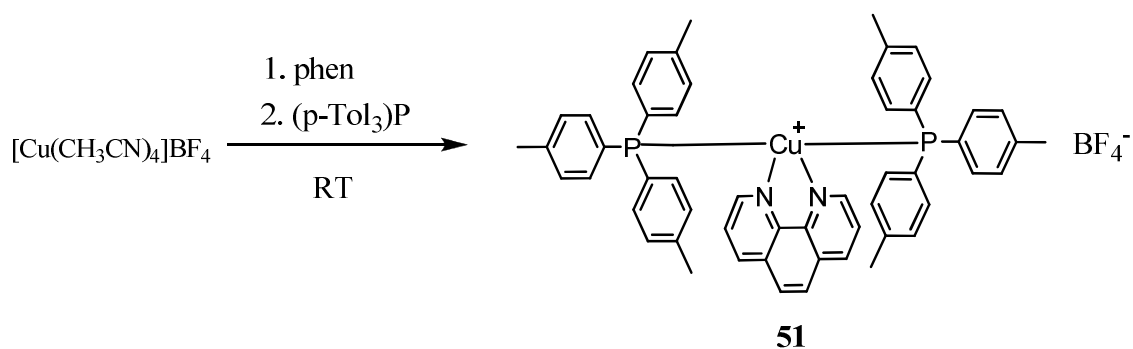
The compound was obtained as yellow crystalline material. Yield, 51%



Scheme 8.10

8.1.11 $[\text{Cu}(\text{p-Tol}_3\text{P})_2(\text{phen})][\text{BF}_4]$ (51)

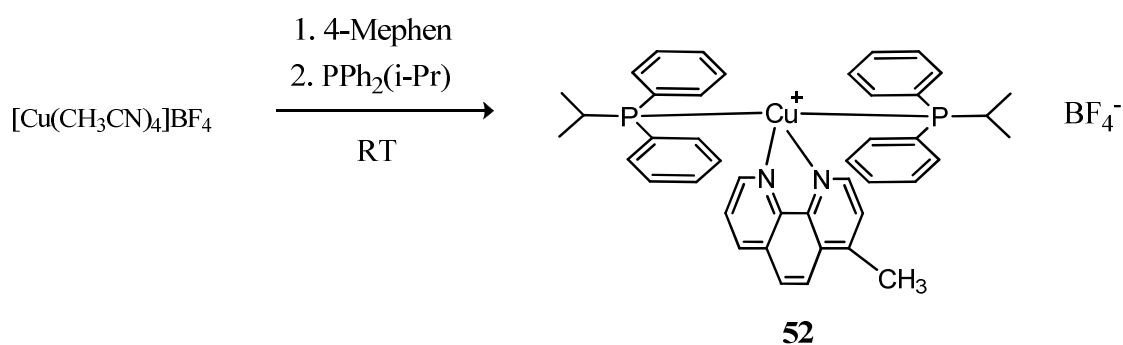
The compound was obtained as yellow crystalline material. Yield, 68%



Scheme 8.11

8.1.12 $[\text{Cu}(\text{PPh}_2(\text{i-Pr}))_2(4\text{-Mephen})][\text{BF}_4]$ (**52**)

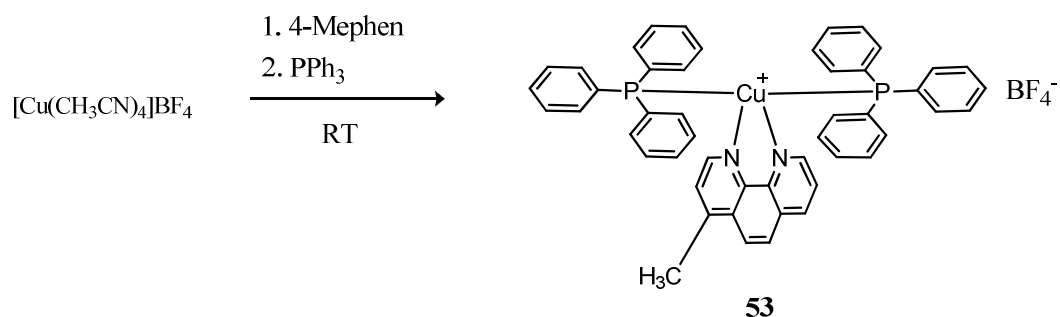
The compound was obtained as yellow crystalline material. Yield, 72 %



Scheme 8.12

8.1.13 $[\text{Cu}(\text{PPh}_3)_2(4\text{-Mephen})][\text{BF}_4]$ (**53**)

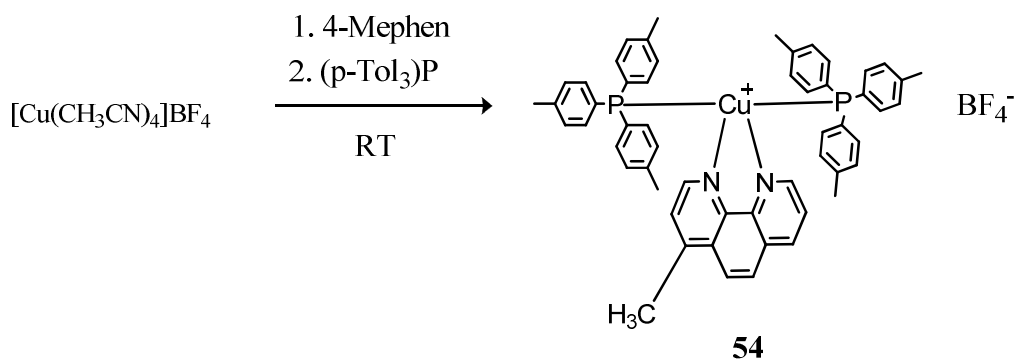
The compound was obtained as yellow crystalline material. Yield, 66 %



Scheme 8.13

8.1.14 [Cu(p-Tol₃P)₂(4-Mephen)][BF₄] (54)

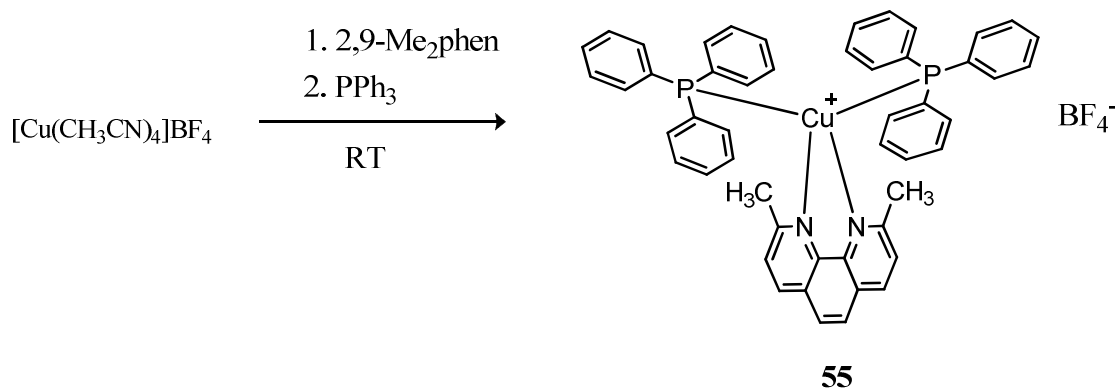
The compound was obtained as yellow crystalline material. Yield, 74 %.



Scheme 8.14

8.1.15 [Cu(PPh₃)₂(2,9-Me₂phen)][BF₄] (55)

The compound was obtained as yellow crystalline material. Yield, 73 %.



Scheme 8.15

8.2 Characterization of the complexes (41-55)

8.2.1 Elemental Analysis

Elemental analysis was performed on Perkin Elmer EA 3000 Elemental Analyzer. The samples were dried prior to analysis. The results of the complexes are given in table 47

Table 47. Results of Elemental Analysis of the Complexes 41-55

Complex	C %	H %	N %
41	Calc: 68.26	5.46	3.06
	Found: 67.98	5.75	3.24
42	63.12	5.25	3.68
	63.40	5.45	3.90
43	68.26	5.46	3.06
	68.15	5.64	3.19
44	65.35	5.44	6.09
	65.65	5.25	6.24
45	63.78	5.81	3.54
	63.59	5.96	3.74
46	67.12	4.89	3.26
	67.37	4.83	3.27
	68.78	5.72	2.96

47	68.52	5.78	3.06
48	63.78	5.81	3.54
	63.88	5.85	3.65
49	68.78	5.72	2.96
	69.05	5.86	3.16
50	46.24	4.11	3.59
	46.50	4.14	3.70
51	69.03	5.85	2.98
	69.19	5.88	3.15
52	64.49	5.36	3.49
	64.57	5.30	3.35
53	67.73	4.60	3.22
	67.93	4.82	3.45
54	69.47	5.46	2.94
	69.77	5.24	3.06
55	68.01	4.75	3.17
	68.29	4.78	3.27

8.2.2 Electronic Spectra of Complexes

The absorption data of complexes (41-55) is given in table 48. The absorption maxima are listed for all energy bands. UV-Vis spectra are given in Appendix A-II. A representative spectrum of complex 46 is given below in figure 41.

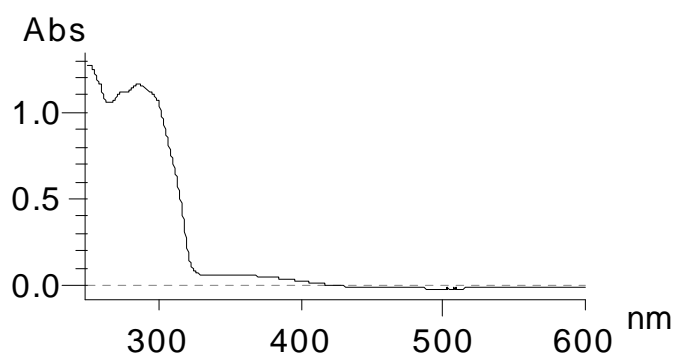


Figure 41. UV-Visible Spectrum of Complex 46

Table 48. Results of Ultraviolet and Visible Spectroscopy for free Ligands and Complexes 42-51 and 54-55

Compound	Conc. M	λ_{max} ($\epsilon_{\text{molar}} \times 10^{-3}$)
$t\text{BuPh}_2\text{P}$	8.25×10^{-5}	259.5s(4.65),265.0sh(4.50),272.0sh(3.80)
PPh_3	5.72×10^{-5}	264.0s(2.83),272.5sh(2.63),268.5sh(2.74)
42	6.33×10^{-7}	253.0br(935.38),274.0s(775.67),301.0(417.06),308.0sh(289.09), 378.0br(56.87)
43	3.98×10^{-7}	228.5s(100),308.0sh(50.50),366.0br(11.8)

44	1.63×10^{-4}	259.0s(9.18), 380.5br(.245)
45	1.64×10^{-6}	252.5sh(773.74),259.5sh(700.60),273.0br(678.65)286.0s(707.92), 359.0br(35.97)
46	1.33×10^{-6}	255.0br(788.63),308.0sh(242.85),357.5br(63.15)
48	3.81×10^{-7}	228.0s(10476),268.5s(1892.3),289.5sh(1283.46),304.0sh(803.14),329.0br(314.96), 362.0br(146.98)
49	2.27×10^{-7}	252.0s(1133.45),283.5s(1039.64),348.0br(83.70),478.5br(39.64)
50	2.33×10^{-7}	264.0s(917.18),272.0s(939.91),287.5s(1042.91), 299.5s(1103.00), 313.5s(1025.75)
51	3.40×10^{-7}	271.5s(1350.0),299.0sh(923.52),314.5sh(438.23), 381.0br(58.82)
54	2.49×10^{-7}	270.5s(1148.59),297.0sh(477.91),303.0sh(349.3),315.0sh(184.73), 329.0sh(72.07)
55	2.58×10^{-6}	269.5s(505.44),288.0sh(211.24),372.0br(28.29)

Wavelength (λ_{\max}) is in nanometer (nm) and molar extinction coefficient ($\epsilon_{\text{molar}} \text{ M}^{-1} \text{ cm}^{-1} \times 10^3$) is given in parenthesis. (s = sharp, sh = shoulder, br = broad)

Free phosphines show strong absorption in region-IV from 259.5 (4.65) to 272.5 (2.63) nm which are typical ligand-centred (LC) bands involving $\pi\text{-}\pi^*$ transitions. This LC band shifts by 6.0-14.0 nm upon complexation with diimines. Visible part of the

spectrum of the complexes consists of weak absorption bands at 359.0 (63.15) to 478.5(39.64) which arise from metal-to-ligand charge-transfer (MLCT) electronic transitions. These MLCT bands in the case of complexes occur because the Cu^+ ion can be easily oxidized as the diimine ligands possess low energy empty π^* orbitals. Substituted diimines exhibit intense absorption maxima than those of unsubstituted ones.

8.2.3 Excitation and Emission spectroscopy

8.2.3.1 Excitation and emission study of diimines

Excitation and Emission spectra of coordination complexes 42-44 & 47 and 52 were recorded in dichloromethane. Excitation and emission spectrum are given in Appendix-III

Table 49. Excitation and Emission Wavelengths of Complexes 42-44, 47 and 52

Complex	λ_{ex}	λ_{em}
42	320	422
43	310	440
44	340	477
47	310	358
52	340	380

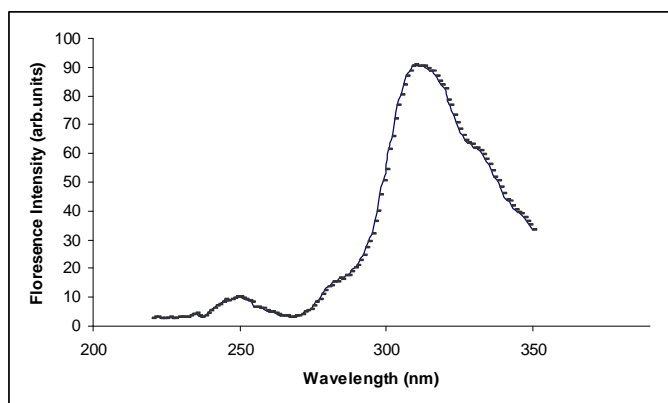


Figure 42. Excitation Spectrum of Complex 42

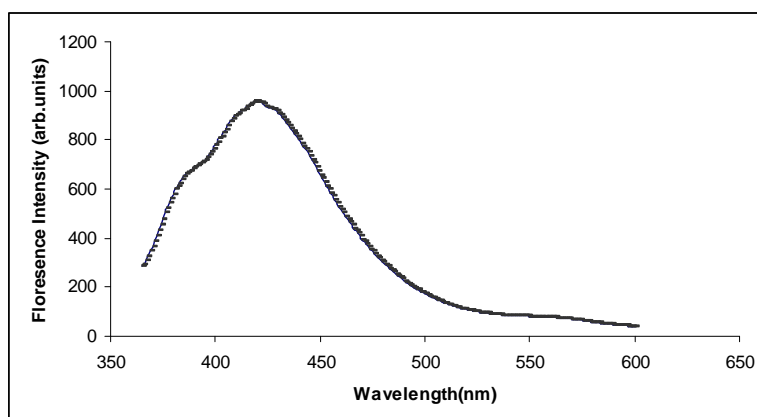


Figure 43. Emission Spectrum of Complex 42

All complexes show excitation maxima in the range of 310.0-340.0 nm and emission maxima 380.0-477.0 nm.

8.2.4 Fourier-Transformed Infrared Spectroscopy (FT-IR)

The FT-IR spectra were recorded using KBr pellets in the range of 4000-400 cm^{-1} . FT-IR spectrum are listed in Appendix-V

Table 50. Infrared frequencies (cm^{-1}) and assignment for Ligand and Complexes 42-46 & 48-49

Assignment	42	43	44	45	46	48	49
C-H stretch aromatics	3035w	3054w	3016w	3050w	3050w	3042w	3023w
C-H stretch alkanes	2907w	2922w	2918w	2925w	2920w	2953w	2921w
C-H bend	1690w	1663w	1659m	1604s	1650w	1605m	1608m
C-H ring stretch	1590s	1593s	1593s	1550w	1595 m	1551m	1551w
C-H in plane bend aromatic ring	1473m	1470m	1490w	1501m	1473m	1477m	1492w
Aromatic ring stretch and bend	1049s	1033s	1054s	1055s	1050s	1041s	1060s
C-H OOP bend aromatic	884w	813m	806s	854m	811m	814m	805m
CH OOP bend	780s	755m	764m	744m	749s	741m	707m
Ring bend	692s	696m	657w	696m	699s	697m	627w
Ring bend	520w	514w	515s	518m	516m	514m	512m
Interring bend	452s	419w	435w	431w	493m		427w

In complexes (17-25) C-H in plane bending of the aromatic ring is observed at 1033.8 to 1060.0 cm^{-1} and 804.9 to 814.6 cm^{-1} CH OOP bend. The aromatic C=C stretching are found in the range of 1403 to 1663 cm^{-1} . Shift of 26.2 cm^{-1} from 1034 to 1060 cm^{-1} and 9.7 cm^{-1} from 810-839 cm^{-1} is attributed to complexation of diimines with the bridging ligand. These shifts are the consequence of the change in electron density of diimine ring when the non-bonding pair of electrons on the nitrogen atom is donated to the metal ion [9]. The aromatic C=C stretching are found in the range of 1426-1672 cm^{-1} .

8.2.5 Single Crystal X-ray Analysis

The crystallographic data of complexes for which single crystal were successfully grown are given in tables 51 and 52 selected bond lengths and bond angles are given in table 53 and 54 respectively.

Table 51. Crystallographic Data Collection and Structure Refinement Parameters for Complexes 41-44

Complexes	41	42	43	44
Chemical Formula	$\text{C}_{62} \text{H}_{66} \text{B}_2 \text{Cu}_2 \text{F}_8 \text{N}_4 \text{P}_2$	$\text{C}_{38} \text{H}_{37} \text{B Cu F}_4 \text{N}_3 \text{P}$	$\text{C}_{50} \text{H}_{48} \text{B Cu F}_4 \text{N}_4 \text{P}_2$	$\text{C}_{38} \text{H}_{37} \text{B Cu F}_4 \text{N}_3 \text{P}$
Formula Mass, Da	1229.83	717.03	917.21	717.03
Space Group	P2(1)2(1)2(1)	P2(1)/c	Pnma	P2(1)/n
a, Å	14.9687(11)	11.6379(12)	24.166(2)	16.2198(6)
b, Å	15.0719(11)	20.173(2)	19.5652(18)	12.6790(5)
c, Å	20.9511(16)	21.786(2)	9.6477(9)	20.8484(8)
α , deg	90.00	90.00	90.00	90.00
β , deg	90.00	97.270(2)	90.00	111.7530(10)

γ , deg	90.00	90.00	90.00	90.00
V , Å ³	4726.7(6)	5073.5(9)	4561.6(7)	3982.2(3)
ρ_{calcd} , gcm ⁻³	1.296	1.408	1.336	1.495
Z	3	6	4	5
μ , mm ⁻¹	0.789	0.748	0.605	0.794
T , K	273(2)	298(2)	298(2)	298(2)
λ , Å	0.71073	0.71073	0.71073	0.71073
$R1(\text{Fo}2)^{\text{a}}$	0.1158	0.0634	0.0494	0.1509
$Wr(\text{Fo}2)^{\text{b}}$	0.3521	0.2244	0.1552	0.4727
GOF	1.222	1.048	1.037	1.737

Table 52. Crystallographic Data Collection and Structure Refinement Parameters for Complexes 45-48 and 53, 55

Complexes	45	46	47	48
Chemical Formula	C ₆₂ H ₆₆ B ₂ Cu ₂ F ₈ N ₄ P ₂	C ₅₄ H ₅₄ B Cu F ₄ N ₂ P ₂	C ₃₈ H ₃₇ B Cu F N ₃ P	C ₆₂ H ₆₆ B ₂ Cu ₂ F ₈ N ₄ P ₂
Formula Mass, Da	1229.83	943.28	660.03	1229.83
Space Group	P2(1)2(1)2(1)	Pna2(1)	P2(1)	P2(1)/n
a , Å	14.9687(11)	21.4078(13)	10.314(3)	12.3735(15)
b , Å	15.0719(11)	12.3391(7)	18.880(5)	21.013(3)
c , Å	20.9511(16)	18.7586(11)	10.669(3)	12.8678(16)
α , deg	90.00	90.00	90.00	90.00

β , deg	90.00	90.00	99.256(5)	95.527(2)
γ , deg	90.00	90.00	90.00	90.00
V , Å ³	4726.7(6)	4955.1(5)	2050.5(9)	3330.1(7)
ρ_{calcd} , gcm ⁻³	1.296	1.264	1.604	1.226
Z	3	4	3	2
μ , mm ⁻¹	0.789	0.558	0.902	0.747
T , K	273(2)	298(2)	298(2)	294(2)
λ , Å	0.71073	0.71073	0.71073	0.71073
$R1(\text{Fo}2)^a$	0.1158	0.0509	0.0436	0.2276
$Wr(\text{Fo}2)^b$	0.3521	0.1317	0.0968	0.5795
GOF	1.222	1.008	0.977	2.051

Table 52 (continued)

Complexes	53	55
Chemical Formula	C ₃₅ H ₄₂ B Cu F ₄ N ₂ P ₂	C ₃₈ H ₃₇ B Cu F ₄ N ₂ P ₂
Formula Mass, Da	881.37	717.03
Space Group	P-1	P-1
a , Å	12.9091(14)	13.0765(17)
b , Å	13.5822(15)	18.550(2)
c , Å	16.6623(18)	20.078(3)
α , deg	111.998(2)	111.825(2)

β , deg	93.658(2)	98.768(2)
γ , deg	95.763(2)	102.150(2)
V , Å ³	2678.7(5)	4274.8(10)
ρ_{calcd} , gcm ⁻³	1.639	1.393
Z	3	5
μ , mm ⁻¹	1.356	0.739
T , K	294(2)	298(2)
λ , Å	0.71073	0.71073
$R1(\text{Fo}2)^{\text{a}}$	0.1318	0.1703
$Wr(\text{Fo}2)^{\text{b}}$	0.4206	0.4919
GOF	0.966	1.529

Table 53. Selected bond lengths (Å) and bond angles (°) of Complexes 41-44

41	42	43	44
Cu1- N2 2.069(5)	Cu1- N3 2.079(3)	Cu1- N1 2.101(3)	Cu1- N1 2.130(7)
Cu1- N1 2.102(5)	Cu1- N4 2.093(3)	Cu1- N2 2.108(3)	Cu1- N2 2.141(7)
Cu1- P2 2.2553(14)	Cu1- P3 2.2562(8)	Cu1- P1 2.2732(6)	Cu1- Cu2 2.269(2)
Cu1- P1 2.2665(15)	Cu1- P2 2.2746(8)	Cu1- P1 2.2732(6)	Cu1- P3 2.295(2)
N2- Cu1- N1 79.7(2)	N3- Cu1- N4 78.93(11)	N1- Cu1- N2 78.77(12)	N1- Cu1- N2 79.5(3)
N2- Cu1- P2 116.70(16)	N3- Cu1- P3 114.95(8)	N1- Cu1- P1 112.73(3)	N1- Cu1- Cu2 112.5(2)
N1- Cu1- P2 106.03(15)	N4- Cu1- P3 113.17(8)	N2- Cu1- P1 107.85(3)	N2- Cu1- Cu2 112.9(2)
N2- Cu1- P1 111.30(16)	N3- Cu1- P2 111.38(8)	N1- Cu1- P1 112.73(3)	N1- Cu1- P3 109.9(2)
N1- Cu1- P1 109.56(14)	N4- Cu1- P2 103.04(8)	N2- Cu1- P1 107.85(3)	N2- Cu1- P3 99.6(2)
P2- Cu1- P1 123.90(6))	P3- Cu1- P2 125.07(3)	P1- Cu1- P1 126.17(3)	P2- Cu1- P3 130.04(9)

Table 54. Selected Bond Lengths (Å) and Bond Angles (°) (of Complexes 45-49 and 53, 55)

45		47		48	
Cu1- N1	2.073(3)	Cu1- N1	2.072(3)	Cu1- N2	2.073(2)
Cu1- N2	2.105(3)	Cu1- N2	2.104(3)	Cu1- N1	2.115(3)
Cu1- P1	2.2444(9)	Cu1- P1	2.2523(9)	Cu1- P2	2.2340(9)
Cu1- P2	2.2610(10)	Cu1- P2	2.2793(10)	Cu1- P1	2.2742(9)
N1- Cu1- N2	78.97(11)	N1- Cu1- N2	79.01(11)	N2- Cu1- N1	79.13(11)
N1- Cu1- P1	115.20(8)	N1- Cu1- P1	122.93(9)	N2- Cu1- P2	119.66(8)
N2- Cu1- P1	104.40(8)	N2- Cu1- P1	111.37(8)	N1- Cu1- P2	109.86(8)
N1- Cu1- P2	112.39(8)	N1- Cu1- P2	110.18(8)	N2- Cu1- P1	105.60(8)
N2- Cu1- P2	106.40(8)				
P1- Cu1- P2	126.93(4)				
C1- N1- Cu1	127.1(2)				
49		53		55	
Cu1- N1	2.116(9)	Cu1- N3	2.068(15)	Cu2- N2	2.071(8)
Cu1- N2	2.103(9)	Cu1- N4	2.134(18)	Cu2- N1	2.079(7)
Cu1- P3	2.226(4)	Cu1- P1	2.238(6)	Cu2- P5	2.239(3)
Cu1- P2	2.293(6)	Cu1- P4	2.378(4)	Cu2- P6	2.254(3)
N1- Cu1- P3	114.3(3)	N3- Cu1- N4	81.9(6)	N4- Cu1- N3	79.4(3)
N2- Cu1- P3	114.0(3)	N3- Cu1- P1	116.0(4)	N4- Cu1- P4	111.2(2)
N1- Cu1- P2	103.6(3)	N4- Cu1- P1	115.0(5)	N3- Cu1- P4	123.7(2)
N2- Cu1- P2	110.8(3)			N4- Cu1- P3	108.8(2)
N1- Cu1- N2	80.6(4)			N3- Cu1- P3	99.2(2)
				P4- Cu1- P3	125.10(9)

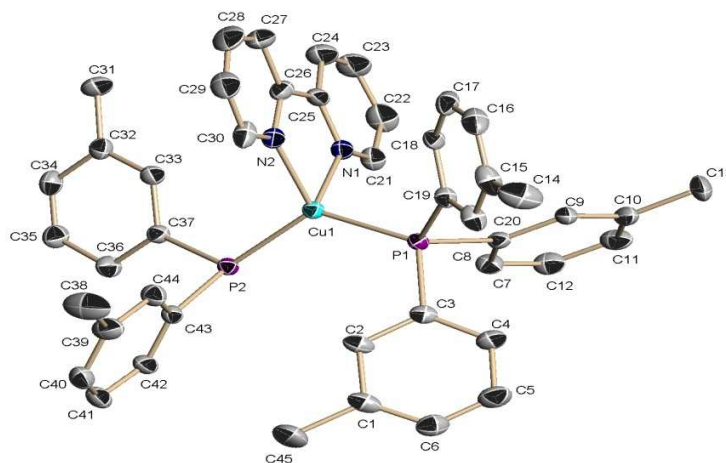


Figure 44. X-ray structure of Complex 42 showing thermal ellipsoid drawn at 15 %. Hydrogen atoms, BF_4^- anion and one meta-tolyl ring is omitted for clarity

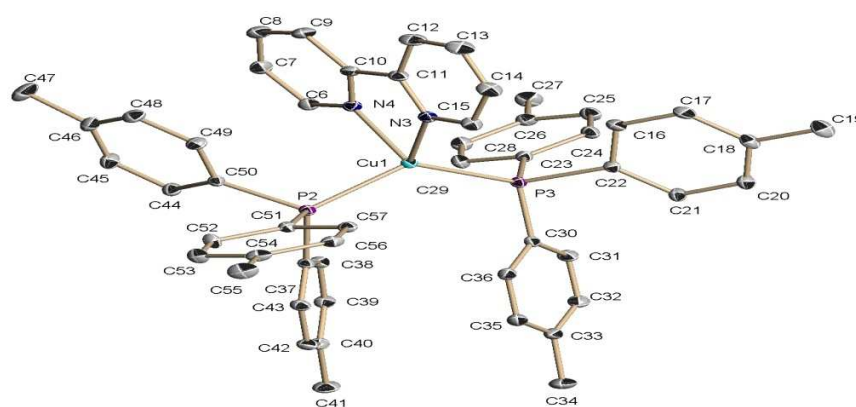


Figure 45. X-ray structure of Complex 43 showing thermal ellipsoid drawn at 15 %. Hydrogen atoms, BF_4^- anion are omitted for clarity

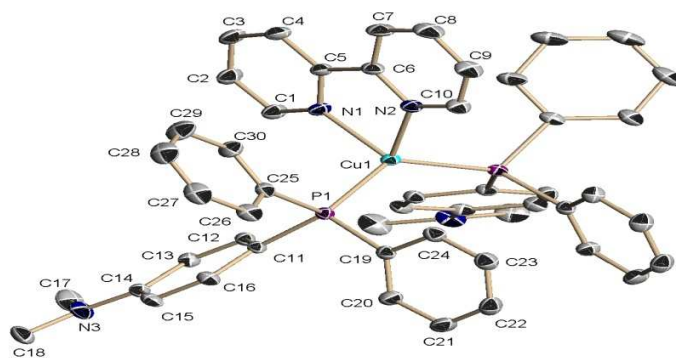


Figure 33. X-ray structure of Complex 44 showing thermal ellipsoid drawn at 15 %. Hydrogen atoms, BF₄⁻ anion are omitted for clarity

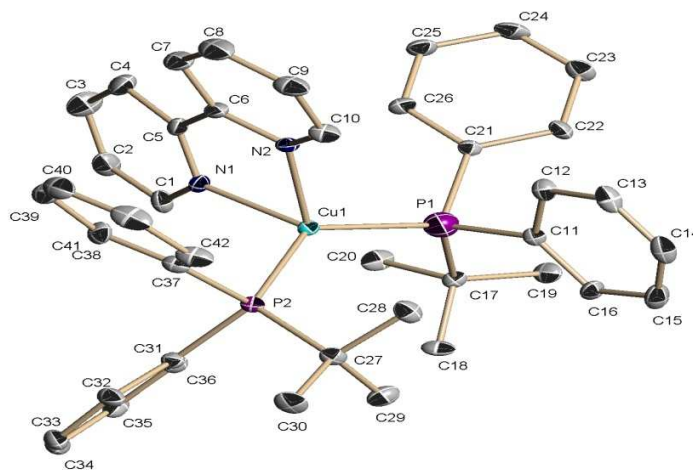


Figure 47. X-ray structure of Complex 45 showing thermal ellipsoid drawn at 15 %. Hydrogen atoms, BF₄⁻ anion are omitted for clarity

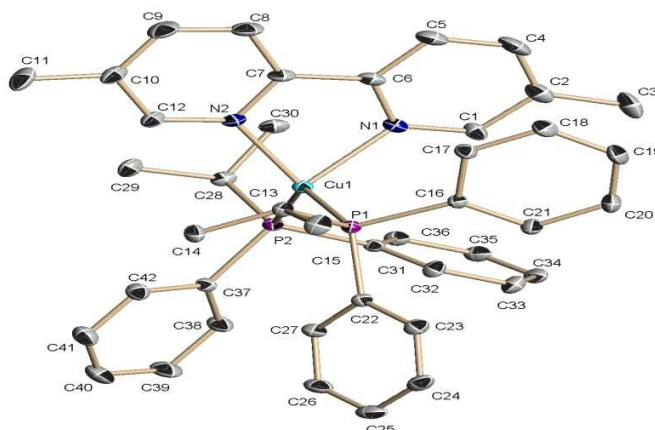


Figure 48. X-ray Structure of Complex 47 showing thermal ellipsoid drawn at 15 %. Hydrogen atoms, BF_4^- anion are omitted for clarity

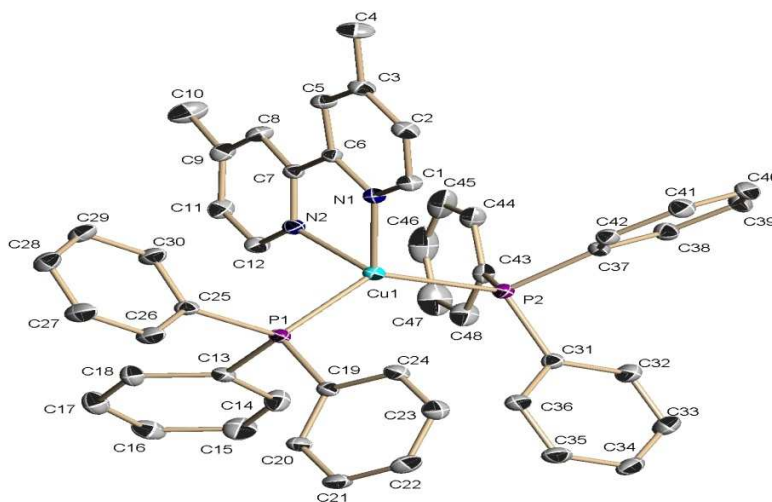


Figure 34. X-ray structure of Complex 49 showing thermal ellipsoid drawn at 15 %. Hydrogen atoms, BF_4^- anion are omitted for clarity

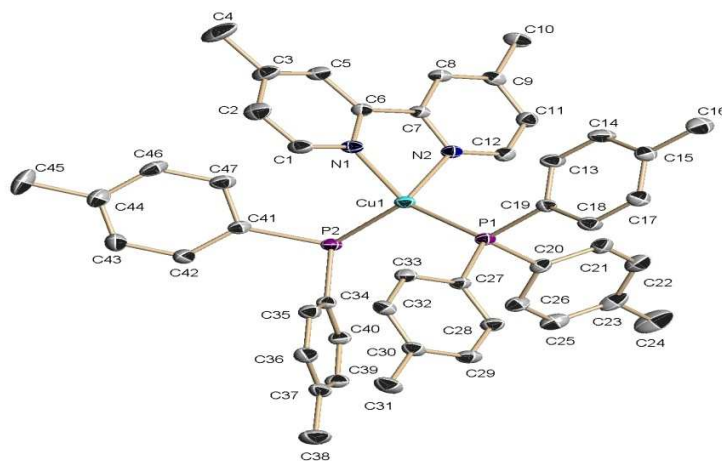


Figure 50. X-ray structure of Complex 50 showing thermal ellipsoid drawn at 15 %. Hydrogen atoms, BF_4^- anion are omitted for clarity

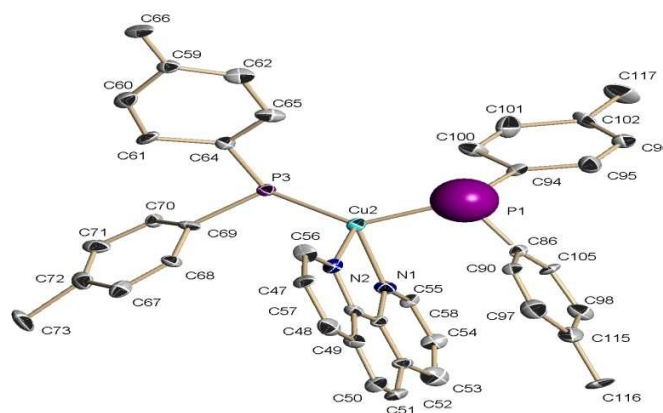


Figure 51. X-ray structure of Complex 52 showing thermal ellipsoid drawn at 15 %. Hydrogen atoms, BF_4^- anions, two para-tolyl rings and DMF molecule are omitted for clarity

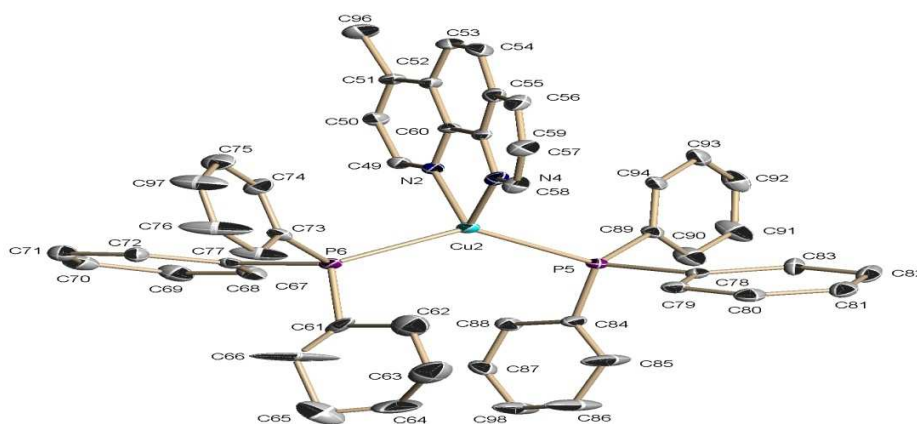


Figure 52. X-ray structure Complex 55 showing thermal ellipsoid drawn at 15 %. Hydrogen atoms, BF_4^- anion are omitted for clarity

In all complexes Copper(I) is linked to two phosphines and one diimine making a $\text{Cu}(\text{PR}_3)_2(\text{diimine})$ structure. Diimine is on the mirror plane in each of the crystal structure. In all complexes N-Cu-P angles range from 111.2(2) to 122.93(9) showing average with deviation of 13.0° from normal tetrahedral angle of 109.5° . N-Cu-N bite angle ranges from 78.77(12) to N-Cu-N 80.6(4) for all complexes. P-Cu-P bite shows tetrahedral angles in the range of 123.90(6) P-Cu-P 130.04(9). Which show deviation of $14.0\text{--}21.0^\circ$. Complex 46 shows P-Cu-P 130.04(9) largest deviation which may be the result of bulky tert-butylphenyl phosphine. The large deviation observed from normal tetrahedral angle is a result of diimine being on the mirror and pushing the angle further.

8.2.6 Nuclear Magnetic Resonance Spectroscopy

^1H NMR and ^{31}P spectra were recorded for free ligands and binuclear Cu(I) complexes in deuterated solvent (DMSO-d_6). Representative ^1H -NMR of complex 45 is given in figures 50 and 51. NMR spectra are given in appendix-VI & VII. Results are tabulated in table 51.

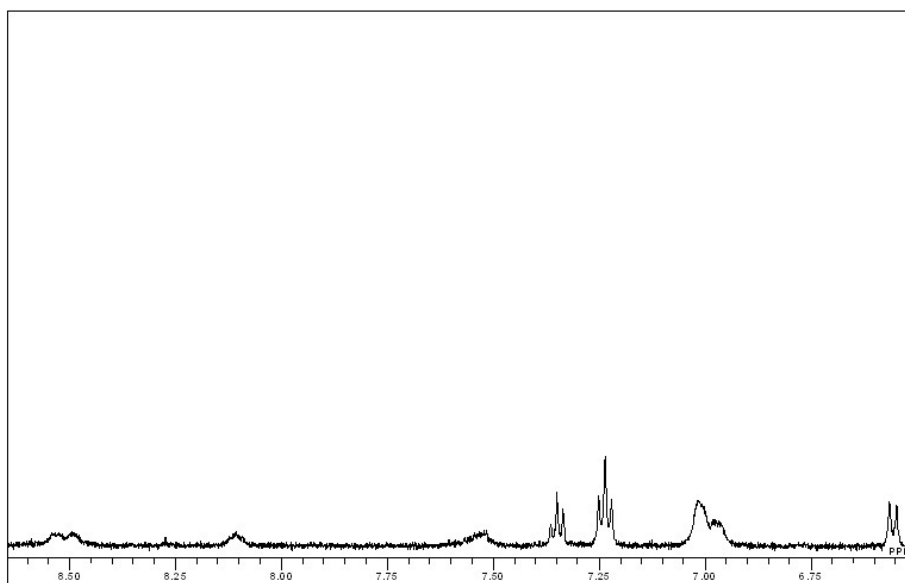


Figure 35. ^1H -NMR (only the aromatic region) of Complex 45

Table 55. ^1H and ^{31}P NMR shifts of Complexes 42-54

Compound	H^1 -NMR shifts $\delta(\text{PPM})$	^{31}P -NMR $\delta(\text{PPM})$
42	2.00(s), 2.06(s), 2.48(s), 2.49(s), 6.81(d), 7.17(d), 7.40(m), 7.50(s), 7.82(s), 8.14(s), 8.47(s), 8.59(s)	1.17
43	1.20(s), 2.16(m), 7.39(s), 7.48(s), 7.72(s), 8.24(s), 8.68(s), 8.72(s)	58.01
44	2.25(s), 2.33(s), 6.93(s), 7.05(d), 7.33(s), 7.43(s), 7.82(s), 8.12(s), 8.49(s), 8.74(s)	26.82

45	2.06(d),2.48(d),2.87(s),6.54(d),7.01(s),7.23(t),7.33(d),7.51(s),8.11(s),8.49(d)	0.907
46	0.89(d),1.09(d),2.06(t),2.48(s),7.25(d),7.40(s),7.56(t),7.61(s),7.91(s),8.01(s),8.42(s)	23.70,37.25
48	2.45(d),7.04(s),7.21(d),7.40(t),7.51(s),7.64(s),8.33(s),8.44(s)	1.91
49	2.25(s),2.49(s),6.91(s),7.04(d),7.34(s),8.28(s),8.39(s)	0.17
50	1.95(s),2.04(s),2.48(s),6.88(s),7.17(s),7.80(s),7.95(s),8.21(s),8.76(s),8.88(s)	1.35
51	1.79(t),2.04(m),7.81(m),8.69(m)	-24.80
52	2.48(s),2.83(s),7.09(s),7.24(s),7.35(d),7.52(s),7.60(s),7.74(s),7.87(s),8.22(s),8.30(s),8.60(s),8.70(d),8.91(s)	-3.56
53	2.06(s),2.83(s),6.90(d),7.51(s),7.61(s),7.76(s),7.92(s),8.20(s),8.27(s),8.56(s),8.74(s),8.88(s)	-2.70
54	2.06(t),2.48(t),7.51(m),7.94(s),8.11(s),8.18(s),8.69(s)	-3.25

Shifts from 0.89-2.83 ppm in ^1H -NMR are attributed to the methyl protons of phosphines by comparing with the spectra of free phosphines. Shifts of 6.88-8.88 are the aromatic

ring shifts of phosphines and. $\Delta(\delta^{31}\text{P})$ shift range after complexation of phosphines is observed from -2.70 to 37.25 ppm

Chapter 9

Catalytic Application in the coupling of phenylacetylene with halobenzene

9.1 Introduction

Aryl-acetylene bonds are prevalent in many compounds that are of biological, pharmaceutical and materials interest. The coupling of phenylacetylene with halobenzenes is an important reaction both from organic synthesis viewpoint and industrial manufacturing. In recognition of the widespread importance, over the years, many synthetic methods have emerged for the coupling of phenylacetylene with halobenzenes. Traditional Hartwig-Büchwald [78-79] and Sonagashira coupling [80] utilizes expensive metal Pd(0) and air-sensitive phosphine ligands as catalysts; Ullmann and Stephens-Castro coupling [81] involves Copper-mediation. These methods have few drawbacks. Most copper(i) salts are insoluble in organic solvents, and hence, the reactions are often heterogeneous and require high reaction temperatures. Moreover, the reactions are sensitive to functional groups on aryl halides and the yields are often irreproducible. It was shown by Weingarten in 1964 [87], Cohen in 1976 [88], and more recently, by others that if the solubility of copper salts is increased then the aryl coupling reactions tend to occur at milder temperatures. D. Venkataraman et al; [46] have

shown that $\text{Cu}(\text{phen})(\text{PPh}_3)\text{Br}$ can be used as catalysts for coupling of aryl iodides with aryl acetylenes using K_2CO_3 as the base, in toluene at 110 -120 °C. This mononuclear copper(I)-based catalytic system shows catalytic conversions under mild conditions and is tolerant to functional groups and does not require the use of expensive metal like palladium.

On the basis of the catalytic system mentioned above, we reasoned that our complexes with copper(I) are potential catalyst for the same reaction. We initiated a study of chemically well-defined, mononuclear and binuclear copper(I) diimine, phosphine and binuclear copper(I)-bpm or copper(I)-dpp based mixed ligand complexes that can be systematically modified to act as catalysts for the formation of aryl-carbon bonds. Based on these facts the complexes synthesized were tested as catalysts for the coupling of phenylacetylene with halobenzene.

9.2 Catalytic properties of some mononuclear copper(I) mixed ligand complexes

The four complexes $[\text{Cu}(\text{Phen})\text{P}[(\text{CH}_2)_2\text{CN}]_3\text{I}]$ (56) $\text{Cu}(\text{bipy})\text{P}[(\text{Ph})_2(\text{i-Pr})]\text{Br}$ (57) $\text{Cu}(5,5'\text{-dimethylbipy})\text{P}[(\text{cyhexyl})_3\text{I}]$ (58) $\text{Cu}(5,5'\text{-dimethylbipy})\text{P}[(\text{Ph})_2(\text{i-Pr})]\text{Br} \cdot 0.5 \text{H}_2\text{O}$ (59) were studied as catalysts for the coupling of phenylacetylene with halobenzene. The general experimental procedure is given below:

In a nitrogen-filled glove box, a schlenk tube equipped with a Teflon stirring bar, was charged with potassium carbonate (2.0 mmol) and the catalyst (10.0 mol % with respect to phenylacetylene) and was sealed with a rubber septum. The sealed tube was taken out of the glove box and phenylacetylene (2.50 mmol), halo-benzene (2.00 mmol) and toluene or DMF (15.0 mL) were injected into the tube through the septum. The mixture was then stirred at 115 °C for 24 hours. The reaction mixture was then cooled to room temperature and filtered to remove any insoluble materials. The solvent was removed and the residue was re-crystallized from hexane giving the product as a white solid.

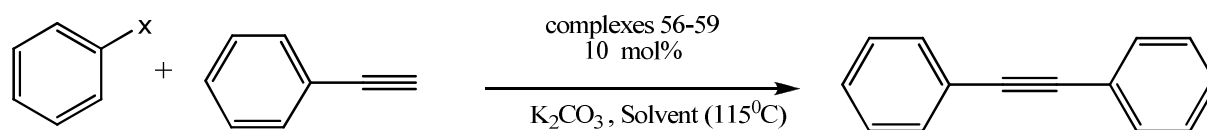


Table 56. Isolated yields of the Reaction of Aryl-halides with Phenylacetylene in the Presence 10 mol % of 56-59

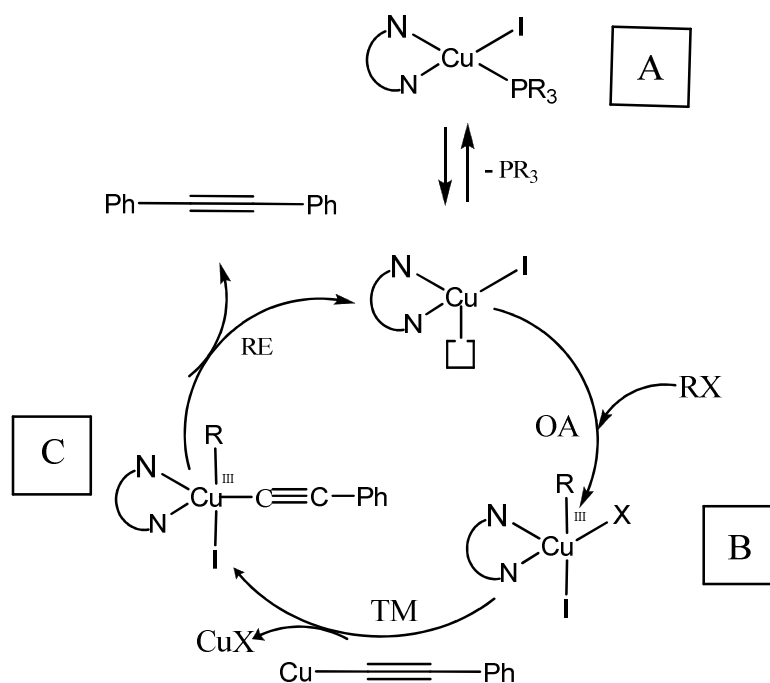
X	Catalyst							
	56		57		58		59	
I	69 ^a	45 ^b	66	55	95	75	73	59
Br	7	25	6	28	23	43	16	39
Cl	4	14	3	5	6	28	6	22

^a in Toluene ; ^b in DMF

Good yields were obtained in the case of iodobenzene. Complex 58 showed the highest activity. Lower yields were obtained for bromo and chlorobenzene. Compound 3 appears to be more active for the formation of diphenylacetylene than the previously reported Cu(phen)(PPh₃)Br compound [47]. For iodobenzene, the use of toluene as a solvent gives higher yields than dimethylformamide, however the opposite is observed for bromo and chlorobenzene

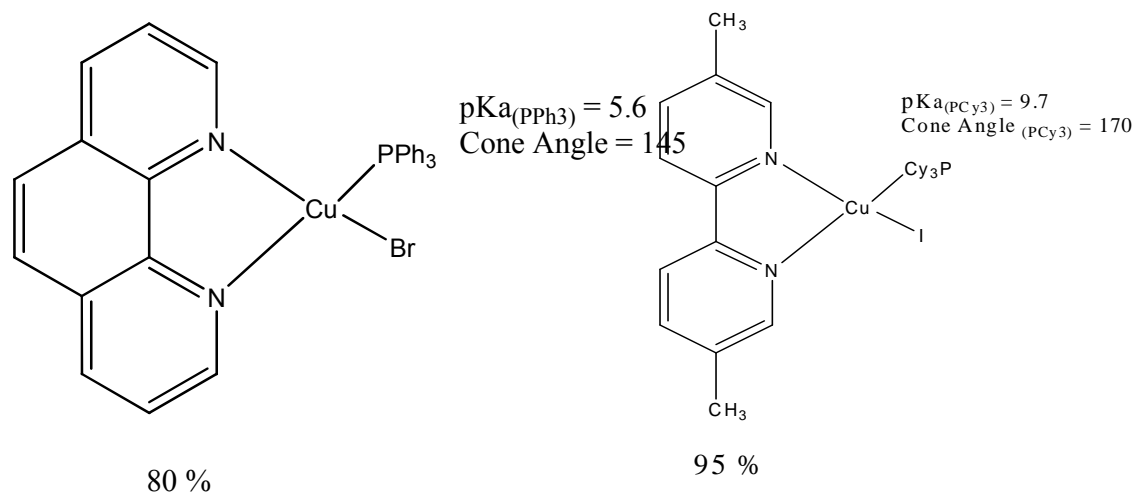
9.2.1 Suggested Mechanism

The active copper(I) catalyst is the 18 electron compound Cu(diimine)(X)(PR₃) (**A**). Suggested reaction mechanism involves four distinct steps; dissociation (favored by the steric effect of phosphine), oxidative addition (favored by electron donating ability of the ligand), transmetallation and reductive elimination (favored by the steric effect of diimine). Steps are shown in scheme 9.1

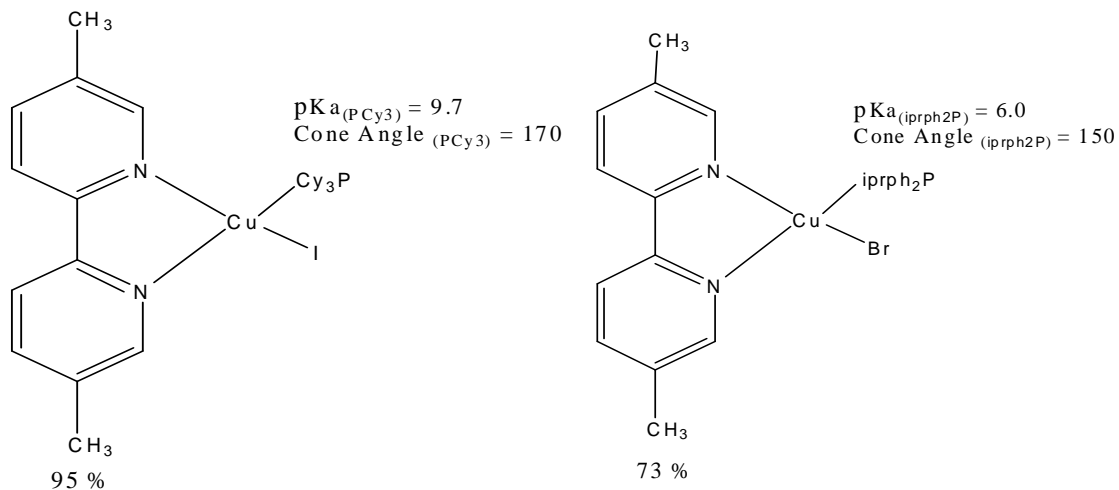


Scheme 9.1

- Complex **A** undergoes dissociation of phosphine in the first step to give Cu(diimine)(X).
- Which reacts in second step with the aryl halide in an oxidative addition to give Cu(III) (complex **B**)
- This complex reacts in a rate limiting transmetalation (whereby exchange of ligand occurs between two metal centers) with the copper acetylide produced in the copper cycle to complex **C** expelling the copper halide CuX.
- In the final step the product is released in a reductive elimination with regeneration of Cu(I).

**Scheme 9.2**

Comparison of our most active catalysts 59 with $\text{Cu}(\text{PPh}_3)(\text{phen})(\text{Br})$ supports our approximation that first step in catalytic cycle is favored by the steric parameter (Tolman cone angle) of phosphine. Tricyclohexylphosphine ($\text{TCA} = 170^\circ$) is bulkier than triphenylphosphine ($\text{TCA} = 145^\circ$) and favors the first step; subsequently favoring the whole catalytic cycle. Resulting in high efficiency of complex 59 in the coupling reaction.

**Scheme 9.3**

Same approximations (dissociation step is favored by steric parameter of phosphine) is valid when we compare our two catalysts 58 & 59. Catalyst 59 has

isopropylidiphenylphosphine with TCA = 1500; comparable to triphenylphosphine. Catalyst 59 is observed to be less efficient than catalyst 58.

9.3 Binuclear copper(I) catalysts for phenylacetylene and halobenzene coupling.

Encouraged by the promising results from mononuclear copper(I) catalysts. We initiated the catalytic properties of binuclear copper(I) catalysts involving 2,2'-bipyrimidine, 2,3-bis(2-pyridyl)pyrazine a bridging ligands and different phosphines. To our knowledge, this is the first well defined binuclear copper(I)-based catalytic system that can be used for the formation of aryl-acetylene bonds from aryl halides under mild conditions. The experimental conditions are identical to those used for the mononuclear (section 9.2) except that 5.0 mol% of the catalyst was used. The results are given in table 57.

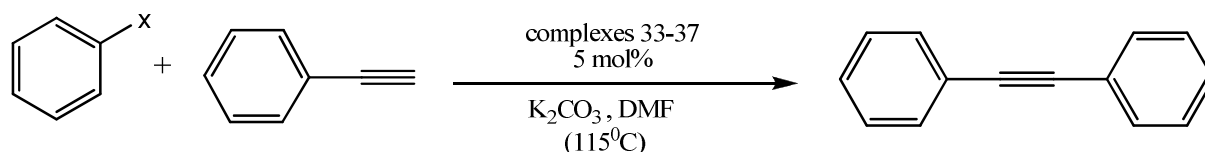


Table 57. Isolated yields of the Reaction of Aryl-halides with Phenylacetylene in the Presence 5 mol % of 33-37

X	Catalyst				
	33	34	35	36	37
I	8.90	30.00	28.6	8.42	22.4
Br	10.47	23.6	18.01	8.02	14.10
Cl	13.70	21.34	16.3	7.30	11.23

Toluene was replaced by dimethylformamide as solvent to enhance the solubility of mixed ligand binuclear copper(i) complexes. Good yields were obtained in the case of iodobenzene. Complex 34 showed the highest activity. Lower yields were obtained for bromo and chlorobenzene. Compound 34 appears to be more active for the formation of diphenylacetylene. For bromo and chlorobenzene comparative yields are obtained.

Chapter 10

Conclusion

In the present work 37 new binuclear copper(I) diimine and phosphine mixed ligand complexes have been successfully synthesised by varying diphosphine and dinitrogen bridges. Diphosphine bridges employed for the synthesis include bis(diphenylphosphino)acetylene and trans-1,2-bis(diphenylphosphino)ethylene. While dinitrogen bridges include 4,4'-bipyridine, trans-1,2-bis(4-pyridyl)ethylene, 2,2'-bipyrimidine and 2,3-bis(2-pyridyl)pyrazine. The diimine used are 2,2'-bipyridyl, 4,4'-dimethyl-2,2'-bipyridyl, 5,5'-dimethyl-2,2'-bipyridyl, 6,6'-dimethyl-2,2'-bipyridyl, 1,10-phenanthroline, 4-methyl-1,10-phenanthroline, 2,9-dimethyl-1,10-phenanthroline and 4,7-dimethyl-1,10-phenanthroline. The phosphines used in the present study are isopropylidiphenylphosphine, tri-cyclohexylphosphine, dicyclohexylphenylphosphine, tri-meta-tolylphosphine, tri-ortho-tolylphosphine, tri-para-tolylphosphine, tert-butylidiphenylphosphine, triphenylphosphine, 4-(dimethylaminophenyl)diphenylphosphine and tris-(2-cyanoethylphosphine). In general these complexes have been characterized by elemental analysis, UV-Visible, solution luminescence, FT-IR, NMR (^1H & ^{31}P) and Single Crystal X-ray diffraction. Beside the above-mentioned techniques complexes (1-8) based on bis(diphenylphosphino)acetylene bridge were also characterized by Raman Spectroscopy. UV-Visible studies showed strong absorption bands, which were typical of the ligand centered $\pi\text{-}\pi^*$ transitions. The Visible part of the spectrum consists of weaker absorption bands, which arise from metal-to-ligand charge-transfer (MLCT) electronic transitions. The visible luminescence from Cu(I)-diimine arises in most of the

cases from two MLCT excited states in thermal equilibrium, i.e. a singlet ($^1\text{MLCT}$) and a triplet ($^3\text{MLCT}$).

Far-Infrared studies were carried out for complexes 33-41. Empirical relationship $\nu/\text{cm}^{-1} = b(r/A^0)^{-m}$ proposed by Bowmaker et al [131] where $b = 13800$ and 18000 and $m = 4.9$ and 5.2 for $X = \text{C1}$ and Br , was used to assign Cu-X stretching frequency from the bond lengths. ^{31}P -NMR for the binuclear complexes gave one broad signal for all complexes. Binuclear complexes having 6,6'-Me₂bipy and 2,9-Me₂phen substituents bonded to the metal show highly shielded phosphorous consistent with high sigma donation power of 6,6'-Me₂bipy and 2,9-Me₂phen ligands enhance π -back bonding from the metal to the phosphine. Many binuclear complexes were obtained as single crystals by careful layering of the solution with diethyl ether or by recrystallizing in dimethylformamide. Single crystal X-ray structure of complexes (1-8) showed the Cu(I) ion adopts a distorted tetrahedral coordination. In these three complexes Cu₂(dppa)₂ moiety can be considered as a 10-membered chair like dimetallacycle. The chair conformation is twisted in complex 3 & 7 possibly due to steric hindrance of bipyridyl rings substituted at 6 and 2,9 positions. Complexes 2, 3, 5 and 7 are centrosymmetric. The X-ray structure of complexes 17, 20, 21, 22 and 25 confirm the binuclear nature with 4,4'-bipy bridging. Each copper(I) ion is bonded to two nitrogen atoms of chelating diimine, one nitrogen of the bridging ligand and a phosphorous atom of the phosphine. The geometry is distorted tetrahedral. Except in complex 20 the binuclear molecule has crystallographic center of symmetry and the two pyridyl rings of the bridging ligand are almost coplanar. In complexes 26 and 28 the crystal structure confirm the presence of trans-1,2-bis(4-pyridyl)ethylene as a bridge; linking CuN₂P moieties on either side. In complexes 33-36 the bridging ligand is 2,2'-bipyrimidine. Copper(I) ion is bonded to two nitrogen atoms of bpm; one phosphorous atom of the phosphine and halide (Br⁻ or I⁻). In complex 38 the presence of the 2,3-bis(2-pyridyl)pyrazine bridge is confirmed by the x-ray structure linking Cu(TCP)(Br) moieties are bonded on either side through nitrogen atoms. The geometry is distorted tetrahedral and the distortion is likely the result of steric effects imposed by the bulky phosphine and halide ions.

During the synthesis attempts of the binuclear complexes, new mononuclear copper(I) mixed ligand complexes 41-55 were obtained. These complexes have been characterized by elemental analysis, UV-Vis, Solution luminescence, FT-IR, NMR (^1H & ^{31}P) and Single Crystal X-ray diffraction. Strong absorption bands and various shoulders were observed for these complexes in the UV region of the spectrum; these are assigned to ligand centered transitions. The visible region showed broad bands typical of metal to ligand charge transfer electronic transitions. ^{31}P -NMR for the mononuclear complexes gave one broad signal. The single crystal X-ray analysis of the mononuclear complexes showed the general formula $[\text{Cu}(\text{PR}_3)_2(\text{diimine})]^+$. copper(I) is linked to two phosphines and one diimine in a distorted tetrahedral geometry.

The mononuclear complexes (56-59) were found to be effective catalysts for the coupling of phenylacetylene with halobenzene to give diphenylacetylene. Five binuclear copper(I) complexes with 2,2'-bipyrimidine and 2,3-bis(2-pyridyl)pyrazine bridge were also successfully tested as catalysts for the same reaction; relatively low yields were obtained, however more studies are required to explore the best catalytic conditions. Such as the nature of the base, temperature, solvent, % of catalyst. To our knowledge, these are the first well defined binuclear copper(I)-based catalytic system that can be used for the formation of aryl-acetylene bonds from aryl halides under mild conditions.

References

- [1] Demadis, K. D.; Hartshorn, C. M.; Meyer, T. J. *Chem. Rev.* 2001, *101*, 2655-2686.
- [2] Paul, F.; Lapinte, C. *Coord. Chem. Rev.* 1998, *178-180*, 431-509.
- [3] Ziessel, R.; Hissler, M.; El-ghayoury, A.; Harriman, A. *Coord. Chem. Rev.* 1998, *178-180*, 1251-1298.
- [4] Cotton, F. A.; Lin, C.; Murillo, C. A. *Acc. Chem. Res.* 2001, *34*, 759-771.
- [5] Barigelletti, F.; Flamigni, L. *Chem. Soc. Rev.* 2000, *29*, 1-12.
- [6] Astruc, D. *Acc. Chem. Res.* 1997, *30*, 383-391.
- [7] Kaim, W.; Klein, A.; Glöckle, M. *Acc. Chem. Res.* 2000, *33*, 755-763.
- [8] Carroll, R. L.; Gorman, C. B. *Angew. Chem., Int. Ed.* 2002, *41*, 4378-4400.
- [9] Creutz, C. Taube, H. *J. Am. Chem. Soc.* 1973, *95*, 1086-1094.
- [10] Richardson, D. E.; Taube, H. *Coord. Chem. Rev.* 1984, *60*, 107-129.
- [11] Callahan, R. W.; Keene, F. R.; Meyer, T. J.; Salmon, D. J. *J. Am. Chem. Soc.* 1977, *99*, 1064-1073.
- [12] Hoshino, Y.; Higuchi, S.; Fiedler, J.; Su, C.-Y.; Knodler, A.; Schwederski, B.; Sarkar, B.; Hartmann, H.; Kaim, W. *Angew. Chem., Int. Ed.* 2003, *42*, 674-677.
- [13] Patoux, C.; Launay, J.-P.; Beley, M.; Chodorowski-Kimmes, S.; Collin, J.-P.; James, S.; Sauvage, J.-P. *J. Am. Chem. Soc.* 1998, *120*, 3717-3725.
- [14] Laye, R. H.; Couchman, S. M.; Ward, M. D. *Inorg. Chem.* 2001, *40*, 4089-4092.
- [15] Mosher, P. J.; Yap, G. P. A.; Crutchley, R. J. *Inorg. Chem.* 2001, *40*, 1189-1195.
- [16] Cameron, C. C.; Pickup, P. G. *J. Am. Chem. Soc.* 1999, *121*, 7710-7711.
- [17] Ganesamoorthy, Chelladurai; Balakrishna, Maravanji S.; George, Paulose P.; Mague, Joel T. *Inorganic Chemistry* 2007, *46*(3), 848-858
- [18] Li, R; *Inorg Chem Commun*, 2003, *V6*, P1017

- [19] Maeyer, J; Polyhedron , 2003, V22, P419
- [20] Pike, R; Inorg Chem, 2002, V41, P631
- [21] Bowmaker, G; J Chem Soc, Dalton Trans 2002, P2722
- [22] Graham, P; Inorg Chem 2000, V39, P5121
- [23] Bernardi, L.; Gothelf, A. S.; Hazell, R. G.; Jørgensen, K. A.
J.Org. Chem. 2003, 68, 2583-2591.
- [24] Shi, W.-J.; Wang, L.-X.; Fu, Y.; Zhu, S.-F.; Zhou, Q.-L.
Tetrahedron: Asymmetry 2003, 14, 3867- 3872.
- [25] Koradin, C.; Polborn, K.; Knochel, P. *Angew. Chem., Int.Ed.*
2002, 41, 2535-2538.
- [26] Liang, L.; Chan, A. S. C. *Tetrahedron: Asymmetry* 2002, 13, 1393-1396.
- [27] Martorell, A.; Naasz, R.; Feringa, B. L.; Pringle, P. G.
Tetrahedron: Asymmetry 2001, 12, 2497-2499.
- [28] Chen, J.-X.; Daeuble, J. F.; Brestensky, D. M.; Stryker, J. M.
Tetrahedron 2000, 56, 2153-2166.
- [29] Yao, S.; Saaby, S.; Hazell, R. G.; Jørgensen, K. A. *Chem.sEur. J.*
2000, 6, 2435-2448.
- [30] Harkins, S. B.; Peters, J. C. *J. Am. Chem. Soc.* 2005, 127, 2030-2031.
- [31] Araki, H.; Tsuge, K.; Sasaki, Y.; Ishizaka, S.;
Kitamura, N. *Inorg. Chem.* 2005, 44, 9667-9675.

- [32] Cuttell, D. G.; Kuang, S.- M.; Fanwick, P. E.; McMillin, D. R.; Walton, R. A. *J. Am. Chem.Soc* 2002, *124*, 6-7.
- [33] Song, H.-B.; Wang, Q.-M.; Zhang, Z.-Z.;Mak, T. C. W. *Chem. Commun.*2001, 1658-1659.
- [34] Yam, V. W.- W.; Lo, K. K.-W. *Chem. Soc. ReV.* 1999, *28*, 323-334.
- [35] Ford, P. C.; Cariati, E.; Bourassa, J. *Chem. ReV.* 1999, *99*, 3625-3647.
- [36] Marzano, C.; Pellei, M.; Alidori, S.; Brossa, A.; Lobbia, G. G.;
Tisato, F.; Santini, C. *J. Inorg. Biochem.* 2006, *100*, 299-304.
- [37] Pellei, M.; Lobbia, G. G.; Santini, C.; Spagna, R.; Camalli, M.;
Fedeli,D.; Falcioni, G. *Dalton Trans.* 2004, 2822-2828.
- [38] McKeage, M. J.; Papathanasiou, P.; Salem, G.; Sjaarda, A.; Swiegers,
G. F.; Waring, P.; Wild, S. B. *Met.-Based Drugs* 1998, *5*, 217-223.
- [39] Saito, K.; Tsukuda, T.; Tsubomura, T. *Bull. Chem. Soc. Jpn.* 79 2006 437-441.
- [40] Suboyama, A.; Okada, S.; Takiguchi, T.; Kamatani, J.; Furugori, M.;Kuge, K.:
Light-emitting device. U.S. Pat. Appl. Publ. 2005 p. 30.
- [41] Cuttell, D. G.; Kuang, S.-M.; Fanwick, P. E.;McMillin, D. R.; Walton, R.A. *J. Am. Chem. Soc.* 124 2002 6-7.
- [42] Henary, M.; Wootton, J. L.; Khan, S. I.; Zink, J. I., *Inorg. Chem.*1997, *36*, 796-801.
- [43] Blaskie, M.W.;McMillin, D.R. *Inorg.Chem.*1980,19,3519
- [44] McMillin, D.R.; McNett,K.M. *Chem.Rev.*1998,98,1201
- [45] Eggleston,M.K.; McMillin, D.R.;Koeing,K.S.;Pallenberg,A.J. *Inorg.Chem.*

1997, 36,172

- [46] Gujadhur, R. K.; Bates, C. G.; Venkataraman, D. *Org. Lett.*, 2001, 3, 4315-4317.
- [47] Derek Van Allen and D. Venkataraman. *J. Org. Chem.* 68 2003 4590- 4593
- [48] Scaltrito,D.V.; Thompson, D. W.; O'Callaghan, J.A.; Meyer,G.J.
*Coord.Chem.Rev.*2000,208,243-266.
- [49] Pallenberg,A.J.; Koeing,K.S.;Barnhart,D.M. *Inorg.Chem.*1995,34,11,2833-2840
- [50] Miller,M.T.; Gantzel, P.K.; Karpishin,T.B. *J,Am.Chem.Soc.*1999,121,17,4292-4293.
- [51] Miller,M.T.; Gantzel, P.K.; Karpishin,T.B.*Angew.Chem.,Int.Ed.*1998,37,11,1556-1558.
- [52] McMillin,D.R.; Buckner,M.T.; Ahn,B.T. *Inorg.Chem.*1977,16,4,943-945
- [53] Mo, Juan; Zhang, Su Mei; Ge, Wen Zhong; Liu, Jian Hua,
Acta Crystallographica, Section E: Structure Reports Online 2007,
E63(8), m2096
- [54] Wei, Y.-Q.; Wu, K.-C.; Zhuang, B.-T.; Zhou, Z.-F.
Journal of Coordination Chemistry 2006, 59(7), 713-719.
- [55] Tsukuda, Toshiaki; Nakamura, Ayaka; Arai, Takashi; Tsubomura, Taro,
Bulletin of the Chemical Society of Japan 2006, 79(2), 288-290.
- [56] Liu, Huan Yu; Wang, Fen Ying; Wang, Guo Yong; Huang, Chang Gan; Peng,
Da. Yong *Acta Crystallographica, Section E: Structure Reports*
Online 2006, E62(1), m111-m112.

- [57] Sun, Yuan; Zhang, Shaowen; Li, Guanliang; Xie, Yaxiong;
Zhao, Dong *Transition Metal Chemistry* 2003, 28(7), 772-776.
- [58] Ruina, Yang; Kunhua, Lin; Yimin, Hou; Dongmei, Wang;
Douman, Jin *Polyhedron* 1997, 16(23), 4033-4038
- [59] Kitagawa, Susumu; Maruyama, Hideki; Wada, Shigetoshi;
Numakata, Megumu; Nakamura, Masaki; Masuda, Hideki.
Bulletin of the Chemical Society of Japan 1991, 64(9), 2809-13
- [60] P.Manikandan, M.Subramoni, B.Varghese, P.T.Manoharan
1998 *J.Chem.Soc.,Dalton Trans.* ,3219
- [61] M.Gembicky, A.Yu.Kovalevsky, P.Coppens 2004 *Private Communication*
- [62] T.Tsubomura, N.Takahashi, K.Saito, T.Tsukuda 2004 *Chem.Lett.* ,33,678
- [63] A.J.Carty and A.Efarty, *Can.J.Chem.*, 1969,47,2573
- [64] Wheelock, J.H.Nelson and H.B.Jonassen, *Inorg.Chim.Acta*,1970,20,399
- [65] M.J.Went, *Polyhedron*, 1995, 4, 465
- [66] E.Sappa, *J.organomet.Chem.*, 1988,352,327
- [67] J.R.Glasworthy, C.E.Housecroft and A.L.Rheingold, *J.Chem.Soc.,Dalton Trans.*,
1995,2639.
- [68] B.C.Ward and J.L.Templeton, *J.Am.Chem.Soc.*, 1980,102,1532
- [69] W.A.Anderson, A.J.Carty and A.Efraty, *Can.J.Chem.*, 1969,47.3361
- [70] D.Rodewald, C.Schulzke and D.Rehder, *J.organomet.Chem.*, 1995,498,29
- [71] A.K.Powell and M.J.Went, *J.Chem.Soc, Dalton Trans.*, 1992,439.

- [72] Yu-Chiao Liu, Ching-I Li, Wen-Yann Yeh, Gene-Hsiang Lee, Shie-Ming Peng 2006 *Inorg.Chim.Acta* ,359, 2361
- [73] De-Hui Wang, Li-Qiang Song, Jian-Hua Chen, Yong Chen, Wen-Fu Fu; 2007 , *Acta Crystallogr.,Sect.E:Struct.Rep.Online* ,63,m474
- [74] Wen-Fu Fu, Xin Gan, Jian Jiao, Yong Chen, Mei Yuan,Shao-Ming Chi, Ming-Ming Yu, Shao-Xiang Xiong 2007 *Inorg.Chim.Acta* ,360, 2758
- 75] Jian-Hua Chen, Li-Qiang Song, De-Hui Wang, Jun-Feng Zhang, Wen-Fu Fu; 2007, *Acta Crystallogr., Sect.E:Struct.Rep.Online* ,63,m34
- [76] Ji-Shu Chen, Pin-Hua Liu, Wen-Fu Fu, 2007, *Acta Crystallogr., Sect.E:Struct.Rep.Online* ,63,m1689
- [77] Donatella Armentano, Giovanni de Munno, Francesca Guerra,a Juan Faus, Francesc Lloret, and Miguel Julve,; *J.Chem.Soc. Dalton Trans.*, 2003, 4626 – 4634
- [78] Paul, F.; Patt, J.; Hartwig, J. F. *J. Am. Chem. Soc.* 1994, 116, 5969.
- [79] Anil S. Guram and Stephen L. Buchwald *J. Am. Chem. Soc.* 1994,116 (17): 7901–7902
- [80] R. D. Stephens and C. E. Castro *J. Org. Chem.*; 1963; 28(12); 3313 - 3315;
- [81] K. Sonogashira, Y. Tohda, N. Hagihara; *Tetrahedron Letters*. 1975, 16 (50): 4467–4470.
- [82] Karl Wilhelm Rosenmund, Erich Struck *Chemische Berichte*, 1919,52: 1749..
- [83] F. Ullmann, Jean Bielecki; *Chemische Berichte* , 1901, 34 (2): 2174–2185

- [84] J. Hassan, M. Sevignon, C. Gozzi, E. Schulz, M. Lemaire.; *Chemical Reviews*, 2002. 102: 1359–1470.
- [85] Derek van Allen, PhD Thesis, University of Massachusetts at Amherst 2004.
- [86] Iram Goldberg; *Berichte der deutschen chemischen Gesellschaft* , 1906, 39 (2): 1691–169275-76
- [87] Weingarten, H. *J. Am. Chem. Soc.* 1964, 29, 3624-3626.
- [88] Cohen, T.; Crostea, I. *J. Am. Chem. Soc.* 1976, 98, 748-753.
- [89] R.H. Crabtree, *The Organometallic Chemistry of the Transition Metals*, 3rd ed., Wiley, New York, 2001.
- [90] B.F.G. Johnson, J. Lewis, A.D. Massey, P.R. Raithby, W.T. Wong, *J. Organomet. Chem.* 397 (1990) C28.
- [91] E. Louattani, J. Suades, *J. Organomet. Chem.* 604 (2000) 234.
- [92] L.R. Falvello, J. Fornie's, J. Go'mez, E. Lalinde, A. Marti'n, F. Marti'nez, M.T. Moreno, *J. Chem. Soc., Dalton Trans.* (2001) 2132.
- [93] G. Hogarth, T. Norman, *Polyhedron* 15 (1996) 2859.
- [94] O. Orama, *J. Organomet. Chem.* 314 (1986) 273.
- [95] John J. McGarvey, Steven E. J. Bell, Keith C. Gordon, *Inorg. Chem.*, 1988, 27 (22), 4003–4006
- [96] Colin G. Coates, Tia E. Keyes, John J. McGarvey, Helen P. Hughes, Johannes G. Vos and Pradeep M. Jayaweera *Coordination. Chemistry Reviews*, 1998, 171, 323-330
- [97] Walton, R.A; *Cn.J.Chem.*, 1996, 44, 1480

- [98] Jawroska, J.K.; Puszko, A.; Kubaik, M.; Pelczynska, M.; J. Inorg. Biochem., 2004, 98, 1447
- [99] Durig, J.R.; Mitchell, B.R.; Sink, D.W.; Wills Jr., J.N.; Wilson, A.S.; Spectrochimica acta, 1967, 23A, 1121 and reference therein.
- [100] G.M. Sheldrick, SHELXTL V5.1 Software, Bruker AXS, Inc., Madison, Wisconsin, USA, 1997
- [101] G.M. Sheldrick, SADABS. Program for Empirical Absorption correction of Area detector Data, University of Gottingen, Germany, 1996.
- [105] Qi-Bing Bo, Guo-Xin Sun, and Dong-Ling Geng Inorg. Chem. 2010, 49, 561–571
- [106]. Abrahams, B.F.; Hoskins, B.F.; Michael, D.M.; Robson, R.
Nature 1994, 369, 727.
- [107]. Yaghi, O.M.; Li, G. *Nature* 1995, 378, 703.
- [108]. Kondo, M. *Bull. Chem. Soc. Jpn.* 1998, 71, 1.
- [109]. Chui, S.S.Y.; Lo, S.M.F.; Charmant, J.P.H.; Orpen, A.G.;
Williams, I.D. *Science* 1999, 283, 1148
- [110] Víctor Blanco, Albert Gutiérrez, Carlos Platas-Iglesias, Carlos Peinador and
Jose M. Quintela, J. Org. Chem. Vol. 74, No. 17, 2009
- [111] Yaghi, O.M.; Li, G. *Nature* 1995, 378, 703.
- [112] J.-M. Lehn, *Supramolecular Chemistry*, VCH, Weinheim, 1995;
- [113] G. De Munno and M. Julve, in *Metal–Ligand Interactions. Structure and Reactivity*, ed. N. Russo and D. R. Salahub, Kluwer, Dordrecht, NATO ASI Ser. C, 1996, vol. 474, pp. 139–162;

- [114] G. DeMunno, T. Poerio, G. Viau, M. Julve and F. Lloret, *Angew. Chem., Int. Ed. Engl.*, 1997, 36, 1459;
- [115] G. De Munno, W. Ventura, G. Viau, F. Lloret, J. Faus and M. Julve, *Inorg. Chem.*, 1998, 37, 1458;
- [116] J. Sletten, H. Daraghmeh, F. Lloret and M. Julve, *Inorg. Chim. Acta*, 1998, 279, 127;
- [117] G. De Munno, T. Poerio, M. Julve, F. Lloret and G. Viau, *New J. Chem.*, 1998, 299
- [118] D. Armentano, G. De Munno, F. Lloret and M. Julve, *Inorg. Chem.*, 1999, 38, 3744;
- [119] G. De Munno, T. Poerio, M. Julve, F. Lloret, J. Faus and A. Caneschi, *J. Chem. Soc., Dalton Trans.*, 1998, 1679;
- [120] G. De Munno, D. Armentano, M. Julve, F. Lloret, R. Lescouëzec and J. Faus, *Inorg. Chem.*, 1999, 38, 2234;
- [121] D. Armentano, G. De Munno, J. Faus, F. Lloret and M. Julve, *Inorg. Chem.*, 2001, 40, 655;
- [122] Y. Rodríguez-Martín, J. Sanchiz, C. Ruiz-Pérez, F. Lloret and M. Julve, *Inorg. Chim. Acta*, 2001, 326, 20;
- [123] B. Vangdal, J. Carranza, F. Lloret, M. Julve and J. Sletten, *J. Chem. Soc., Dalton Trans.*, 2002, 566.
- [124] S. Decurtins, H. W. Schmalle, P. Schneuwly, L. M. Zheng, J. Ensling and A. Hauser, *Inorg. Chem.*, 1995, 34, 5501;
- [125] S. Decurtins, H. W. Schmalle, P. Schneuwly and L. M. Zheng, *Acta Crystallogr., Sect. C*, 1996, 52, 561.

- [126] S. Kawata, S. Kitagawa, M. Enomoto, H. Kumagai and M. Katada, *Inorg. Chim. Acta*, 1998, 283, 80;
- [127] M. K. Kabir, M. Kawahara, H. Kumagai, K. Adachi, S. Kawata, T. Ishii and K. Kitagawa, *Polyhedron*, 2001, 20, 1417.
- [128] S. R. Marshall, C. D. Incarvito, J. L. Manson, A. L. Rheinholt and J. S. Miller, *Inorg. Chem.*, 2000, 39, 1969.
- [129] J. S. Sun, H. Zhao, X. Ouyang, R. Clérac, J. A. Smith, J. M. Clemente-Juan, C. Gómez-Gracia, E. Coronado and K. Dunbar, *Inorg. Chem.*, 1999, 38, 5841
- [130] S. Martín, M. G. Barandika, J. I. Ruiz de Larramendi, R. Cortés, M. Font-Bardía, L. Lezama, Z. E. Serna, X. Solans and T. Rojo, *Inorg. Chem.*, 2001, 40, 3687.
- [131] Graham.A.Bowmaker; Jeffery.C.Dyson;Peter.C.Healy; *J.Chem.Soc.Dalton.Trans*, 1987, 1089-1097
- [132] The Crystal as a Supramolecular Entity, from Perspectives in Supramolecular Chemistry, ed. G. R. Desiraju, Wiley, Chichester, 1996, vol. 2;
- [133] N. T. Huang, W. T. Pennington and J. D. Petersen, *Acta Crystallogr., Sect. C*, 1991, 47, 2011.
- [134] V. W. W. Yam, V. W. M. Lee and K. K. Cheung, *Organometallics*, 1997, 16, 2833;
- [135] M. B. Ferrari, G. G. Fava, G. Pelosi, G. Predieri, C. Vignali, G. Denti and S. Serroni, *Inorg. Chim. Acta*, 1998, 275–276, 320;
- [136] J. R. Kirchhoff and K. Kirschbaum, *Polyhedron*, 1998, 17, 4033; (d) Y. Y. Choi and W. T. Wong, *J. Chem. Soc., Dalton Trans.*, 1999, 331;
- [137] L. W. Morgan, K. V. Goodvin, W. T. Pennington and J. D. Peterson, *Inorg. Chem.*, 1992, 31, 1103; (b) J. Sletten and O. Bjorsvik,
- [138] *Acta Chem. Scand.*, 1998, 52, 770;

- [139] H. Grove, J. Sletten, M. Julve, F. Lloret and L. Lezama, *Inorg. Chim. Acta*, 2000, 310, 217;
- [140] H. Grove, M. Julve, F. Lloret, P. E. Kruger, K. W. Törnroos and J. Sletten, *Inorg. Chim. Acta*, 2001, 325, 115
- [141] S. M. Scott, K. C. Gordon and A.K. Burrell, *J. Chem. Soc., Dalton Trans.*, 1999, 2669.
- [142] D. J. Chesnut, A. Kusnetzow, R. R. Birge and J. Zubieta, *Inorg. Chem.*, 1999, 38, 2663.
- [143] Graham.A.Bowmaker, Peter C.Healy, John D.Kildea, Allan H.White; *Spectrochimica Acta*, 1998, Vol.44A, No.11, 1219-1213

Appendices

A-I

Experimental Techniques

The different characterization techniques used in the studies are as follow.

Melting Temperature

The Buchi 510 melting point apparatus was used to determine the melting point of the complexes. Few mg of clean, finely ground appropriate sample was packed in small capillary and immersed in silicone oil. The temperature of the oil was raised at slow heating rate to get the exact melting point.

Ultraviolet Visible Spectroscopy

The UV-Vis spectroscopy of the sample was carried out using Perkin Elmer Lambda EZ 210 spectrometer. 1.5-3.5 mg of appropriate sample was dissolved in 20 ml of dichloromethane. 0.5 ml was then diluted with 2.5 ml of DCM for analysis.

Emission Spectroscopy

1.5-3.5 mg of appropriate sample was dissolved in 20 ml of dichloromethane and the emission spectra were recorded at room temperature Shimadzu on PF-5301 PC spectrofluorometer.

Fourier-Transformed Infra Red Spectroscopy (FT-IR)

About 1-2 mg sample were dispersed in 150 mg of anhydrous KBr to make pellet. These pellets were used to take FT-IR spectra on Perkin Elmer FTIR 16FPC spectrometer.

Far-Infrared Spectroscopy

About 10 mg of the sample were mixed and grinded with 90-100 mg of high density polyethylene (HDPE) to make pellet. These pellets were used to take Far-IR spectra on

Nicolet 6700 FT-IR spectrometer. Typically 600-800 scans were used for spectra collection

Raman Spectroscopy

Raman spectra were collected for solid samples on NIOCLET NXR 967 FT Raman spectrometer. Typically 128 scans were used for spectra collection.

Nuclear Magnetic Resonance Spectroscopy

^1H NMR and ^{31}P NMR were recorded on a JEOL LAMBDA 500 spectrometer. About 10-12 mg of the solid sample was dissolved in $\text{DMSO}-d_6$ or Cd_2Cl_2 for ^1H NMR and ^{31}P NMR. Tetramethylsilane and 85% H_3PO_4 were used as internal and external references respectively

Single Crystal X-ray Analysis

The single crystal X-ray structures were carried out on Bruker-AXS SMART APEX CCD diffractometer. Single crystal of appropriate size was glued on glass needle with araldite. This needle was mounted on a sample holder and fixed in the X-ray goniometer. The dimension of the crystal were measured and the X-ray diffraction pattern collected using SHLEXTL (5.1 V). The structural parameters were refined using the same program. SADABS were also run for samples. Some of the graphics were done using WinGX program.

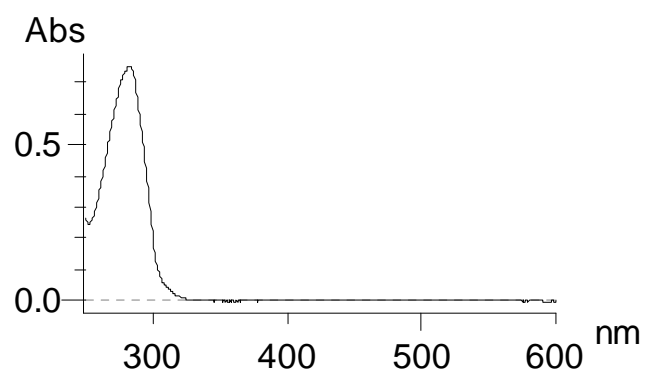
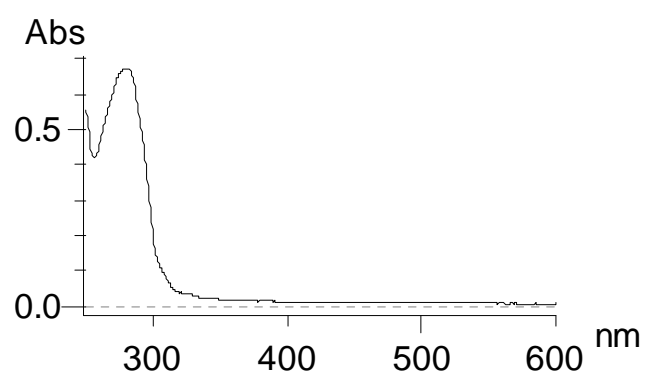
Gas Chromatography and Mass Spectrometry

A screening of the reactant and product for the coupling of phenylacetylene with halobenzene was carried out using GC-MS (Varian CP-3800 GC coupled with MS Varian Saturn 2000).

GC equipment and experimental conditions

Agilent GC 6890 plus series gas chromatograph equipped with split-splitless injector (split ratios of 20:1) was used for the GC analysis. The temperature of the injector was

2500C, with 10 psi constant pressure. the column was an HP-5 Column (30 m x 0.25 mm i.d., 0.25um film thickness) consisting of CrossbondR (5% phenyl-95% dimethylpolysiloxane). Helium was the carrier gas at a flow rate of 15.8 ml/ min and tprogrammed temperature was applied to obtain the seperation of compounds; precisely the initial temperature was 500C, hold 2 min, then ramped at 10 0C/min to 140 0C (hold time 0 min), then finely ramped at 200C/min to 2500C (hold time 20 min).

A-II**Figure 1** UV-Visible Spectrum of bipy**Figure 2.** Figure 1 UV-Visible Spectrum of 4,4'-Me₂bipy

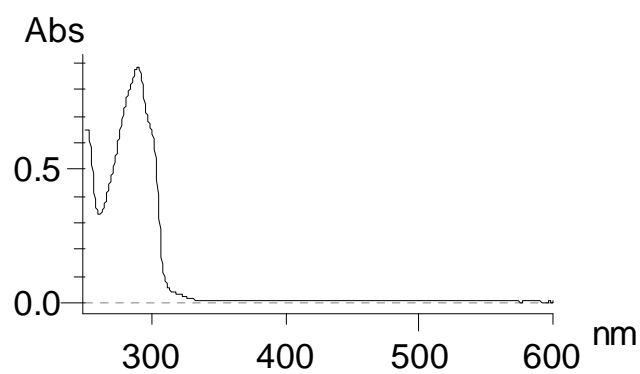


Figure 3. UV-Visible Spectrum of 5,5'-Me₂bipy

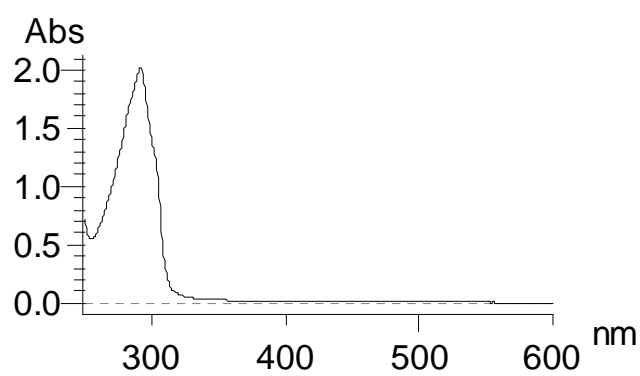


Figure 4. UV-Visible Spectrum of 6,6'-Me₂bipy

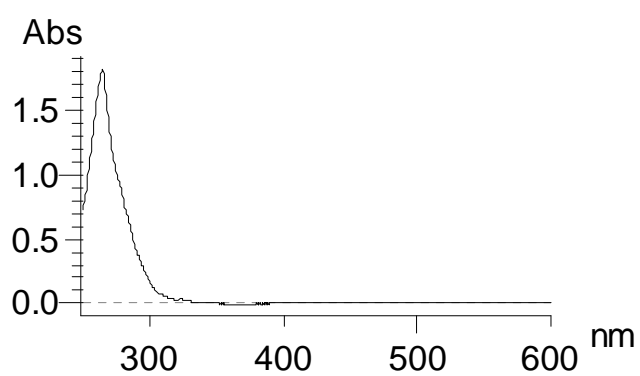


Figure 5. UV-Visible Spectrum of phen

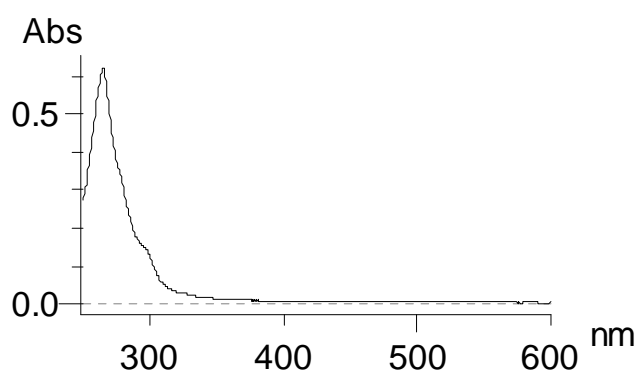


Figure 6. UV-Visible Spectrum of 4-Mephen

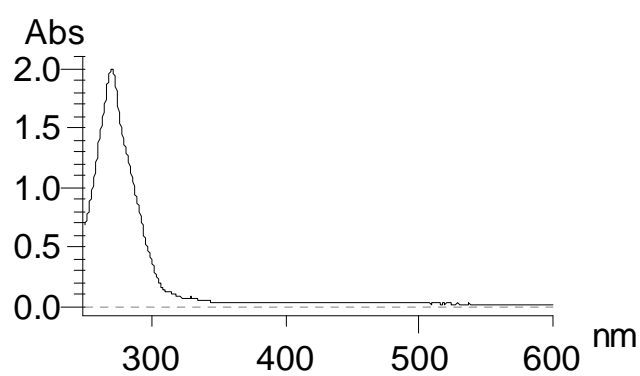


Figure 7. UV-Visible Spectrum of 2,9-Me₂phen

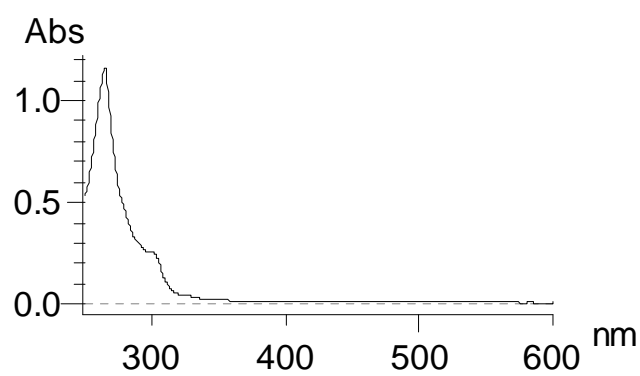


Figure 8. UV-Visible Spectrum of 4,7-Me₂phen

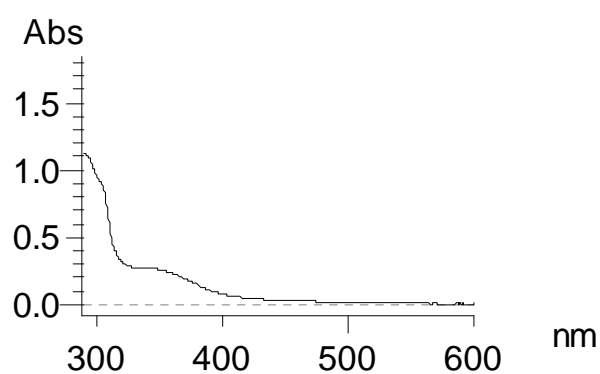


Figure 9. UV-Visible Spectrum of Complex 2

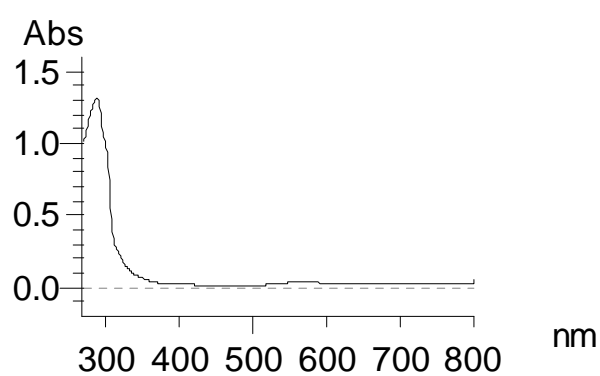


Figure 10. UV-Visible Spectrum of Complex 3

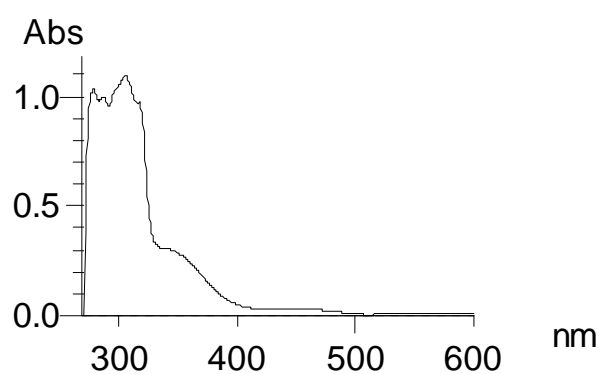


Figure 11. UV-Visible Spectrum of Complex 4

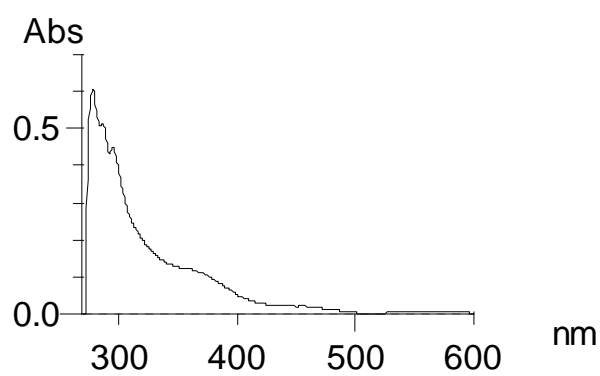


Figure 12. UV-Visible Spectrum of Complex 5

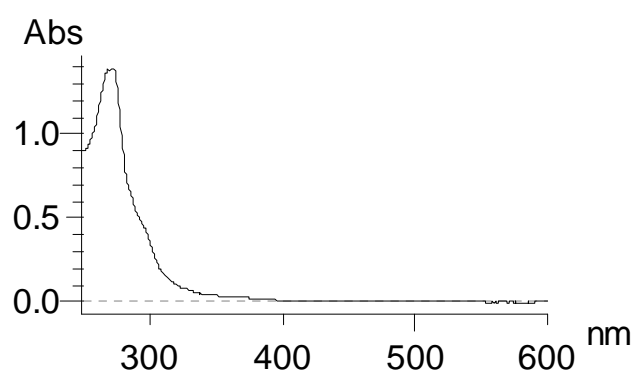


Figure 13. UV-Visible Spectrum of Complex 6

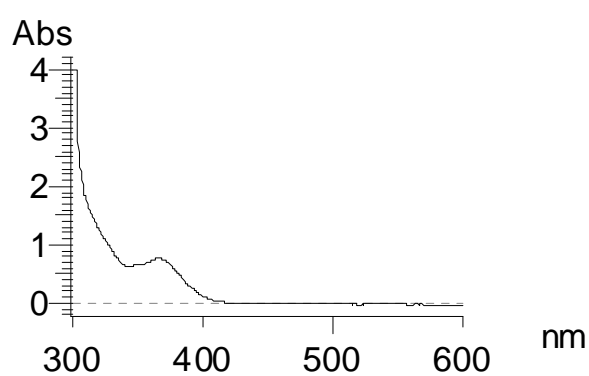


Figure 14. UV-Visible Spectrum of Complex 7

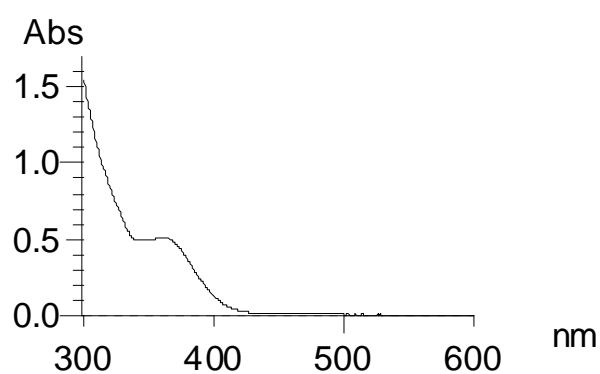


Figure 15. UV-Visible Spectrum of Complex 8

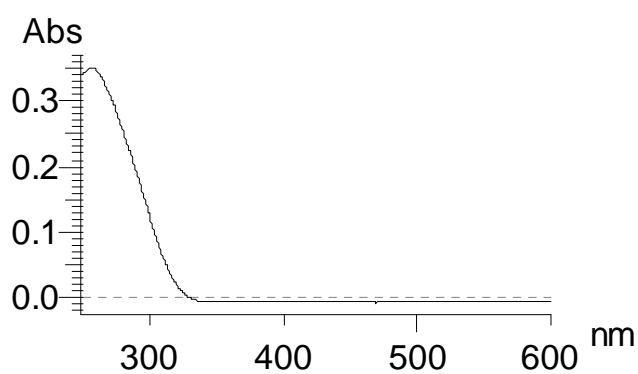


Figure 16. UV-Visible Spectrum of DPPETHY

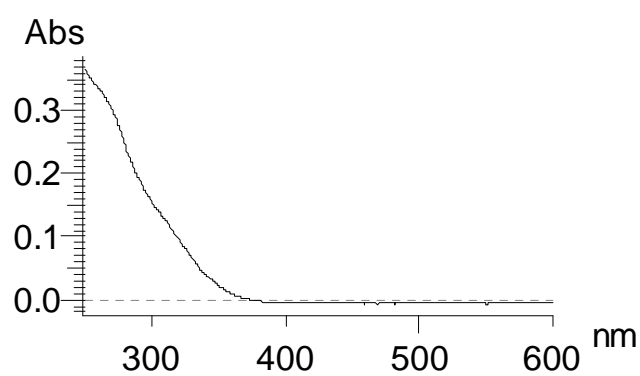


Figure 17. UV-Visible spectrum of precursor-B

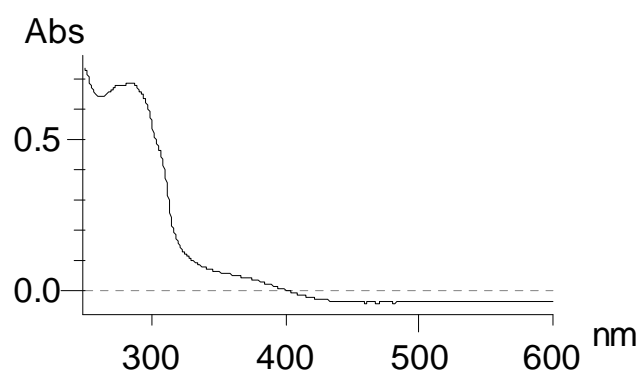


Figure 18. UV-Visible Spectrum of Complex 9

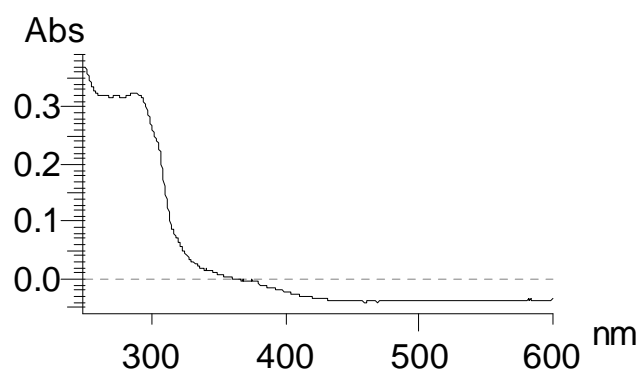


Figure 19. UV-Visible Spectrum of Complex 10

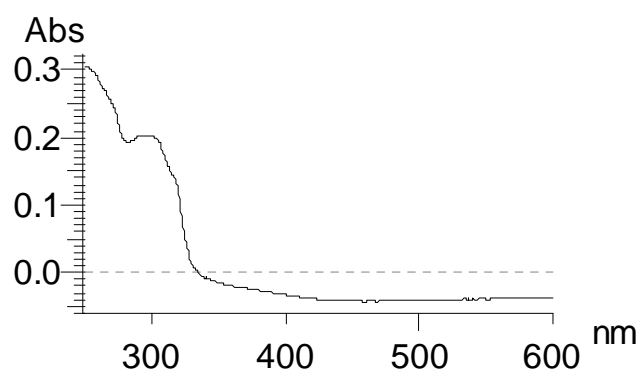


Figure 20. UV-Visible Spectrum of Complex 11

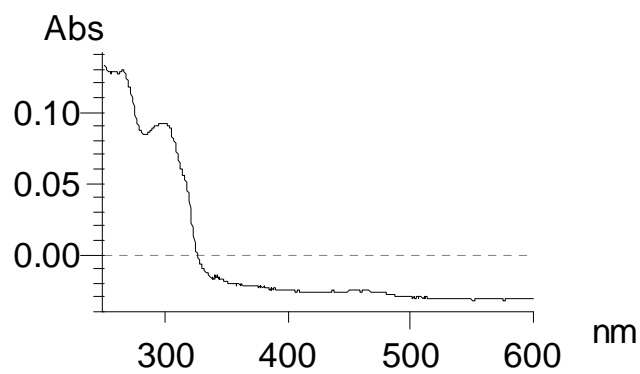


Figure 21. UV-Visible Spectrum of complex 12

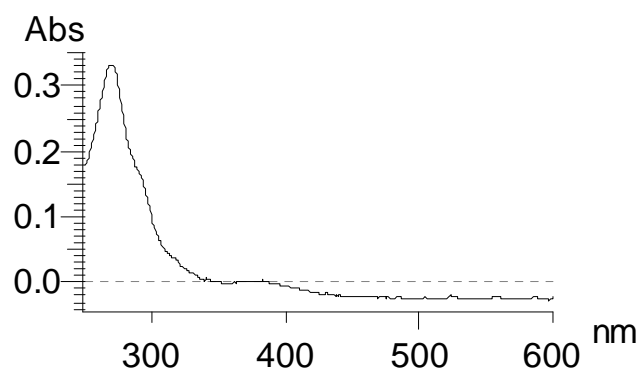


Figure 22. UV-Visible Spectrum of complex 13

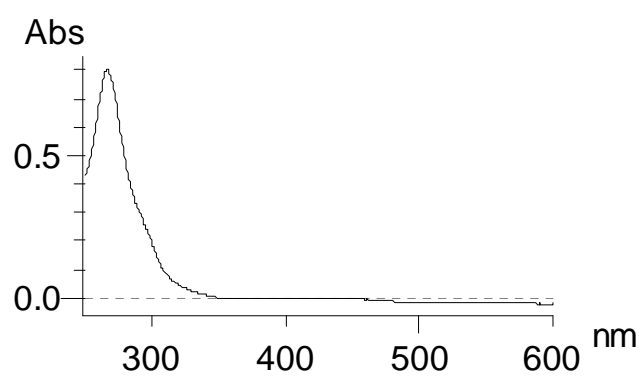


Figure 23. UV-Visible Spectrum of complex 14

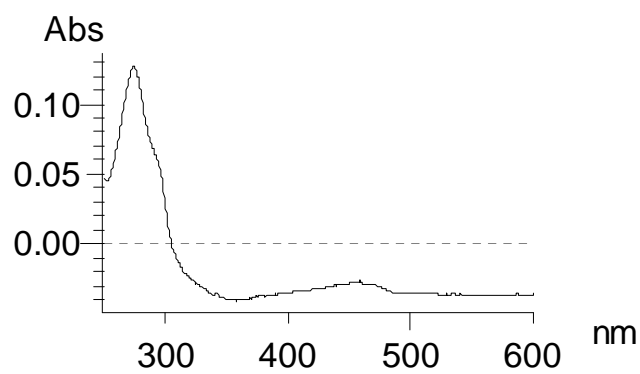


Figure 24. UV-Visible Spectrum of complex 15

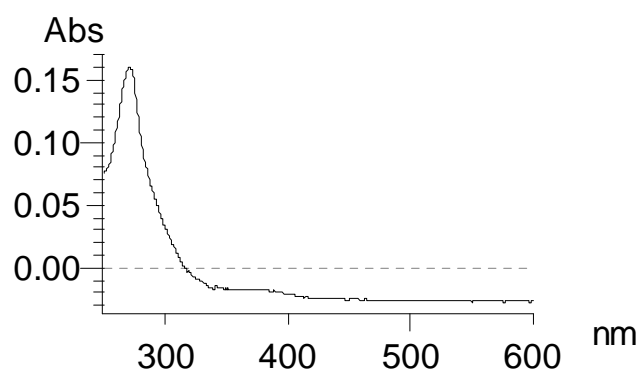


Figure 25. UV-Visible Spectrum of complex 16

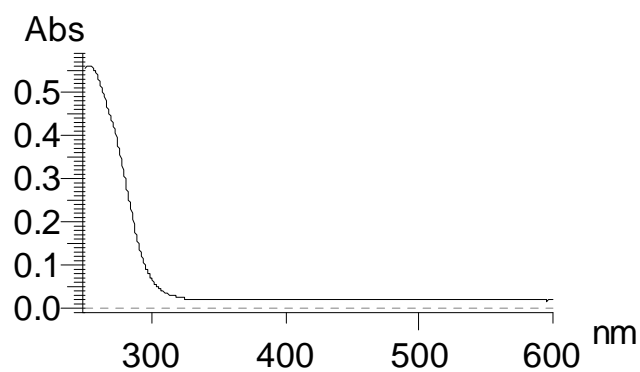


Figure 26. UV-Visible Spectrum of PPh₂(i-Pr)

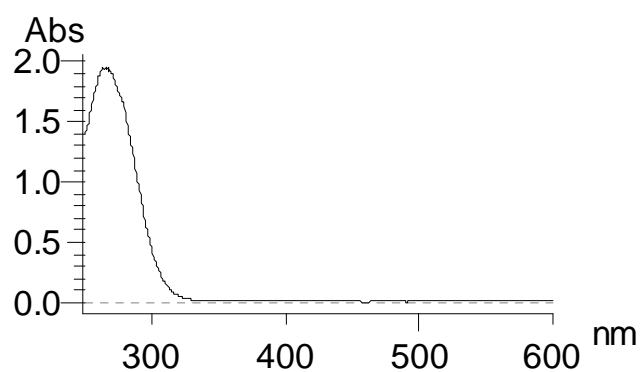


Figure 27. UV-Visible Spectrum of (m-Tol₃)P

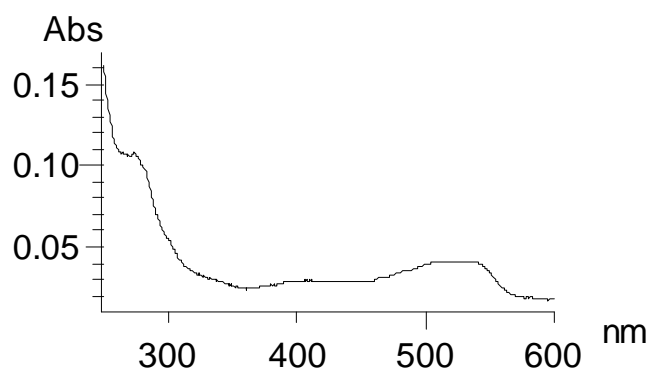


Figure 28. UV-Visible Spectrum of PCy₃

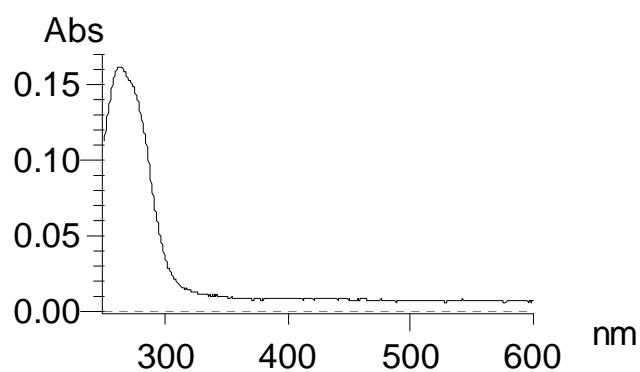


Figure 29. UV-Visible Spectrum of PPh_3

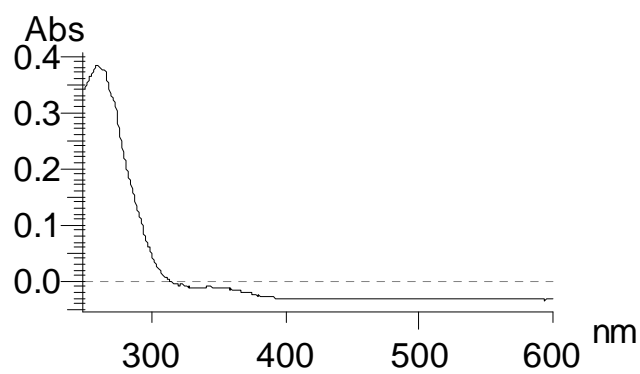


Figure 30. UV-Visible Spectrum of $^t\text{BuPh}_2\text{P}$

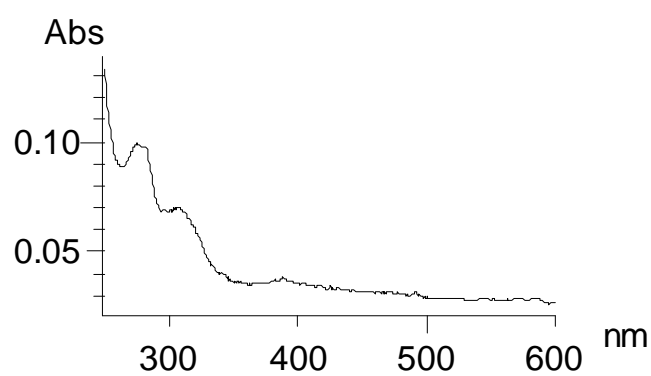


Figure 31. UV-Visible Spectrum of TCP

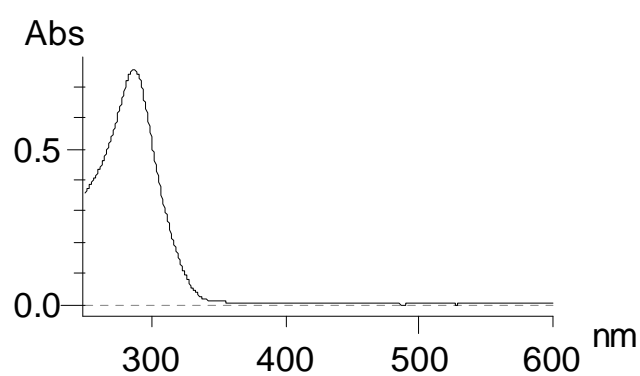


Figure 32. UV-Visible Spectrum of DAP-DP

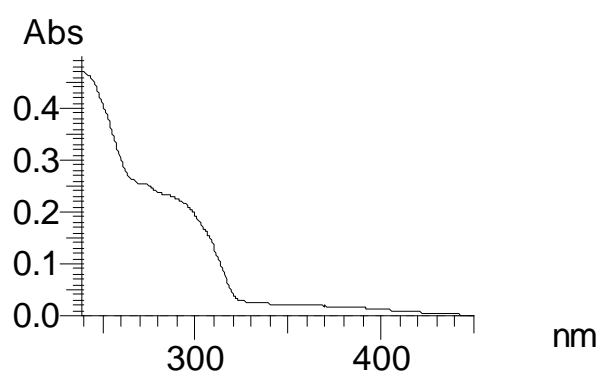


Figure 33. UV-Visible Spectrum of Complex 17

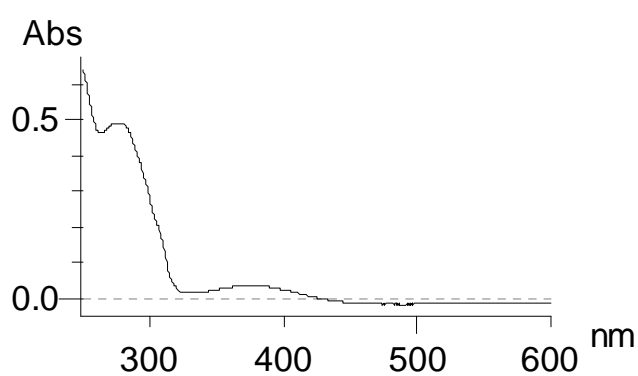


Figure 34. UV-Visible Spectrum of Complex 18

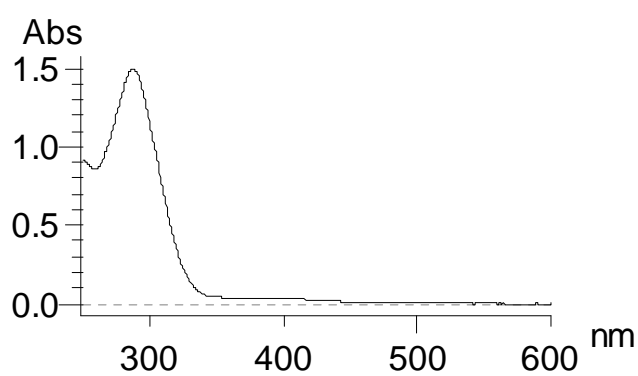


Figure 35. UV-Visible spectrum of complex 19

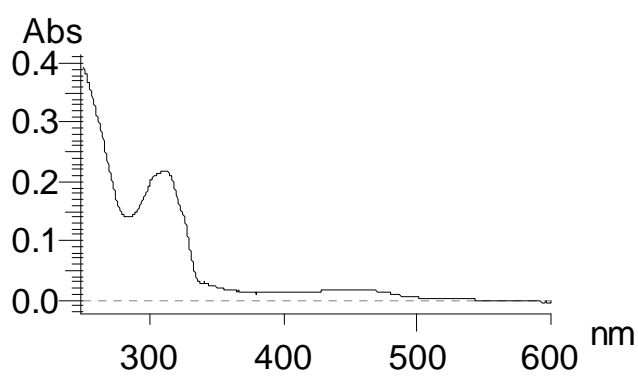


Figure 36. UV-Visible Spectrum of Complex 20

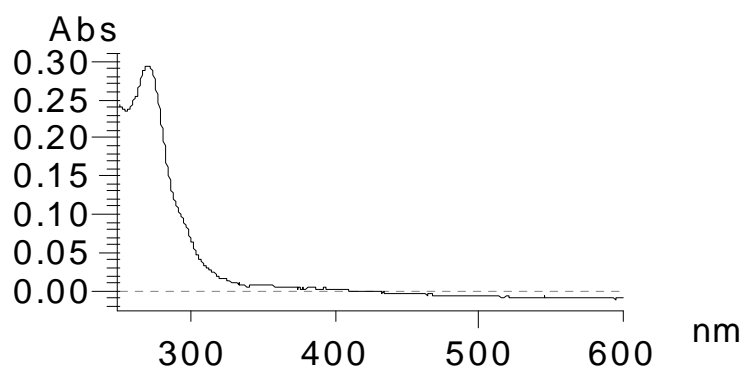


Figure 37. UV-Visible Spectrum of Complex 21

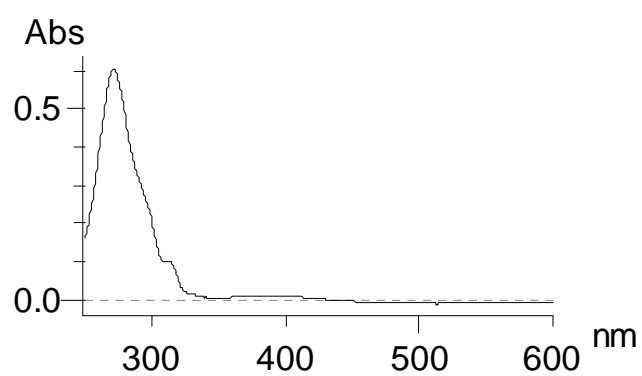


Figure 38. UV-Visible Spectrum of Complex 22

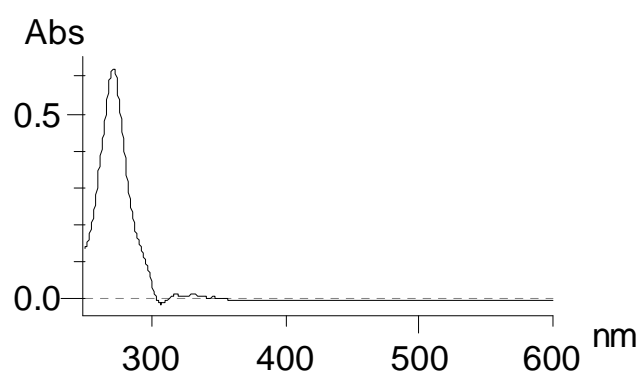


Figure 39. UV-Visible Spectrum of Complex 23

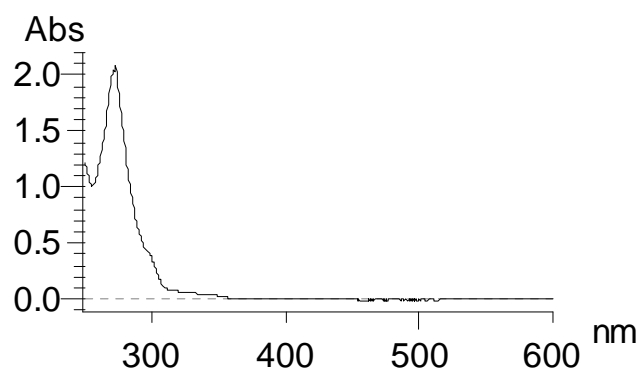


Figure 40. UV-Visible Spectrum of Complex 24

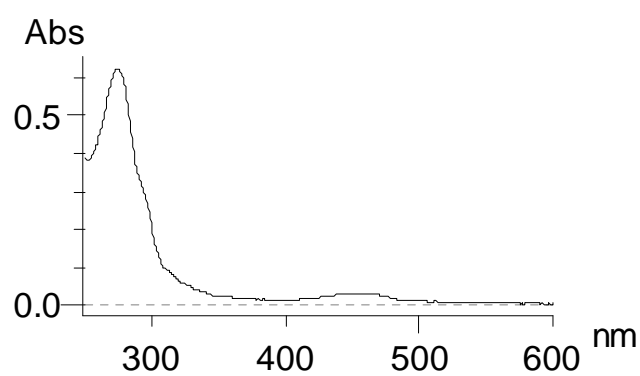


Figure 41. UV-Visible Spectrum of Complex 25

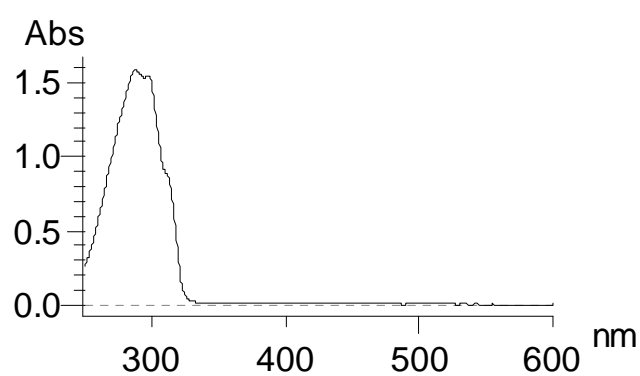


Figure 42. UV-Visible Spectrum of bpe

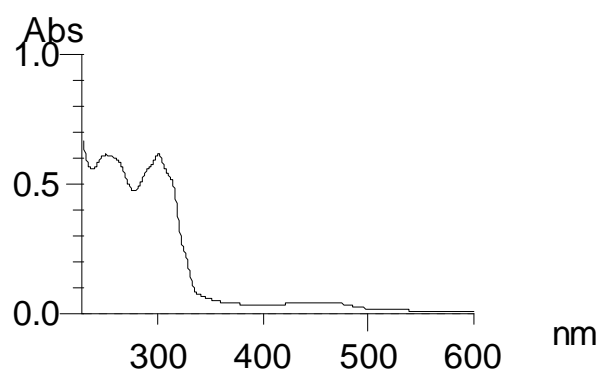


Figure 43. UV-Visible Spectrum of Complex 26

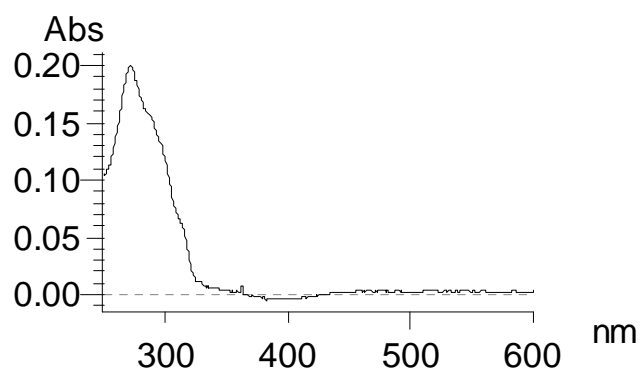


Figure 44. UV-Visible Spectrum of Complex 27

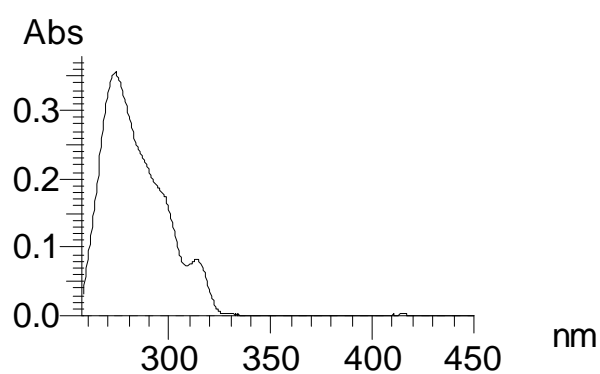


Figure 45. UV-Visible Spectrum of Complex 28

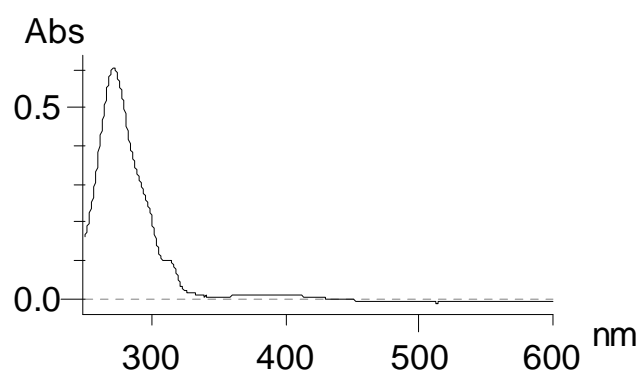


Figure 46. UV-Visible Spectrum of Complex 30

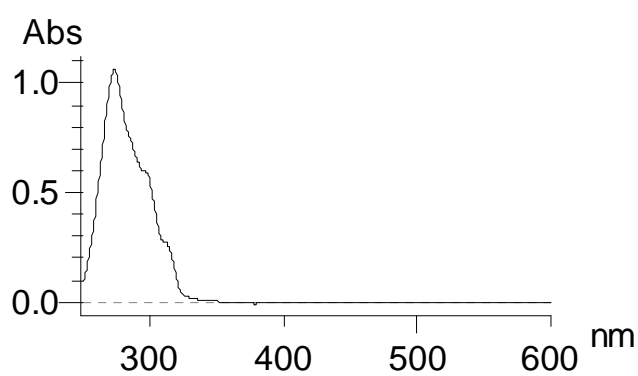


Figure 47. UV-Visible Spectrum of Complex 31

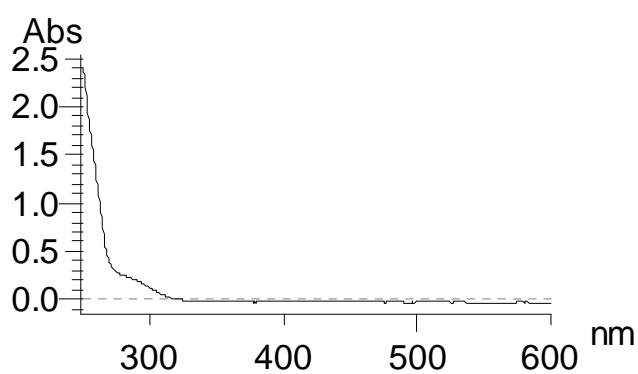


Figure 48. UV-Visible Spectrum of bpm

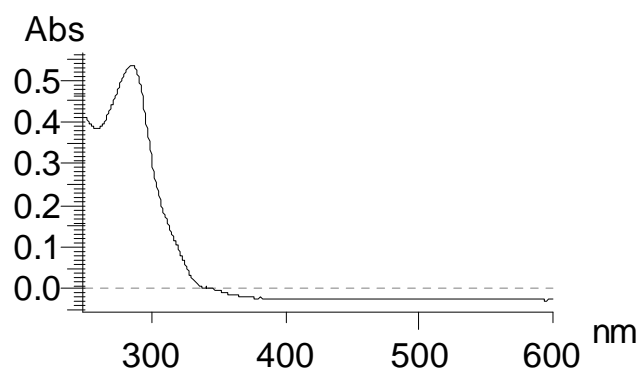


Figure 49. UV-Visible Spectrum of bpp

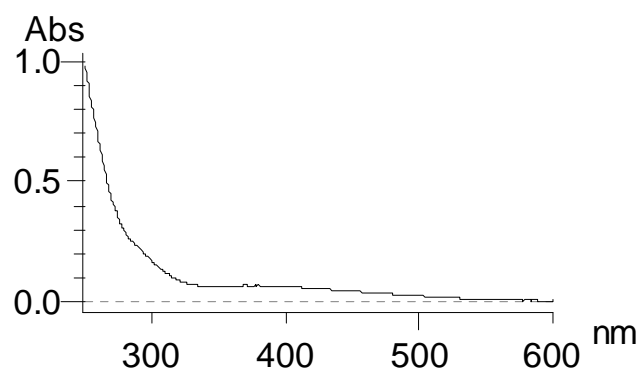


Figure 50. UV-Visible Spectrum of Complex 33

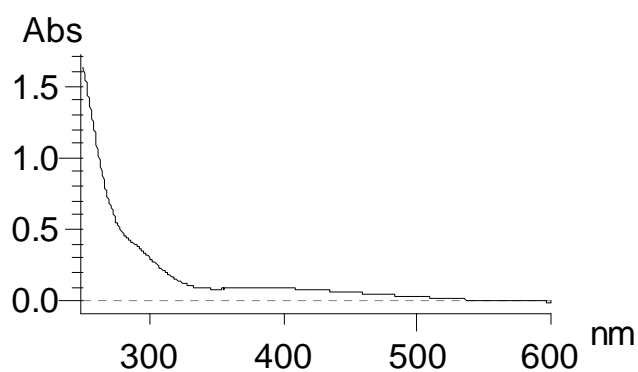


Figure 51. UV-Visible Spectrum of Complex 34

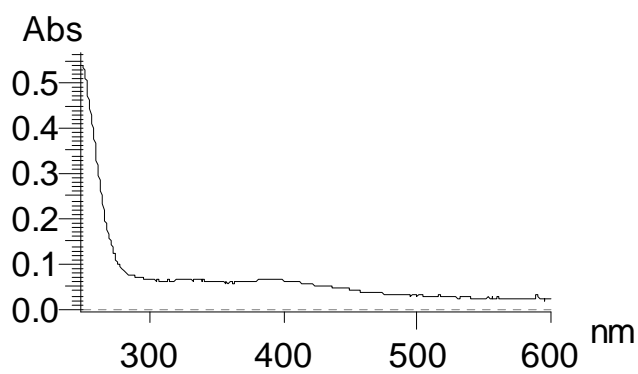


Figure 52. UV-Visible Spectrum of Complex 35

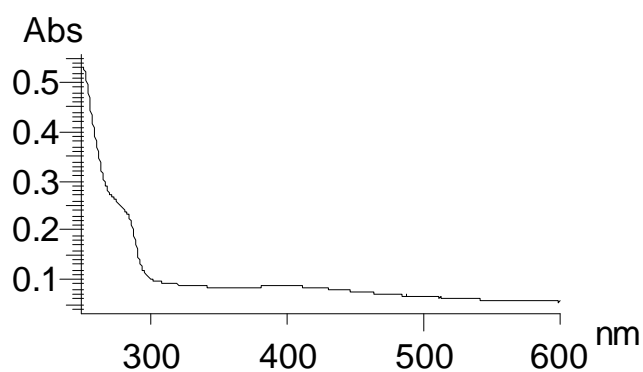


Figure 53. UV-Visible Spectrum of Complex 36

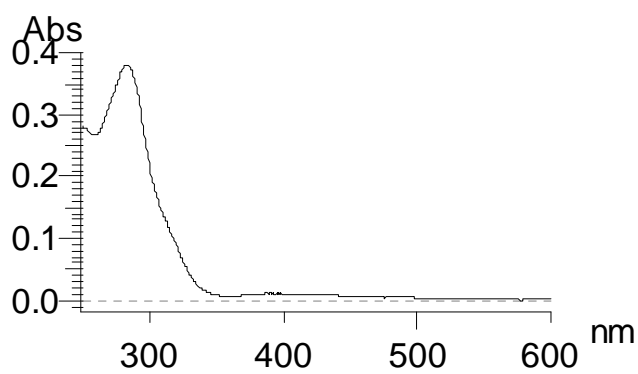


Figure 54. UV-Visible Spectrum of Complex 37

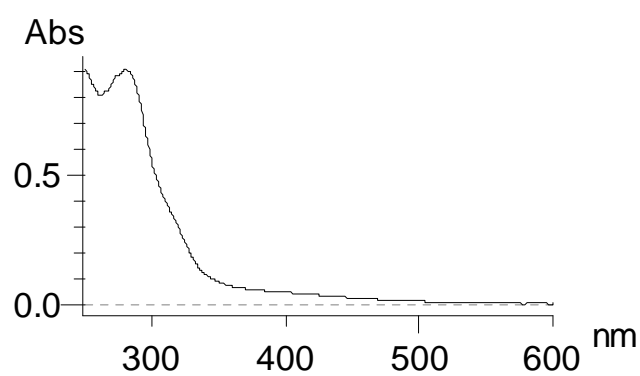


Figure 55. UV-Visible Spectrum of Complex 38

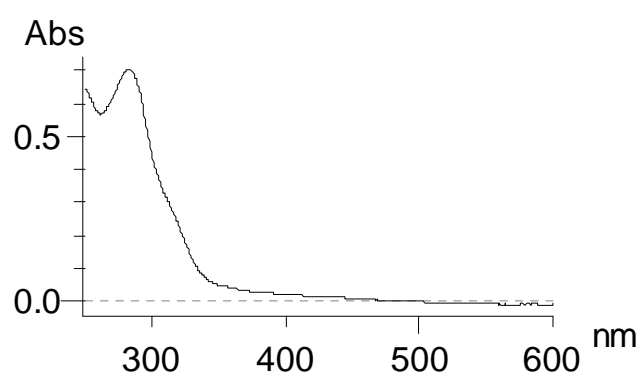


Figure 56. UV-Visible Spectrum of Complex 39

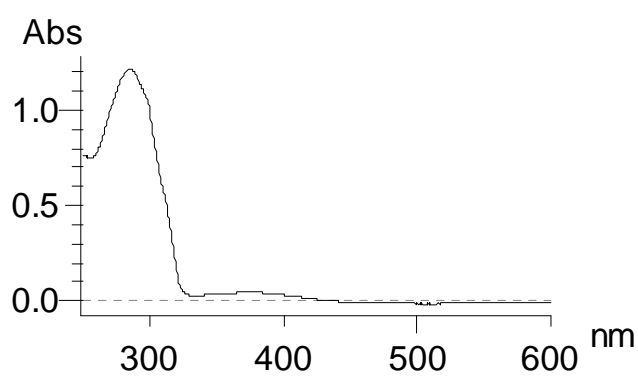


Figure 57. UV-Visible Spectrum of Complex 41

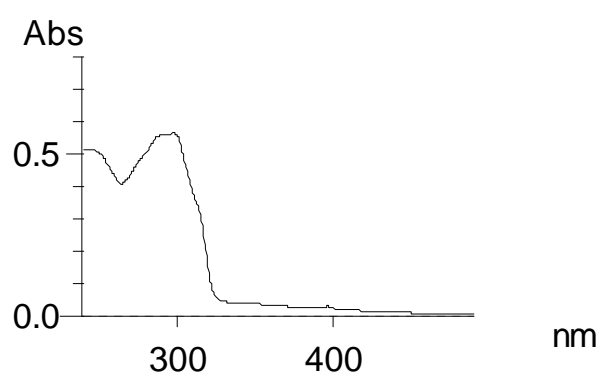


Figure 58. UV-Visible Spectrum of Complex 42

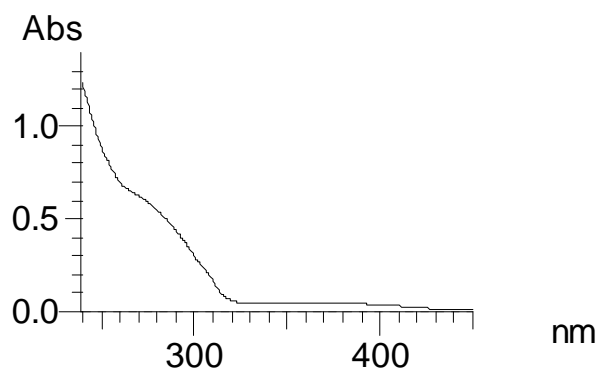


Figure 59. UV-Visible Spectrum of Complex 43

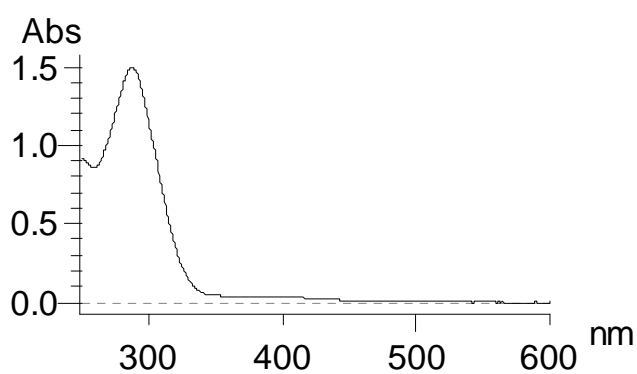


Figure 60. UV-Visible Spectrum of Complex 44

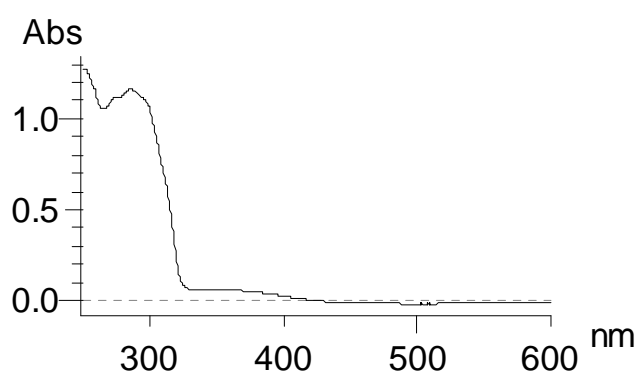


Figure 61. UV-Visible Spectrum of Complex 45

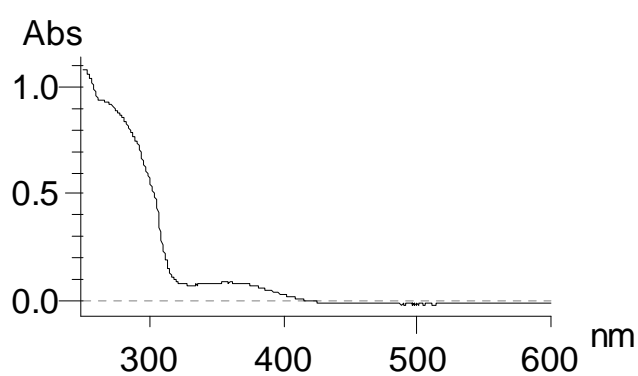


Figure 62. UV-Visible Spectrum of Complex 46

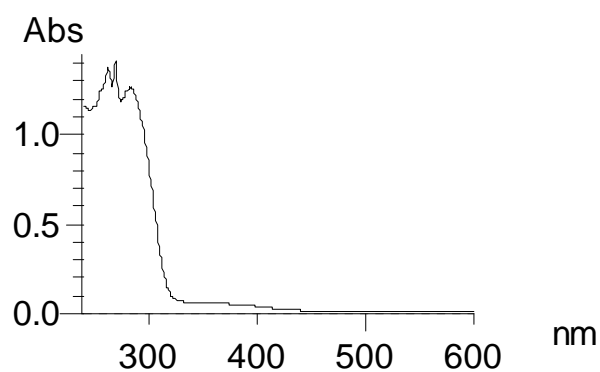


Figure 63. UV-Visible Spectrum of Complex 47

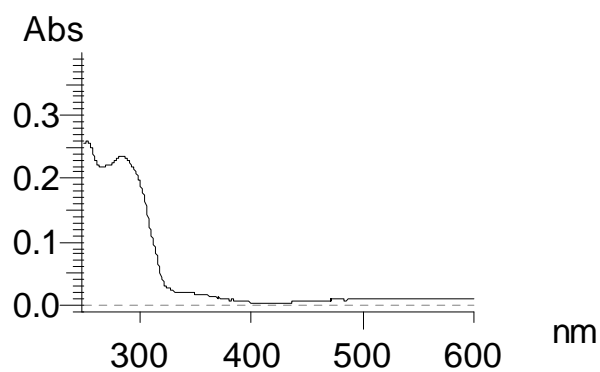


Figure 64. UV-Visible Spectrum of Complex 48

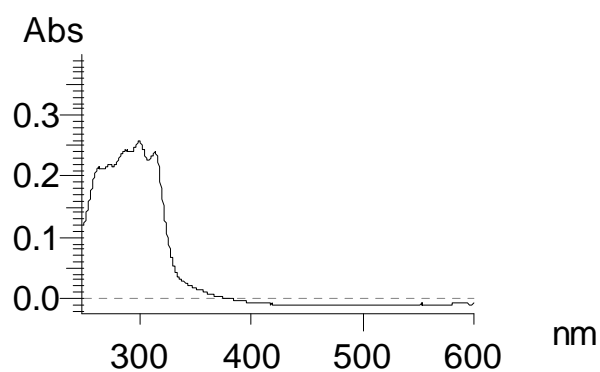


Figure 65. UV-Visible Spectrum of Complex 49

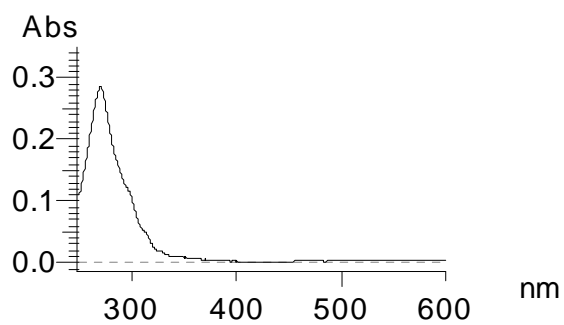


Figure 66. UV-Visible Spectrum of Complex 52

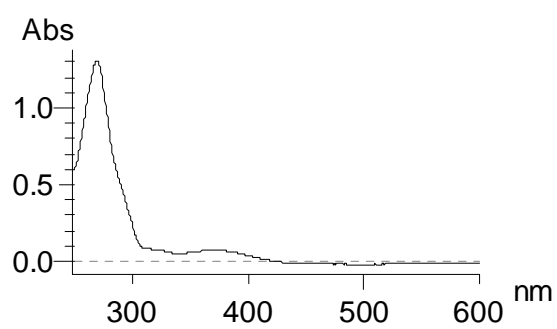


Figure 67. UV-Visible Spectrum of Complex 53

A-III

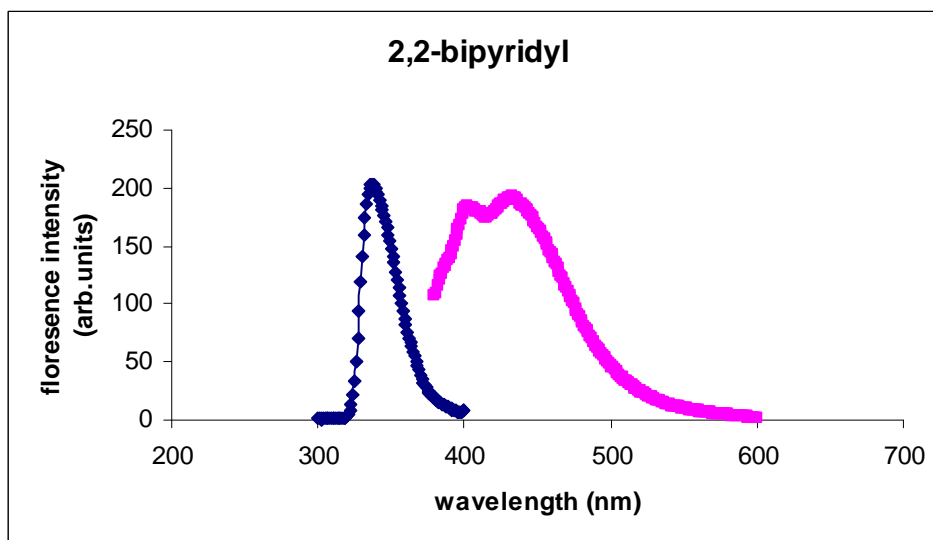


Figure 1. Excitation and Emission Spectrum of bipy

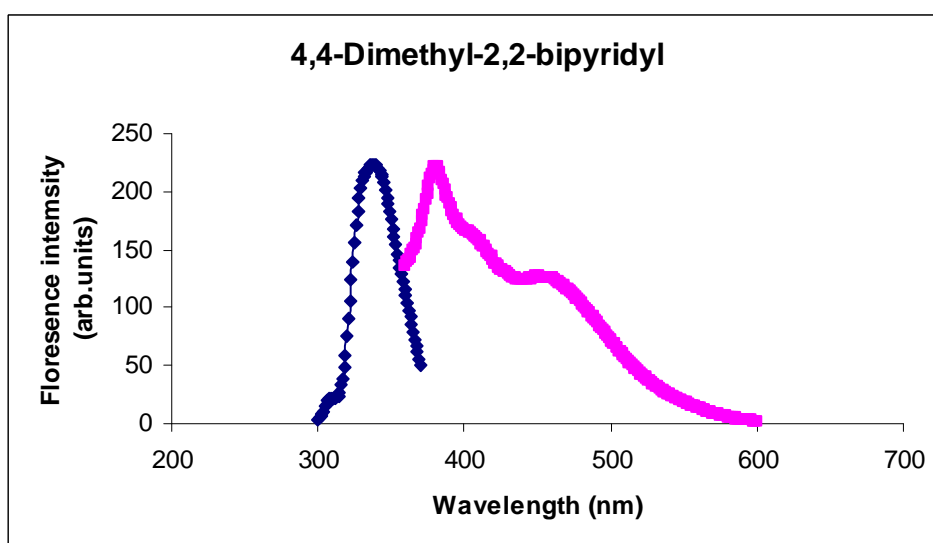


Figure 2. Excitation and Emission Spectrum of 4,4'-Me₂bipy

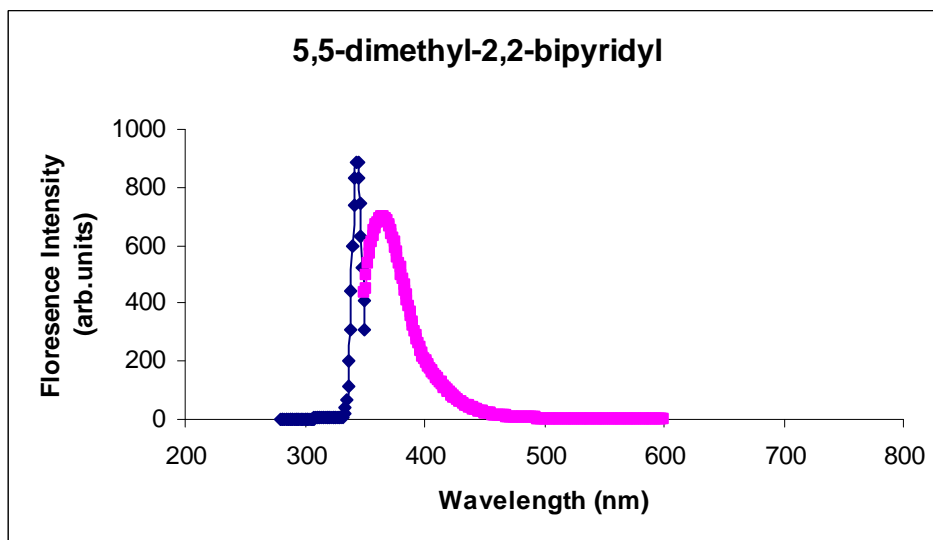


Figure 3. Excitation and Emission Spectrum of 5,5'-Me₂bipy

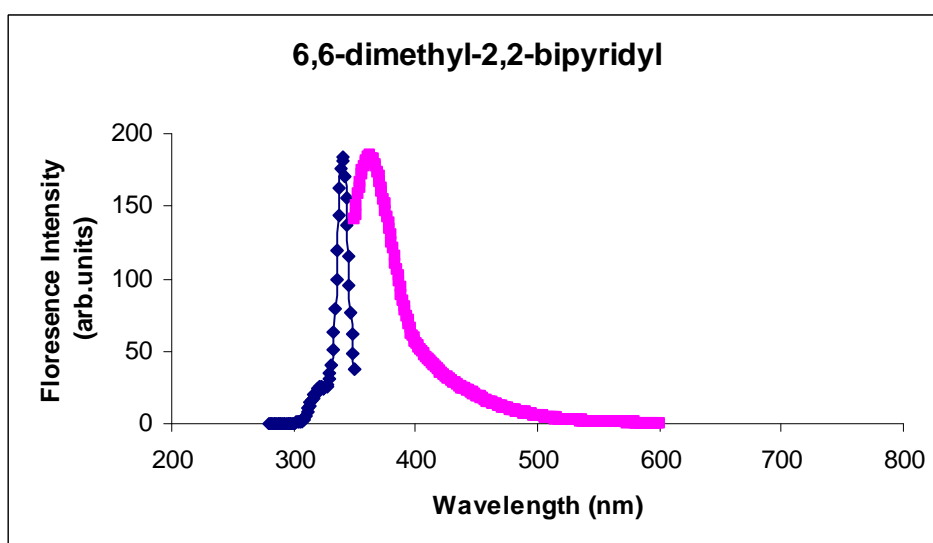


Figure 4. Excitation and Emission Spectrum of 6,6'-Me₂bipy

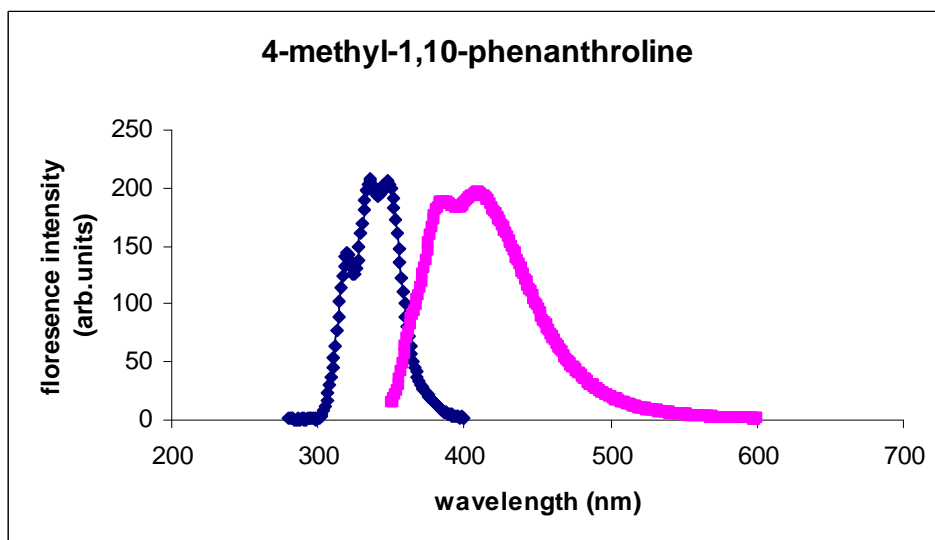


Figure 5. Excitation and Emission Spectrum of 4-Mephen

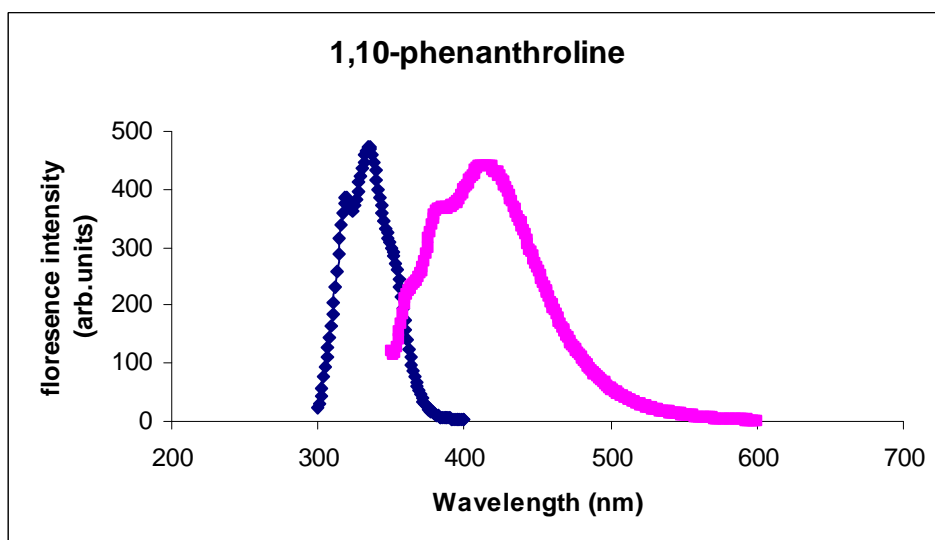


Figure 6. Excitation and Emission Spectrum of phen

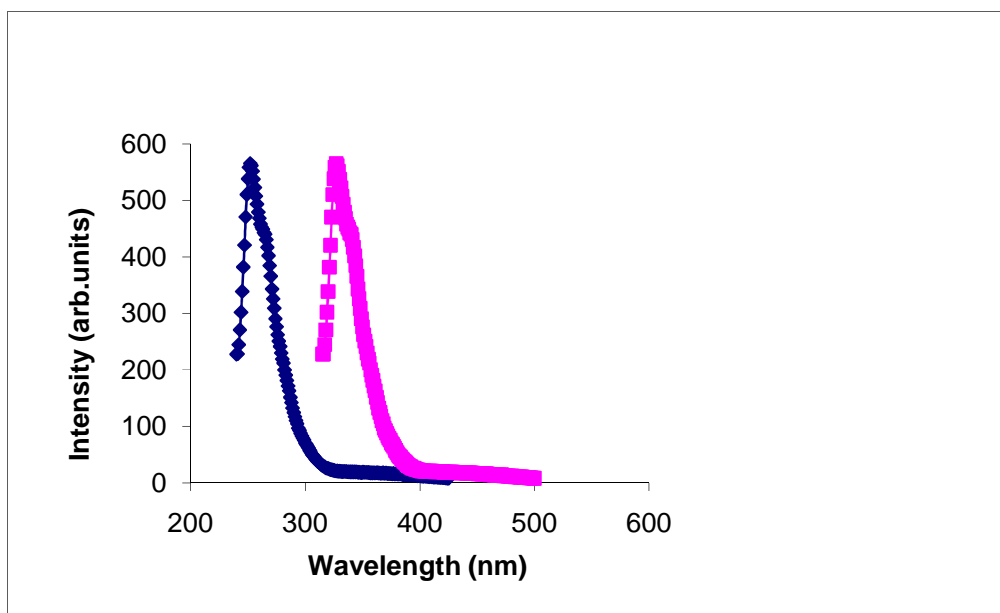


Figure 7. Excitation and Emission Spectrum of Complex 2

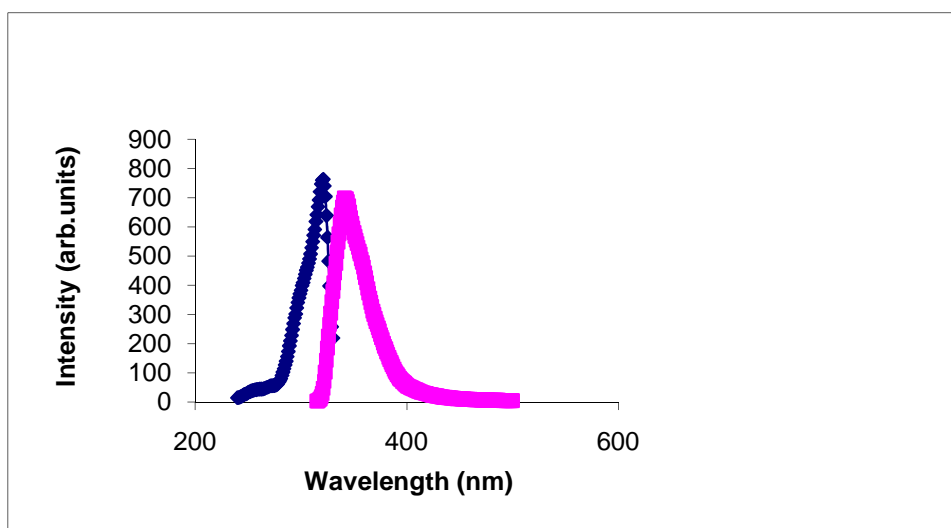


Figure 8. Excitation and Emission Spectrum of Complex 3

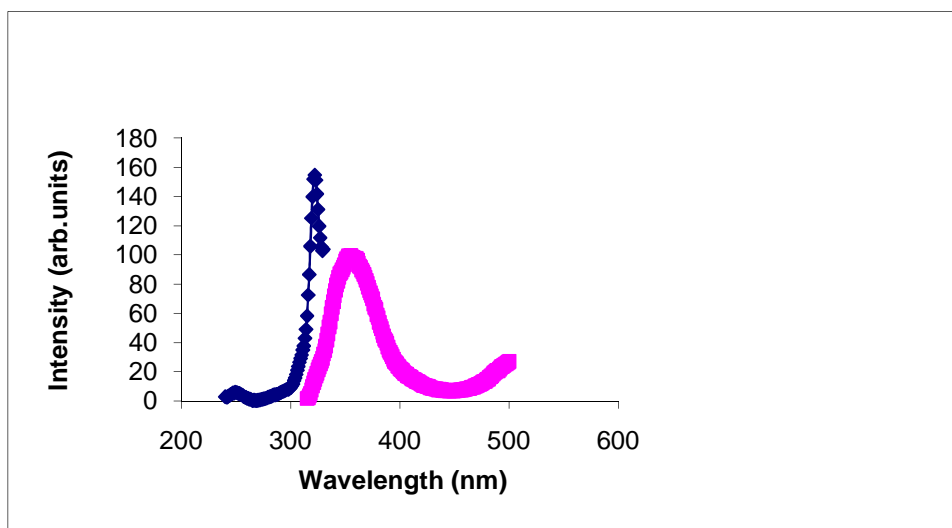


Figure 9. Excitation and Emission Spectrum of Complex 4

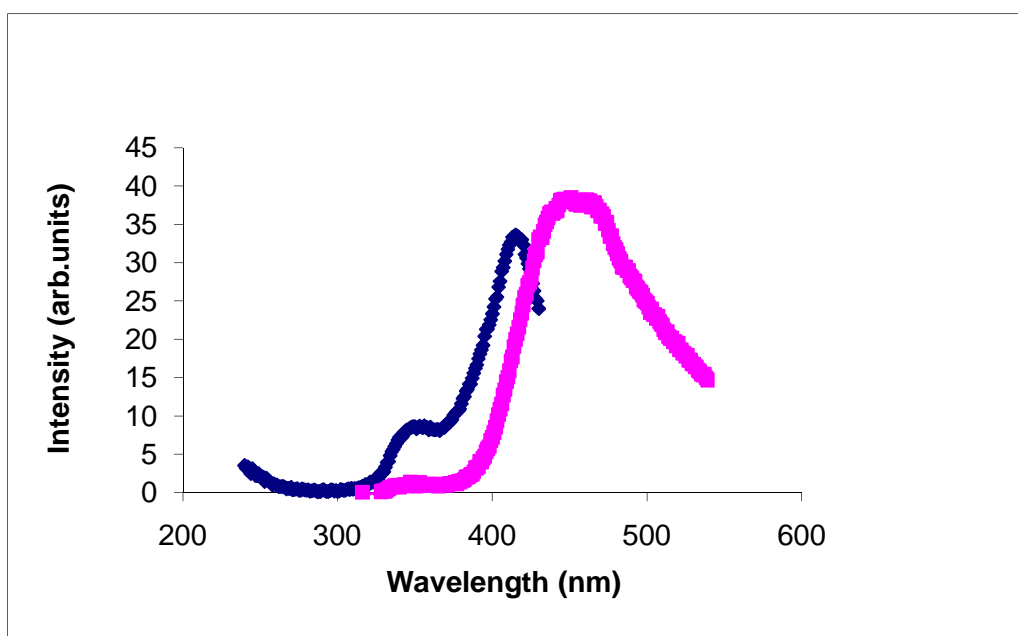


Figure 10. Excitation and Emission Spectrum of Complex 5

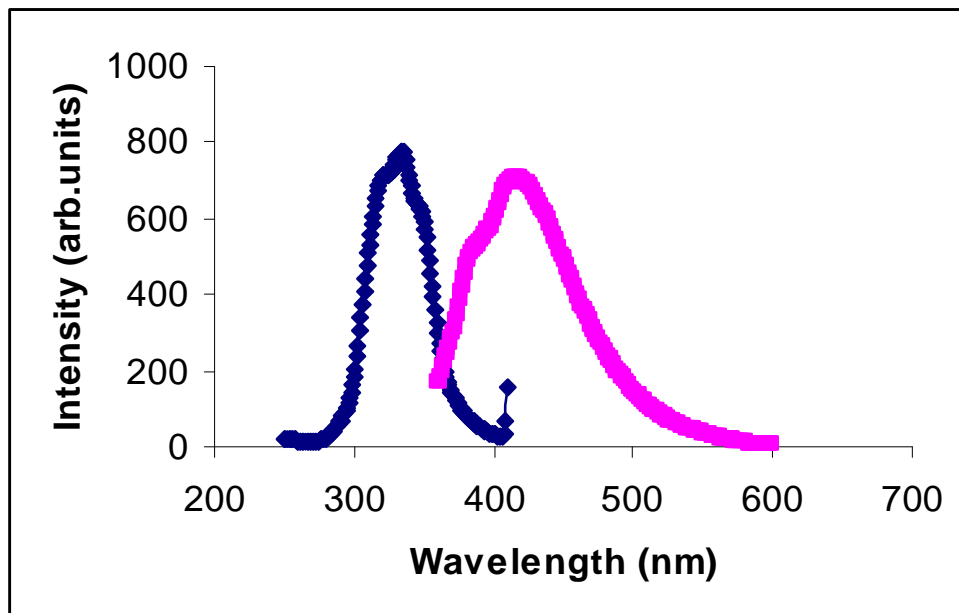


Figure 11. Excitation and Emission Spectrum of Complex 6

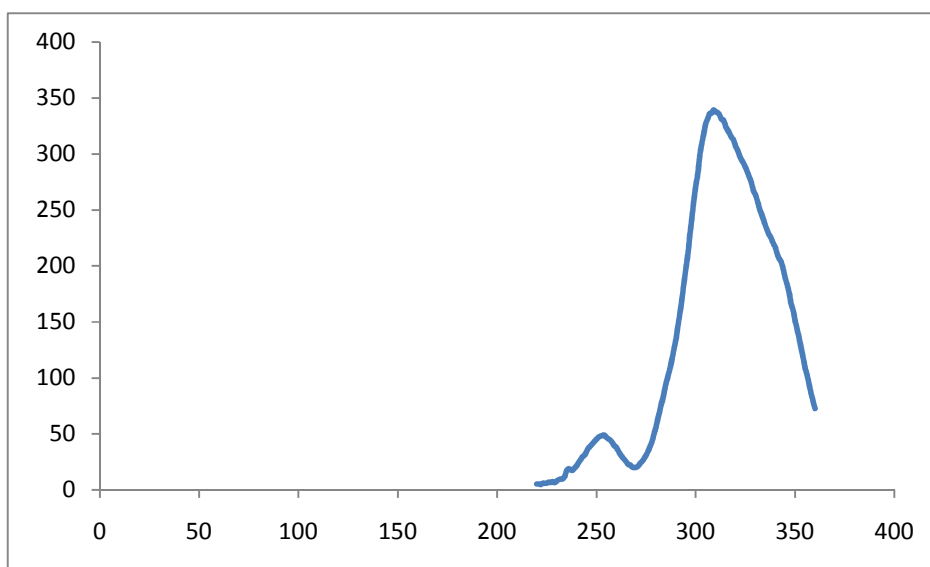


Figure 12. Emission spectrum of Complex 21

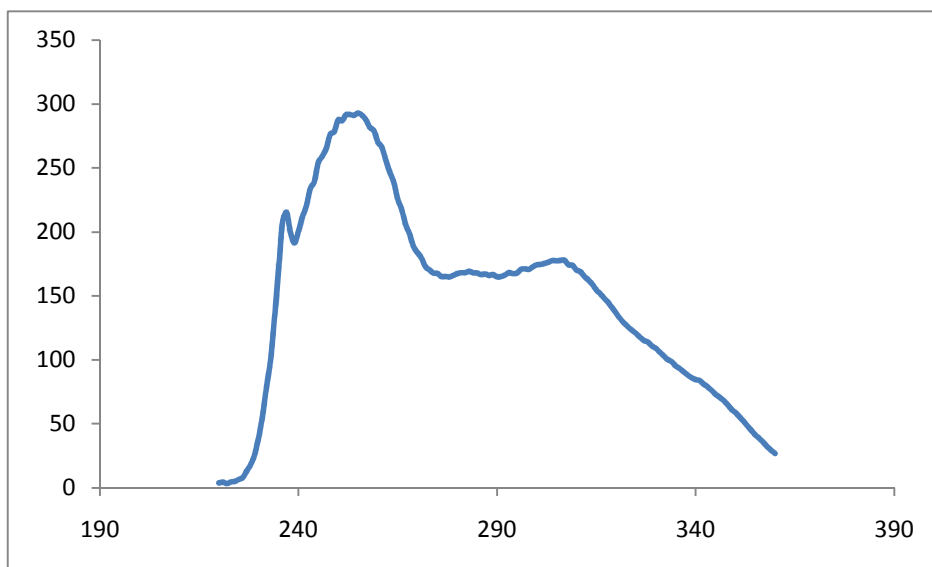


Figure 13. Excitation Spectrum of Complex 27

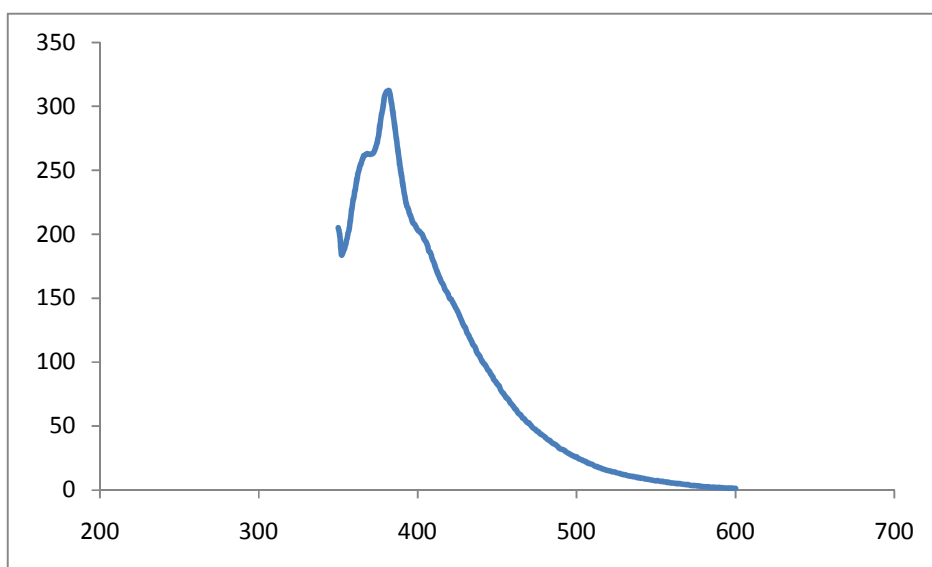


Figure 14. Emission Spectrum of Complex 27

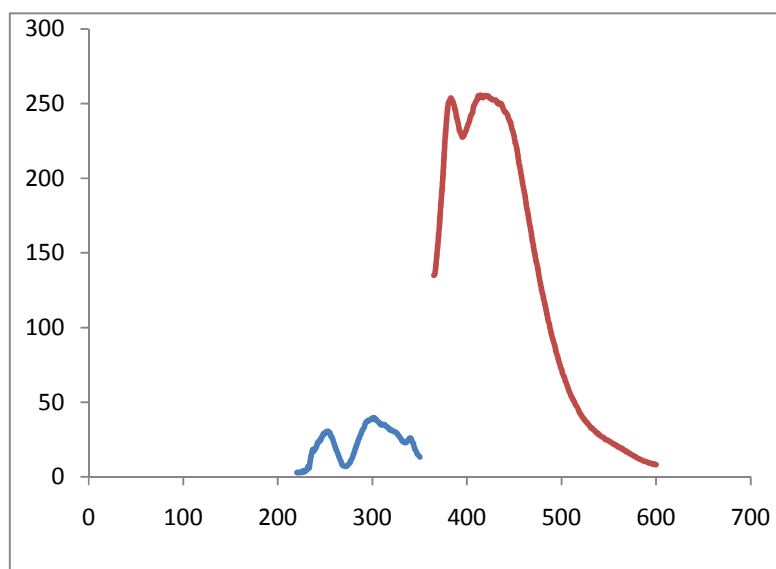


Figure 15. Emission and Excitation Spectrum of Complex 28

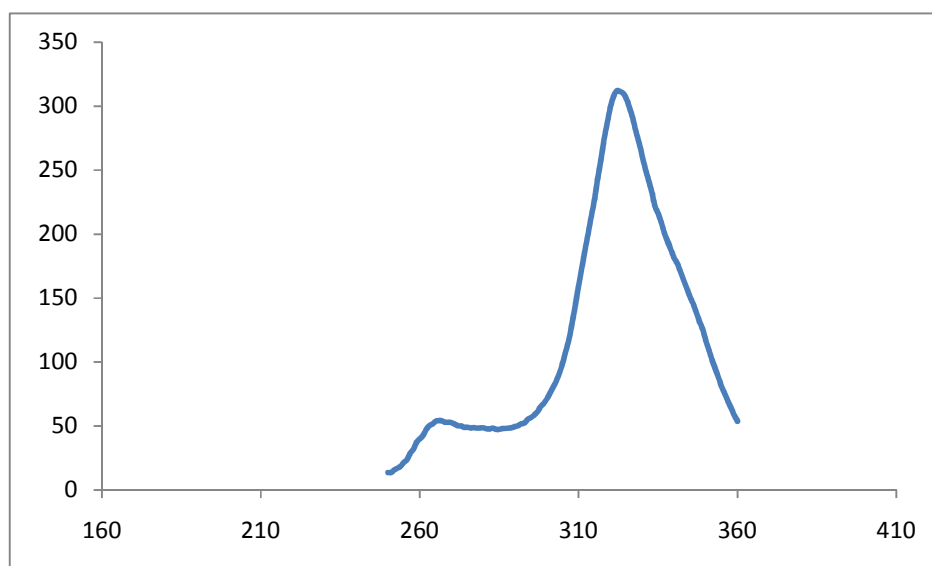


Figure 17. Excitation Spectrum of Complex 42

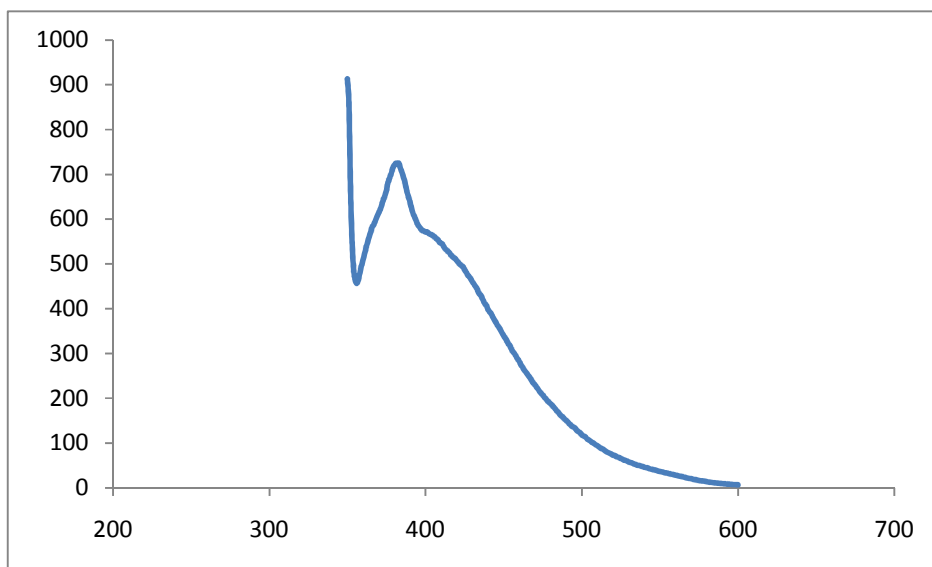


Figure 18. Emission Spectrum of Complex 42

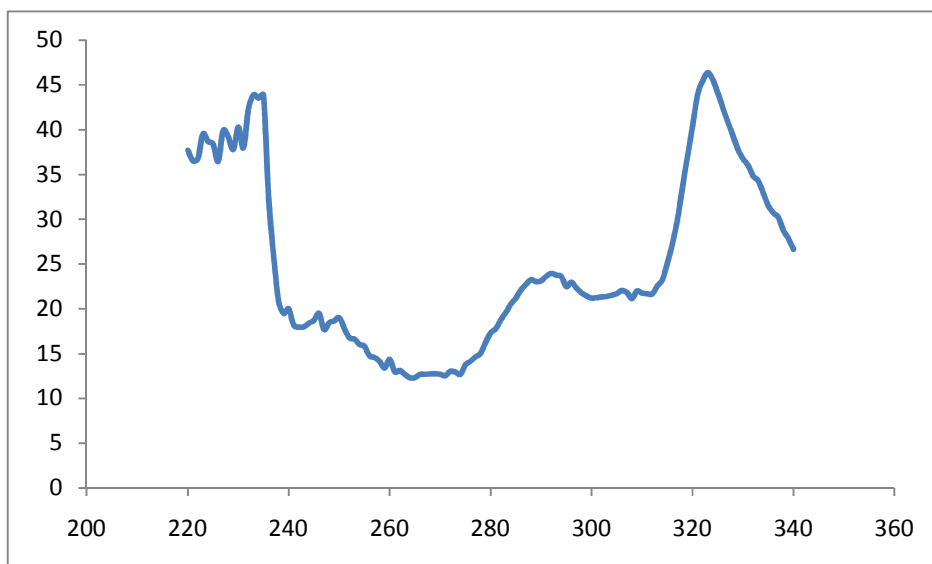


Figure 19. Excitation Spectrum of Complex 43

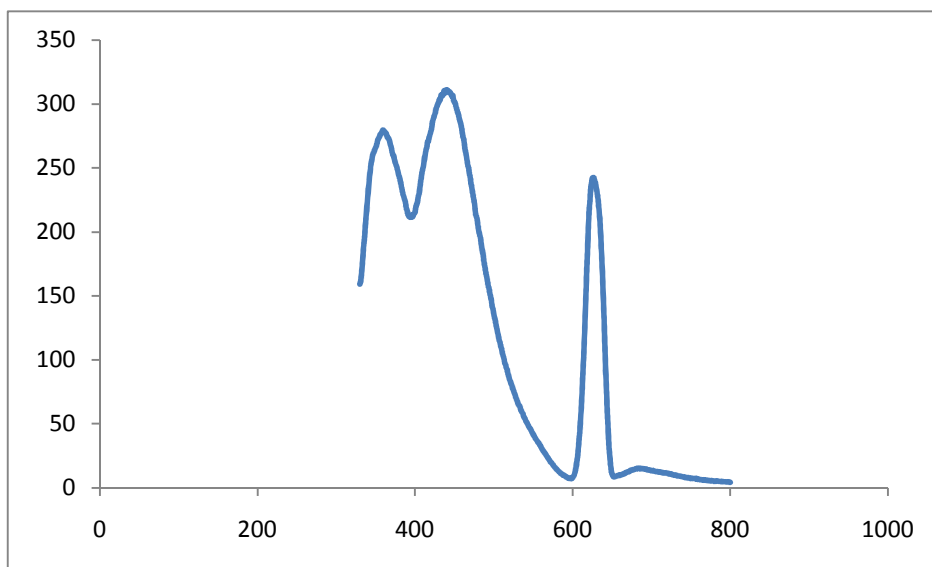


Figure 20. Emission Spectrum of Complex 43

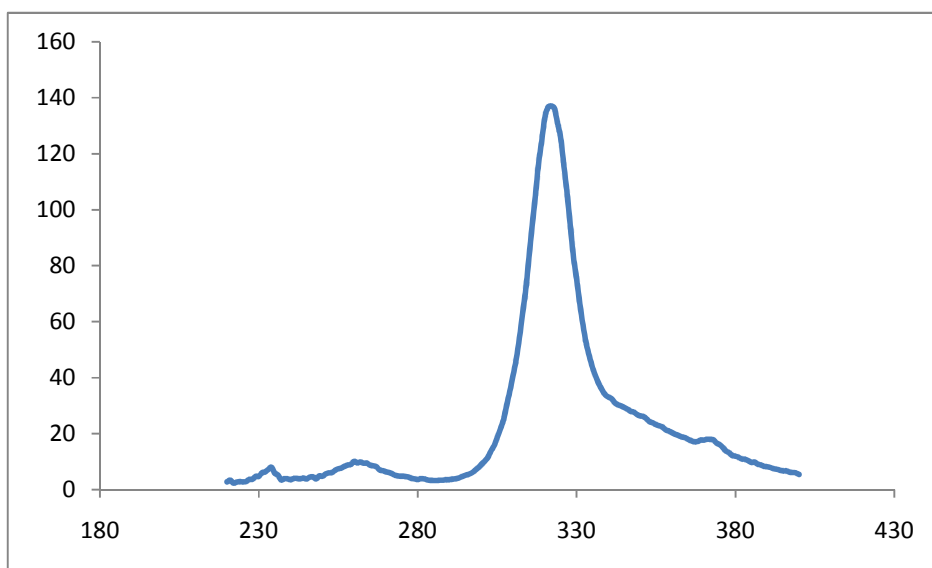


Figure 21. Excitation Spectrum of Complex 44

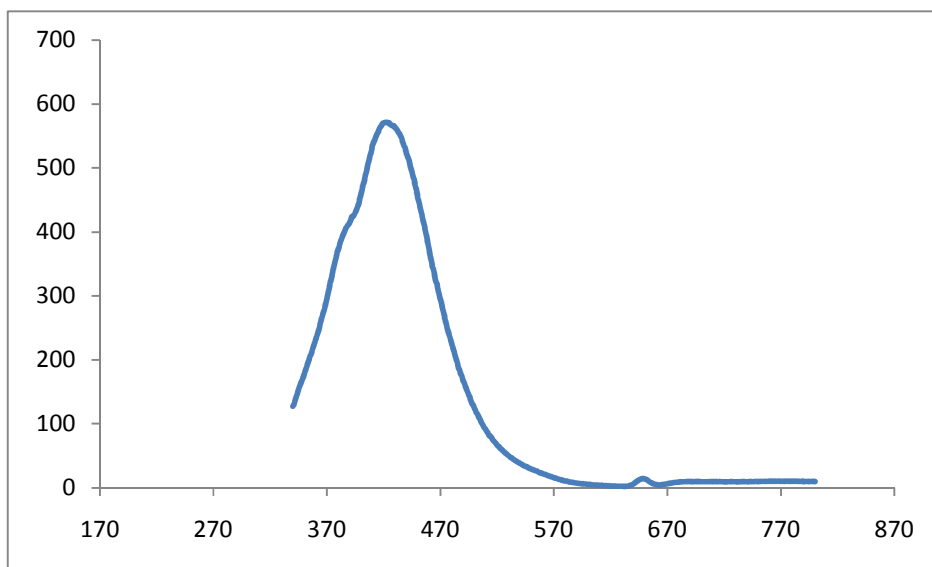


Figure 22. Emission Spectrum of Complex 44

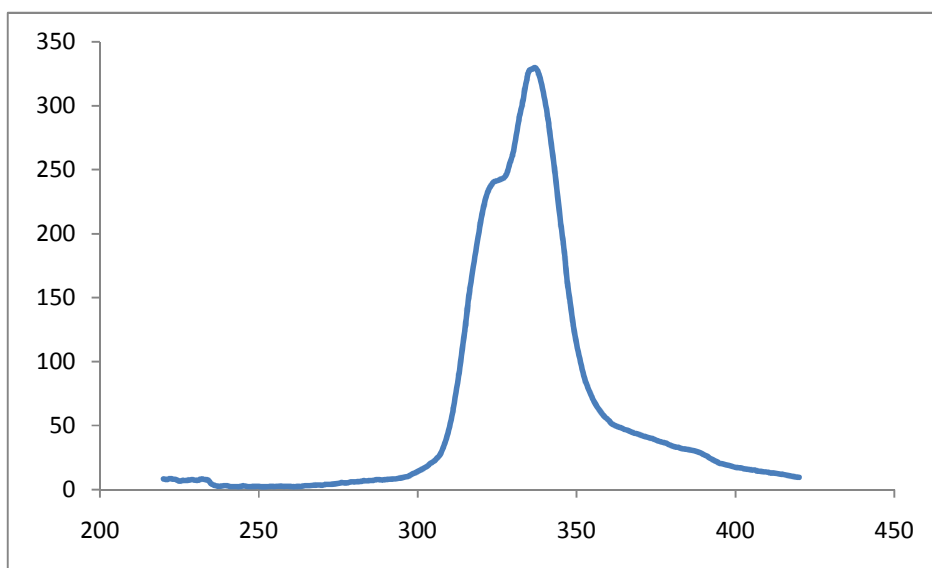


Figure 23. Excitation Spectrum of Complex 47

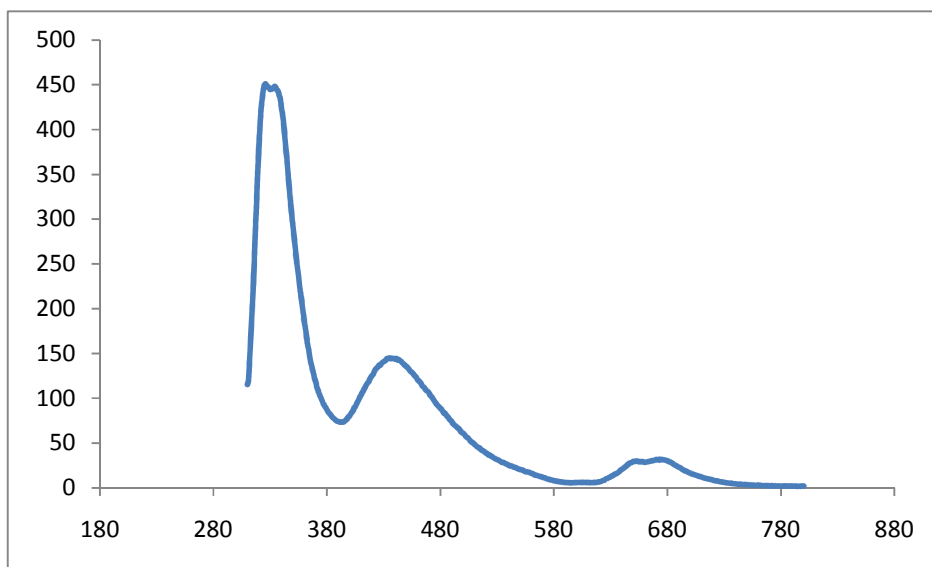


Figure 24. Emission Spectrum of Complex 47

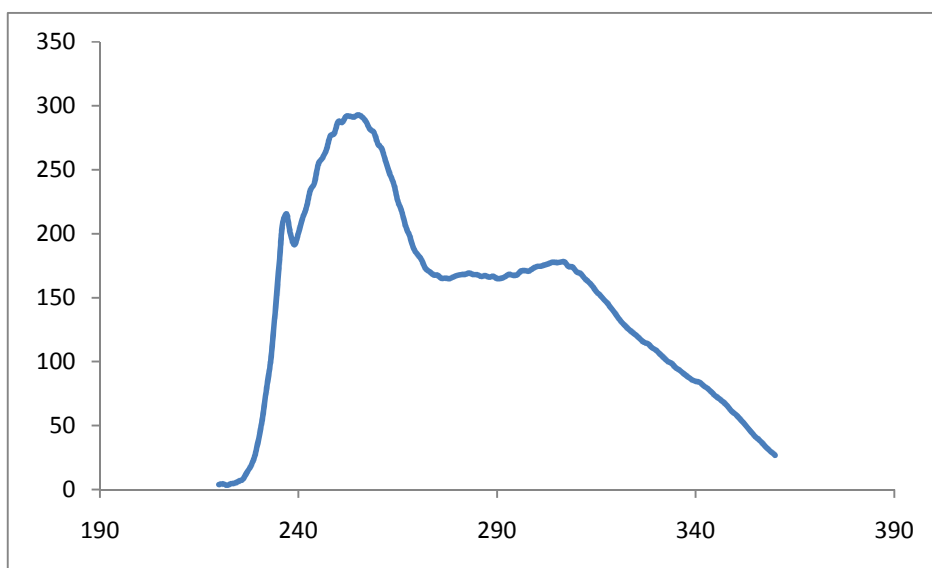


Figure 25. Emission Spectrum of Complex 50

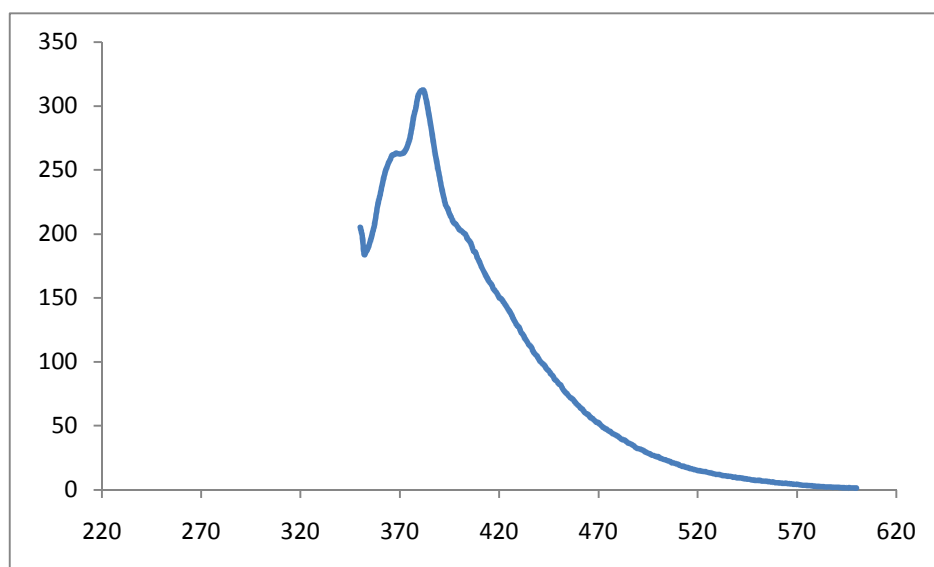
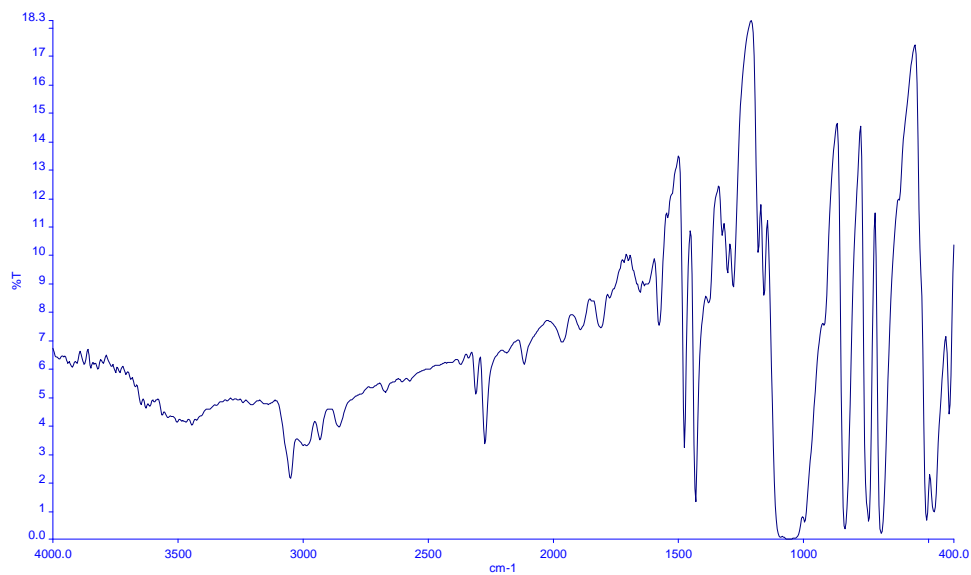
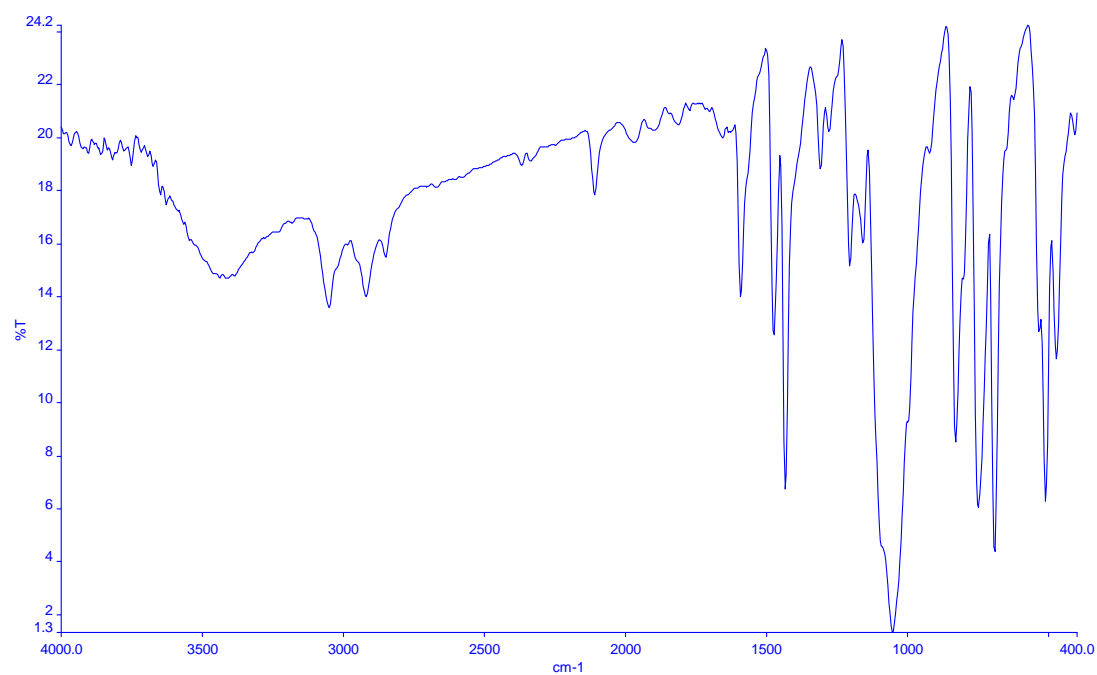


Figure 26. Emission Spectrum of Complex 50

A-IV**Figure 1.** FT-IR Spectrum of precursor-A**Figure 2.** FT-IR Spectrum of Complex 1

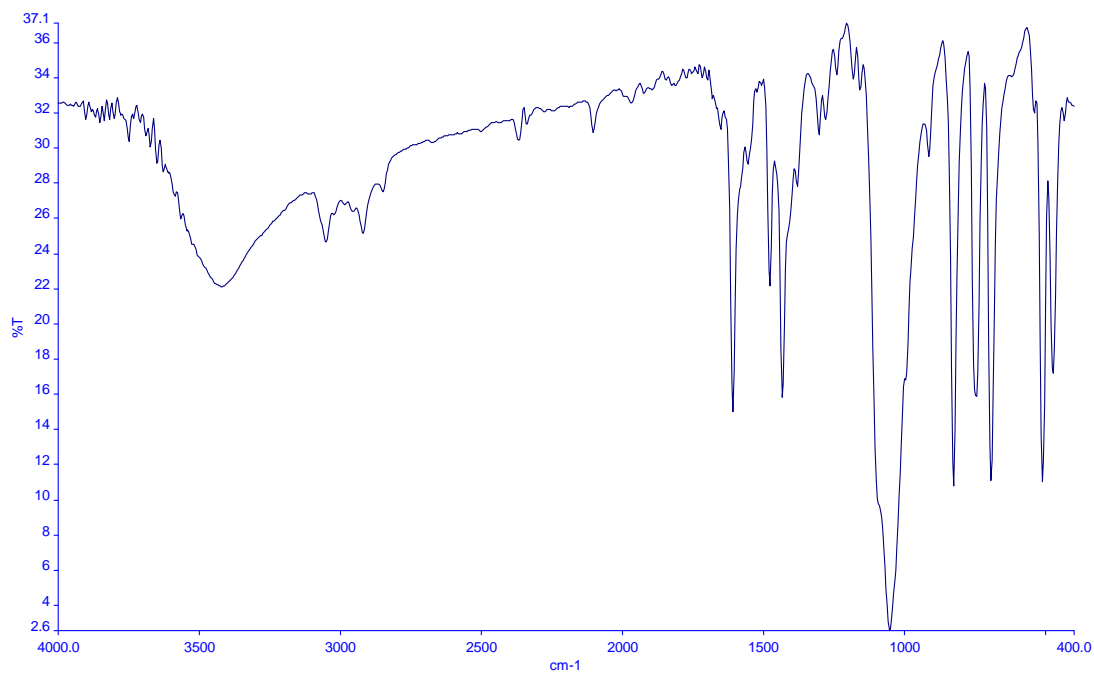


Figure 3. FT-IR Spectrum of Complex 2

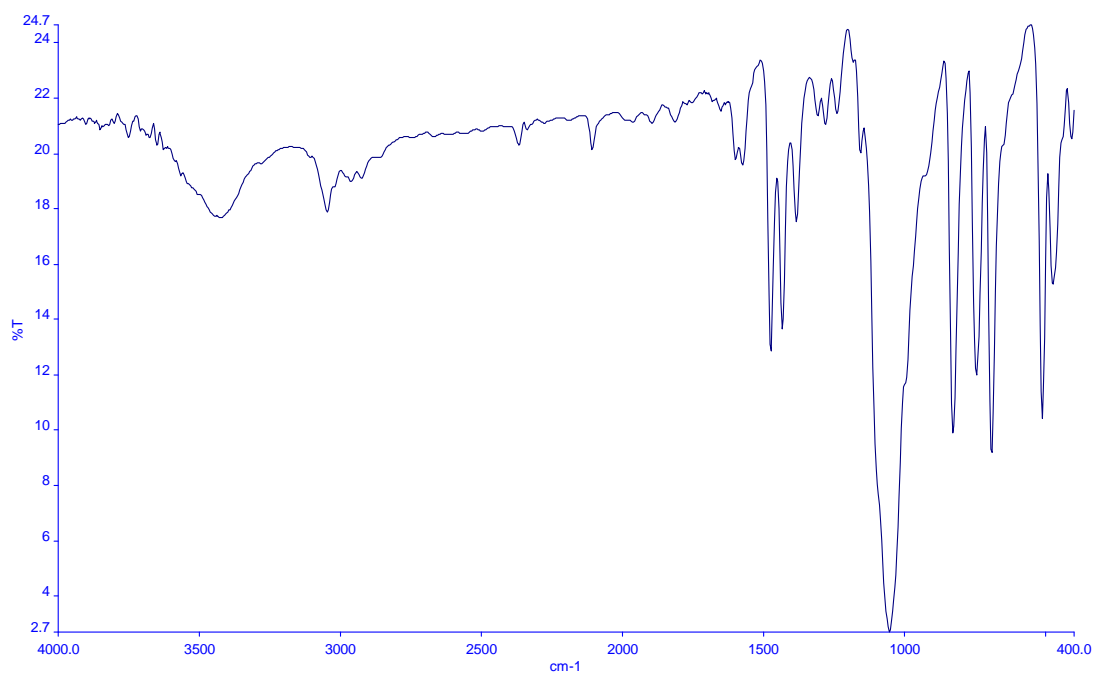


Figure 4. FT-IR Spectrum of Complex 3

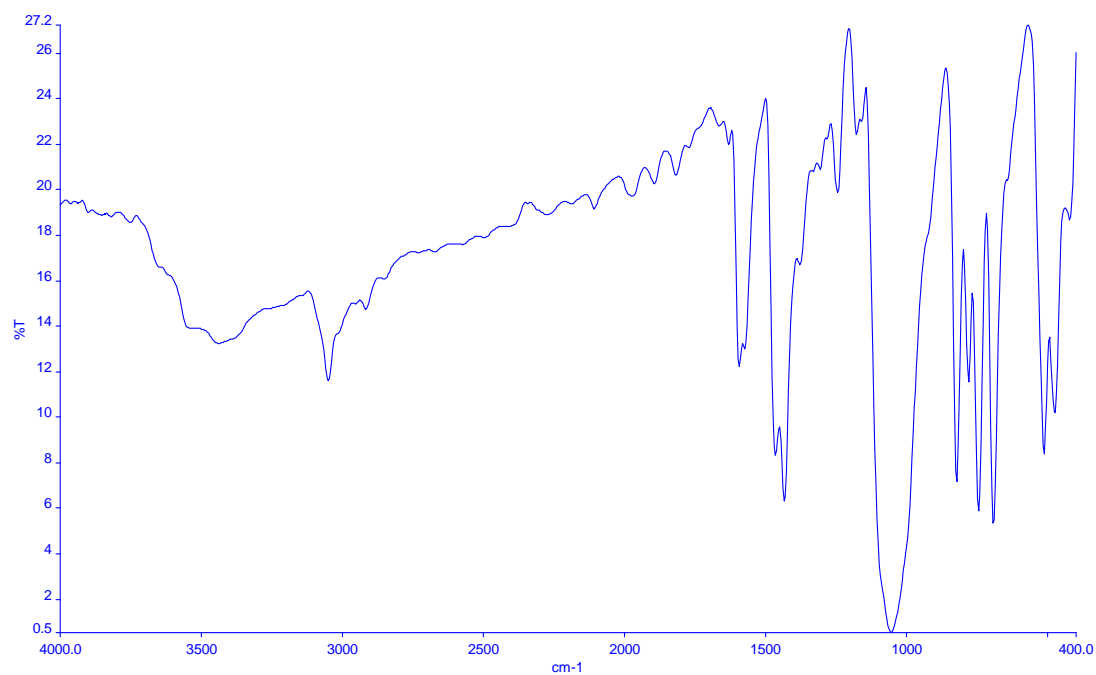


Figure 5. FT-IR Spectrum of Complex 4

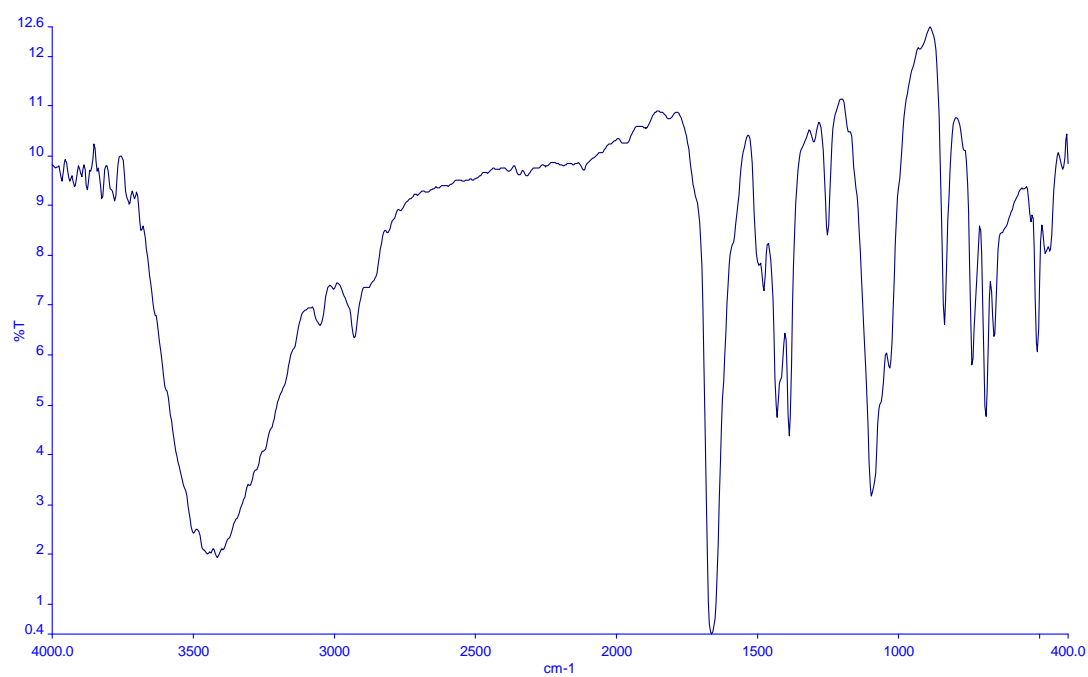


Figure 6. FT-IR Spectrum of Complex 5

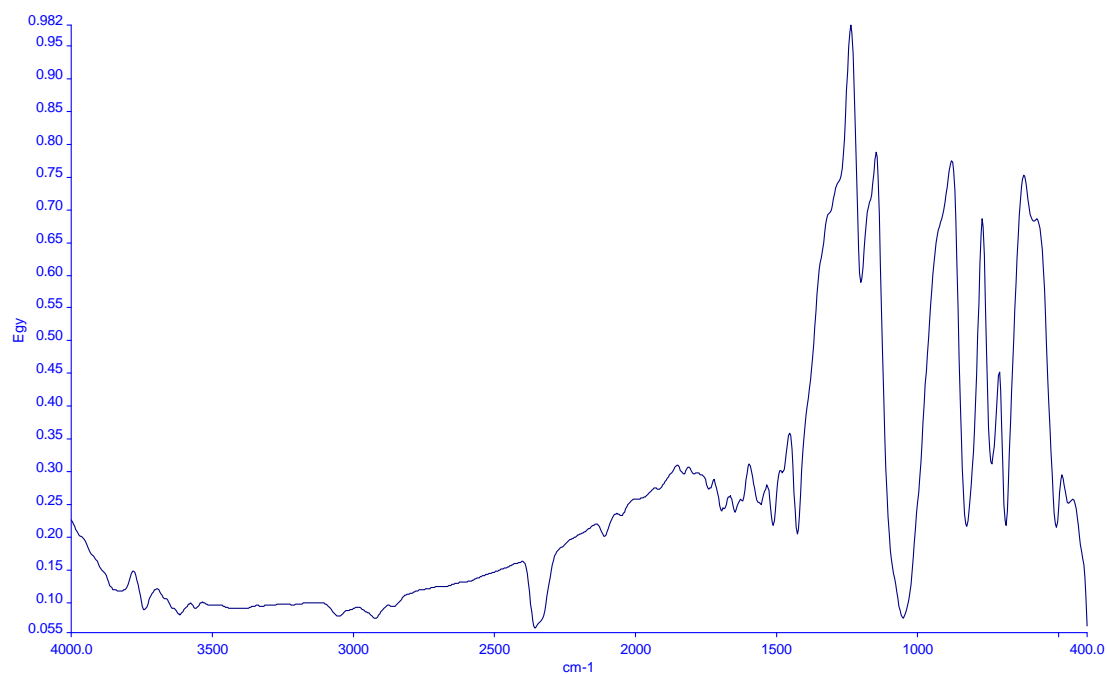


Figure 7. FT-IR Spectrum of Complex 6

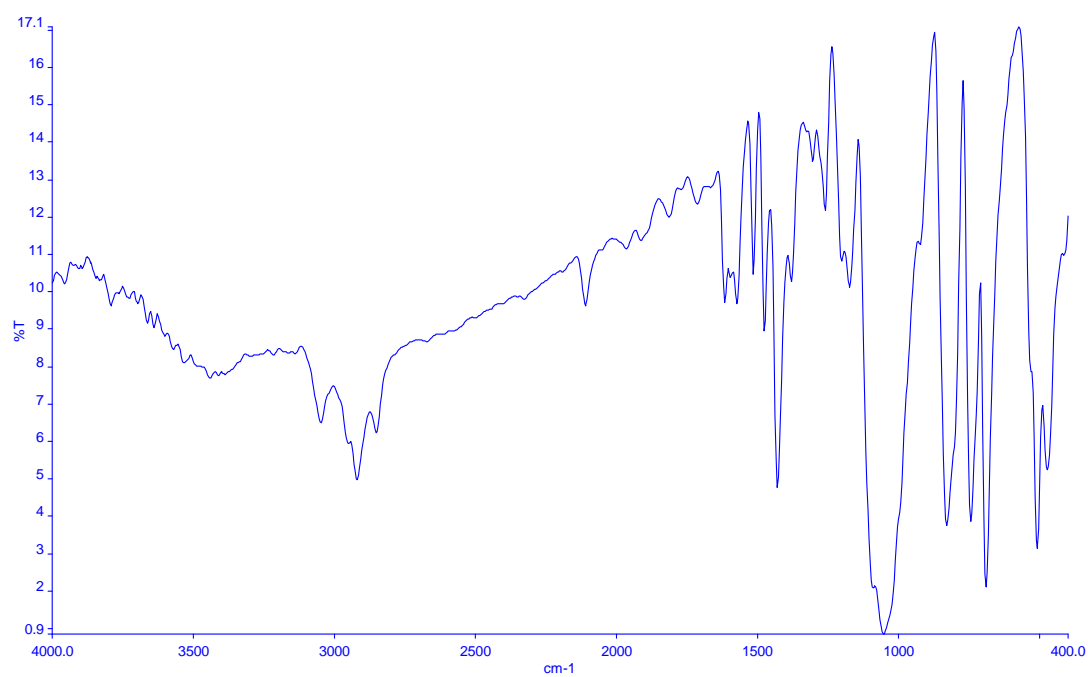


Figure 8. FT-IR Spectrum of Complex 7

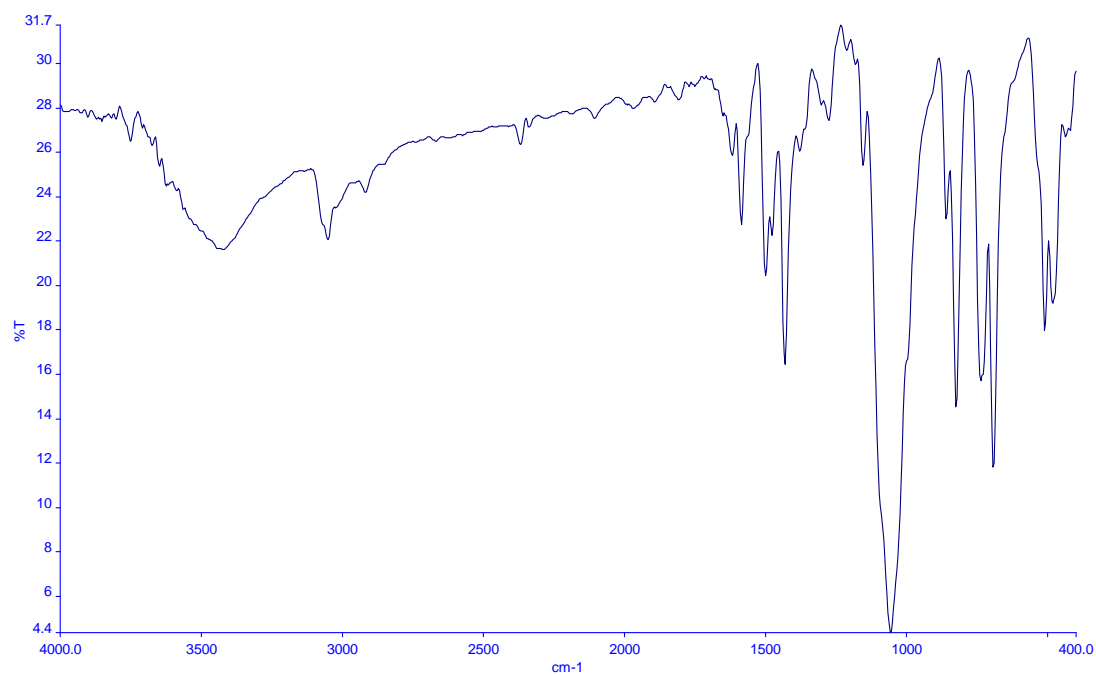


Figure 9. FT-IR Spectrum of Complex 8

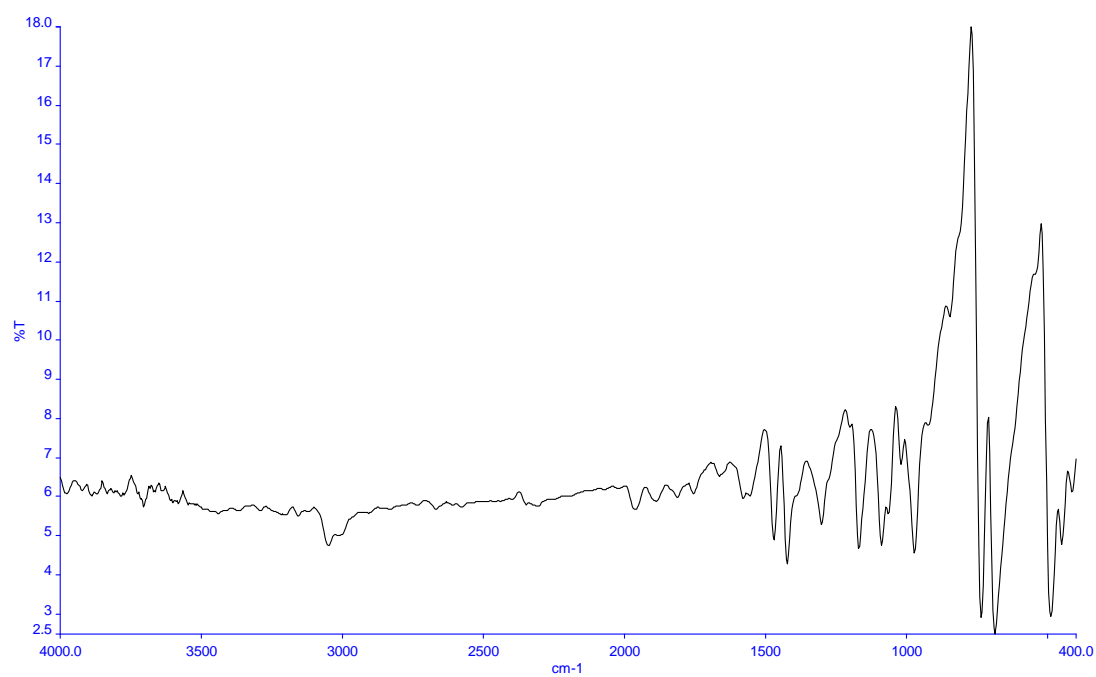


Figure 10. FT-IR Spectrum of trans-1,2-bis(diphenylphosphino)acetylene

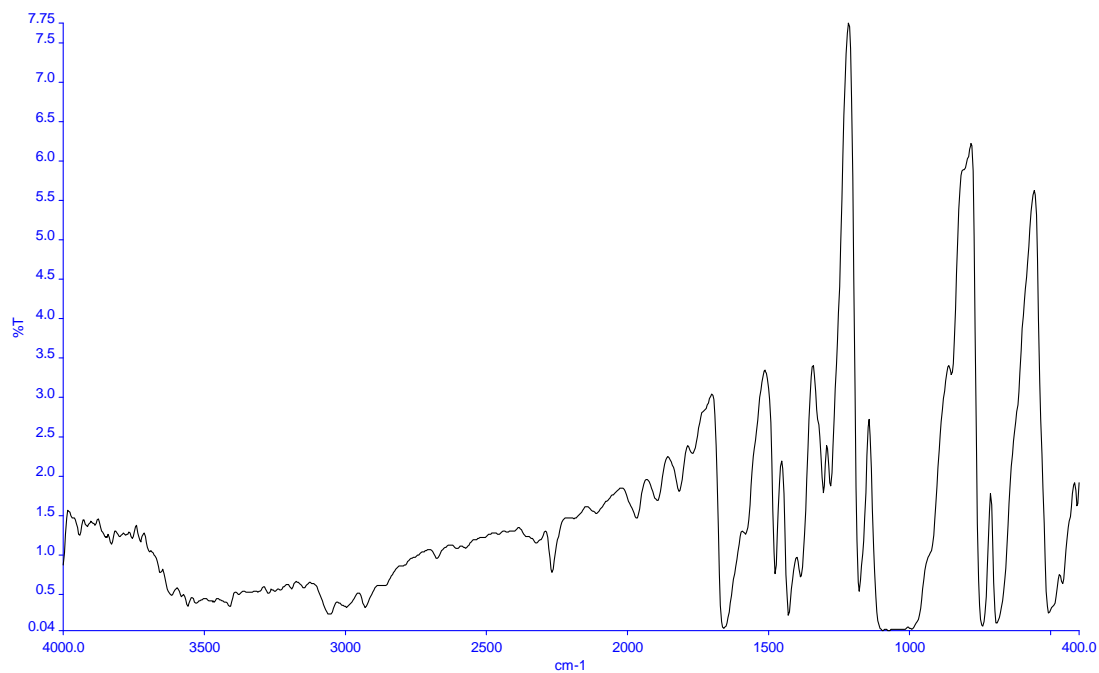


Figure 11. FT-IR Spectrum of Precursor-B

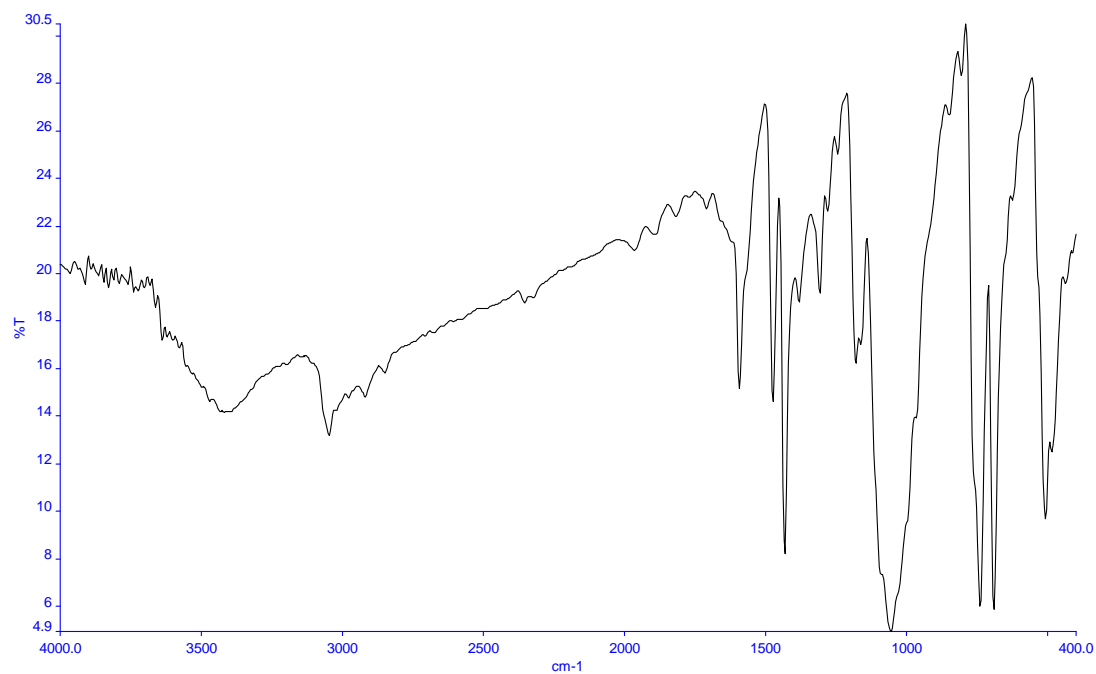


Figure 12. FT-IR Spectrum of Complex 9

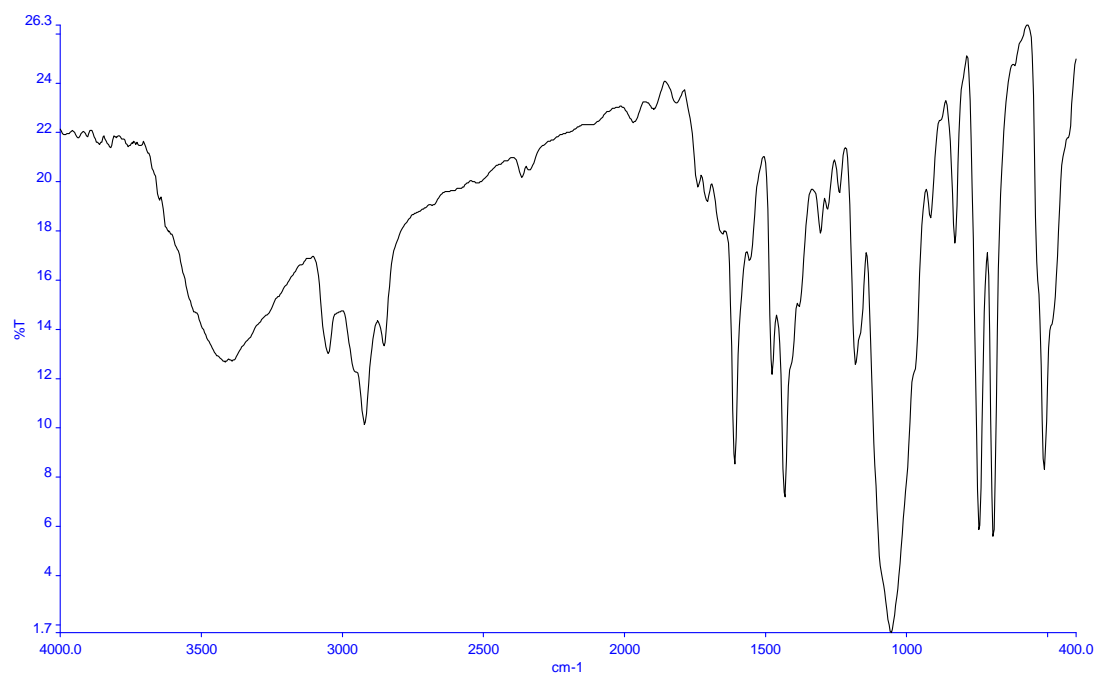


Figure 13. FT-IR Spectrum of Complex 10

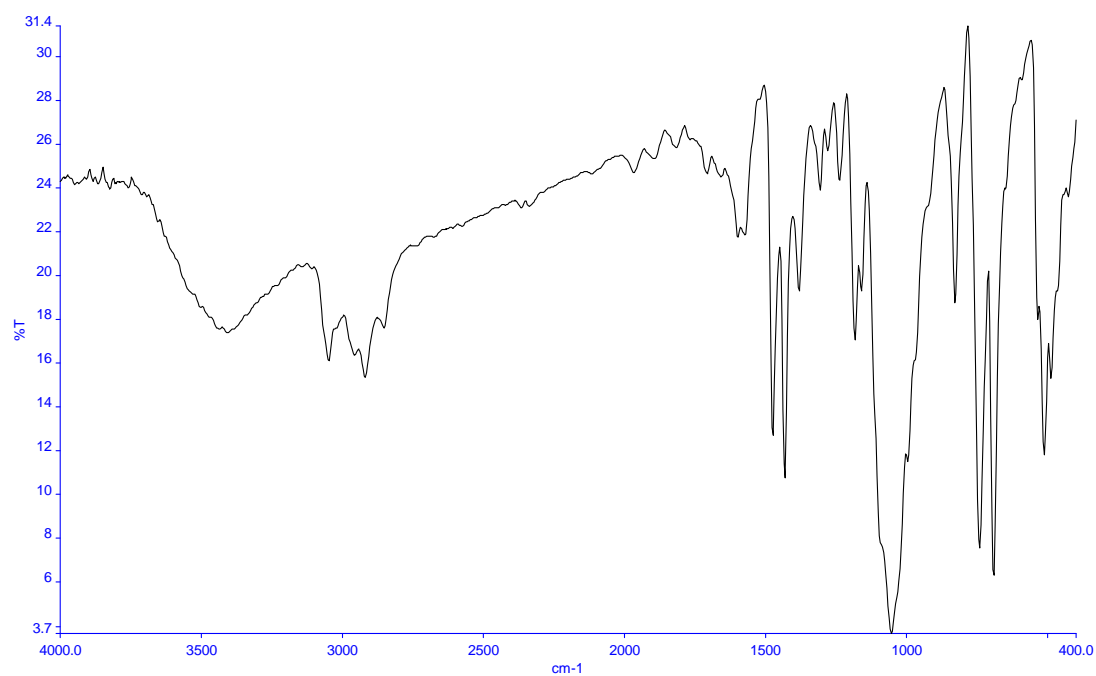


Figure 14. FT-IR Spectrum of Complex 11

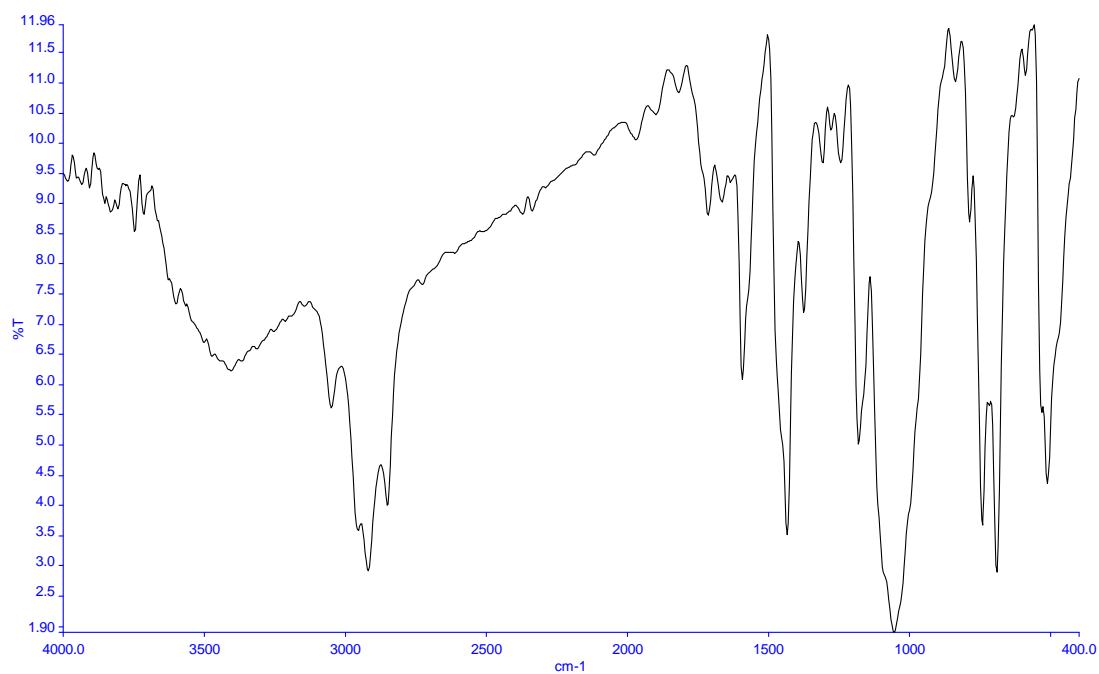


Figure 15. FT-IR Spectrum of Complex 12

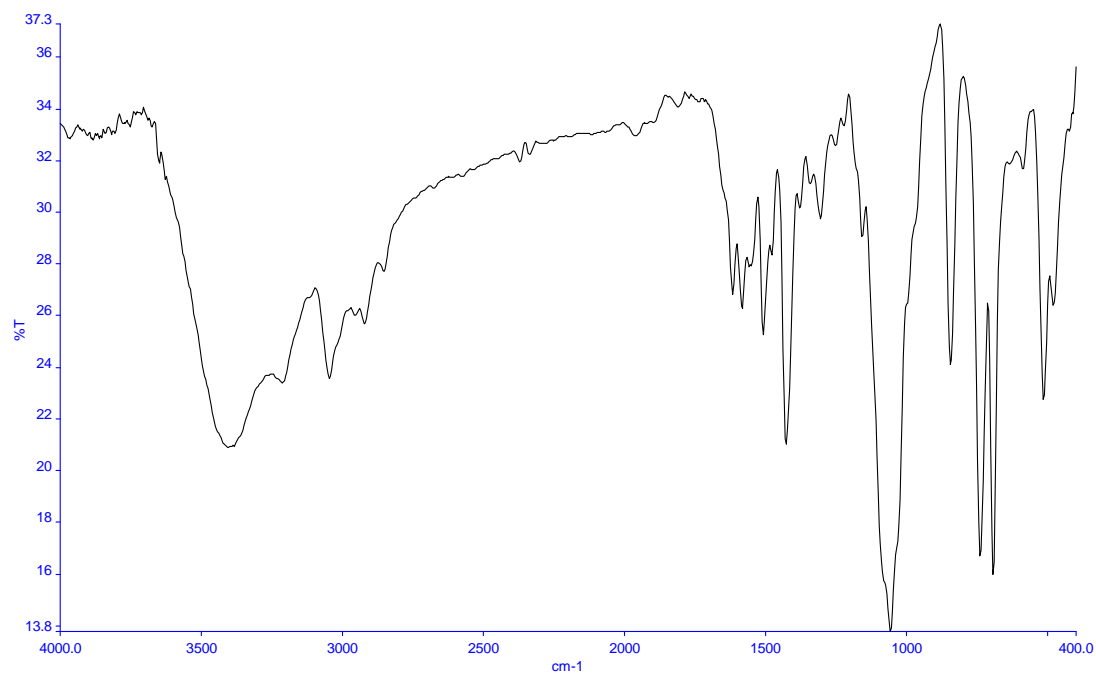


Figure 16. FT-IR Spectrum of Complex 13

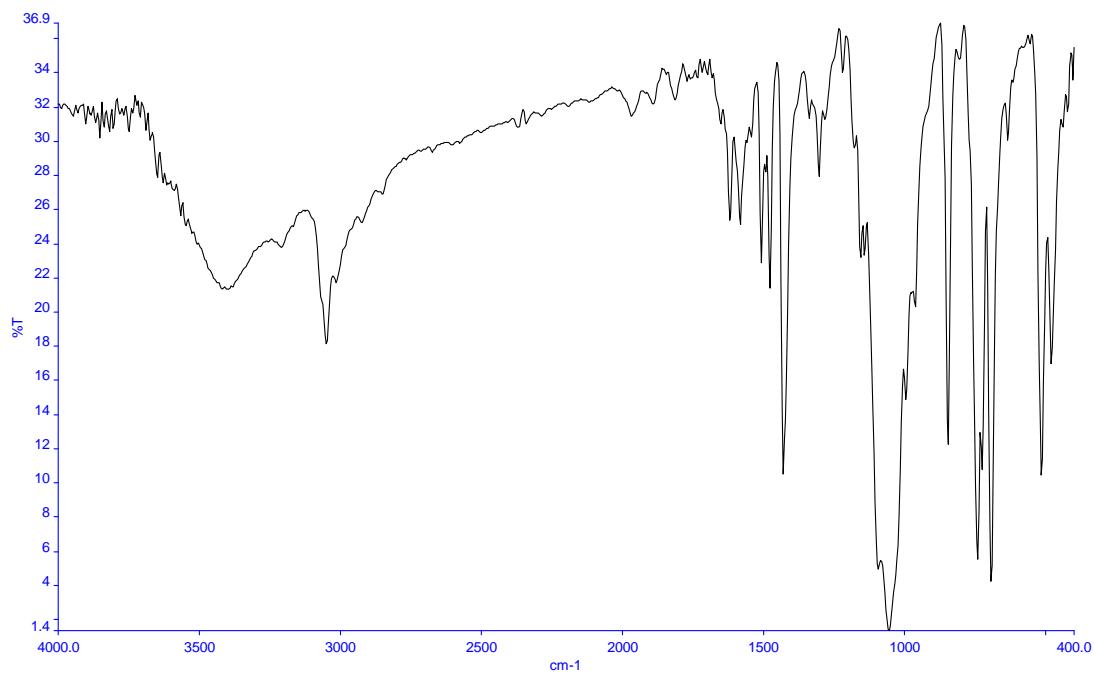


Figure 17. FT-IR Spectrum of Complex 14

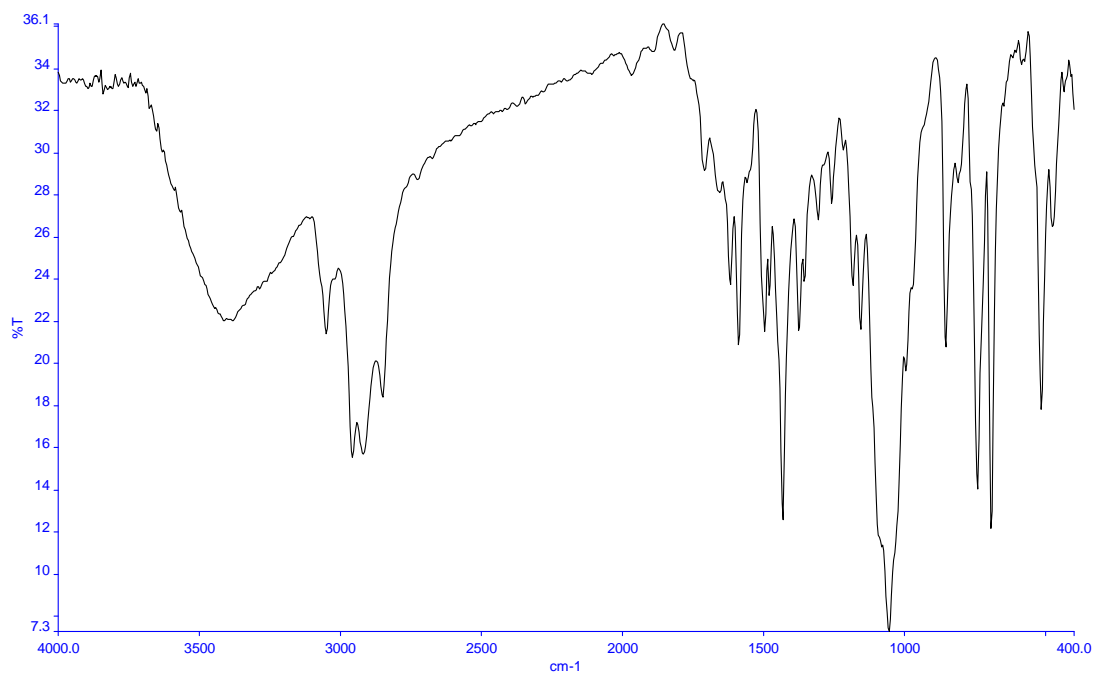


Figure 18. FT-IR Spectrum of Complex 15

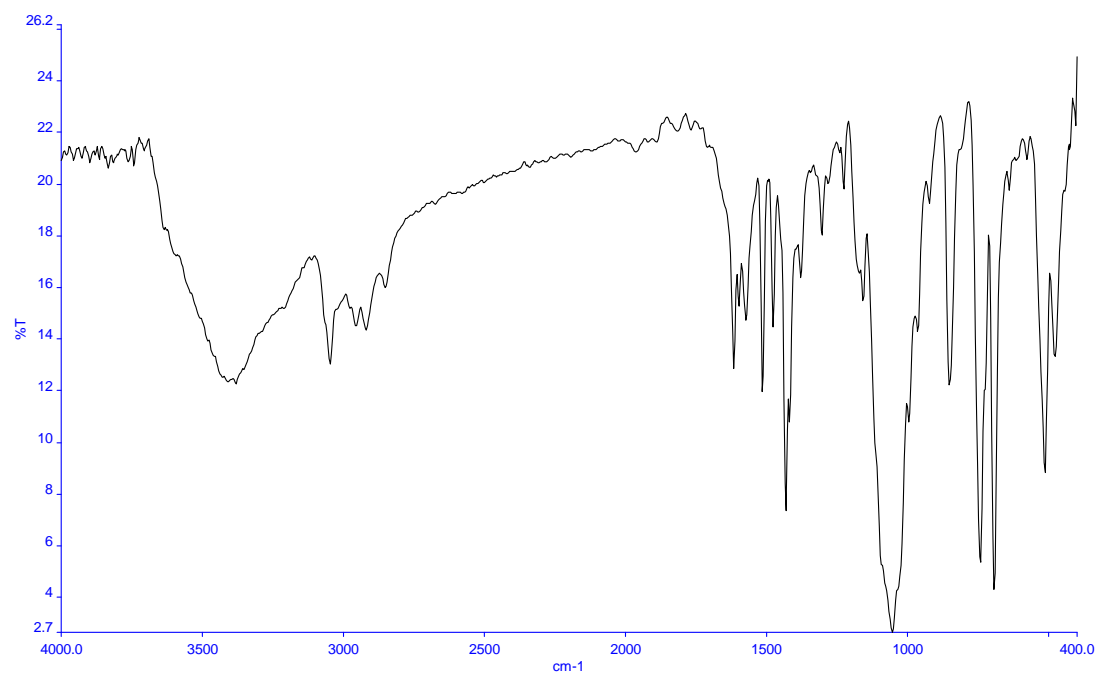


Figure 19. FT-IR Spectrum of Complex 16

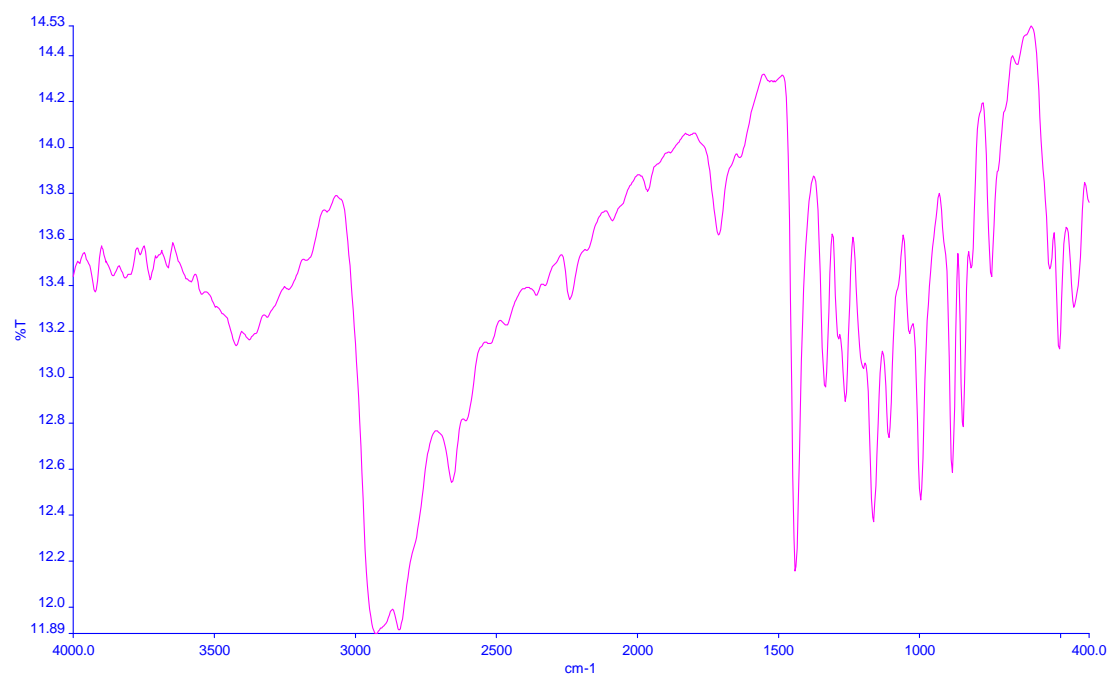


Figure 20. FT-IR Spectrum of PCy₃



Figure 21. FT-IR Spectrum of (m-Tol₃)P

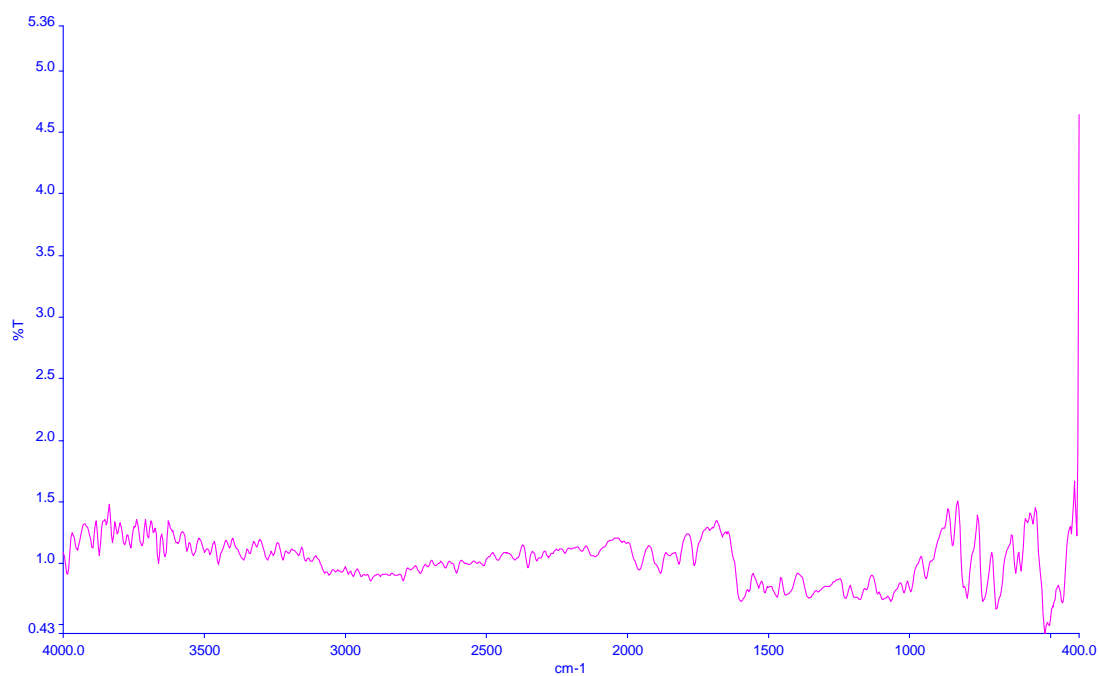


Figure 22. FT-IR Spectrum of DAP-DP



Figure 23. FT-IR Spectrum of Complex 17



Figure 24. FT-IR Spectrum of Complex 18

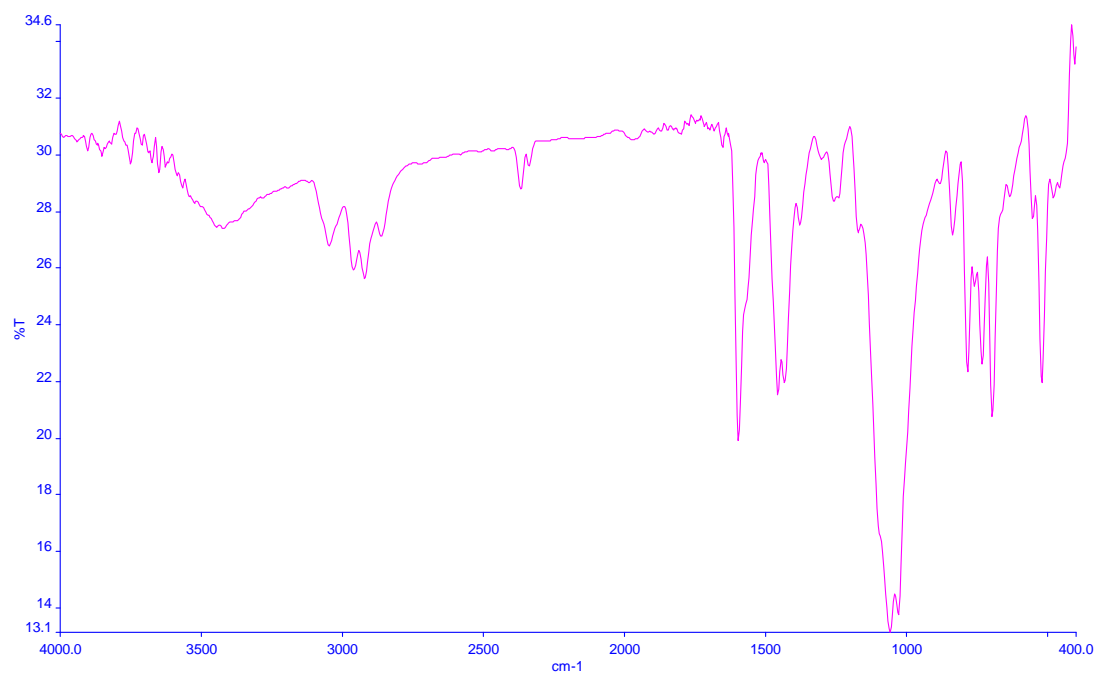


Figure 25. FT-IR Spectrum of Complex 20

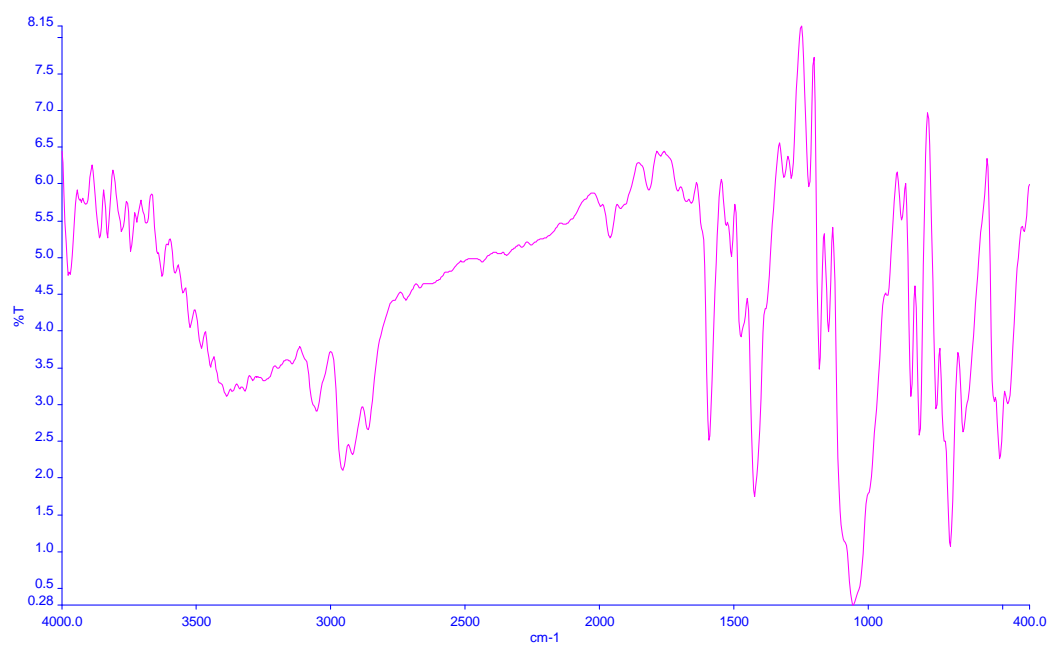


Figure 26. FT-IR Spectrum of Complex 21

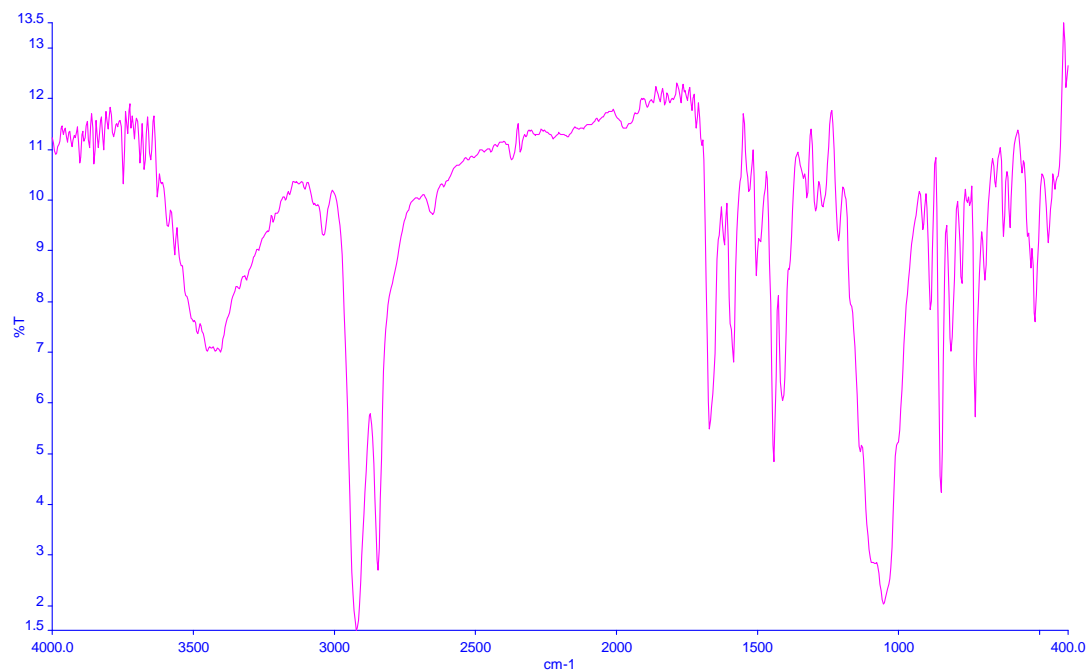


Figure 27. FT-IR Spectrum of Complex 23

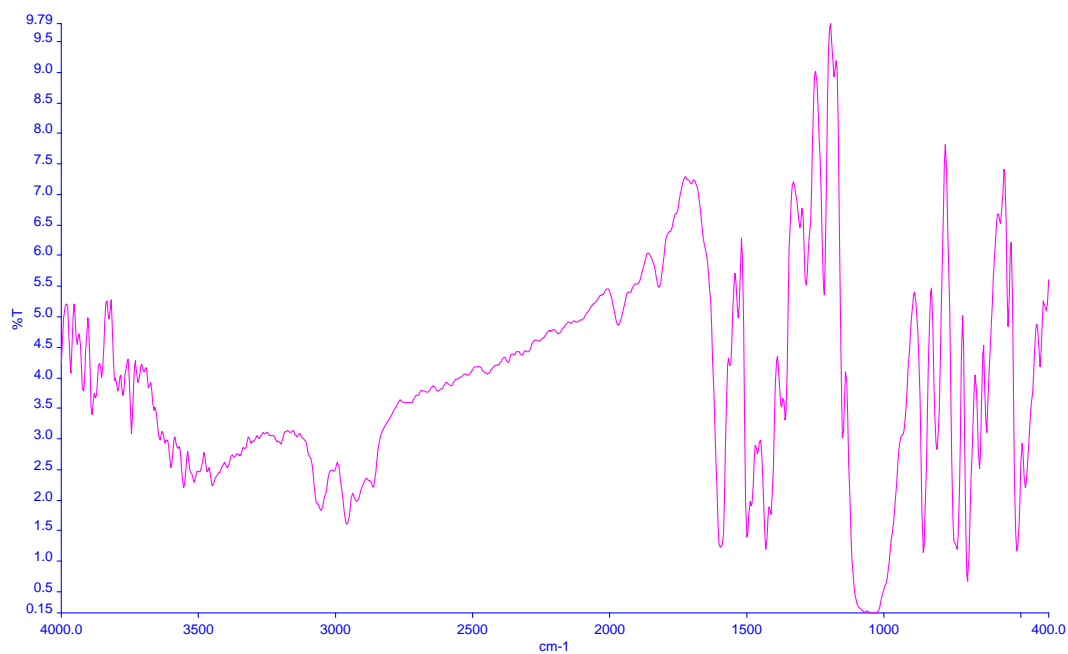
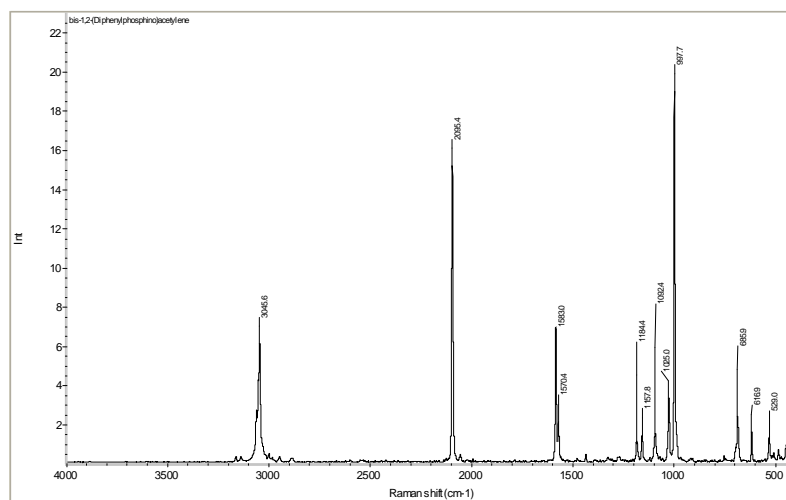
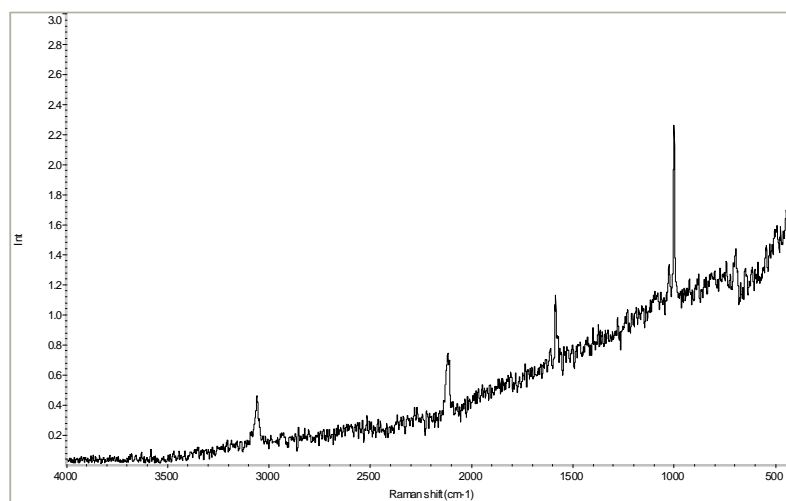


Figure 28. FT-IR Spectrum of Complex 25

A V

**Figure 1.** Raman Spectrum of DPPA**Figure 2.** Raman Spectrum of Precursor-B

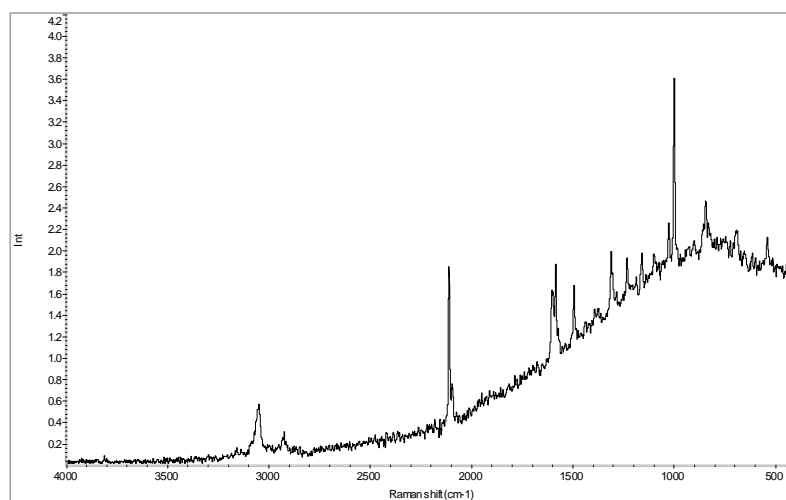


Figure 3. Raman Spectrum of Complex 3

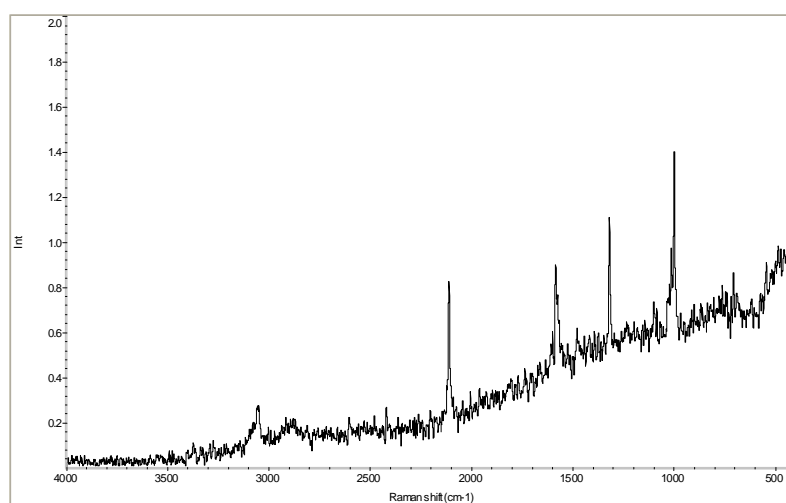


Figure 4. Raman Spectrum of Complex 4

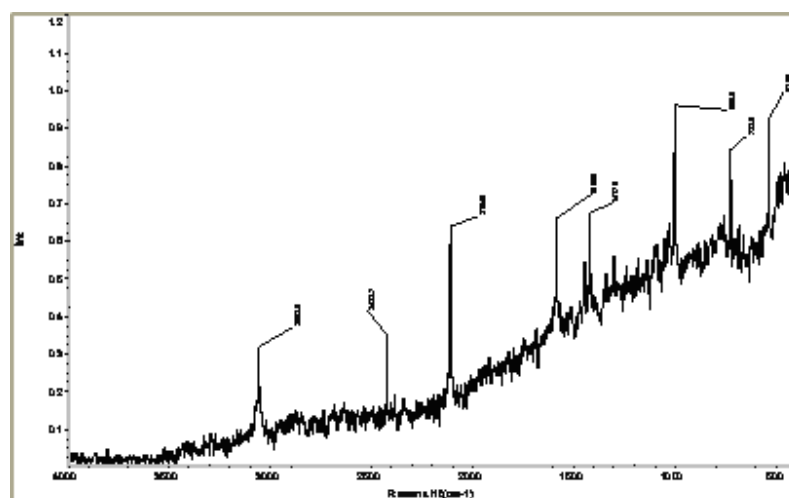


Figure 5. Raman Spectrum of Complex 5

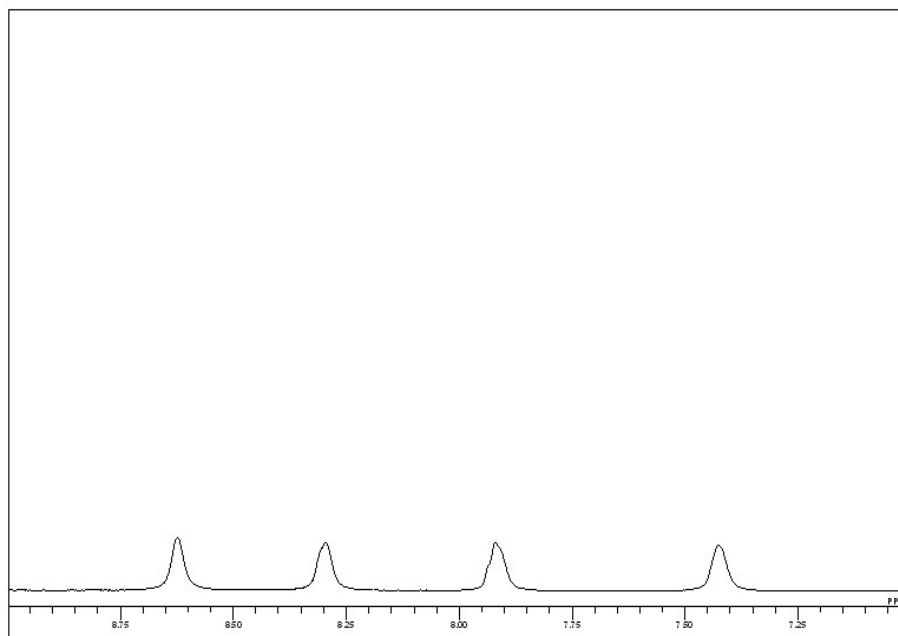
A-VI

Figure 1. ^1H -NMR (only the aromatic region) of bipy

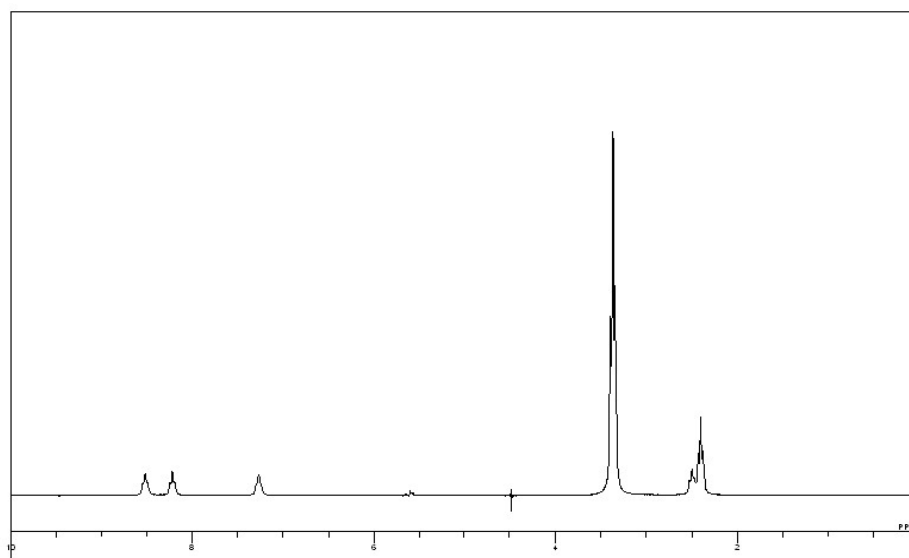


Figure 2. ^1H -NMR 4,4'-Me₂bipy

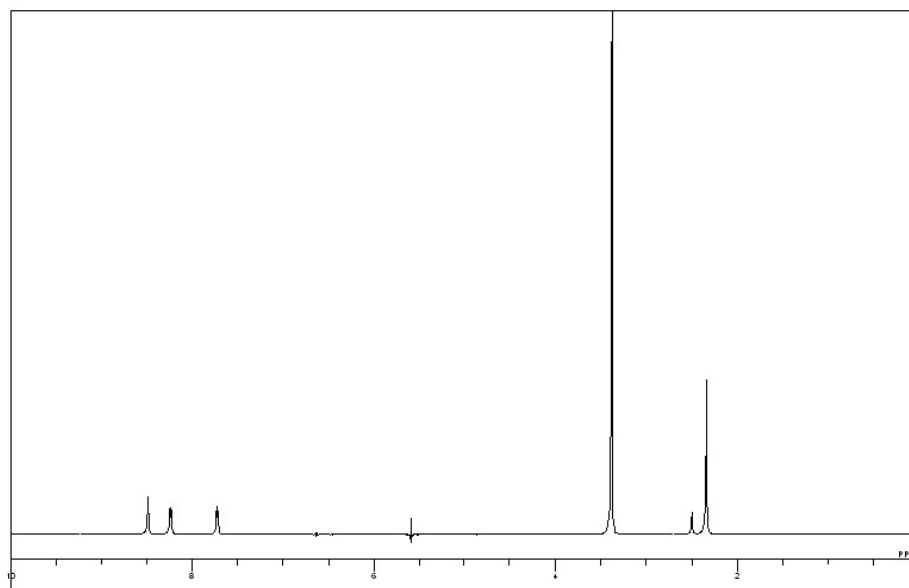


Figure 3. ^1H -NMR 5,5'-Me₂bipy

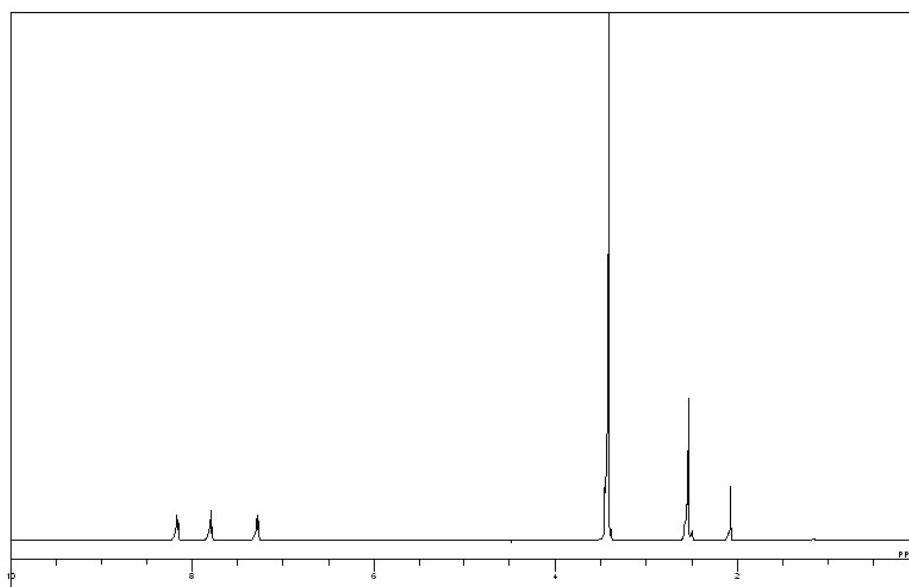


Figure 4. ^1H -NMR 6,6'-Me₂bipy

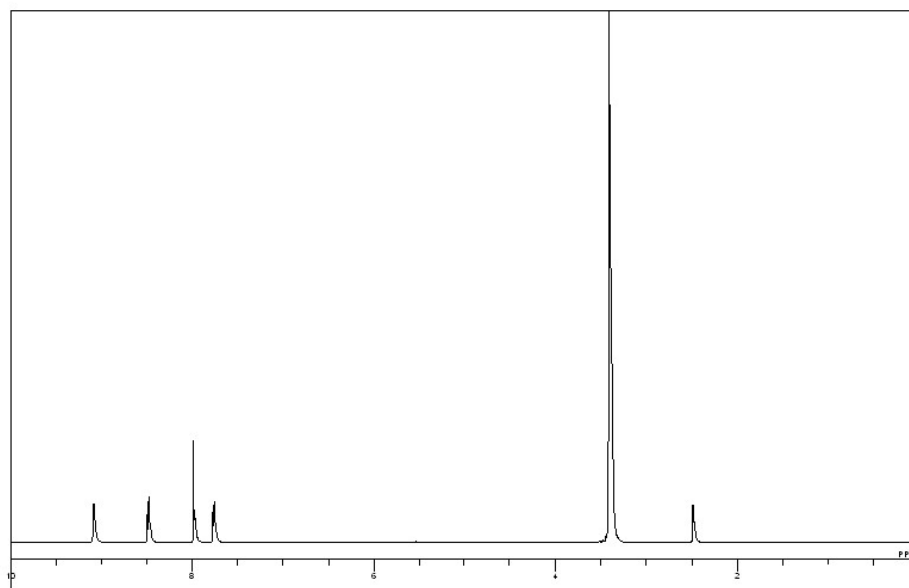


Figure 5. ^1H -NMR spectrum of phen

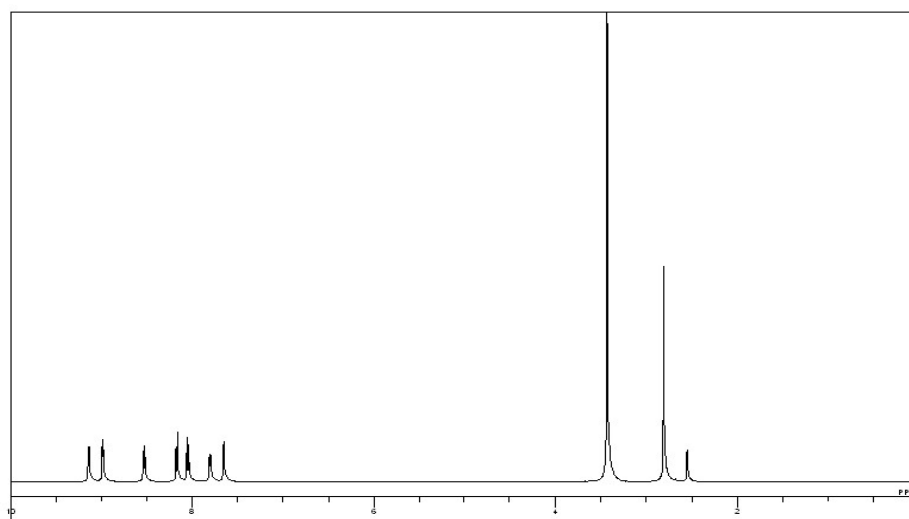


Figure 6. ^1H -NMR spectrum of 4-Mephen

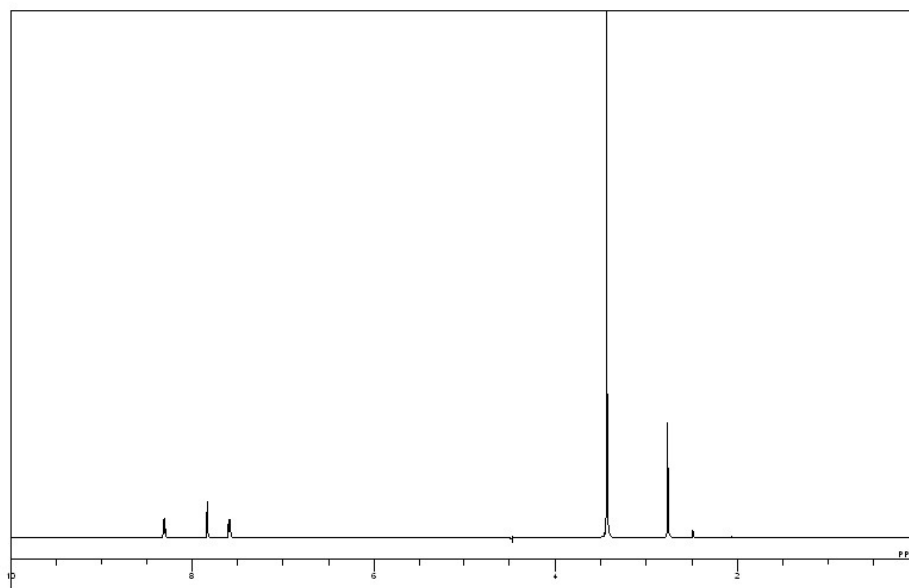


Figure 7. ^1H -NMR spectrum of 2,9- Me_2phen

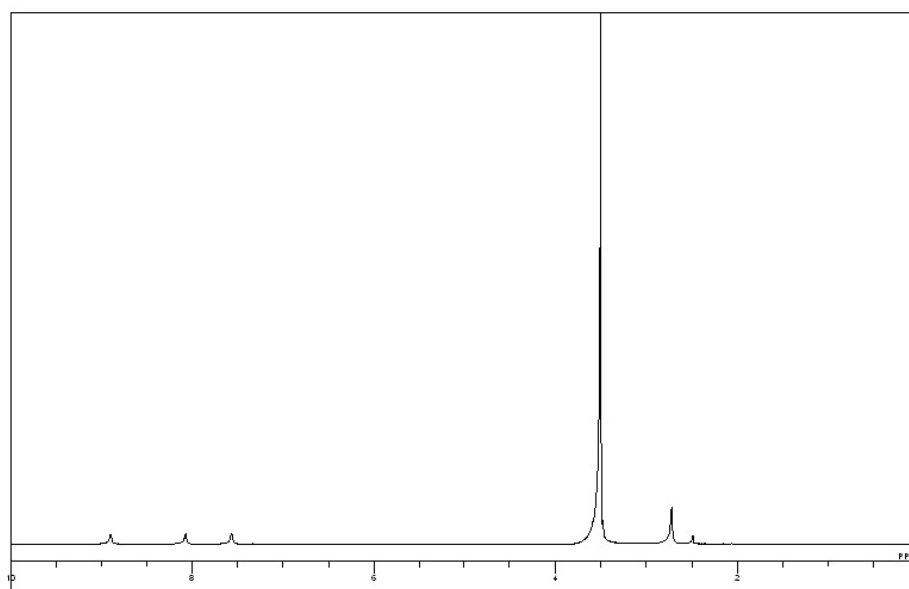


Figure 8. ^1H -NMR spectrum 4,7- Me_2phen

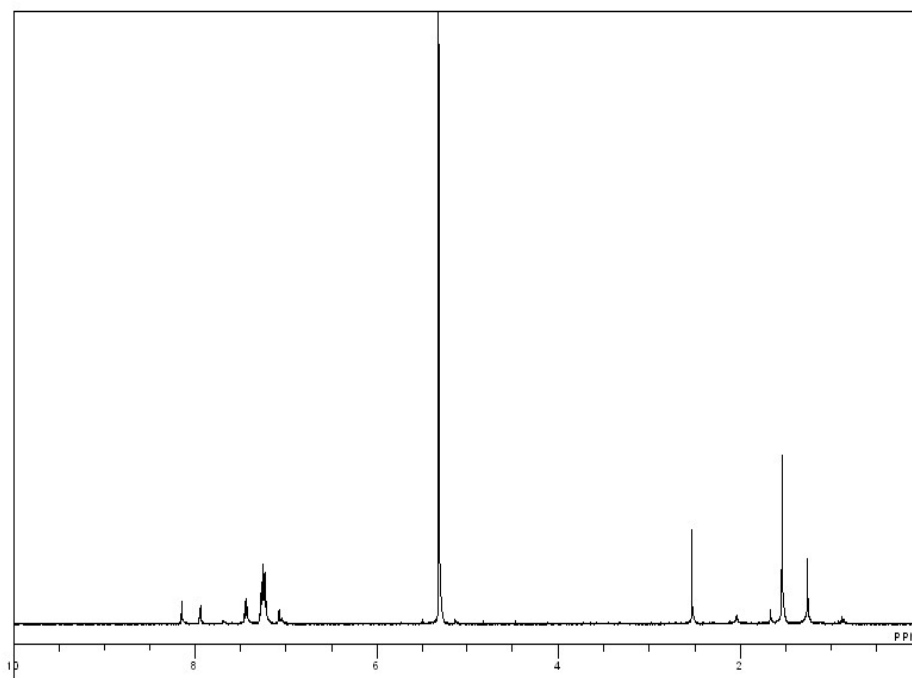


Figure 9. ^1H -NMR spectrum of Complex 2

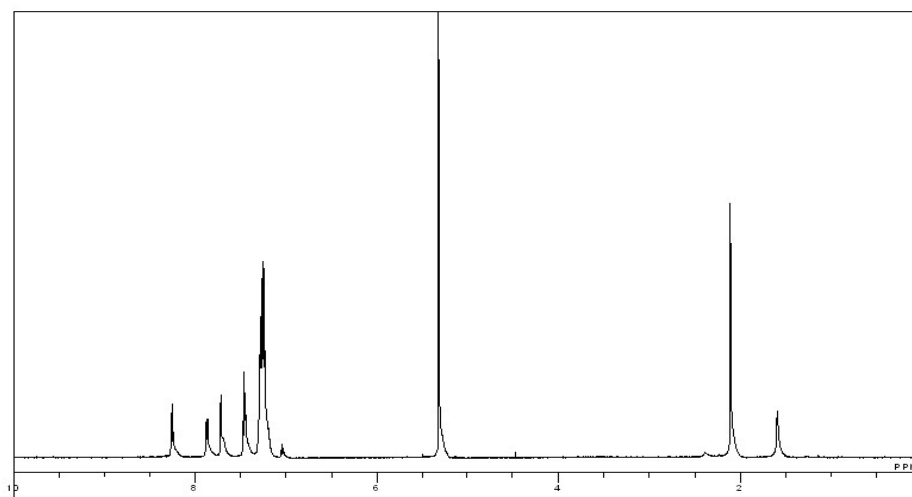


Figure 10. ^1H -NMR Spectrum spectrum of Complex 3

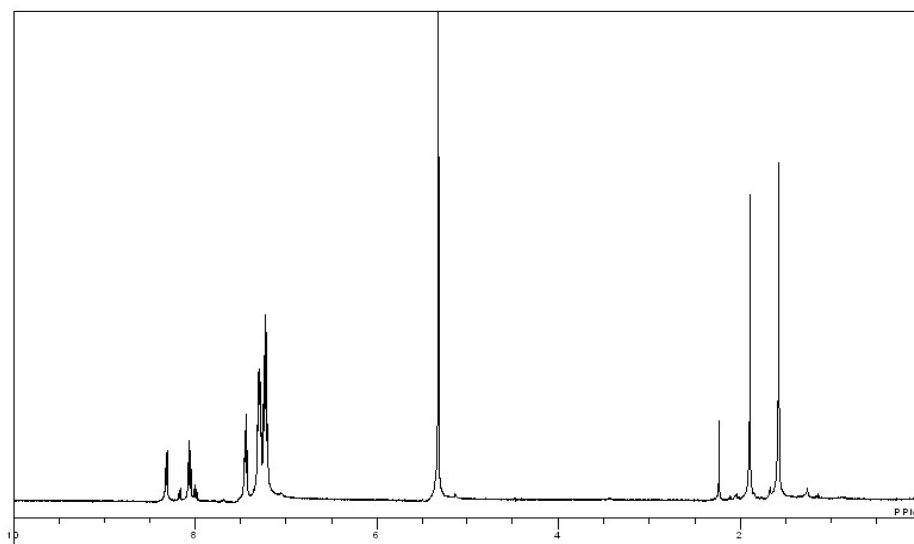


Figure 11. ^1H -NMR Spectrum of Complex 4

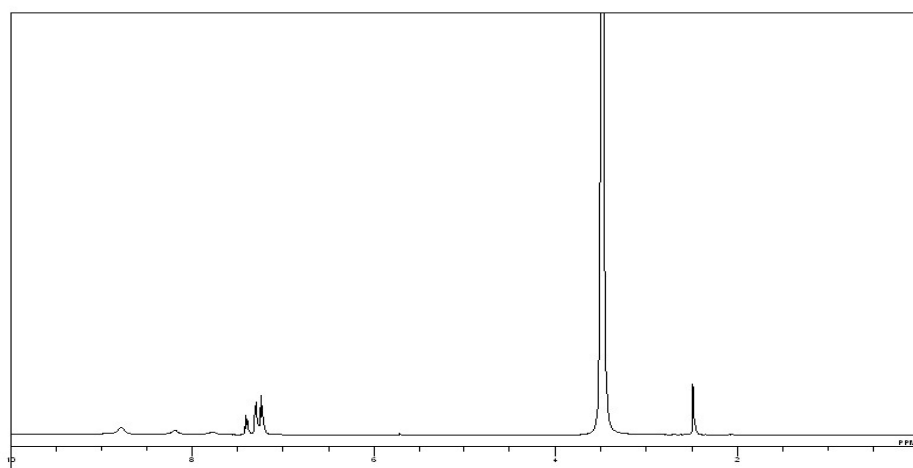


Figure 12. ^1H -NMR Spectrum of Complex 5

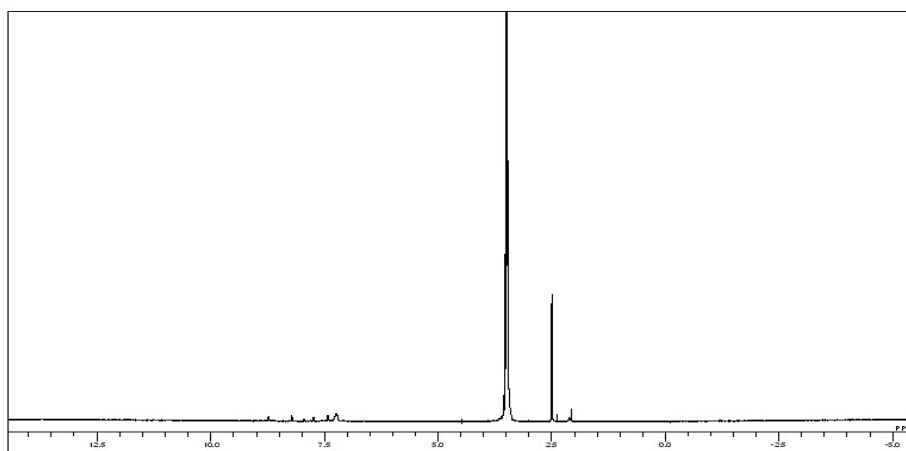


Figure 13. ^1H -NMR Spectrum of Complex 7

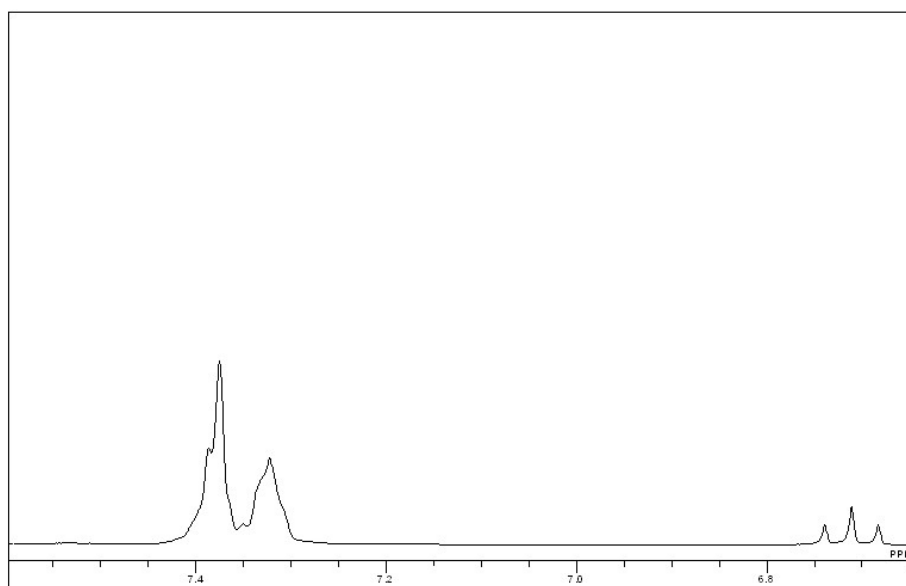


Figure 14. ^1H -NMR Spectrum of DPPETHY

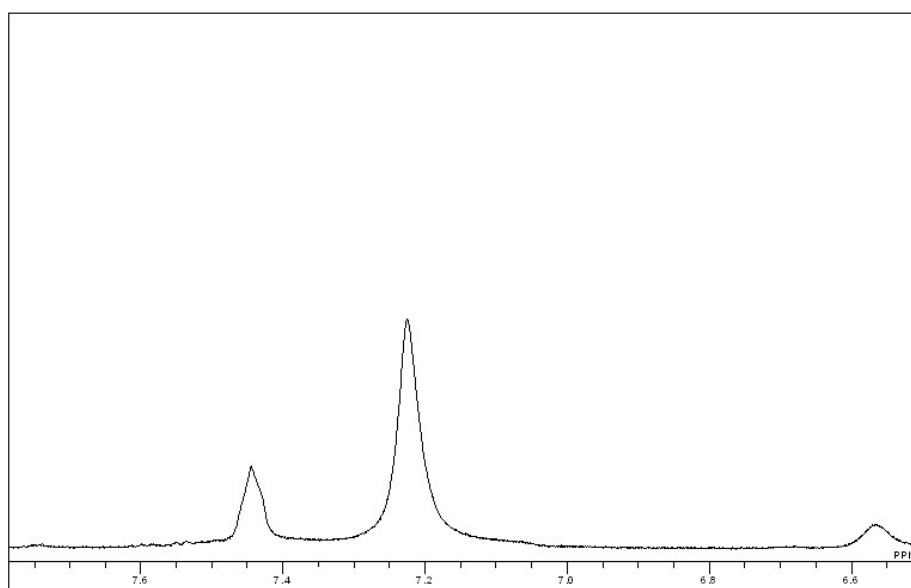


Figure 15. ^1H -NMR Spectrum of Precursor-B

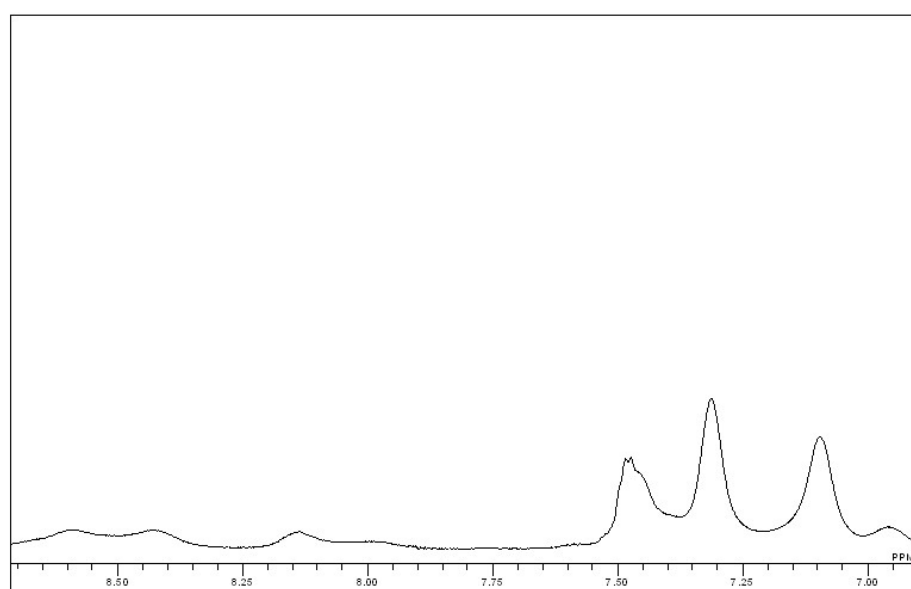


Figure 16. ^1H -NMR Spectrum of Complex 9

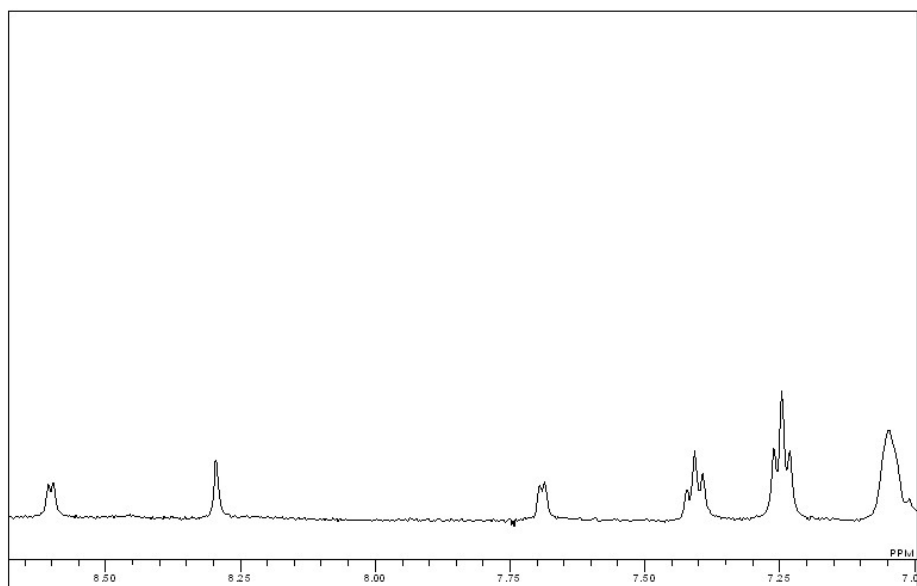


Figure 17. ^1H -NMR Spectrum of Complex 10

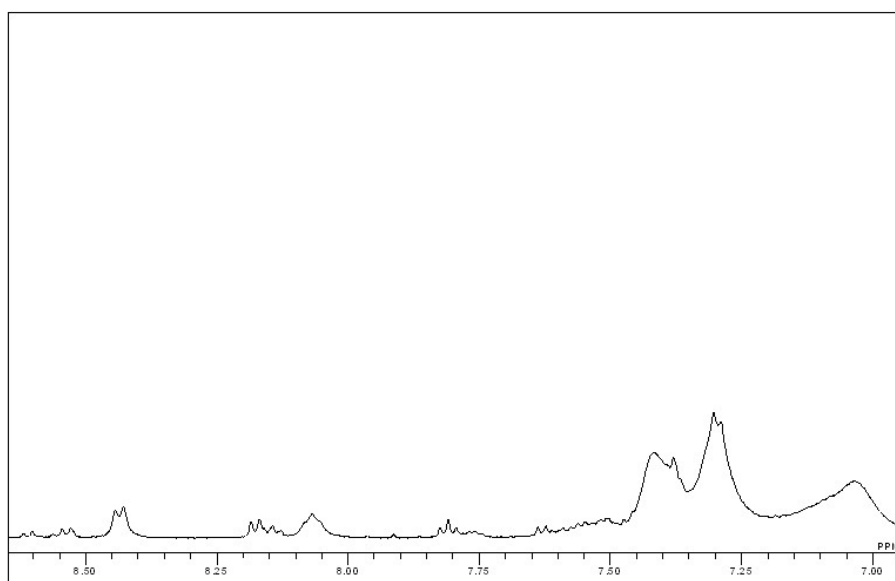


Figure 18. ^1H -NMR Spectrum of Complex 12

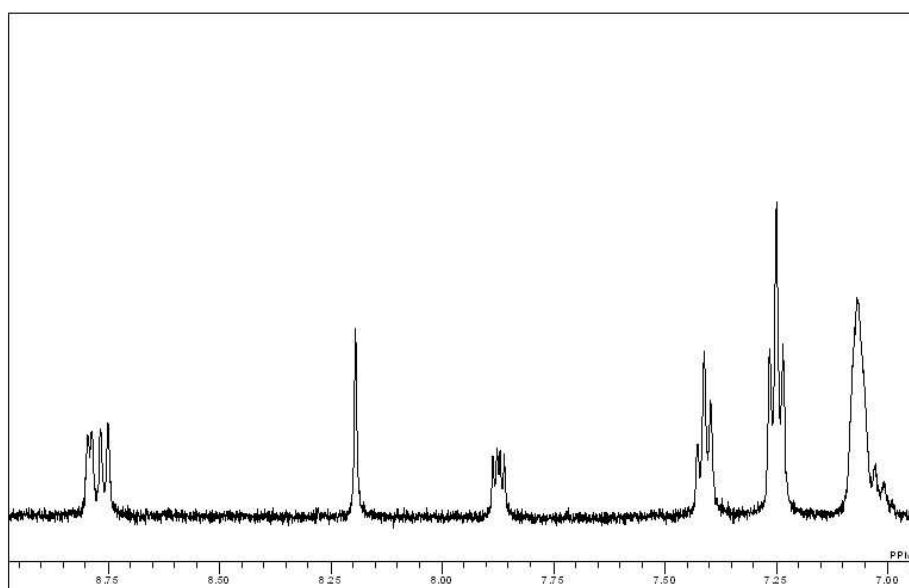


Figure 19. ^1H -NMR Spectrum of Complex 13

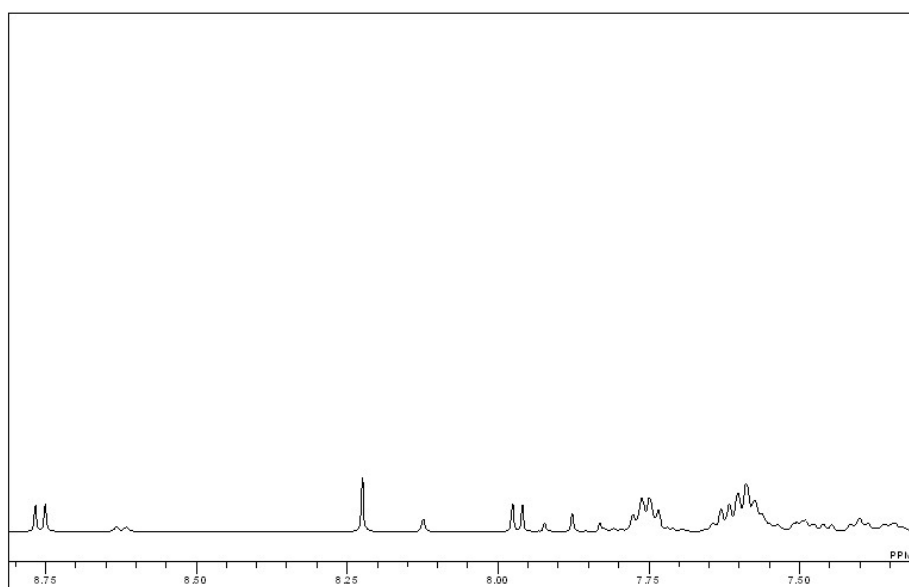


Figure 20. ^1H -NMR Spectrum of Complex 15

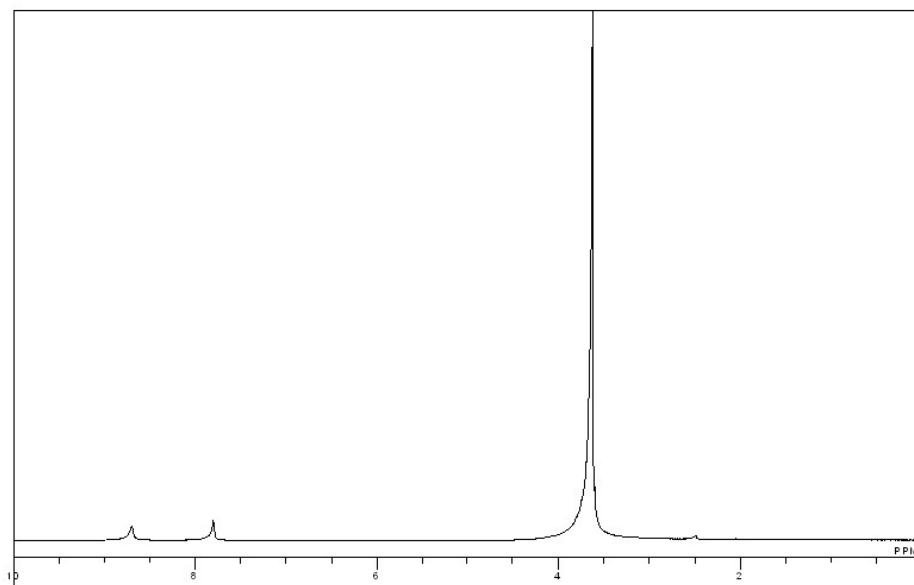


Figure 21. ^1H -NMR Spectrum of 4,4'-bipy

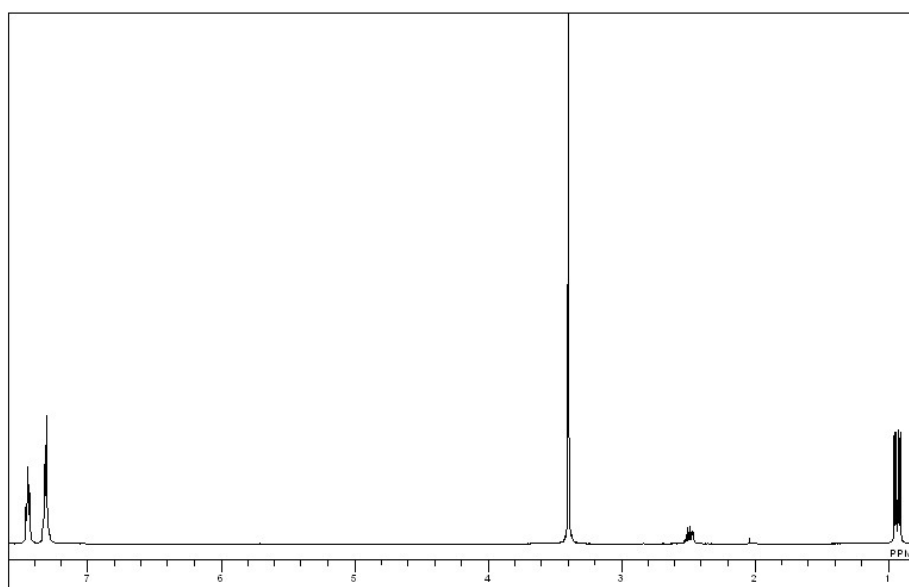


Figure 22. ^1H -NMR Spectrum of PPh₂(i-Pr)

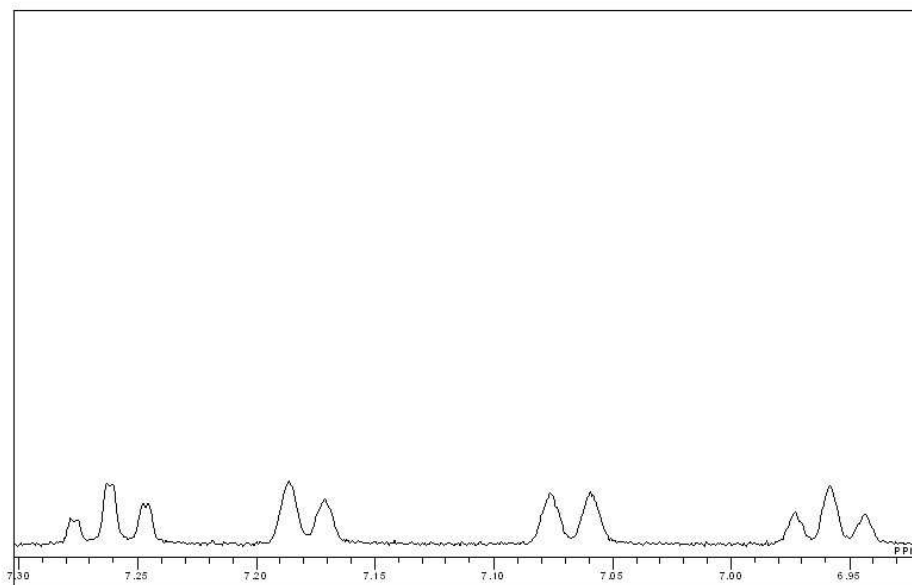


Figure 23. ^1H -NMR Spectrum of (m-Tol₃)P

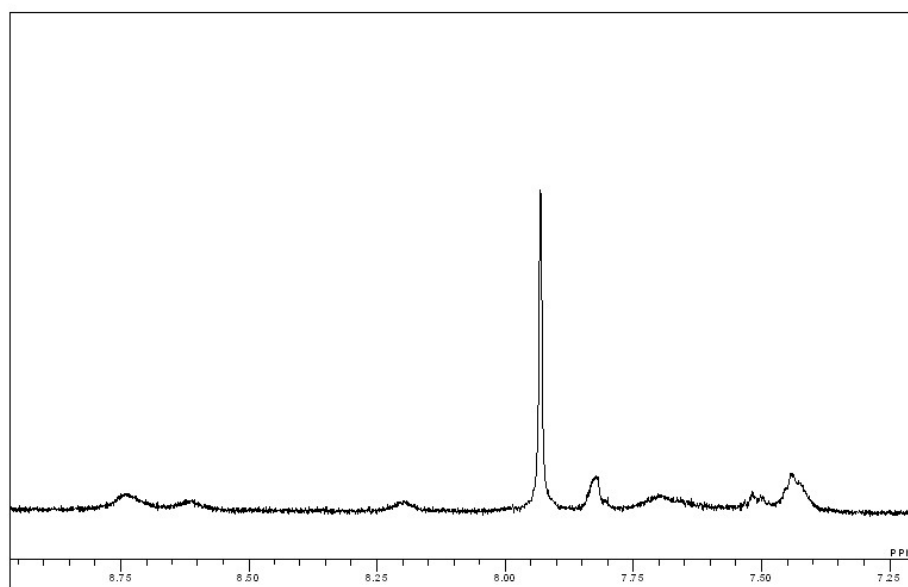


Figure 24. ^1H -NMR Spectrum of Complex 17

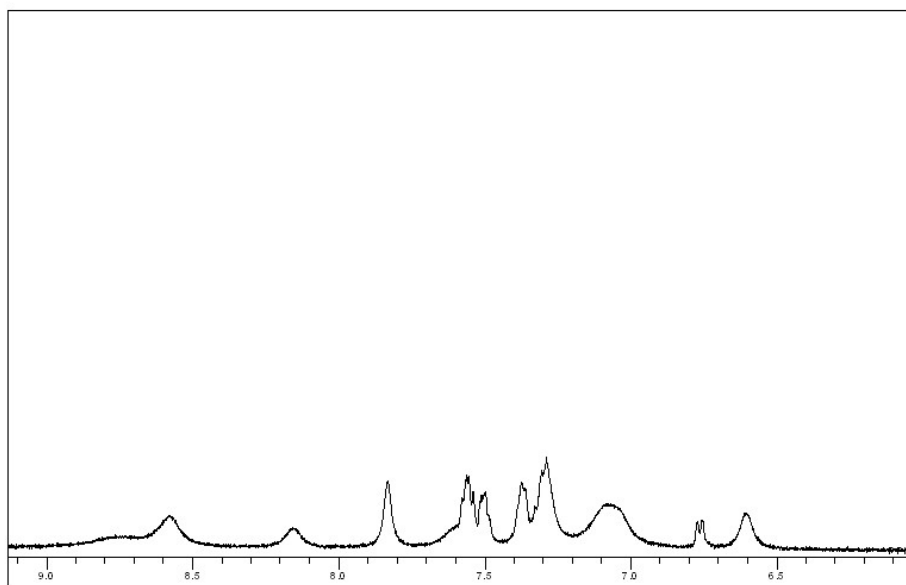


Figure 25. ^1H -NMR Spectrum of Complex 19

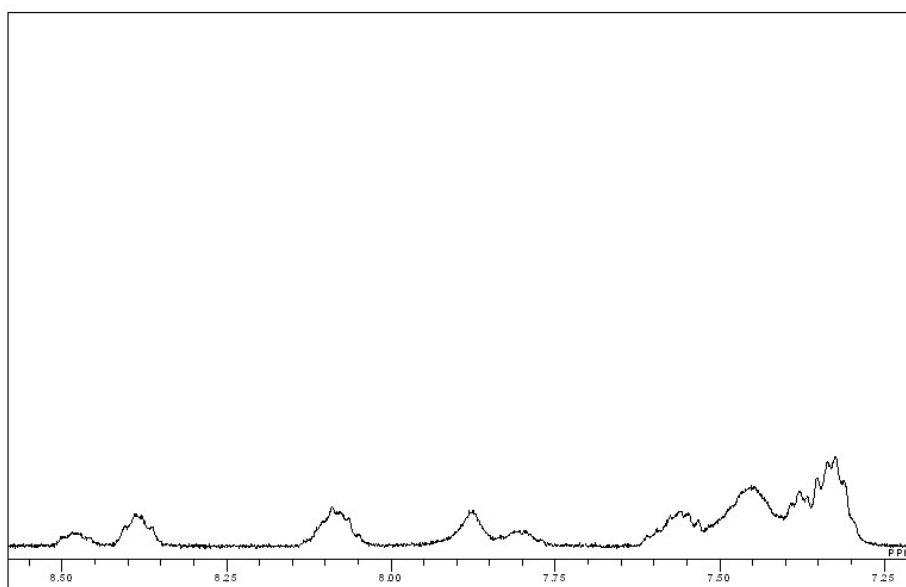


Figure 26. ^1H -NMR Spectrum of Complex 20

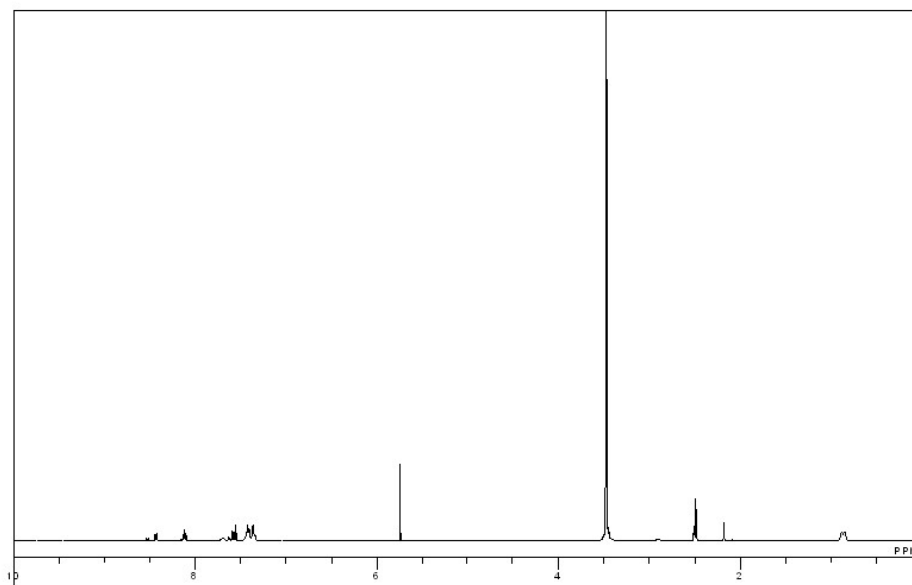


Figure 29. ^1H -NMR Spectrum of Complex 26

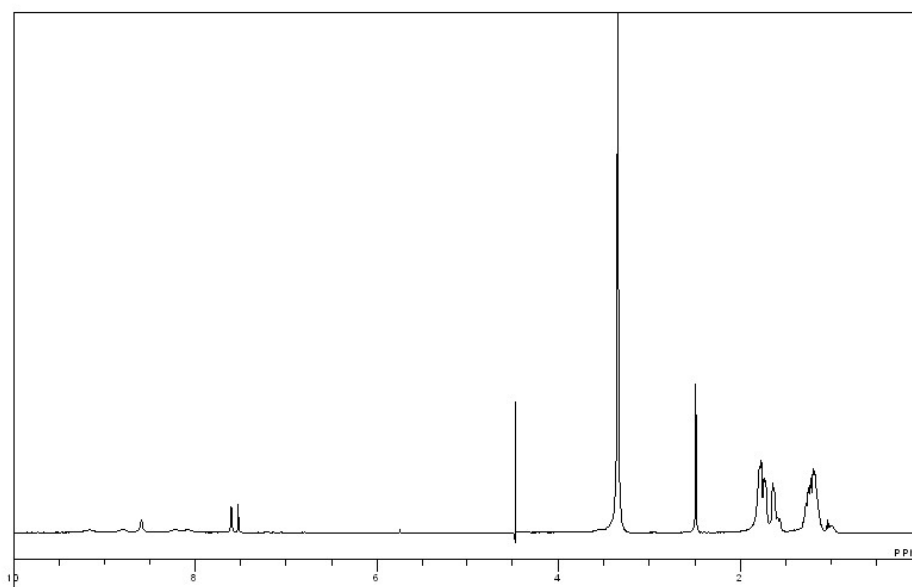


Figure 30. ^1H -NMR Spectrum of Complex 28

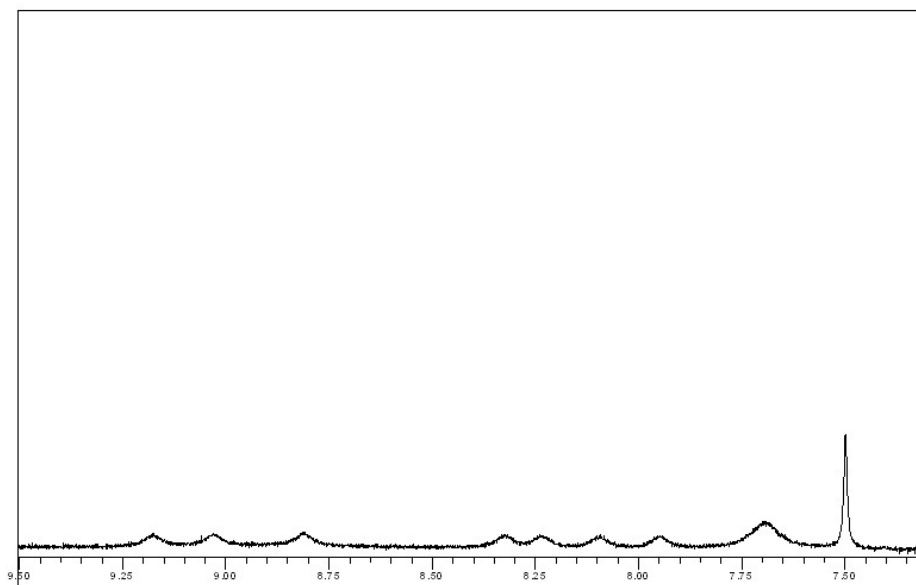


Figure 31. ^1H -NMR Spectrum of Complex 31

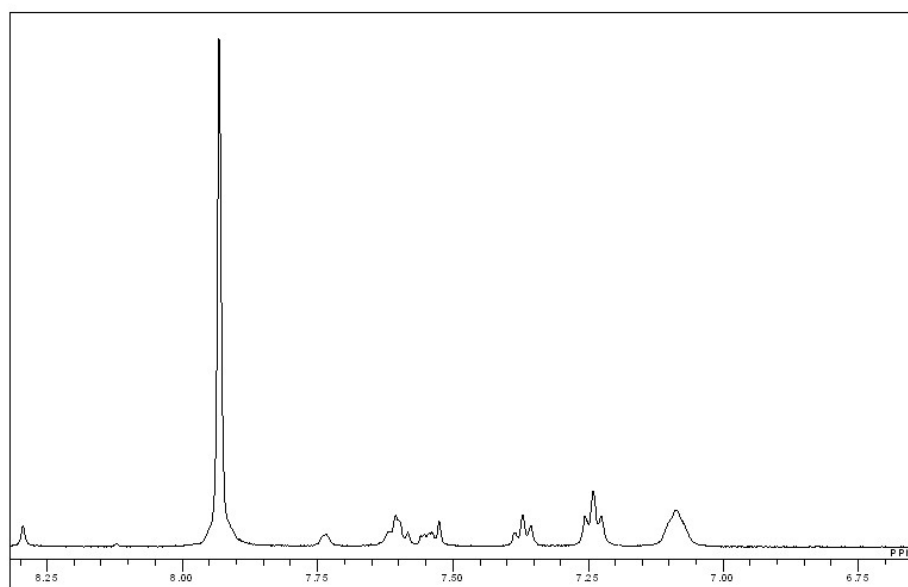


Figure 32. ^1H -NMR Spectrum of Complex 32

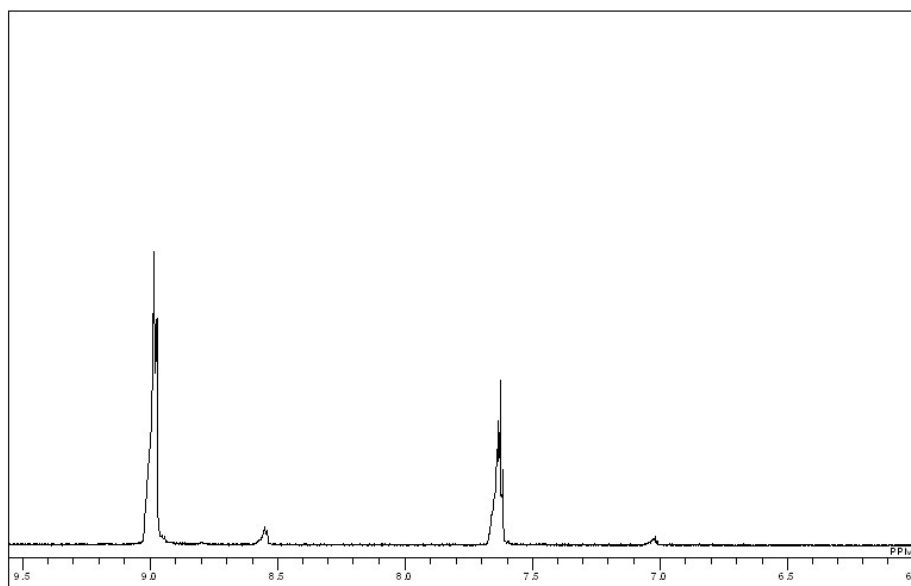


Figure 33. ^1H -NMR Spectrum of bpm

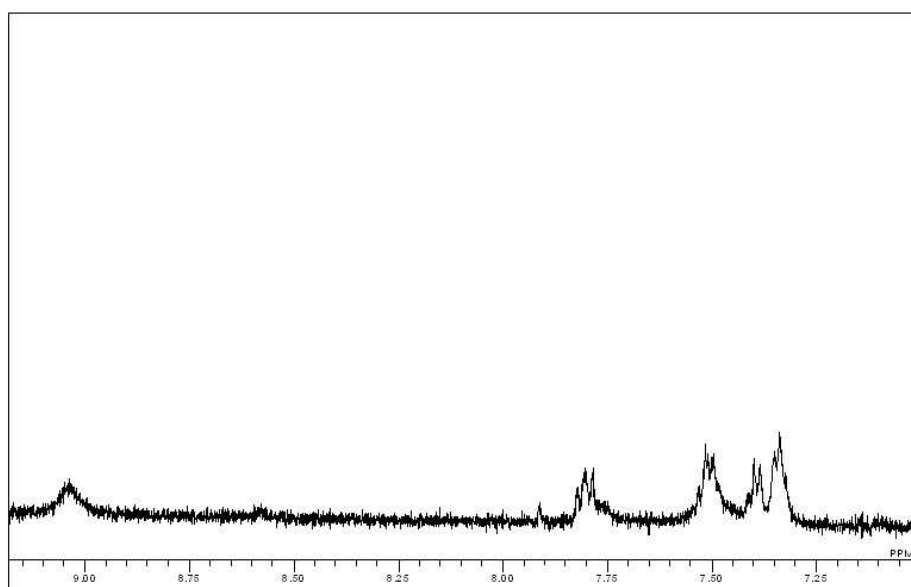


Figure 34. ^1H -NMR Spectrum of Complex 34

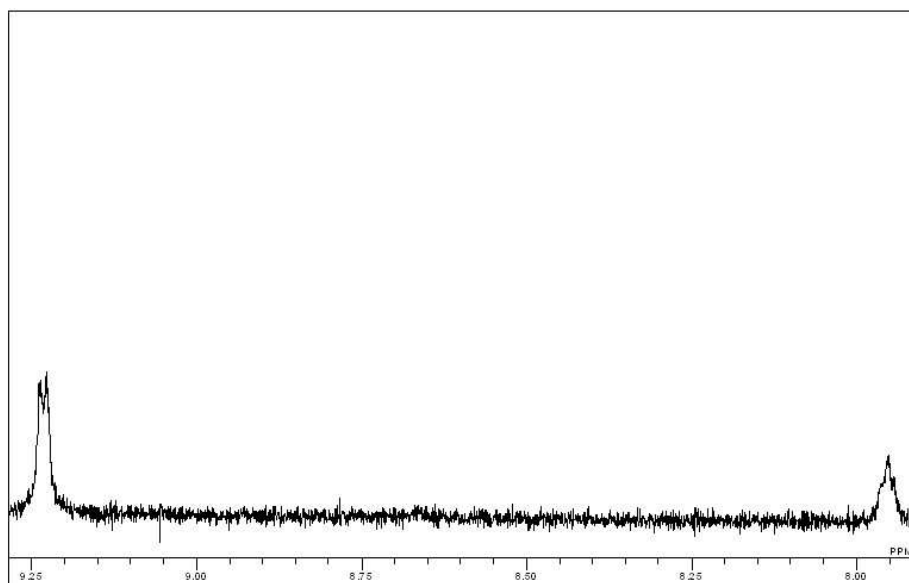


Figure 35. ^1H -NMR Spectrum of Complex 35

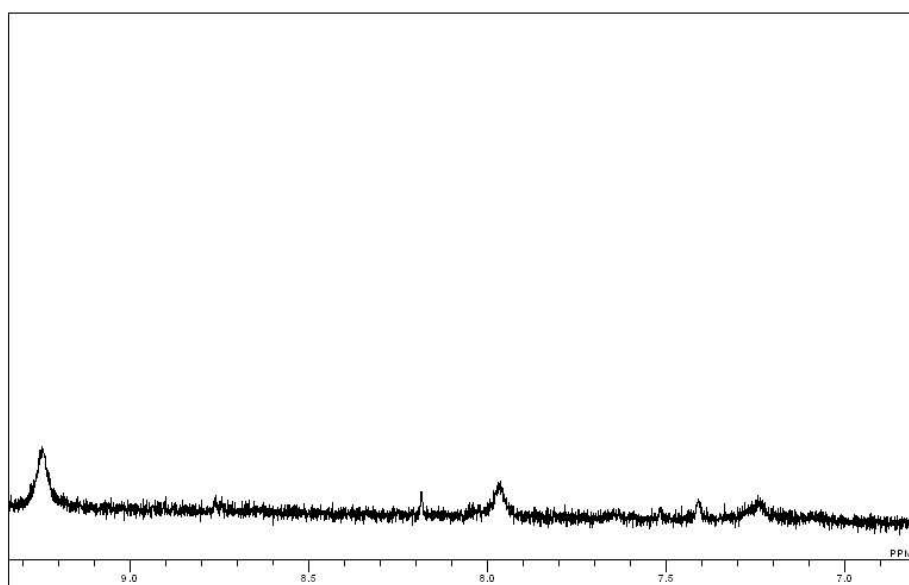


Figure 36. ^1H -NMR Spectrum of Complex 36

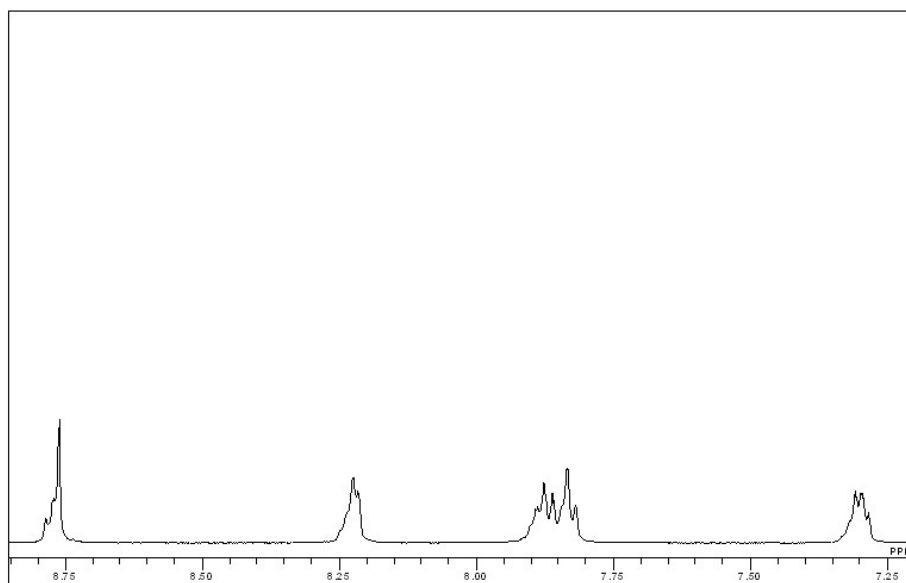


Figure 37. ^1H -NMR Spectrum of *bpp*

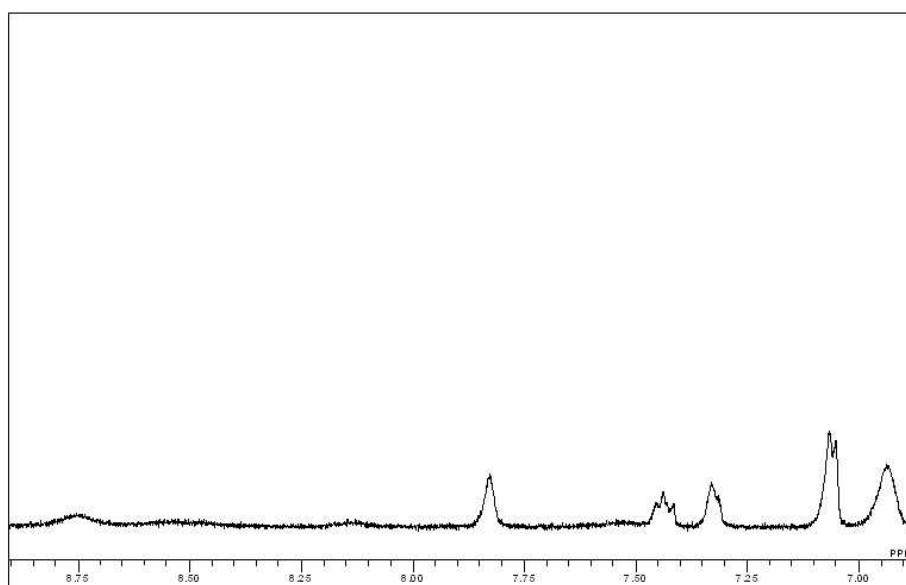


Figure 38. ^1H -NMR Spectrum of Complex 43

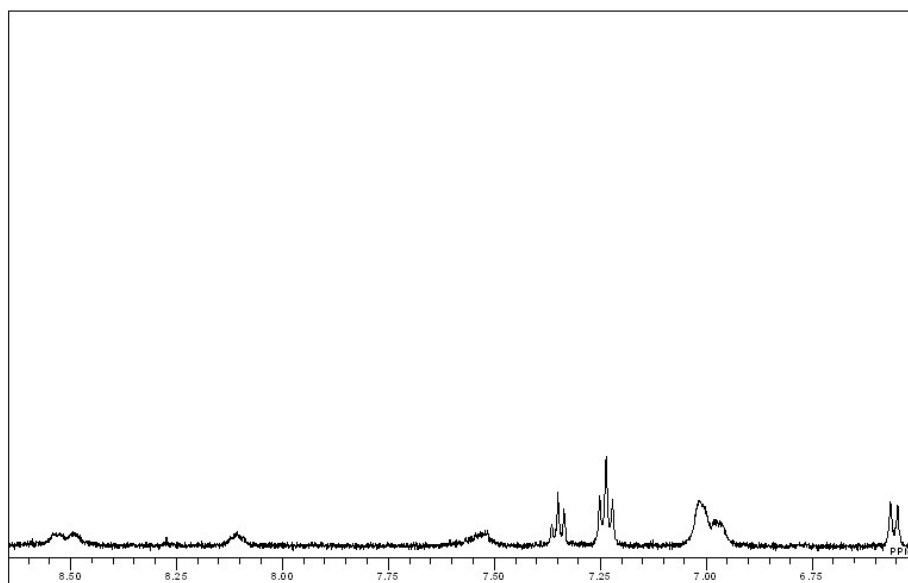


Figure 39. ^1H -NMR Spectrum of Complex 44

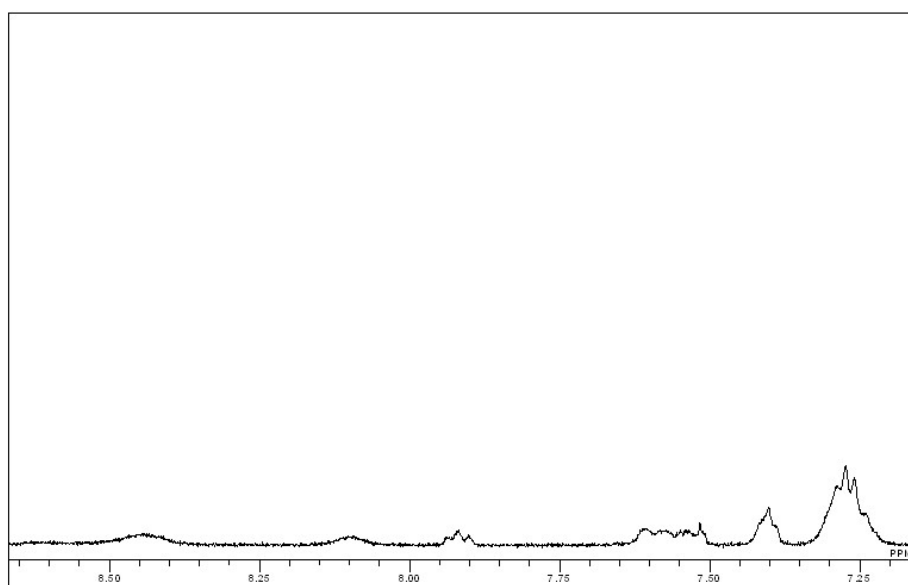


Figure 40. ^1H -NMR Spectrum of Complex 45

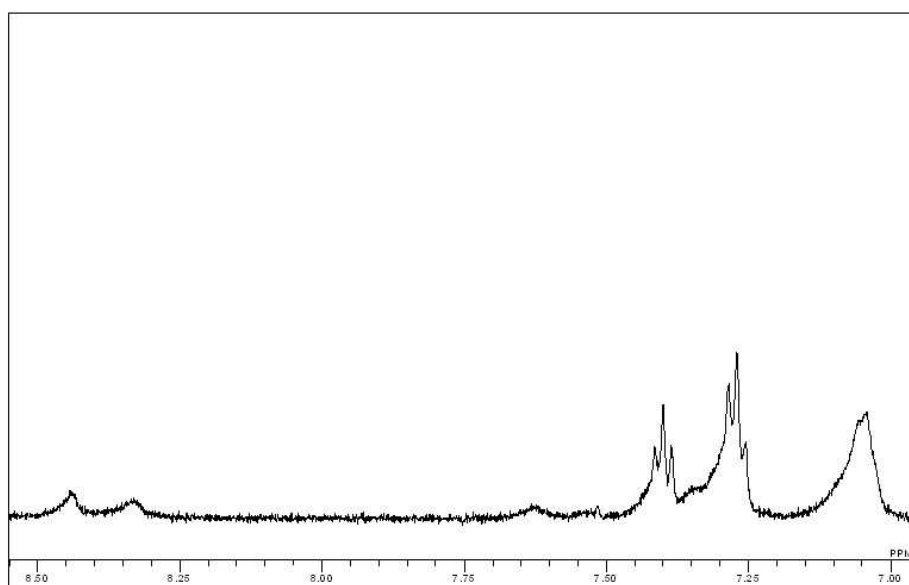


Figure 41. ^1H -NMR Spectrum of Complex 47

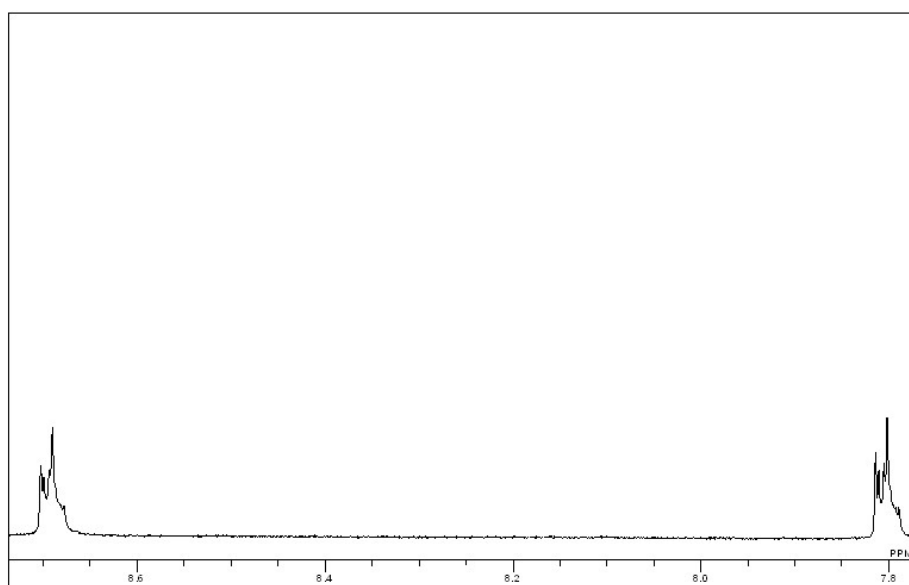


Figure 42. ^1H -NMR Spectrum of Complex 50

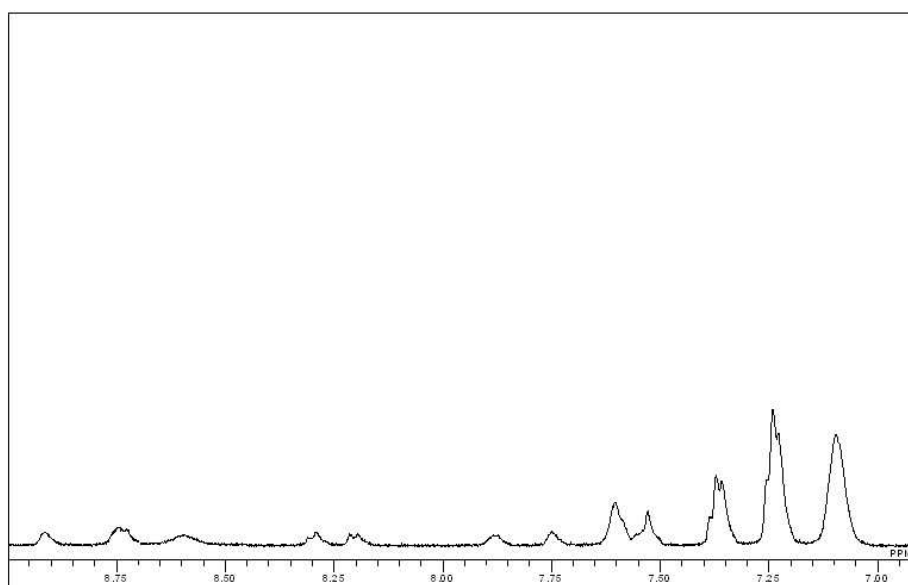


Figure 43. ^1H -NMR Spectrum of Complex 53

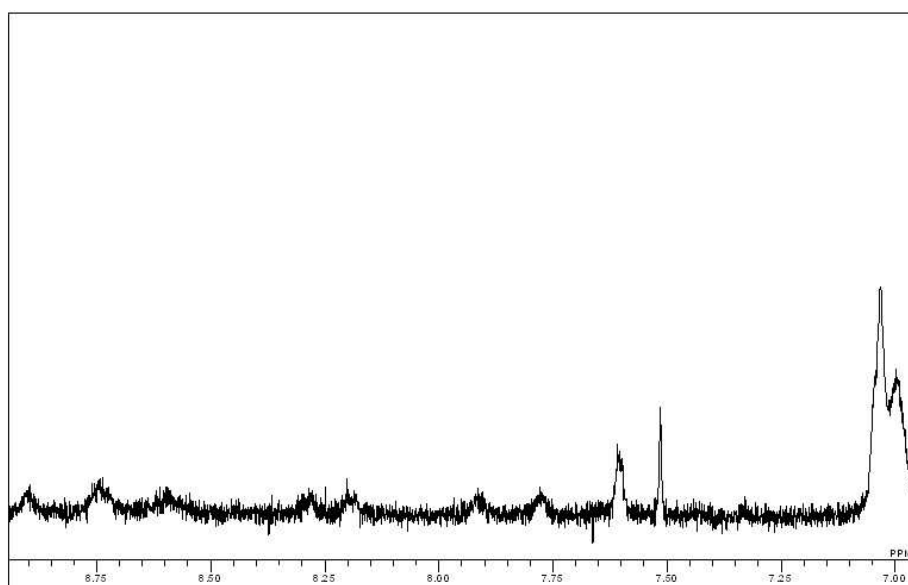


Figure 44. ^1H -NMR Spectrum of Complex 54

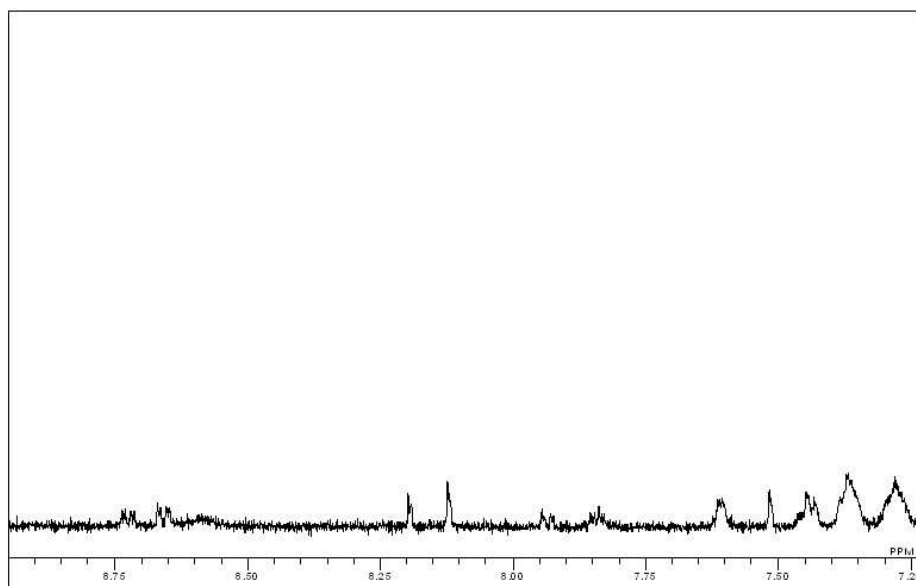
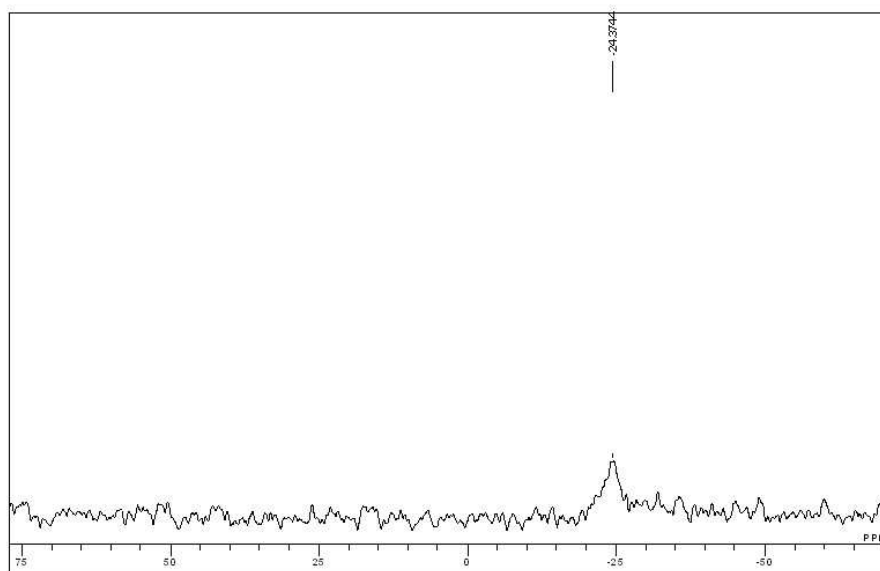
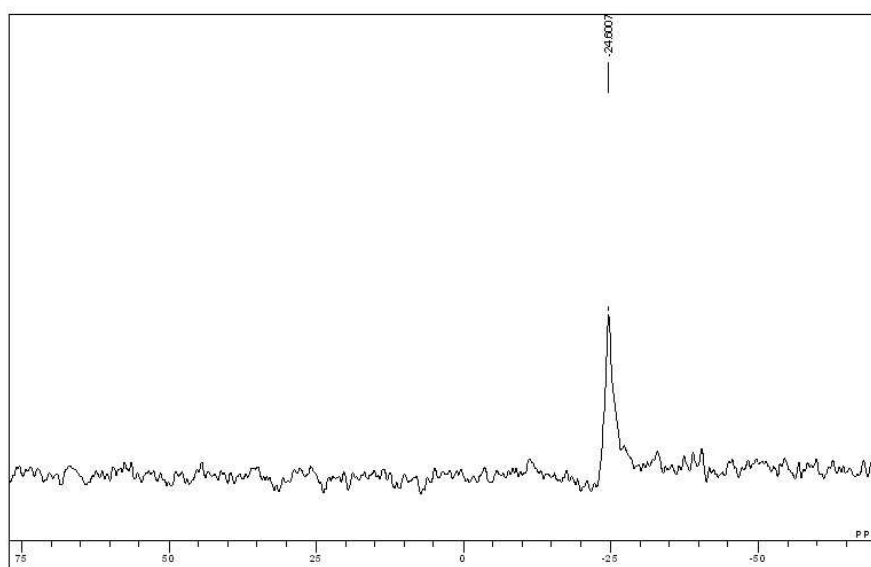


Figure 45. ^1H -NMR Spectrum of Complex 55

A- VII

**Figure 1.** ^{31}P -NMR Spectrum of Complex 1**Figure 2.** ^{31}P -NMR Spectrum of Complex 2

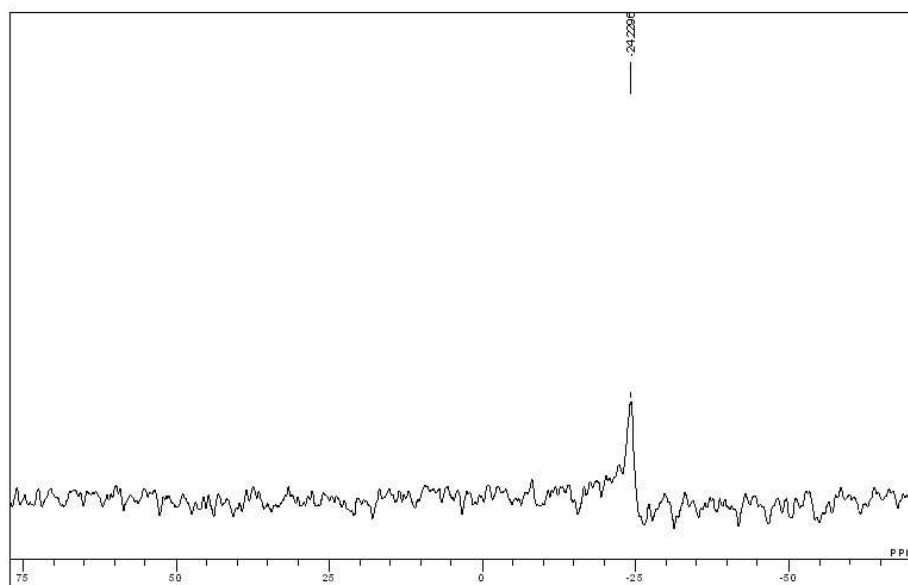


Figure 3. ^{31}P -NMR Spectrum of Complex 3

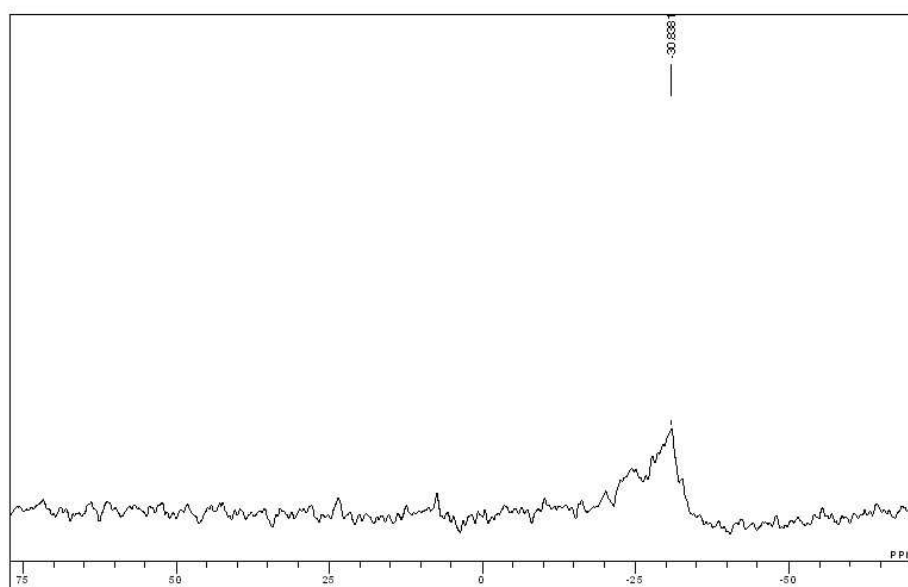


Figure 4. ^{31}P -NMR Spectrum of Complex 4

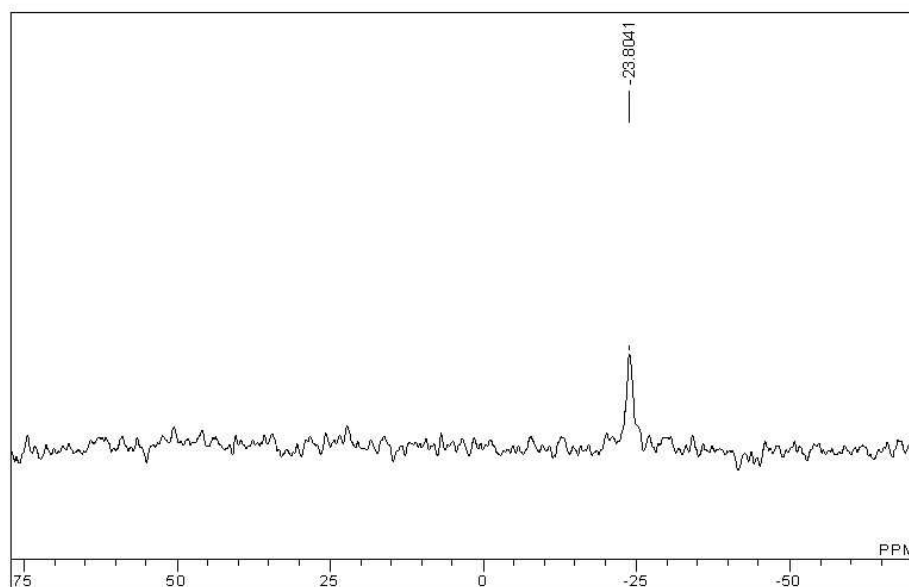


Figure 5. ^{31}P -NMR Spectrum of Complex 5

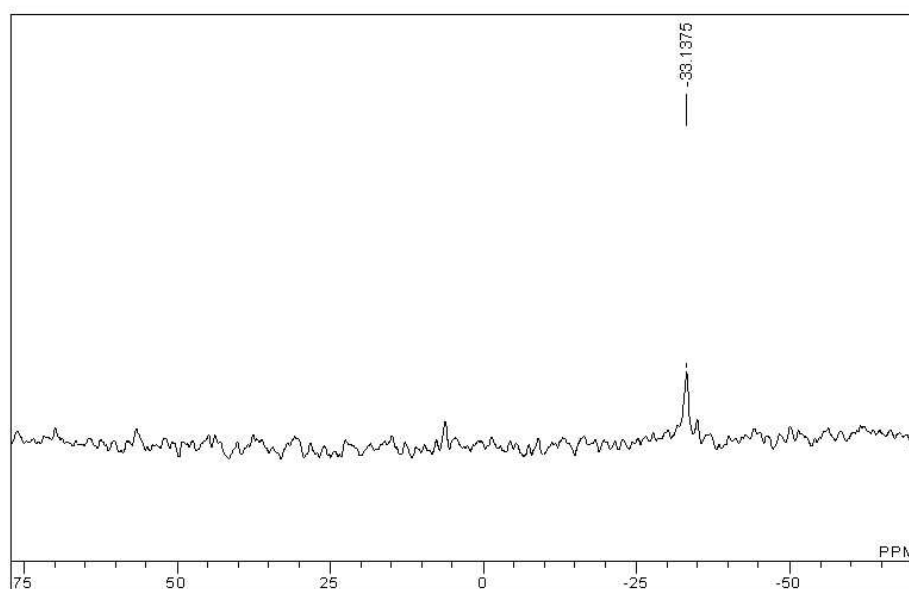


Figure 6. ^{31}P -NMR Spectrum of Complex 7

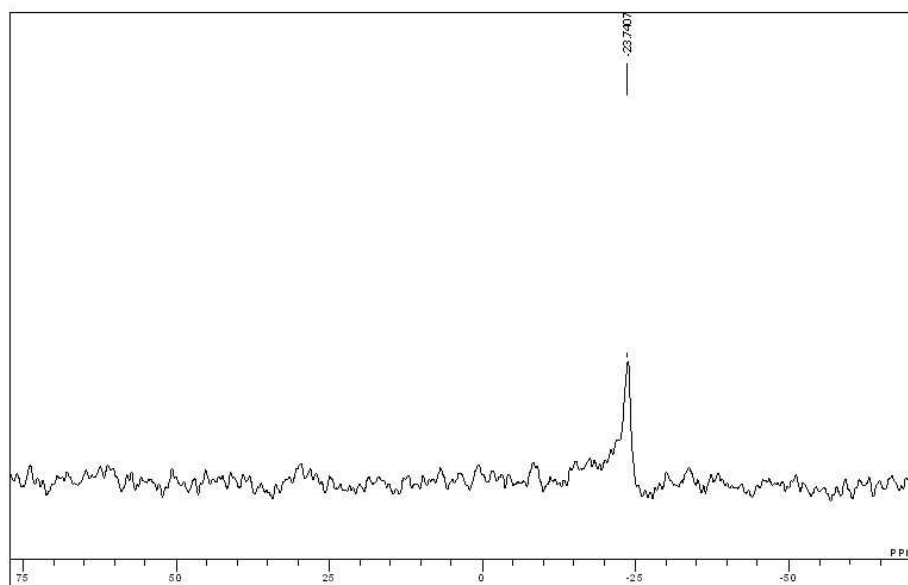


Figure 7. ^{31}P -NMR Spectrum of Complex 8

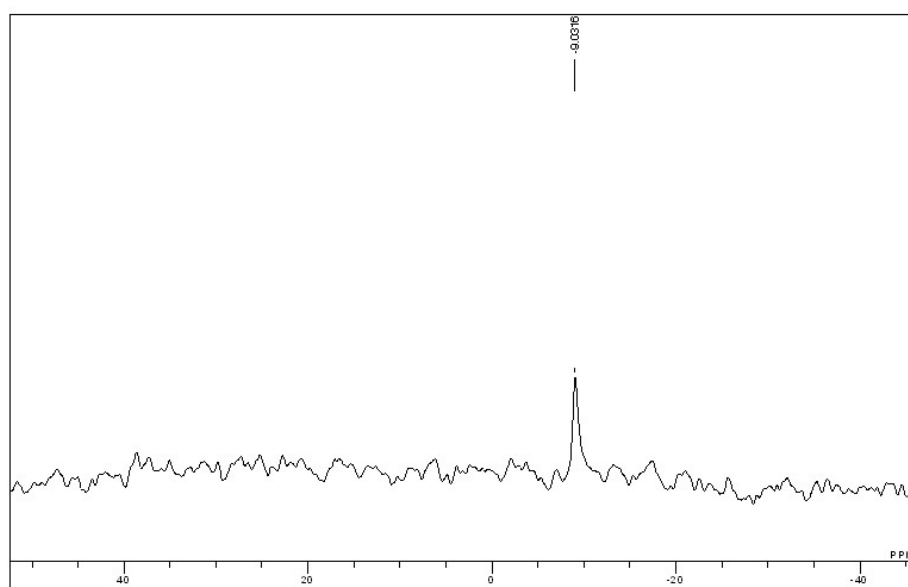


Figure 8. ^{31}P -NMR Spectrum of DPPETHY

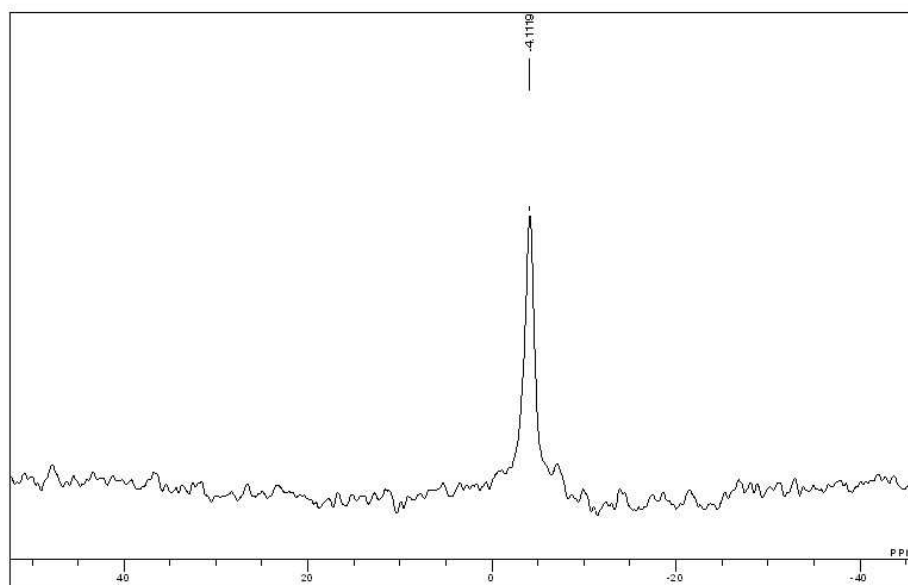


Figure 9. ^{31}P -NMR Spectrum of Precursor-B

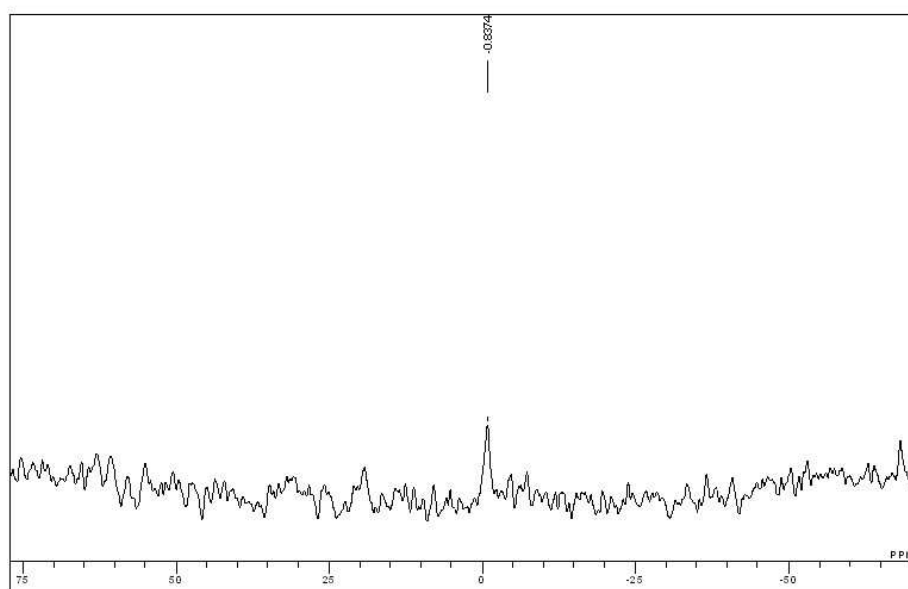


Figure 10. ^{31}P -NMR Spectrum of Complex

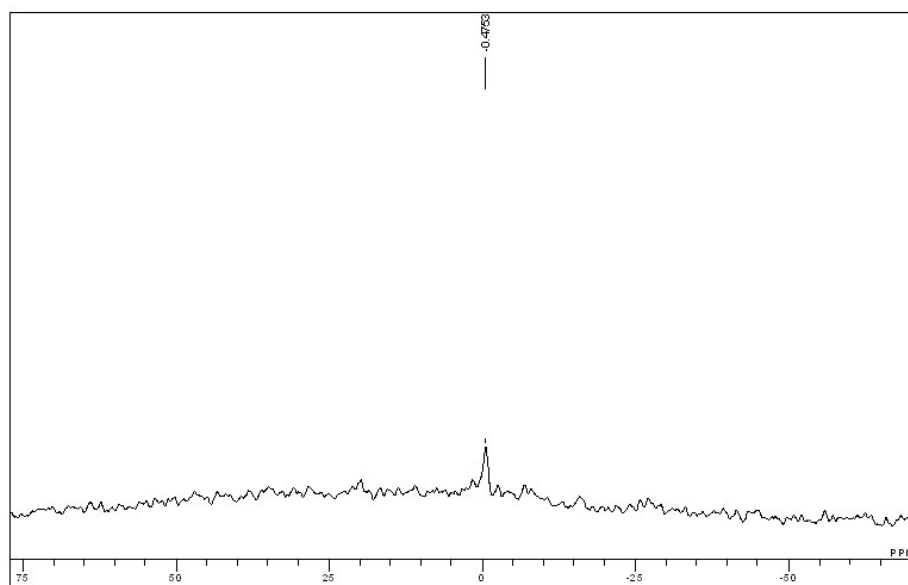


Figure 11. ^{31}P -NMR Spectrum of Complex 10

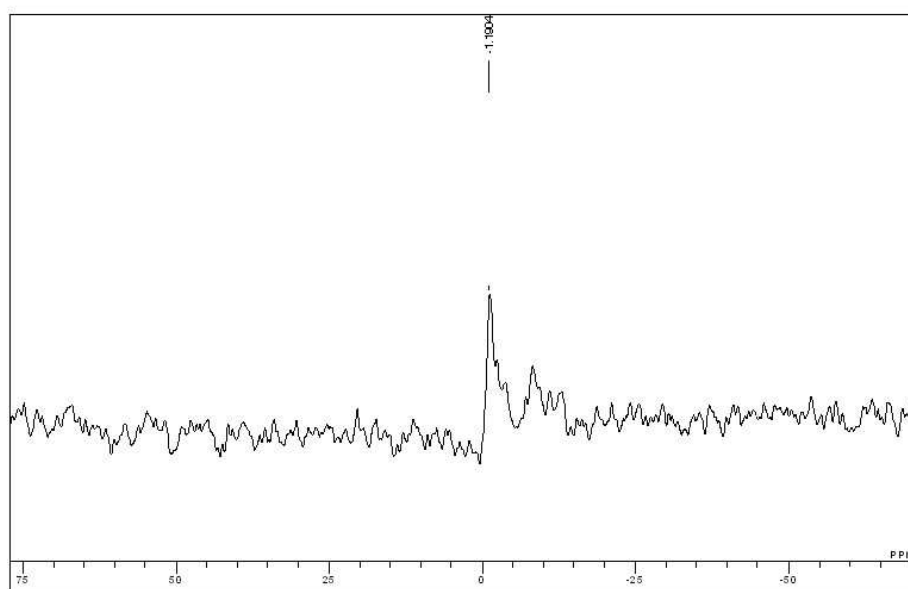


Figure 12. ^{31}P -NMR Spectrum of Complex 11

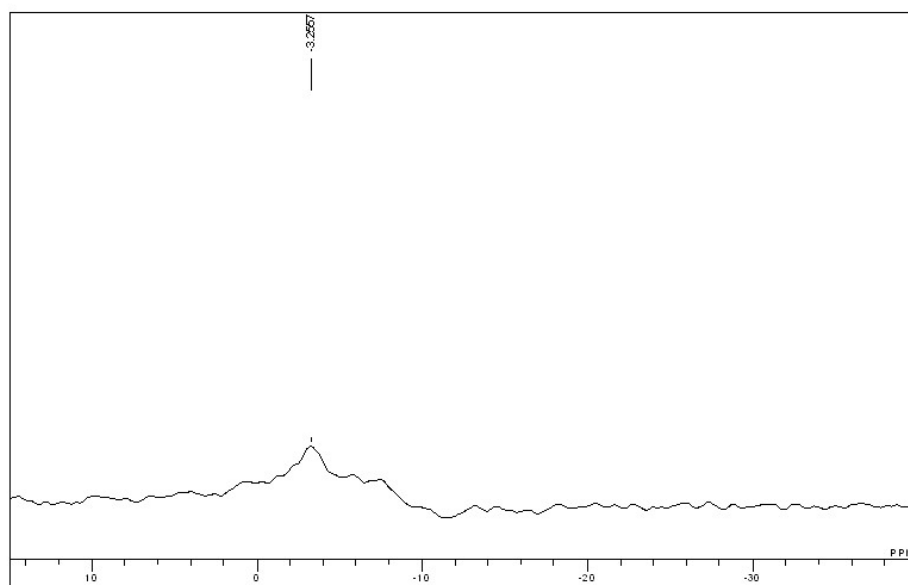


Figure 13. ^{31}P -NMR Spectrum of Complex 12

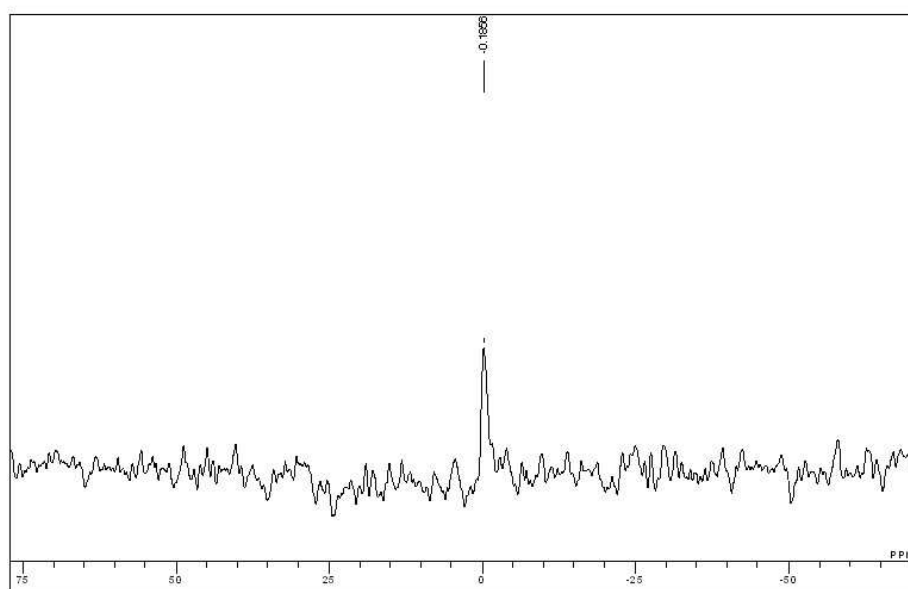


Figure 14. ^{31}P -NMR Spectrum of Complex 13

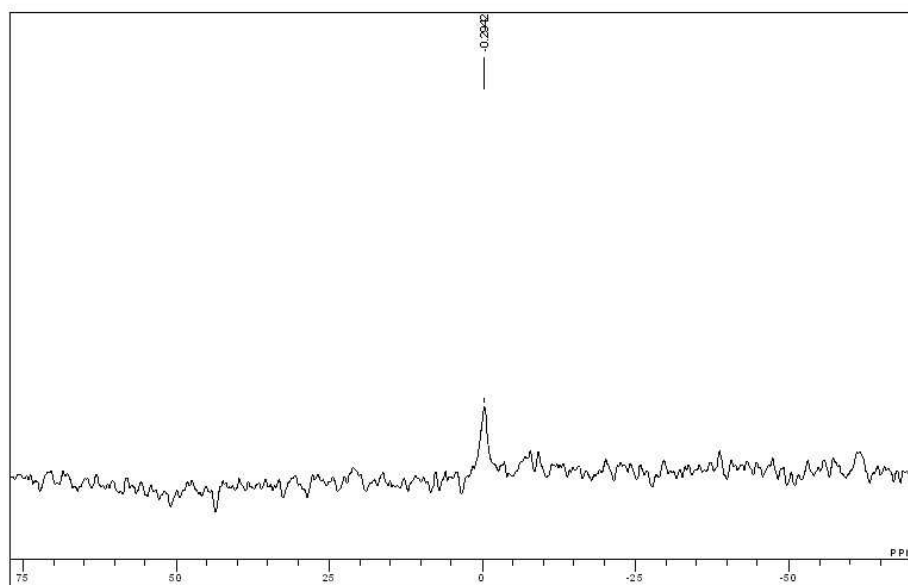


Figure 15. ^{31}P -NMR Spectrum of Complex 14

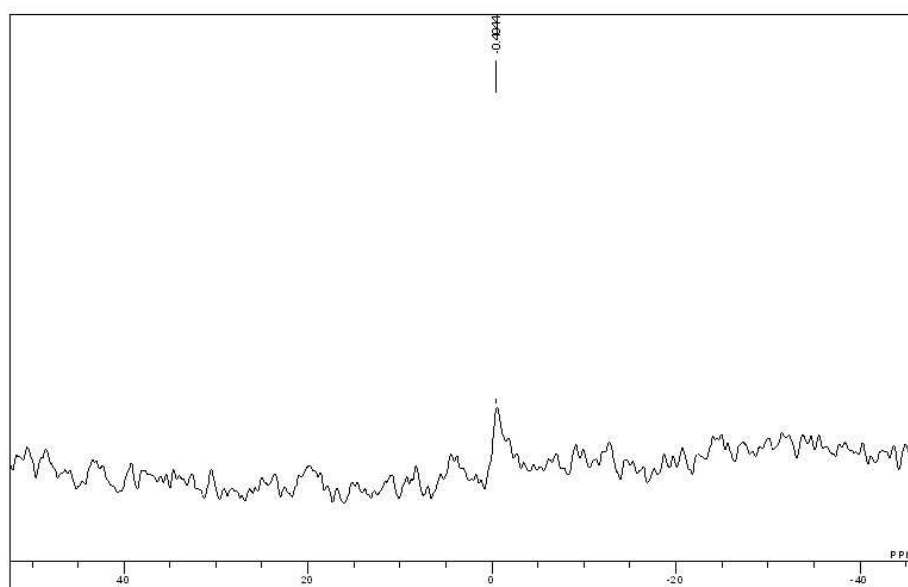


Figure 16. ^{31}P -NMR Spectrum of Complex 15

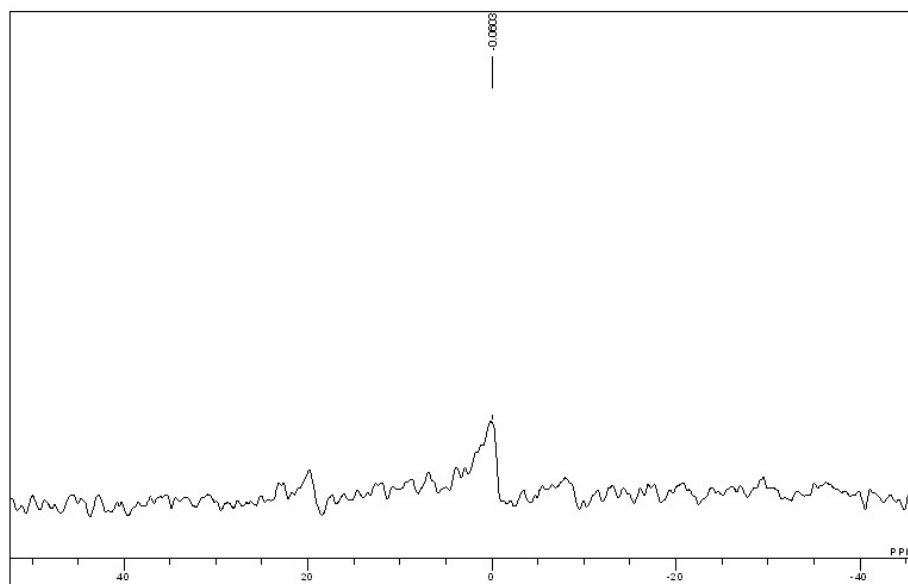


Figure 17. ^{31}P -NMR Spectrum of Complex 16

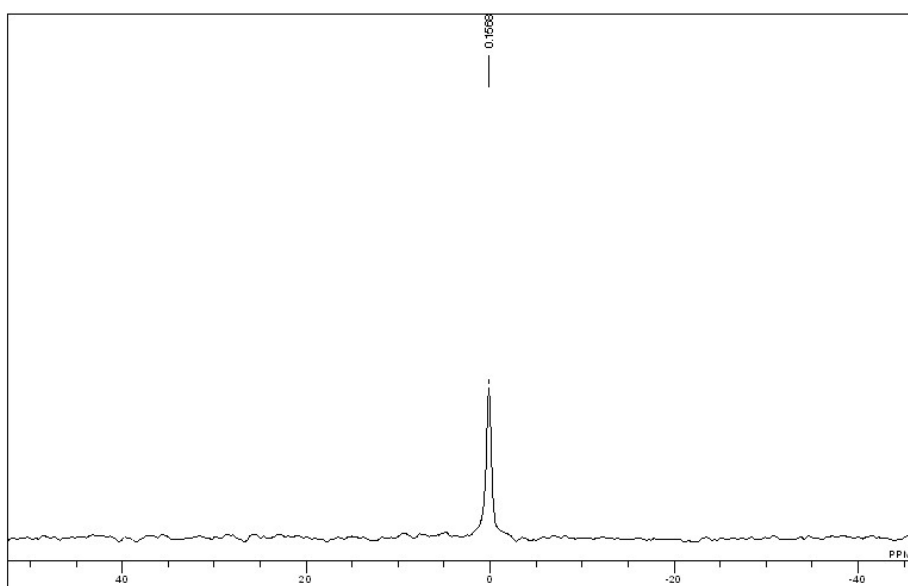


Figure 18. ^{31}P -NMR Spectrum of $\text{PPh}_2(\text{i-Pr})$

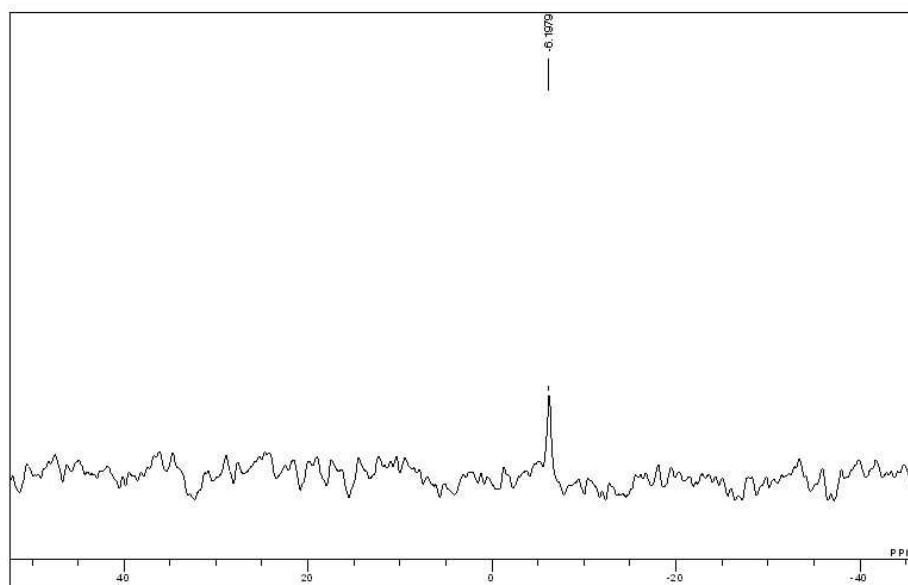


Figure 19. ^{31}P -NMR Spectrum of (m-Tol) $_3\text{P}$

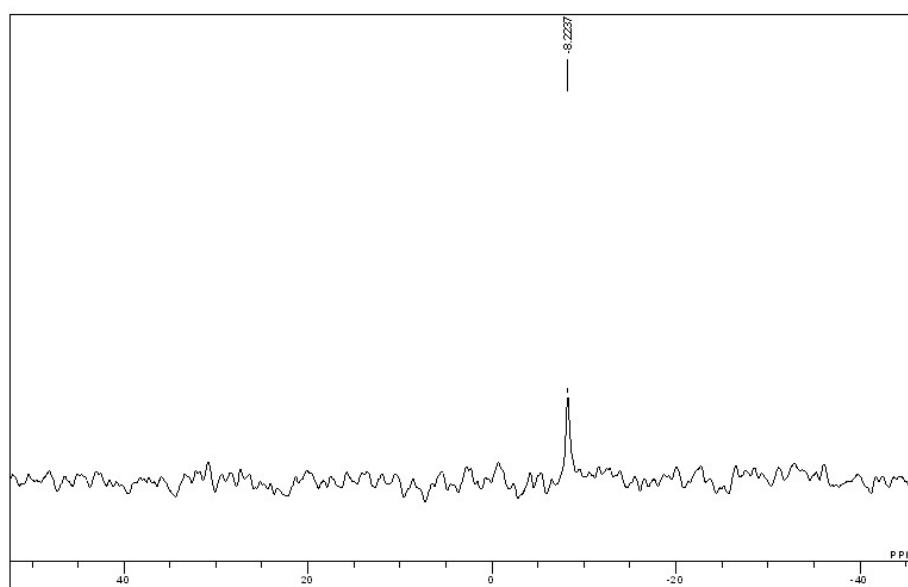


Figure 20. ^{31}P -NMR Spectrum of DAP-DP

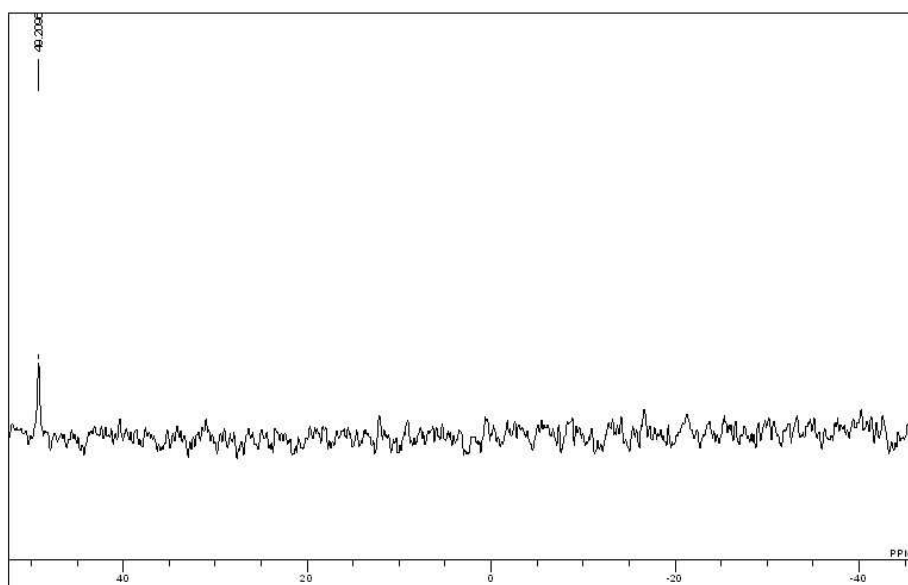


Figure 21. ^{31}P -NMR Spectrum of PCy_3

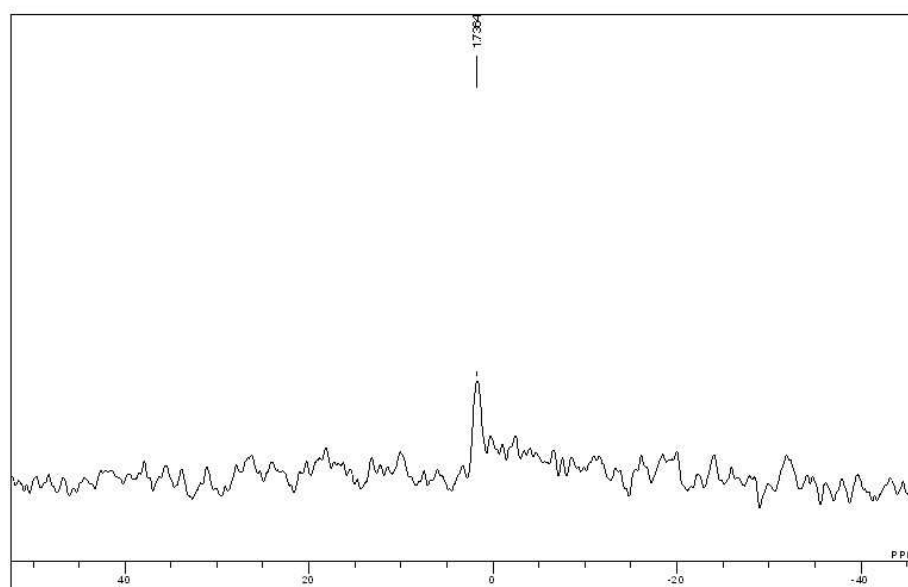


Figure 22. ^{31}P -NMR Spectrum of Complex 18

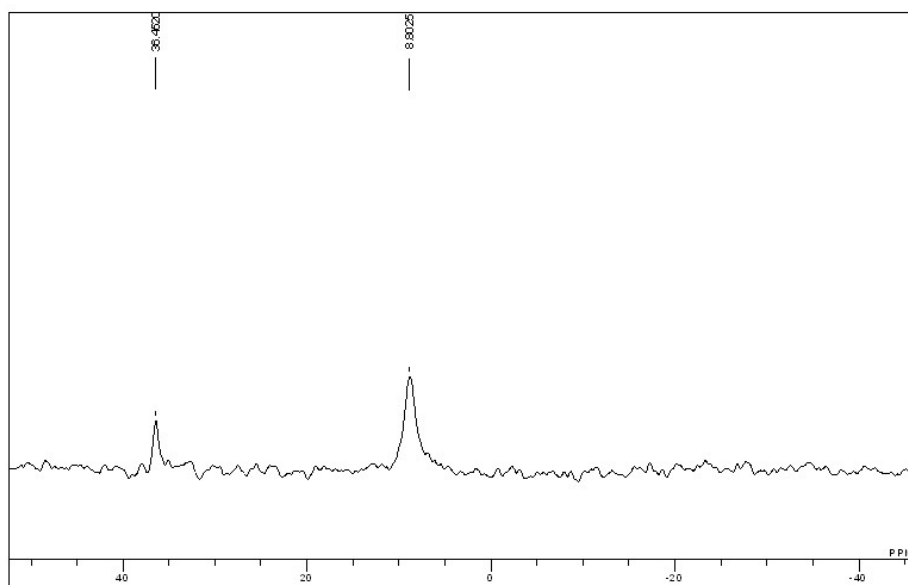


Figure 23. ^{31}P -NMR Spectrum of Complex 20

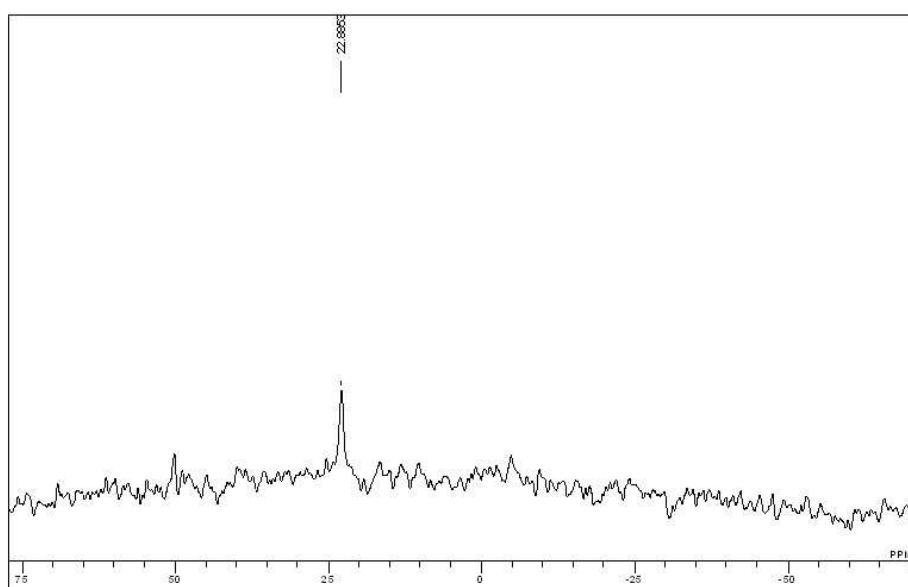


Figure 24. ^{31}P -NMR Spectrum of Complex 23

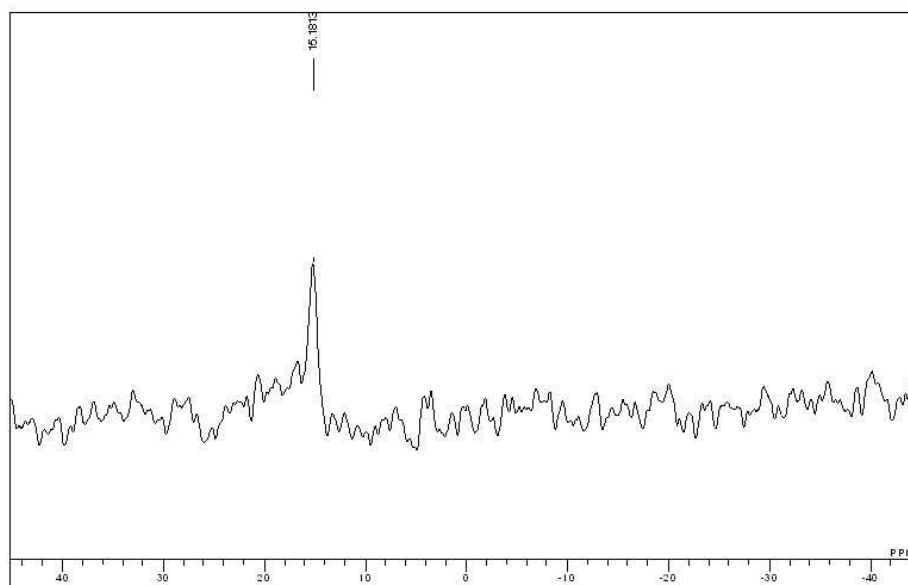


Figure 25. ^{31}P -NMR Spectrum of Complex 24

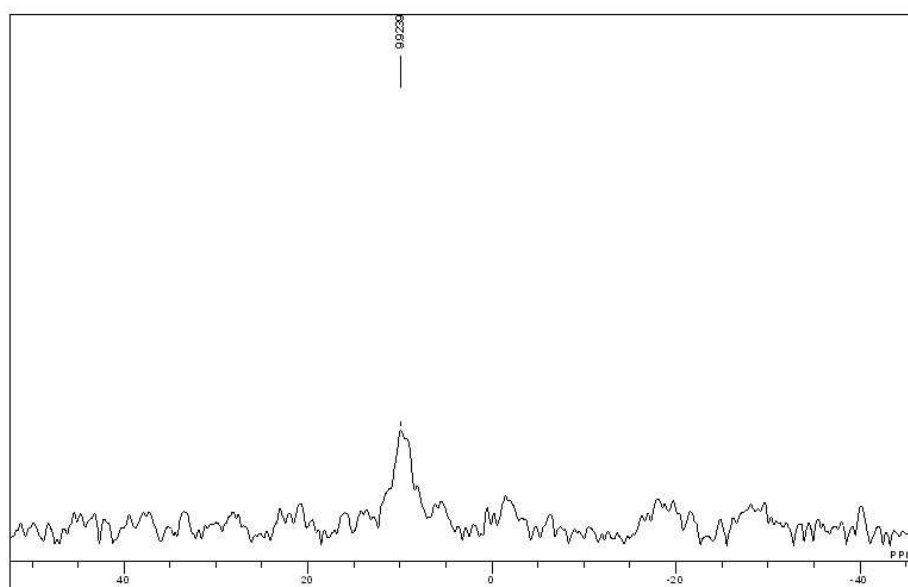


Figure 26. ^{31}P -NMR Spectrum of Complex 25

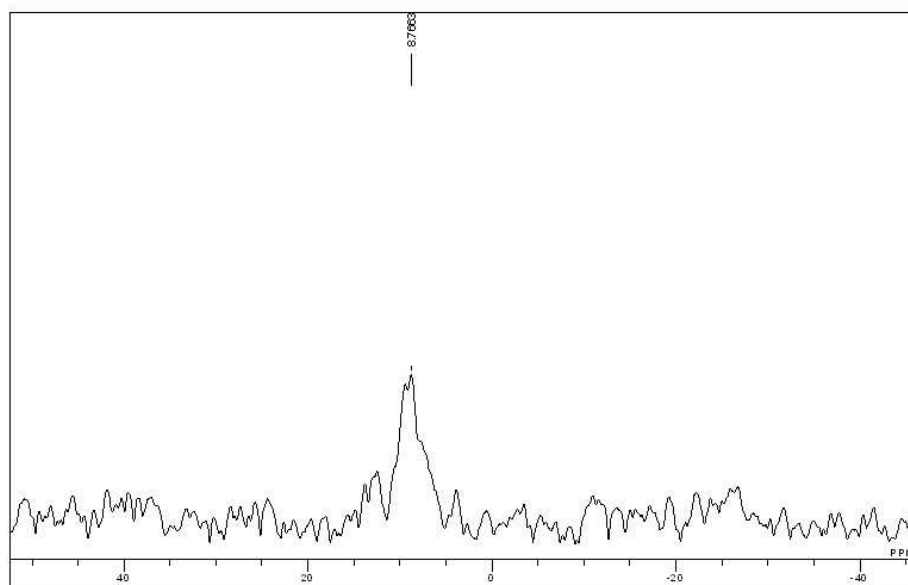


Figure 27. ^{31}P -NMR Spectrum of Complex 26

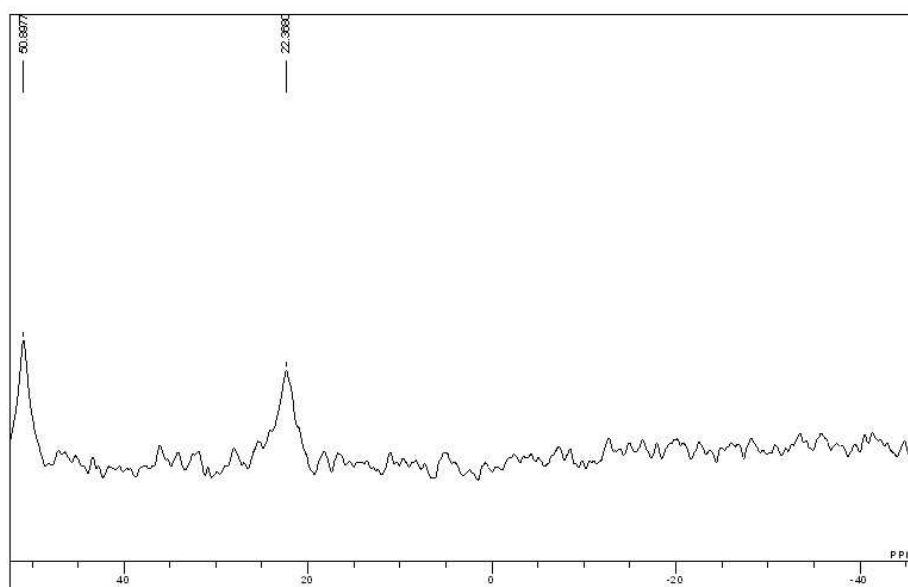


Figure 28. ^{31}P -NMR Spectrum of Complex 31

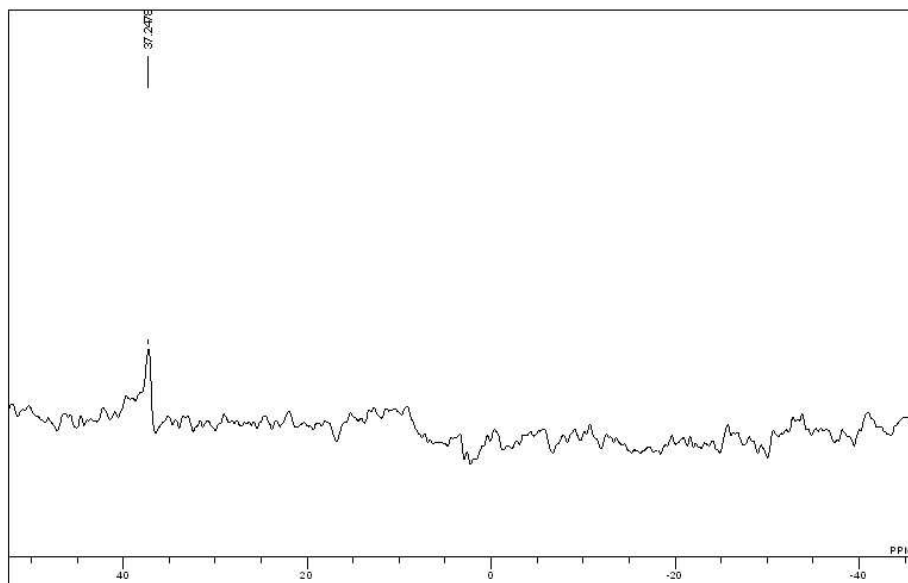


Figure 29. ^{31}P -NMR Spectrum of Complex 34

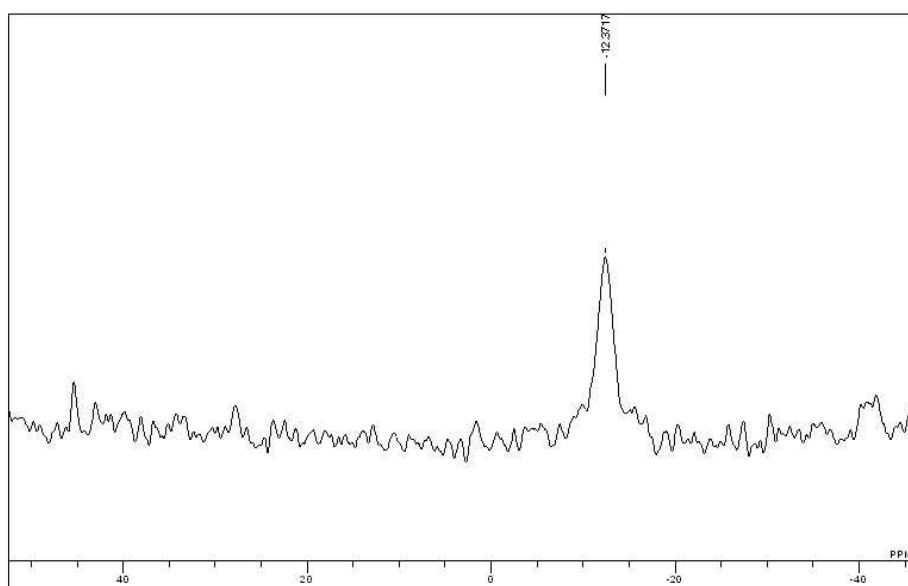


Figure 30. ^{31}P -NMR Spectrum of Complex 35

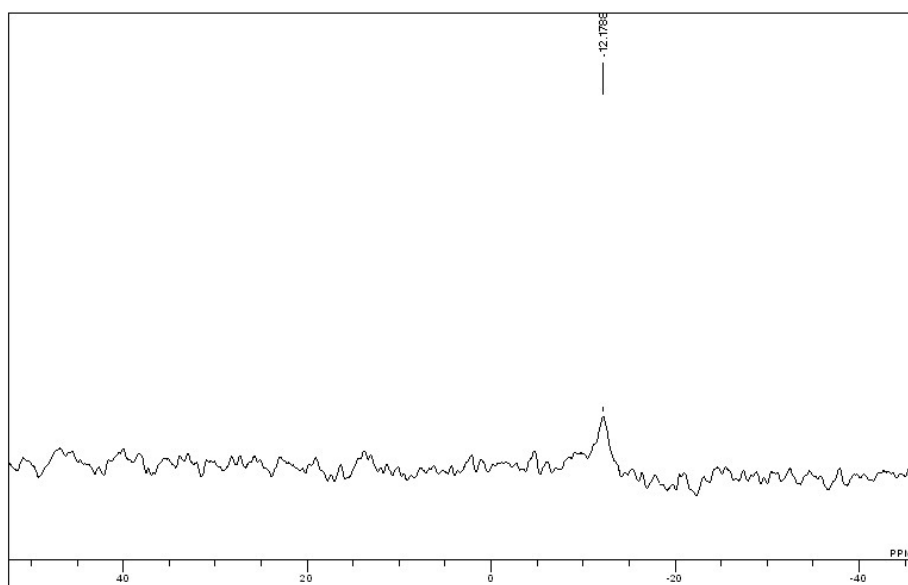


Figure 31. ^{31}P -NMR Spectrum of Complex 36

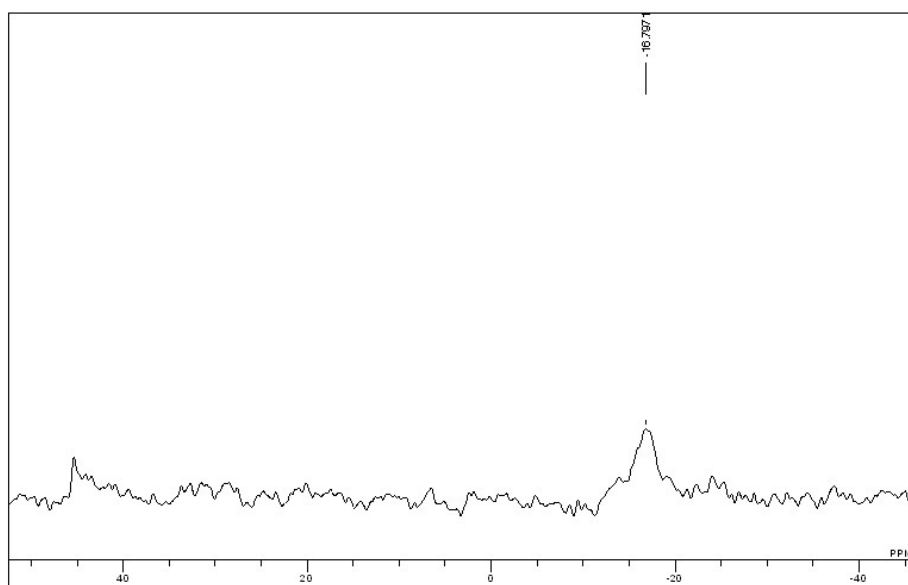


Figure 32. ^{31}P -NMR Spectrum of Complex 37

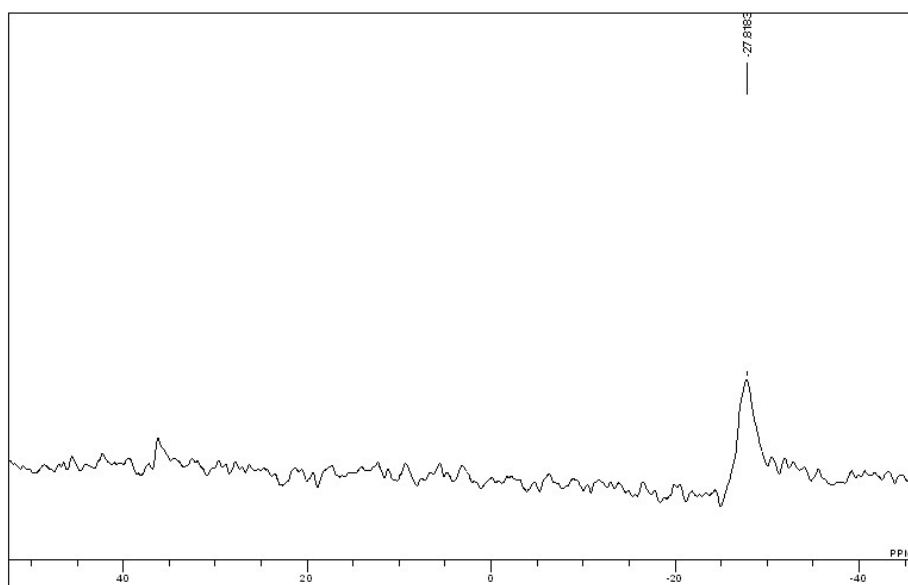


Figure 33. ^{31}P -NMR Spectrum of Complex 39

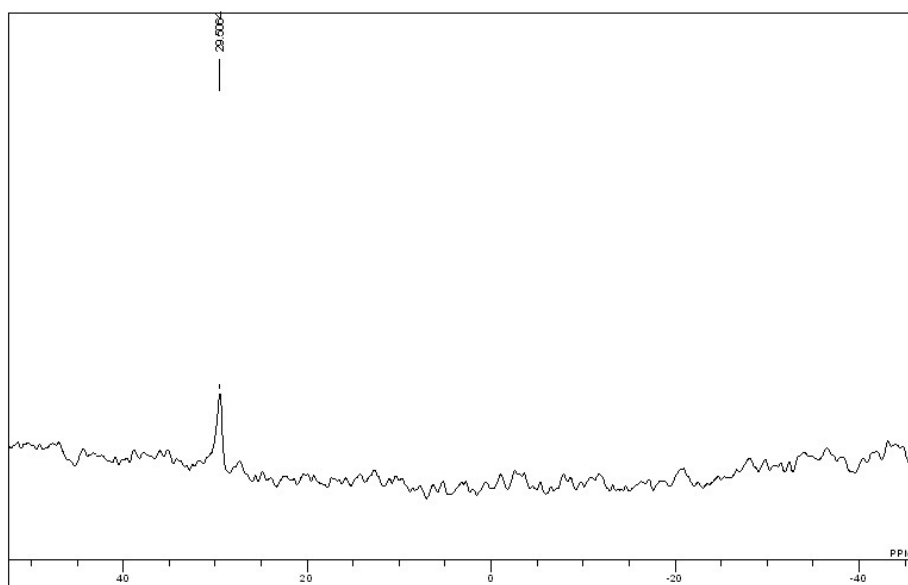


Figure 34. ^{31}P -NMR Spectrum of Complex 40

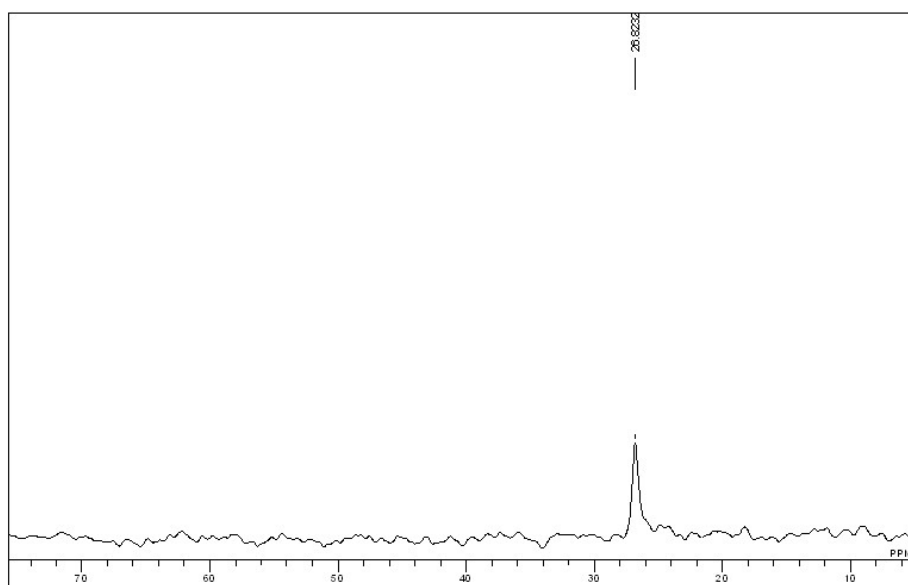


Figure 35. ^{31}P -NMR Spectrum of Complex 43

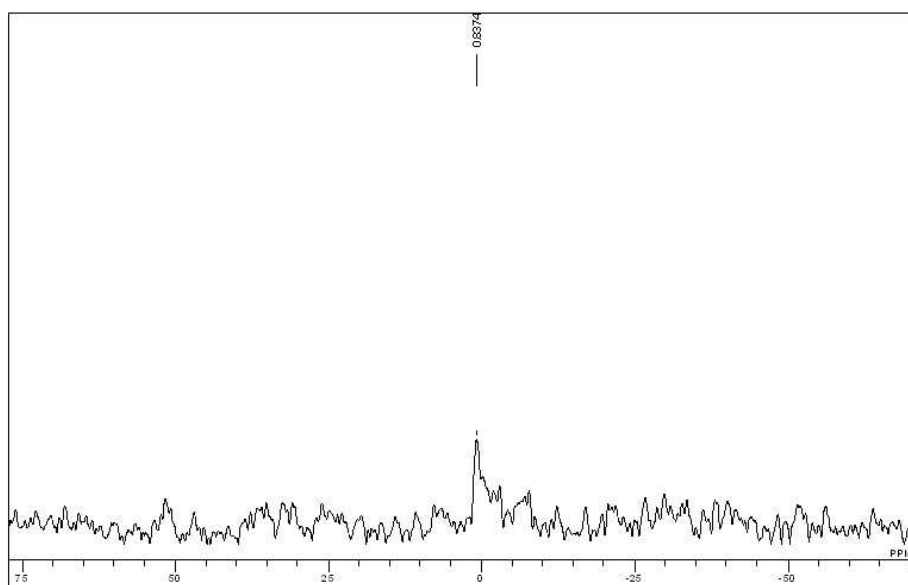


Figure 36. ^{31}P -NMR Spectrum of Complex 44

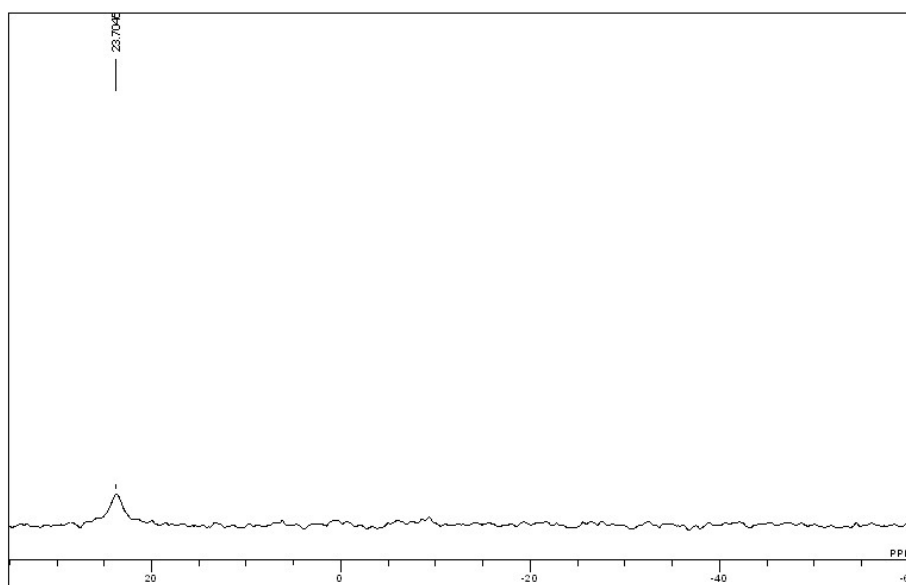


Figure 37. ^{31}P -NMR Spectrum of Complex 45

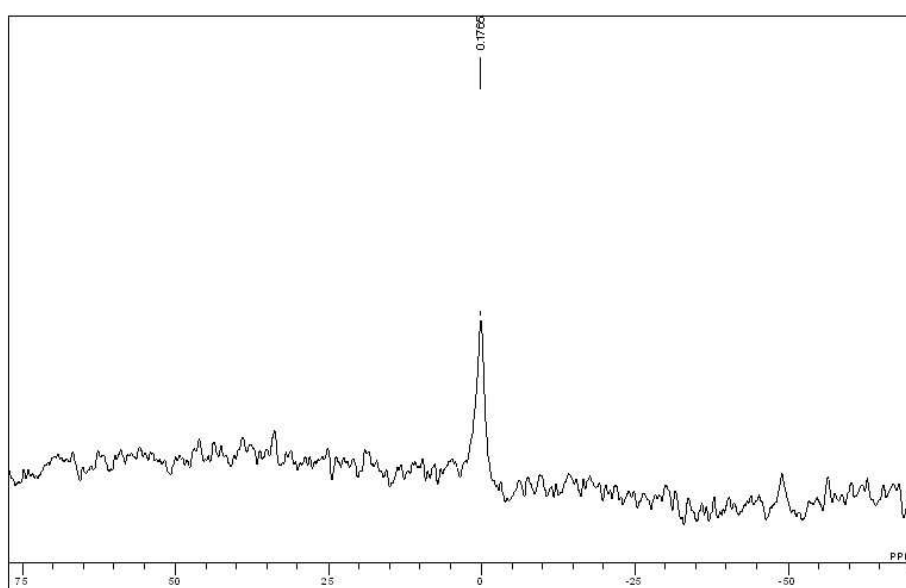


Figure 38. ^{31}P -NMR Spectrum of Complex 47

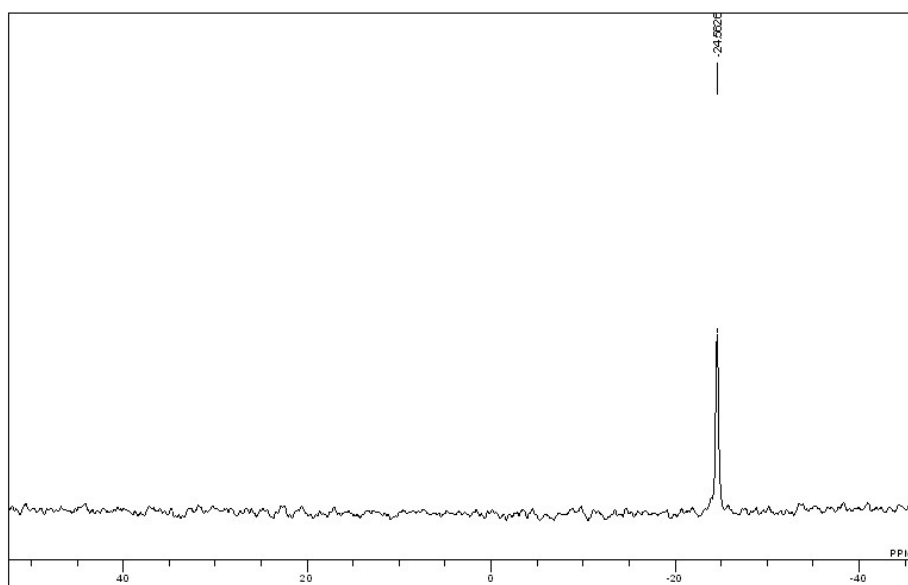


Figure 39. ^{31}P -NMR Spectrum of TCP

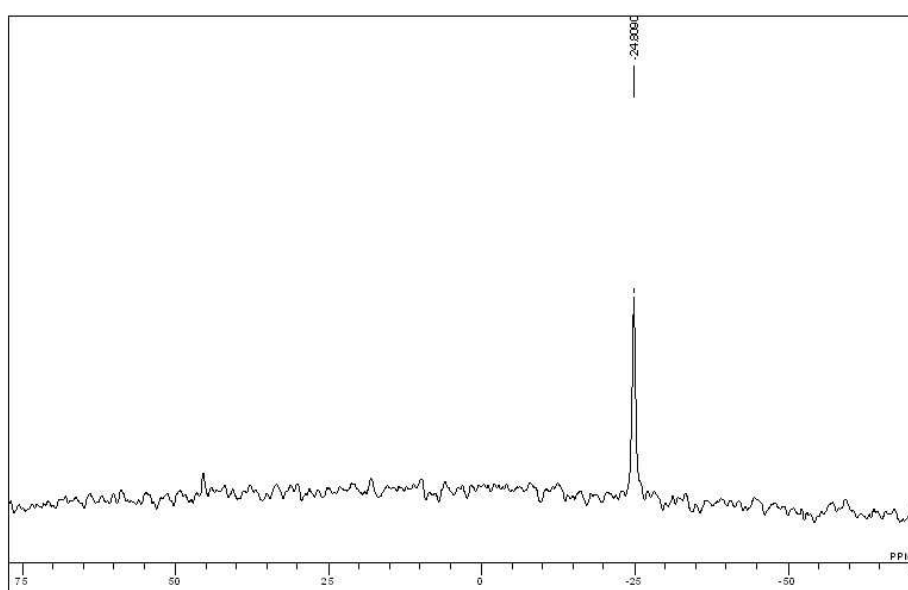


Figure 40. ^{31}P -NMR Spectrum of Complex 50

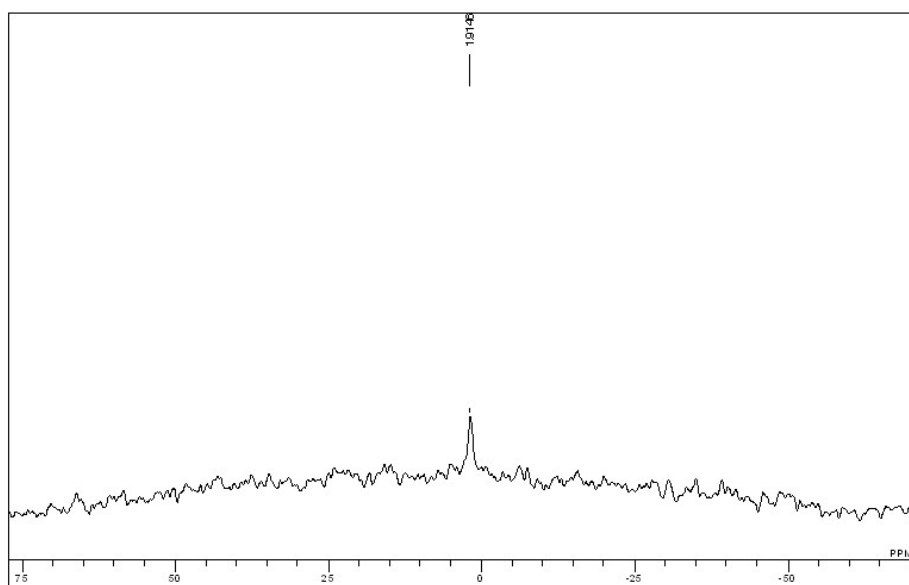
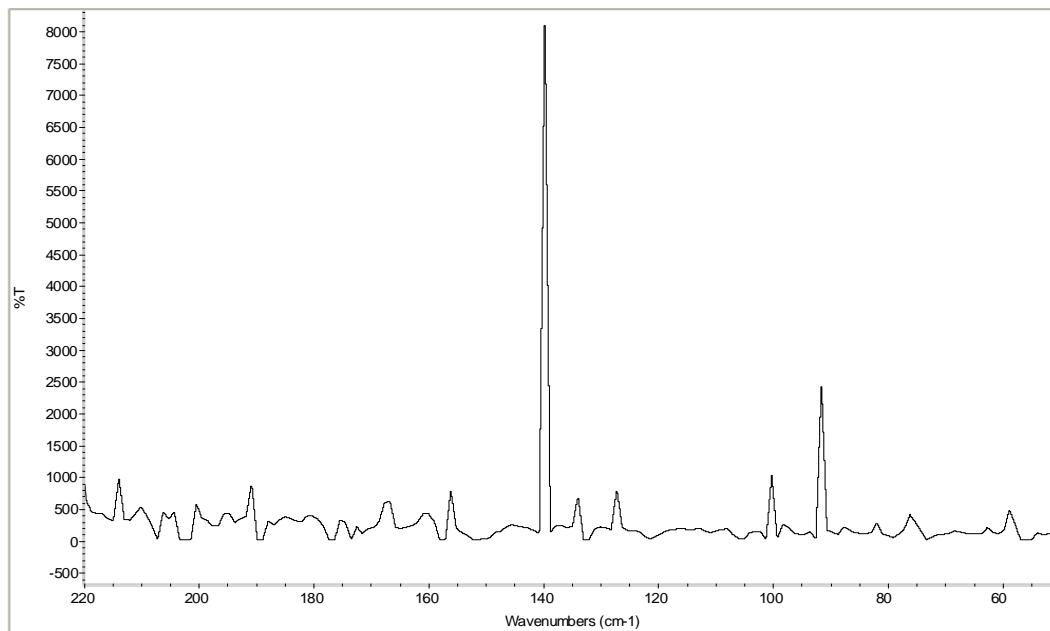
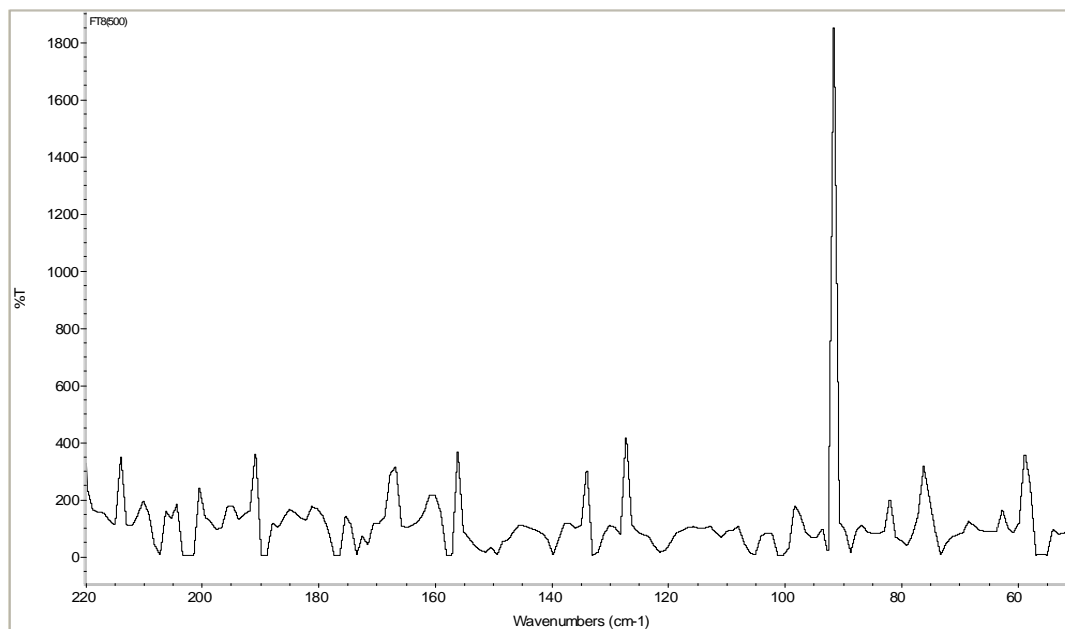


Figure 41. ^{31}P -NMR Spectrum of Complex 55

A-VIII**Figure 1.** Far-Infrared Spectrum of Complex 33**Figure 2.** Far-Infrared Spectrum of Complex 34

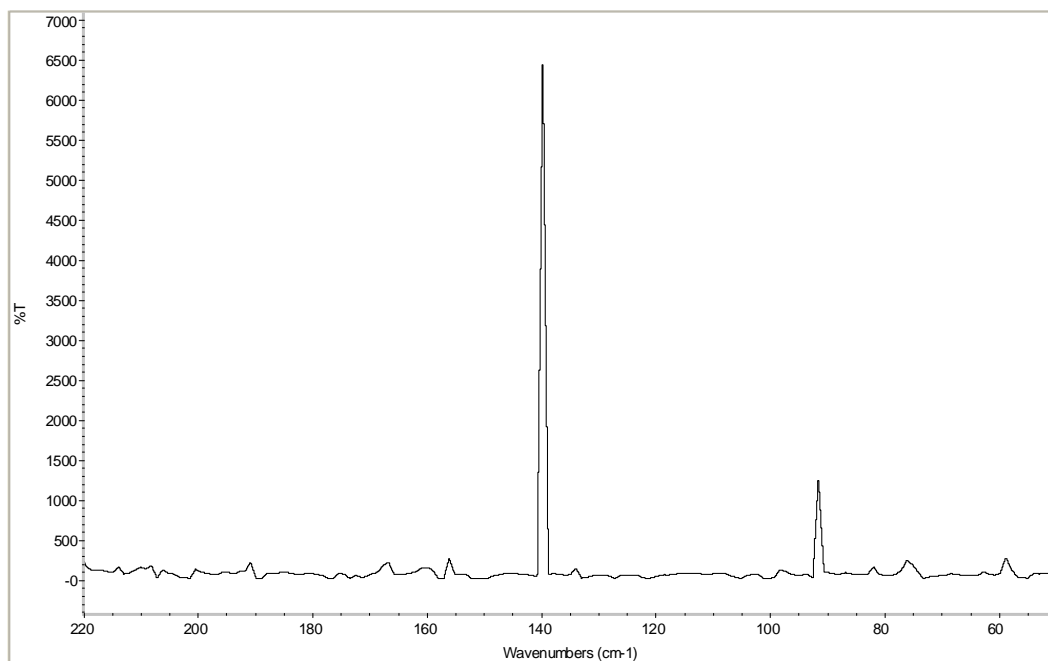


Figure 3. Far-Infrared Spectrum of Complex 35

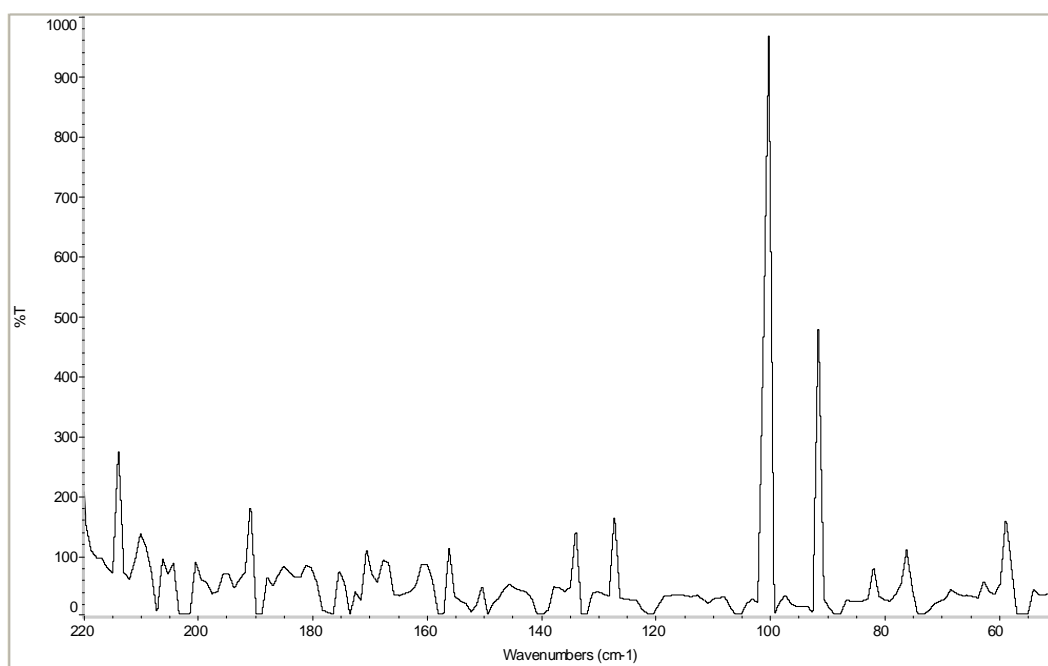


Figure 4. Far-Infrared Spectrum of Complex 36

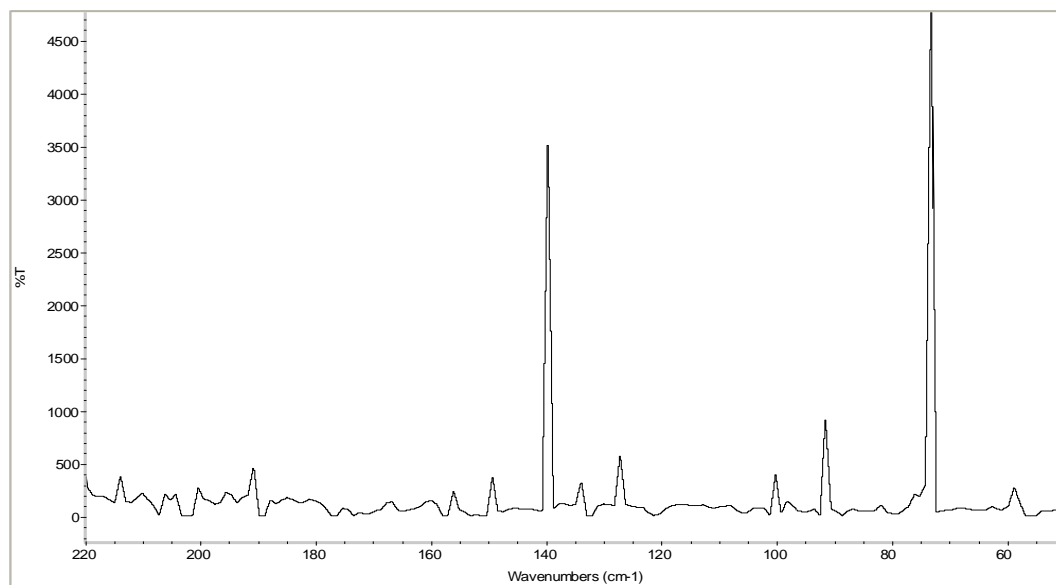


Figure 5. Far-Infrared Spectrum of Complex 37

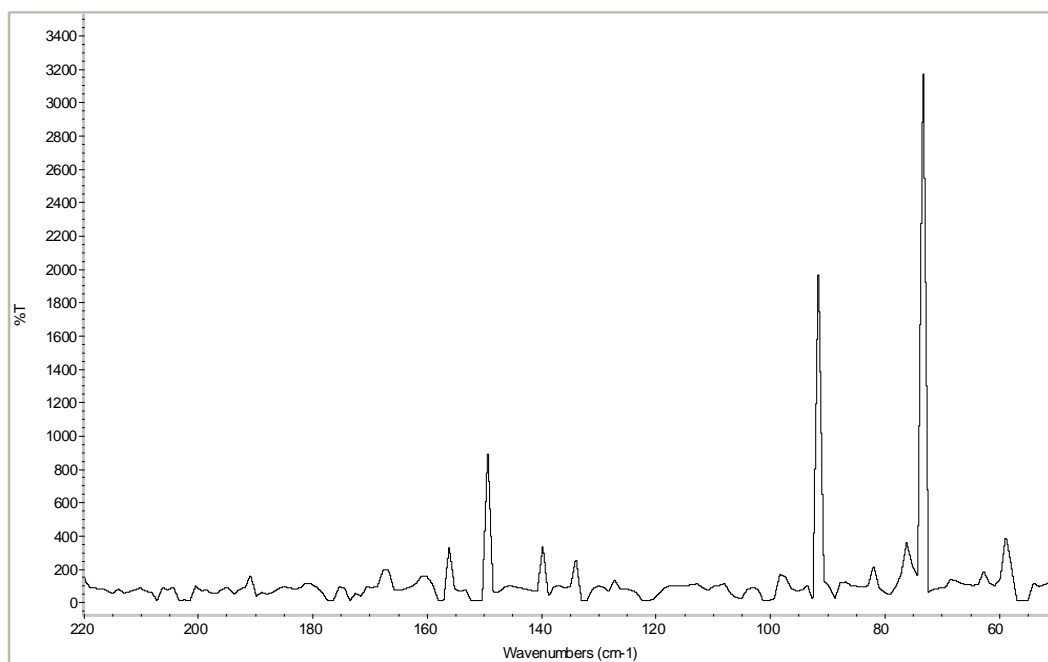


Figure 5. Far-Infrared Spectrum of Complex 38

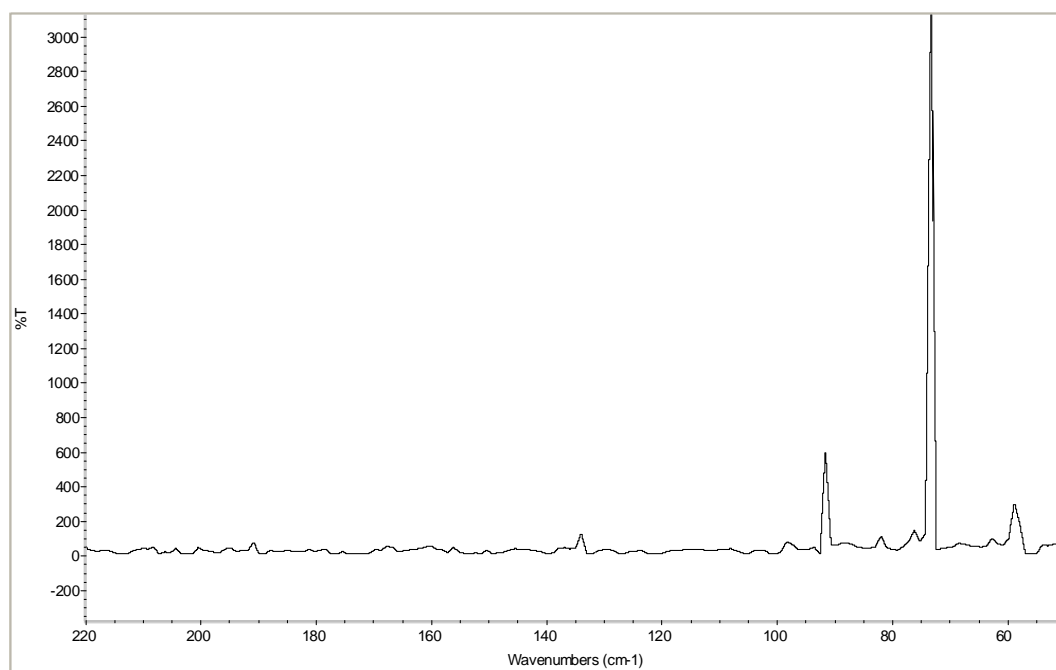


Figure 6. Far-Infrared Spectrum of Complex 40

Curriculum Vitae

Personal Information

Nationality: Pakistani

Place of Birth: The scenic city of Abbottabd located at an altitude of 4120 ft above sea level; in the North West Frontier Province of Pakistan. Abbottabad is also known as The City of Schools and The City of Pines.

Present Address: P.O.BOX 7020, K.F.U.P.M, 31261, Dhahran, Saudi Arabia

Permanent Address: House # K-419 / 2, Kunj Qadeem, Abbottabad, NWFP, Pakistan

Marital Status: Married with a daughter

Family: 7 brothers and 3 sisters (myself being the 8th child)

Tribe: Awan

E-mail: atif_fazal@yahoo.com

Education

S.S.C 1995 from Government High School No.3, Abbottabad

H.S.S.C 1997 from Government Post Graduate College No.1, Abbottabad

B.Sc 1999 from University of Peshawar, Peshawar, Pakistan

M.Sc 2002(Physical Chemistry) from Quaid-i-Azam University, Islamabad, Pakistan

M.Phil 2004(Physical Chemistry) from Quaid-i-Azam University, Islamabad, Pakistan

Joined K.F.U.P.M on February 8, 2005 as Ph.D. student (Lecturer-B)

Completed Ph.D. (Inorganic Chemistry) on January 10, 2010